Facoltà di Scienze Matematiche Fisiche e Naturali

Dipartimento di Chimica

XXX Ciclo Dottorato in Chimica

Evaluation of the effects of PM emitted by specific emission sources on environment and health

Cordinatore

Osvaldo Lanzalunga

Relatore

Dott.ssa Silvia Canepari

Dottorando

Giulia Simonetti

Matricola 1263813

ANNO ACCADEMICO 2017/2018

Sommario

Development of my PhD project

The health burden due to particulate matter (PM) air pollution (PM_{10} and $PM_{2.5}$) is one of the biggest environmental health concerns in the WHO European Region and around the world.

A particular challenge in this research field is about the identification of the physical and chemical characteristics of PM able to reveal the correlation that links fine particle pollutants and respiratory morbidity and mortality.

PM is a complex, heterogeneous mixture, whose chemical and physical characteristics (particle size distribution, chemical composition) changes in time and space and depends on various factors (sources, atmospheric chemistry and weather conditions). In literature, most studies associate PM emitted by the major combustion sources, mobile and stationary, with a range of serious health effects, including increased morbidity and mortality from cardiovascular and respiratory conditions. Current knowledge, however, does not allow a quantification of the health effects of PM emissions from different sources or from individual PM components. Therefore, the study of a depth chemical characterization of the individual emissive sources would be helpful in identification of possible PM toxic effects. Another important factor in the assessment of the aspects that link the human health to particulate pollution is the size of the particle to which the population is exposed. In fact, the size of the particles, together with their chemical composition, are fundamental indicator of health risk. Particle size determines in which region of the respiratory tract particles are deposited, as well as the amount of particles deposited. In this optic, a better understanding of the strength of individual emission sources, of the size of the emitted particles and of their chemical composition could facilitate the design of targeted abatement policies more effective to reduce the burden of diseases due to air pollution. My PhD work was carried out in response to all the above-mentioned needs. In fact, during these three years, I have been studying and deepened all those factors (size, emission sources, chemical composition and indicators of oxidative stress) that could be crucial, to the scientific world, for a better understanding of the PM's harmful effects both on humans and on environment.

I have been involved in the study of possible techniques able to monitor and characterize as well as possible, the different emission sources, some of which can only be identified by using high time-resolved methods. I have been also involved in the study of different methods that can quantify the capacity of inhaled PM to cause oxidative stress within the lung, which seems to be one of the main mechanisms for the adverse cardio-respiratory health effects observed in epidemiological studies.

CHAPTER I: AIRBORNE PARTICULATE MATTER

1.1 Particulate Matter: definitions and classifications

Particulate matter (PM) is a mixture of solid and liquid particles suspended in the atmosphere, with an aerodynamic diameter ranging between 0.01 and 100 μm. The heterogeneous composition of these particles takes in soot, dust, differently originated salts, fly ashes, trace metals and biological micro-organisms (viruses, bacteria, fungi, spores and pollen) (Manahan 2000; EPA 1997). A first general classification of PM concerning the emission sources is divided in:

• *Natural sources*: volcanic eruptions, forest fires, erosion and disintegration of rocks, plants (pollen and plant residues), spores, sea spray.

• *Anthropogenic sources*: combustion engines (trucks, cars, airplanes), domestic heating (especially coal and wood), road surface abrasion, brakes and tires wear, construction works, industries, agricultural processes, incinerators and power plants, tobacco smoke.

The anthropogenic sources are, however, able to introduce into the atmosphere a greater amount of particles toxicologically harmful to health and environment.

Atmospheric particles can also be classified as primary or secondary depending their mechanism of formation.

Primary particles are directly emitted into the atmosphere consisting of fuel combustion, surface erosion and windblown dusts, mechanical break-up from e.g. quarrying and construction activities.

Secondary particles are those formed in the air, generally by chemical reactions of gaseous precursors, sulphur dioxide (SO_2), nitrogen oxides (NOx) and ammonia (NH_3), to form particulate sulphates and nitrates, as well as organic aerosols formed from the photochemically induced oxidation of volatile organic compounds (EC 2004e). The heterogeneous character of PM makes necessary to introduce different detailed classifications, each of them evidencing its peculiar physical – chemical properties. Differently originated particles show very different sizes and shapes as it can be seen in Figures 1.1. The atmospheric particles can be classified referring to the *aerodynamic diameter* (a.d.), defined as the diameter of a unit-density spherical particle ($1g/cm^3$) having the same aerodynamic properties (sedimentation rate) of a given particle (John 2001). The atmospheric particles are divided into three different sub-classifications relating to dimensional characteristics: *modal*, based on the mechanisms of particle formation and consequently on their number, surface area and mass distribution (Whitby 1978); *dimensional (size) cut-off*, based on the efficiency of the sampling head device during the PM collection and *dosimetric*, based on the particles' ability to enter and penetrate into the respiratory system.

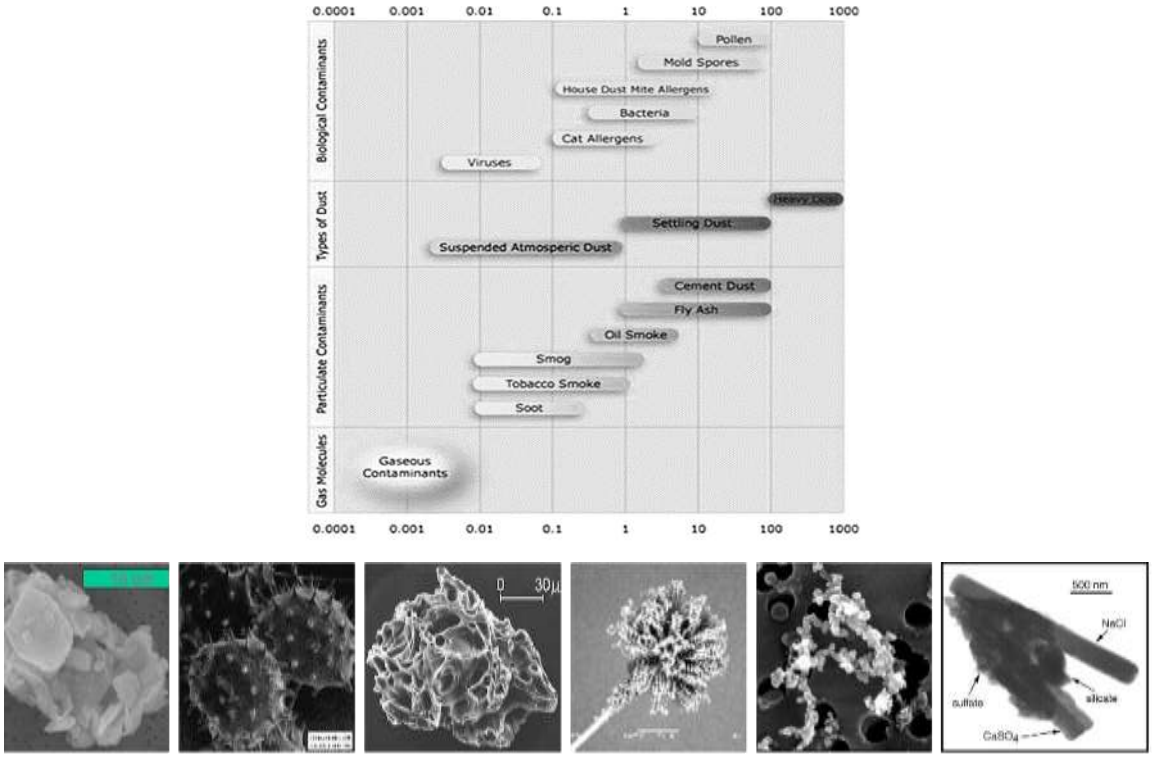

Figure. 1.1: *(Upper panel). Size distribution in micrometres of various types of atmospheric particulate matter. (Lower panel). Scanning electron or transmission electron microscope images.From the left to the right: desertic particle (A. Gaudichet, LISA); hibiscus pollen :http://uq.edu.au/nanoworld); ash particle from the eruption of Mount St. Helens (http://volcanoes.usgs.gov); indoor moulds (M. Boissier, CSTB); soot particle (MPI for Chemistry Mainz); mineral dust from marine thropsphere (Copyright © 1999, The National Academy of Sciences) http://www.env.leeds.ac.uk/envi2150/oldnotes/lecture4/gases.html*

1.1.1 Modal Classification

Particles with less than 0.1 µm aerodynamic diameter ("ultra-fine" fraction) are found in the nucleation mode, including combustion and gas – particle processes. The accumulation mode considers those particles having an aerodynamic diameter between 0.1 and 2.5 µm, generated by coagulation and condensation mechanisms involving nucleation particles, giving altogether the so-called "fine" fraction.

Finally, the coarse mode includes particles with an aerodynamic diameter higher than 2.5 and up to 100 µm, which originate from mechanical processes, such as erosion and abrasion, re-suspension of dust and fragments of organic and vegetable materials, air masses transported from marine or desertic sites (John 2001; Puxbaum 1991). However, by current convention (EC 1997) particles between 2.5 and 10 µm are called "coarse particles", whereas particles less than 2.5 µm are called "fine particles"

and the expression "ultrafine particles" is used mostly in health related literature as notion for particles less than 0.1 µm. By plotting the number of suspended particles versus their size, it will generate a multimodal distribution, as showed in fig 1.2. This refers to the classification by Whitby in 1978 later updated by the EPA in 1997 (John 2001).

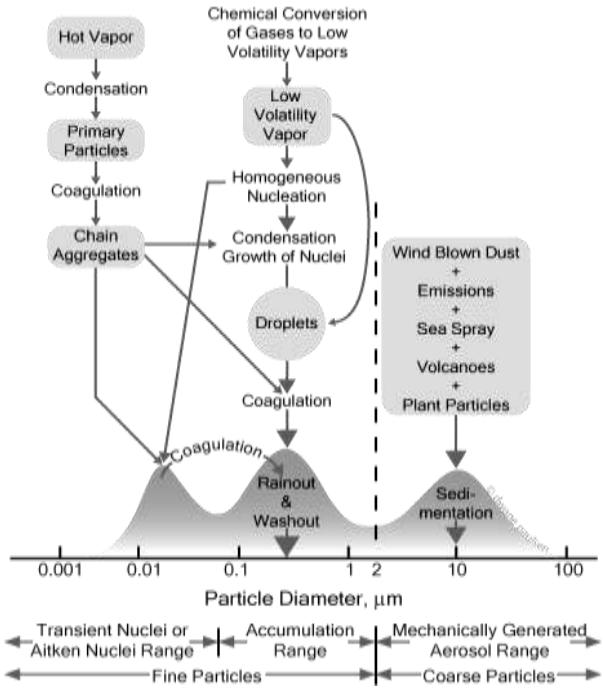

Figure 1.2: *The three ranges for atmospheric particles and the processes leading to their formation.*

1.1.2 Size cut – off classification

PM_X is the fraction of particulate matter that has been collected by a selective inlet impactor with a 50% efficiency cut-off at X µm aerodynamic diameter (EC 1997). Indeed, the instruments usually used in the air sampling stage collect particles that fall within a size range rather than one single size. The most commonly available sampling heads for commercial samplers collect mainly the PM_{10} and $PM_{2.5}$ fractions, being the most interesting for both health/environmental effects and investigations on the life cycle of airborne particles. Nowadays, the PM_1 fraction is gaining more attention, as smaller particles have potentially higher toxicity and capability to infiltrate into the pulmonary system. Therefore, the "*fine*" fraction will be intended for $PM_{2.5}$ fraction, while the "*coarse*" fraction will be intended to include particles with aerodynamic diameter between 2,5 and 10 µm, that is the difference between PM_{10} and $PM_{2.5}$ (EPA 1999). Conventional PM_{10} and $PM_{2.5}$ samplers show a 50% efficiency in collecting particles with 10 ± 0.5 µm or 2.5±0.5 µm aerodynamic diameter.

1.1.3 Dosimetric classification

The dosimetric classification is based on the capability of airborne particles to enter, infiltrate, deposit and react with the different zones of the respiratory system, as showed in figure 1.3. These actions depend on the particle chemical composition its size and solubility.

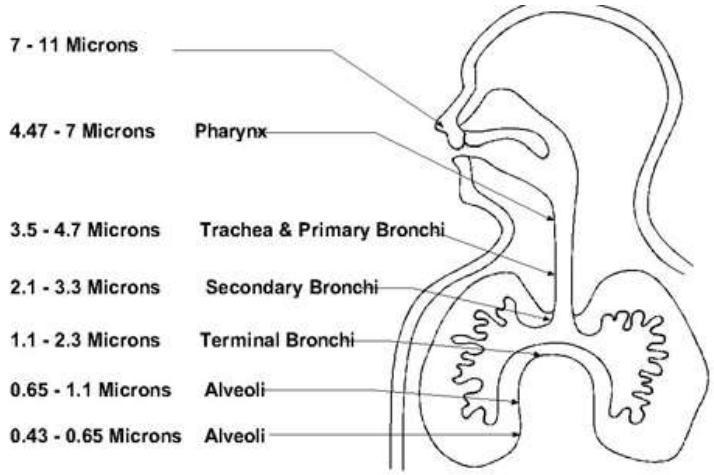

Figure.1.3: *Potential deposition of particles with different sizes into the respiratory system (http://www.acrd.bc.ca/cms.asp?wpID=314).*

Particles greater than 10 µm a.d. are mainly deposited in the upper system, particles between 5 and 10 µm are deposited in the trachea and pharynx, and particles of less than 2 µm penetrate significantly into the bronchi and alveoli. Therefore, under this classification particles are identified by four fractions: *inhalable*, particles which pass through the nose and mouth; *thoracic*, particles that are deposited in the lower respiratory tract, including those particles that reach lungs; *respirable*, particles penetrating significantly up to the gas-exchange region of alveoli; *respirable "high risk"* fraction, which refers to the harmful effects of the respirable fraction on children and people suffering from cardio-pulmonary diseases (Mark 1999).

1.2 PM chemical composition

The chemical composition of the particulate matter includes a large number of species it can be divided into two major classes:

- The *macro-components*: inorganic ions, elements and carbon-containing compounds that exceed more than 1% of the PM mass;
- The *micro-components*: metals present in trace amount (< 1% of PM mass).

The species present in PM are characterized by several parameters as emission sources, chemical-physical processes occurring in the atmosphere and the location of the monitoring site.
In literature, studies testify that the majority of the *fine* fraction is constituted by chemical species such as elemental carbon (EC), sulphates (normally present as ammonium salts) and various organic compounds of primary and secondary origin. However, the *coarse* fraction is mainly formed by elements coming from the earth's crust (Ca, Al, Si, Mg, Fe) and some bio-organic materials such as pollen, spores, plants and animal wastes.

1.2.1 PM macro-components

Among the macro-components it can be found anions, (Cl^-, NO^{3-}, SO_4^{2-}, CO_3^{2-}, SiO_4^{4-}), cations (Na^+, NH_4^+, K^+, Mg^{2+}, Ca^{2+}) and some of elements (Al, Si, Fe). In addition, EC-containing compounds and organic matter constitute a relevant fraction of the macro-components. It is possible to subdivide the ions by in referring to their primary or secondary nature.
The primary ions are: *chlorides* – coming from marine aerosol or from the waste incineration-, *sodium*- coming from marine aerosol and partly from the soil-, *calcium*- coming from soil, wood combustion, fires and industrial activities-, *magnesium*- coming from marine aerosol and soil-, *potassium*- coming from the earth's crust, biomass combustion and agricultural fertilization-, *sulphates*- mainly present as secondary species but a minimal part comes from the marine aerosol-, *silicates and carbonate*- mainly present in the earth's crust.
The secondary compound formation has different gaseous precursors as *sulphide oxides* and *nitrogen oxides* – coming mainly from coal and fuel combustion processes, e.g. power plants, heating plants, vehicular traffic- and *ammonia*- coming from the microbiological activity of the soil and sea; it can be formed also by reduction of NO_x. It is originated by stock farms and, on an urban local scale, by the vehicular exhausts. In general, the formation and the composition of the secondary particles depends largely on the acid-base reactions, oxidation processes, gas-particle interactions that from gaseous precursors give rise to several products (this will be discussed in the next paragraphs). These reactions mainly involve the inorganic species and influence their solubility and their transferability to the surrounding environment (Cirillo, 2016).

1.2.2 Carbon containing compounds

The total carbon fractionin the PM, occurring for 20-60% of the total mass, can be divided into organic carbon (OC) and elemental carbon (EC).

The formation of this fraction, is due to some changes in the physical conditions during the combustion process that lead to a deviation from the ideal combustion. Indeed, there is the emission of CO2, H_2O, other organic gas (such as CH_4, hydrocarbons and volatile organic compounds) and also solid particles, such as soot and aerosol particles in the atmosphere.

While, on the one hand, EC is directly emitted into the atmosphere by combustion processes as either single particles or clusters with variable shape and size (Barone et al., 2006), instead the OC fraction is constituted by a complex mix of numerous compounds of which only a few are known. Some of these are very harmful to the human health such as alkanes, benzoic acids, benzaldehydes, phenols, furans, carboxylic acids, polycarboxylic aromatic acids, aliphatic acids, polycyclic aromatic hydrocarbons (PAHs), polycyclic aromatic ketones, sterols and pesticides. In literature, the organic compounds are divided into *primary* and *secondary*: the former came from combustion processes and from geological and natural sources, e.g. meat cooking, paving roads, chimney emissions, forest fires and cigarette smoke (Gelencsér et al., 2000) and the latter come some reactions occurring in the atmosphere involving volatile organic compounds (VOCs) and oxidant species such as O_3 and OH radical.

1.2.3 PM micro-components

PM includes also a great number of elements with a variable percentage depending on the different nature and origin of the particles. Trace metals coming from natural sources are related to the geological composition of the earth's crust. Also, their suspension in the air is due to the physical, chemical, biological and meteorological processes, such as the soil particles resuspended by wind, or due to the volcanoes (which emit Cd, Hg, As, Cr, Cu, Ni, Pb and Sb), sea spray (which leads to an enrichment in Cd, Cu, Ni, Pb and Zn) and forest fires (which may originate metals such as Cu, Pb and Zn) (Pacyna, 1999).

The release of trace metals into the atmosphere by anthropogenic activity is much more significant and is attributable to the various industrial processes, to the production of electricity, to the combustion of fossil fuels to generate heat and to the vehicular traffic: these sources are responsible for more than 50% of the total emissions of Cr, Mn and V and for 20-30% of the annual release into

the atmosphere of metals such as Cu, Mo, Ni, Pb, Sb, as, Se, Hg, Sn and Zn (Moore,1994). Other sources of trace metals can be identified with the waste incineration and paved roads: the latter emits Al, Si, K, Ca, Ti and Fe, mainly contained in the *coarse* fraction, while the first releases in atmosphere elements mainly included in the *fine* fraction such as Cu, Zn, Cd, Sb, Pb and Ca, Cr, Mn, Ni (Abbas et al., 2001; Phongphiphat et al., 2011). By studying the metal distributions and their emission sources, more information can be obtained about the interpretation of the environmental pollution phenomena. The study of the phenomena (permanence, transport and the removal mechanism) affecting the particulate matter after the emission from the sources are fundamental for the identification of the particles lifetime

1.2.4 Sampling and measurement methods of the PM_{10} and $PM_{2.5}$ fractions

The measure of airborne particulate matter is effectively defined for European regulatory purposes by the European Committee for Standardization (CEN). For PM_{10}, the European Reference Method is described in the CEN standard EN 12341, adopted by CEN in November 1998 (CEN 1998) while for $PM_{2.5}$ the standard are set in the EN 14907 adopted in 2005 (CEN 2005). They define a PM sampling inlet coupled with a filter substrate and a regulated flow device. These systems allow sampling PM according to the particle aerodynamic size. Also by increasing the sampling time, a sufficient quantity of powder can be collected to obtain both an accurate determination of the mass and the subsequent chemical analysis. The standard samplers are constituted by a sampling head that draw the airflow and select the particles of a certain size. The air thus "*purified*" is conveyed through a filtration membrane able to retain the selected particles. Downstream of sampling line, a pump generates the pressure gradient necessary to the airflow. These samples are then constituted by all the particles contained in the *fine* mode and most of the particles belonging to the *coarse* mode, as it is shown in figure 1.4.

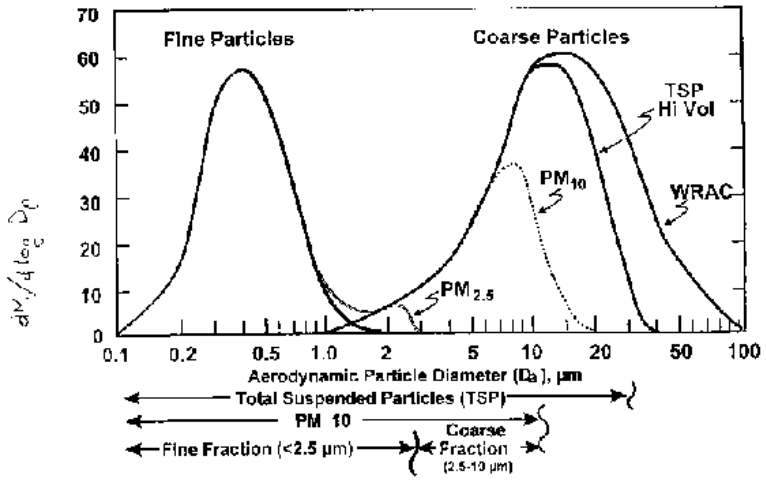

Figure 1.4: *Typical size distribution of atmospheric aerosols.*

The choice of setting the cut to 10 and 2.5 µm was determined by toxicological considerations, since the particles with a.d <10 µm can penetrate into the respiratory system, while the particles with a.d <2.5µm are considered particularly harmful. This choice, however, does not allow an adequate interpretation from the environmental point of view: in fact, it would be useful to distinguish the particles according to the different processes of formation, much more indicative for the identification of the emission sources. From this point of view, it would be appropriate to consider separately the particles belonging to the two coarse and fine modes, because they constitute two independent sets of particles. Samplers can be divided in two main group: the High Volume Samplers (HVS) that allow to collect high amounts of dust on large filters (diameter 150 mm) and the Low Volume Samplers (LVS) that allow to collect small amounts of dust (Few mg) on membranes of 47 mm diameter. The flow rate is critical to maintain the PM cut point and, when using the standard impactor dimension following the criteria for the CEN standard (CEN 1998), a constant flow rate of 68 m^3/h (1133 l/min) is required for a high volume sampler and 2.3 m^3/h (38 l/min) for a low volume sampler.

In figure 1.5 an example of an instrument which is in accordance with CEN standard (1998) for PM_{10} measurements is shown.

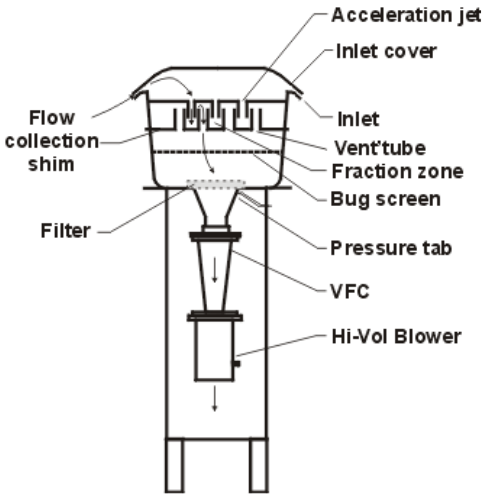

Figure 1.5: *Schematic diagram of Sierra-Andersen/GMW Model 12000 with a volumetric flow controller (VFC).*

Different materials can be used to collect PM depending on the chemical analysis to perform after the sampling phase. In table 1.1 the advantages and disadvantages of the most used materials are reported.

Table 1.1: *Characteristics of the materials used to collect PM.*

Filter material	Advantage	Disadvantage
Glass fiber	High retention capacity.	Release of material due to the fibrous structure.
Quartz	Resistance to high temperatures; available to analyze carbonaceous compounds by means of thermal methods.	Tendency to adsorb volatile organic compounds.
Teflon	No release of material due to the continue structure; low blank value, suitable to analyze trace elements.	Fast clogging with high PM concentrations.

The mass collected on the filter is gravimetrically measured by means of a micro-balance under ambient air conditions. The handling of filters should be made in clean air and all equipment should

be stored in plastic bags in a dust free environment. It is required by EN 12341 (CEN 1998) that the filters are equilibrated, at 20° C (±1) and 50% R.H. (±5), for 48 hours. This equilibration should be performed before the filters are weighed before the sample collection, and after sampling, before the filter is weighed again with the collected sample. This is helpful to make the determination of mass independent from any external condition. Known the flow and the sampling time, the concentration of particulate matter in the air (in mg/m3) is expressed as:

$$C = \frac{m(n) - m(b)}{F\ t}$$

Where *m(n)* is the mass of the sampled filter, *m(b)* is the mass of the blank filter, *F* is the flow value and *t* is the sampling time.

This method has some drawbacks: it is slow, it requires high sampling volumes and the conditioning procedure requires at least 48 hours. Furthermore, the main problem is the low ratio between the mass of the sampled and the blank filter. In these conditions, the uncertainty associated with the measurement is equal to 2-4%.

PM mass determination can be alternatively carried out automatically by measuring the attenuation of the β radiation produced by a radioactive source of C-14 placed inside the sampler. The β radiations pass through the filter before and after the sampling so that the difference in the absorption of β-rays by the filter is proportional to the concentration of PM. In this case, the uncertainty of measurement is influenced especially by the stability of the β source and is equal to 1-2%.

1.2.5 Cascade impactor sampler

Besides to the PM samplers aimed to collect particles with a wide range of aerodynamic parameters, e.g. PM_{10} and $PM_{2.5}$, cascade impactors allow to fractionate the particles in different restricted ranges of aerodynamic diameters. The multiple stages of a cascade impactor can be analyzed to determine aerosol mass distribution (by gravimetric analysis) or to study the chemical composition as a function of the particle size. Simultaneous data on particle size and mass or chemical composition are useful to assess health effects and particle transport in the atmosphere.

Particle impaction refers to the collection of particles on a solid plate when they deviate from the airflow streamlines due to their inertia. Particles contained in the air enter in the device by means of a nozzle and are blocked on a solid plate oriented perpendicularly to the nozzle axis. The airflow is laminar and the particles are accelerated to a uniform velocity. Larger particles are propelled from the streamlines and are collected on the plate, while smaller particles remain in the airflow. A

schematic representation of a multistage cascade impactor is shown in figure 1.6. Airflow enters from the top by means of a pump, it passes through every plate and is exhausted through a back-up filter. Each impactor stage consist of a particular aerodynamic diameter range and successive stages are aimed to collect smaller particles (Hering et al., 1979). Sampling by the cascade impactor should cause some drawbacks, depending on the sampling conditions and on physical and chemical properties of the aerosol sampled. For example, all the aerosol sampled in an impactor should be deposited on the collection plates or be captured by the after filter. In practice, some particles are collected on other interior surfaces and are typically excluded from the analysis. Wall losses result from diffusion of particles in turbulent eddies, from sedimentation of large particles. Therefore, if they are significant, the total mass concentration will contain an error. Another problem occurs when particles bounce off the collection surface and they may be carried to subsequent stages, where they may stick or again bounced off. The result is that subsequent stages collect more mass than is appropriate, and the inferred particle-size distribution is based towards the smaller particles. This phenomenon can severely limit the utility of the collected data. Typically, sticky substances are applied to impaction surfaces to reduce particle bounce.

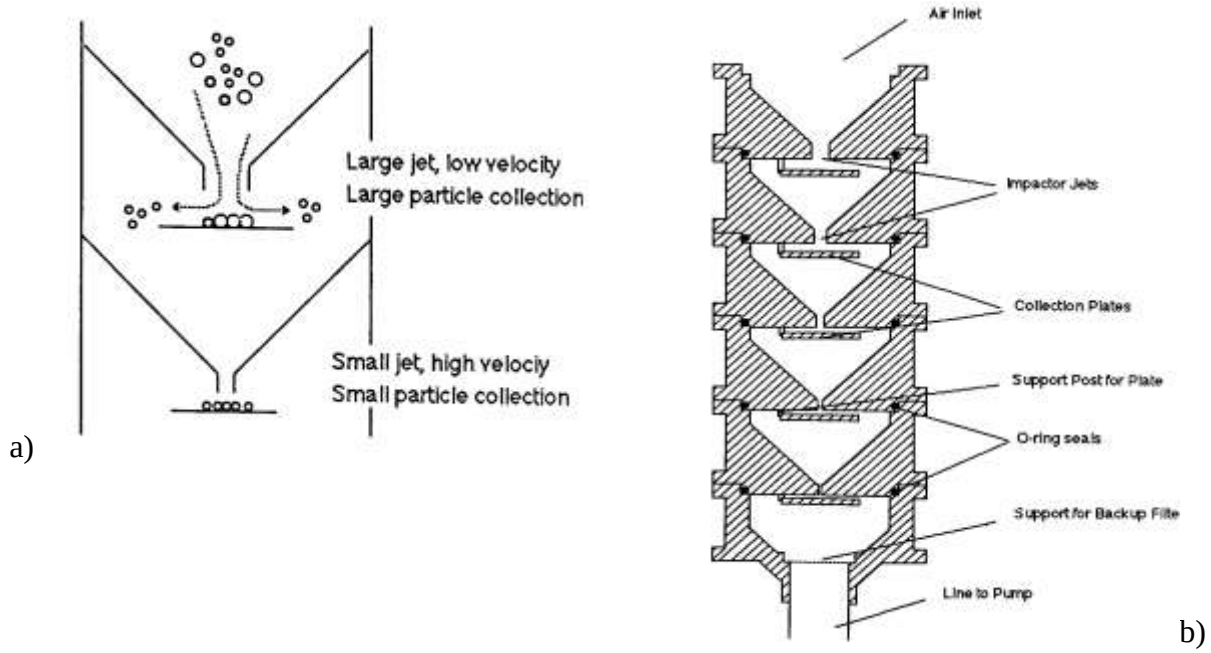

Figure 1.6: *a) Scheme of two impactor stages showing large and small particle trajectory; b) Example of five-stage cascade impactor.*

1.2.6 Sampling devices to reduce sampling artifacts

As it is well known, the secondary species undergo gas-particle equilibria causing positive or negative artefacts. In fact, during the sampling phase there is a displacement of the equilibrium regulated by temperature, concentration and flow rate changes and a kinetic effects leading to the evaporation of the sampled species (negative artifact). In addition, it has to be taken into account the influence of the sampling membrane, since many species can adsorb on the filter before, during or after the sampling (positive artifact). Since the separation of the solid and the gaseous species can be done only during the sampling phase, it was necessary to create some sampling devices able to "*pick up*" the gaseous components that are lost during the sampling due to variations in the equilibrium. To this purpose, the diffusion denuder allows the selective removal of the gas phase on the device's walls and the sampling of the particles on filter membrane placed downstream. It is a cylindrical glass tube (figure 1.7) whose inner surface is coated with a substance capable of chemically reacting with the gaseous species of interest (Ferm, 1979). By means of a pump, the atmospheric air is drawn in through the denuder and, in laminar flow conditions, the molecules in the vapour phase diffuse toward the reactive or adsorbent surface (concentration gradient), while the particles are blocked on the filter (fig.1.7).

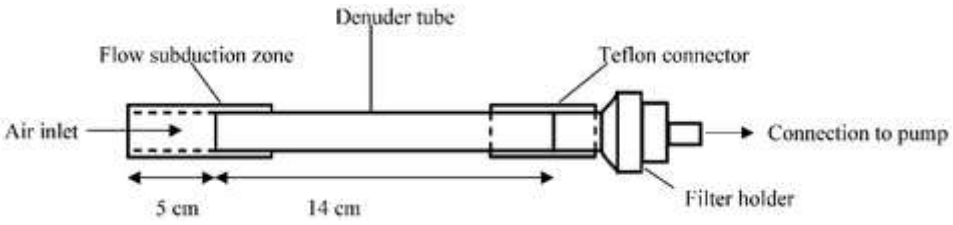

Figure 1.7: *Schematic structure of a cylindrical denuder*

Denuders are especially used to reduce the artifact due to the evaporation of the ammonium nitrate. They give the possibility to determine simultaneously the individual concentrations of HNO_3 (gas) NO_3^-(particle), NH_3 (gas) and NH_4^+ (particle). The air is drawn through a series of annular denuders, and filters. The first two denuders are internally coated with sodium carbonate (Na_2CO_3) and glycerol for the collection of nitric acid and sulphur dioxide respectively (glycerol prevents oxidation of nitrite to nitrate by ozone) and the third is coated with citric acid, oxalic acid or phosphorous acid for the collection of ammonia. The coated denuders are then followed by a three-filter pack system. The first filter is characterized by a high collection efficiency for submicron particles, followed by a filter impregnated with potassium hydroxide for collection of nitric acid, which may have evaporated from the particle filter, and a filter impregnated with oxalic acid for the collection of ammonia, which may

also have evaporated. Nitrous acid (HNO_2) is also absorbed in the alkaline denuders, but will normally not cause a significant interference as it is usually detected as nitrite in the sample extracts.
Regarding the Semi-Volatile Organic Compound there is not a validated sampling method to reduce the artefacts. In fact, sampling devices such as carbon-coated denuders are still under study, for this reason, the only way to reduce and valuate the organic compound artifacts is to collect the evaporated compounds at the bottom of the sampling system. One of the most used materials involved in this phase is the PolyUrethane Foam (PUF); this material, located after the sampling filter, is extracted during the analytical phase to measure organic species such as Polycyclic Aromatic Hydrocarbons.

1.3 Analysis and chemical characterization of particulate matter

Many studies are available in literature concerning the determination and characterization of different chemical species and/or size fractions of particulate matter, eventually combined to source-apportionment applications (EPA 1999; Kleeman et al. 1998; Querol et al. 2003).
A complete chemical characterization of airborne particulate matter includes the determinations of the volatile, hydro-soluble and insoluble fractions of inorganic ions, organics and elements. Since various different analytical methods have been developed and used for these determinations, usually data quality is variable and it is difficult a comparison among the results obtained in different laboratories.

1.3.1 Chemical characterization of the carbon fraction

As described above the carbon fraction typically constitutes more of 30 % of the particulate mass and contains elemental carbon (EC) and a huge number of different organic carbon (OC) compounds. Measurements of EC and OC are important for health and source apportionment studies, as well as for models' validation. Indeed, the ratio between EC and OC (EC/OC) is often used as a valuable tool to understand the origin of the air masses. A variety of methods is available for the measurement of the carbon content of the aerosols (Heintzenberg and Winkler 1991); however, the distinction between organic and elemental carbon remains one of the critical issues and strongly depends on the analytical procedure of the method (EC 2004c).
The recommended method to determine EC is based on the volatilization and oxidation of the sample, and consequently determination of the evolved CO_2, either directly or after conversion to CH_4 by a flame ionization detector (FID). This procedure also gives the total carbon content, and then a quantification of the total amount of the organic materials; the method is not free of artifacts,

particularly the charring or incomplete removal of organic compounds may lead to the overestimation of EC.

Table 1.2. *Recommended and alternatives methods for chemical analysis of inorganic ions (EMEP/CCC 1996).*

METHODS FOR CHEMICAL ANALYSIS OF INORGANIC IONS		
Component or parameter	**Recommended methods**	**Alternative**
Conductivity	Conductivity cell and resistance bridge	
Hydrogen ion (H^+)	Potentiometry (glass electrode) pH<5.0	Titration
Ammonium ion (NH_4^+)	Ion chromatography	Spectrophotometry (indophenol blue colour reaction)
Sodium ion (Na^+)	Atomic absorption spectrophotometry (AAS)	Ion chromatography
Potassium ion (K^+)	AAS	Ion chromatography
Magnesium ion (Mg^{2+})	AAS	Ion chromatography
Calcium (Ca^{2+})	AAS	Ion chromatography
Sulphate ion (SO_4^{2-})	Ion chromatography	
Nitrate ion (NO_3^-)	Ion chromatography	Reduction to nitrite and diazotation
Chloride ion (Cl^-)	Ion chromatography	Displacement of SCN^- in Hg $(SCN)_4^{2-}$, determination of coloured Fe(SCN) complex.

1.3.2 Chemical characterization of the inorganic ionic fraction

The major inorganic ions to be determined in the particulate matter are those indicated in table 1.2, which also reports the recommended analytical methods. When the inorganic ion fraction is to be determined, a special attention should be given to PM sampling, due to the eventual artefacts arising from their gas-particle phase distribution as already discussed in paragraph *1.2.6*

As shown in table 1.2 the analytical method used for ionic determination is mainly the ion chromatography after extraction. The Teflon filter is extracted in water and sonicated for 20 min before the analysis.

1.3.3 Trace elements analysis

Summing the trace elements analysis was usually performed in our laboratory, as usual, while the other chemical analysis (macro elements, ions, EC and OC) were performed at the Atmospheric Pollution Institute of CNR (Montelibretti, Rome). The simultaneous sampling of PM on teflon and quartz filters allowed the chemical determination of several components. Quartz filter were analyzed for their elemental carbon and organic carbon content (EC/OC) by means of a thermo-optical analyzer (OCEC Carbon Aerosol Analyzer, Sunset Laboratory, OR-U.S.A.), by following the procedure described above. Teflon filters were analyzed by following the procedure reported in figure 1.8. This analytical procedure has been previously optimized and validated in our laboratory by evaluating the recovery percentages and the repeatability on both certified material (NIST1648) and real samples (Canepari et al., 2006 a,b; Canepari et al., 2009). Briefly, macro-elements Al, Fe, K, Mg, Ca, Ti, S and Si were analyzed by energy-dispersive X-Ray fluorescence (EPD-XRF, X-Lab 2000, SPECTRO). Then each filter was extracted in an acetate buffer solution using an ultrasonic bath. The solution was divided into two aliquots, one analyzed for anions (Cl^-, NO_3^- , SO_4^{2-}) and cations (Na^+, NH_4^+, Mg^{2+}, Ca^{2+}) using Ion Chromatography (DX 100, DIONEX Co., CA-USA) and the other analyzed for the extractable fraction of the elements (Al, As, Cd, Cu, Fe, Mg, Mn, Ni, Pb, Sb, S, Si, Ti, V, Zn) using inductively coupled plasma with optical (ICP-OES) and mass spectrometer detection (ICP-MS) (Bruker 820, equipped with a reaction cell, CRI, and a 400 μl/min MicroMist nebulizer). The choice of the extracting solution was driven by the intention to increase the selectivity of elements as PM source tracers but also to estimate the environmental mobility and bio-accessible fraction of toxic elements (Canepari et al. 2010).

The residual teflon filter was digested in a mix of HNO_3 and H_2O_2 (2:1) using a microwave oven (Milestone Ethos Touch Control with HPR 1000/6S rotor) and the mineralized fraction was then analyzed by ICP-OES and ICP-MS for its insoluble elemental content. The use of both ICP-OES and ICP-MS allowed the analysis of a larger number of elements. According to the results of the previous studies, we quantified Fe, Cu, Mn and S by ICP-OES and the others elements with ICP-MS. Matrix-matched standard solutions were used for calibration; Y was used as internal standard; the collision reaction interface (CRI) was activated for As, Se, Fe and V determination.

This overall procedure allows the determination of macro-elements (including Al and Si, which show a low recovery after the acid digestion), soluble inorganic ions and the extracted and residual fractions of micro- and trace- elements on individual 24-h filters; furthermore the determination of the same element with different analytical techniques (e.g. Fe, Mg, S) makes it possible to check the quality control of the determinations by means of an inter-techniques comparison (Canepari et al. 2009b).

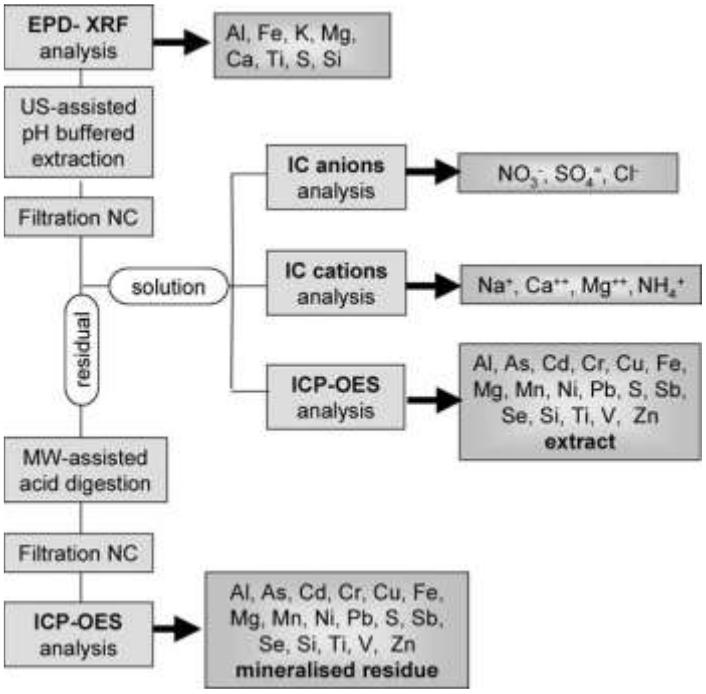

Figur.1.8: *Sequence of the chemical analysis performed on Teflon filters.*

1.4 Mass closure and macro-sources calculation

The chemical analyses described allowed the determination of the main components of atmospheric PM (macro-elements, ions, elemental carbon, and organic matter) and a satisfactory mass closure was obtained. The chemical mass closure is the correspondence between the mass concentration of PM and the sum of the single chemical analyses. It is based on the simple chemical analyses of the PM macro-components which can be then grouped into five main PM macro-sources: crustal matter, marine aerosol, secondary inorganic compounds, combustion products (vehicular emissions) and organics (Perrino et al., 2013a). Micro- components (such as trace elements), because of their low abundance in the PM, are generally considered negligible in the mass balance calculation. Afterwards, the algorithms used to calculate these macro-sources are hereinafter reported:

- ***crustal matter*** contribution is calculated by adding the concentration of elements generally associated with mineral dust (Al, Si, Fe and the insoluble fractions of Na, K, Mg and Ca, calculated as the difference between the XRF and the Ion Chromatography determinations) and carbonate, calculated from calcium and magnesium determined by Ion Chromatography.

A correction factor for oxygen had to be applied for the macro-elements in order to consider them as metal oxides (Chan et al., 1997; Marcazzan et al., 2001).

- **Crustal matter** = 1.89 Al + 2.14 Si + 1.42 Fe + 1.35 $Na_{insoluble}$ + 1.2 $K_{insoluble}$ + 1.67 $Mg_{insoluble}$ + 1.4 $Ca_{unsoluble}$ + CO_3^{2-} (1)

$CO_3^{2-} = 2.5\ Mg^{2+} + 1.5\ Ca^{2+}$ (2)

- ***Marine aerosol*** contribution is calculated from the sum of the concentrations of soluble sodium and chloride, determined by Ion Chromatography, multiplied by 1.176 in order to take into account minor sea water components (sulphate, magnesium, calcium, potassium).

- ***Secondary inorganic components*** are calculated by adding the non-sea-salt sulphate, nitrate and ammonium concentrations.

- ***Combustion products*** (Vehicular emission) are calculated by adding elemental carbon to the same amount multiplied by 1.1 (primary organic carbon), in order to take into account organic species that condense from the exhaust gases and coat the surface of elemental carbon particles (Castro et al., 1999).

Combustion products = EC+ 1.1 EC (3)

- ***Organics*** are calculated by multiplying the non-primary organic carbon by a factor α taking into account the atoms other than C present in the organic molecules. It includes primary OC coming from biomass combustion and biogenic aerosol and secondary organic compounds. α can be assume values from set to 1.6 for urban sites to 2.2 for rural, as suggested in Turpin and Lim (2001) and Viidanoja *et al.* (2002)

Organics= α OC – (1.1 EC). (4)

The empiric factor α used to convert the OC in Organic Matter (αOC) is influenced by the spatial and temporal variability. The organic compound, represent one of the main sources of uncertainty in PM reconstruction due to the particle nature and then difficult to solve; it is important to reduce any other error source that may affect the mass closure calculation. The determination of the ionic species is

not particularly difficult. In fact, the simple, economic, and able analytical method used to determine all the anions and cations required by the Italian Dlgs 155/2010 is the ion chromatography. Much more complex is the determination of EC and OC deposited on the filters. The most used method for the determination of the carbonaceous material is the thermo-optical analysis, implemented by the instrumentation developed and produced by Sunset Laboratory, which is currently the most widely used in Europe (Birch and Cary, 1996). The aerosol sampled on a quartz filter is subjected to two successive stages of analysis. During the first stage, the filter is heated under an inert atmosphere (helium), between 550 and 900° C, to release the organic compounds. A part of it, however, undergoes a process of pyrolysis. In the second stage, the furnace is cooled and then heated again in an oxidizing atmosphere (in the carrier gas is added to 5-10% oxygen) up to 800-900° C. In this phase are released from the filter elemental carbon and pyrolytic carbon (PyC) produced in the previous step. All species released from the filter during the two stages of analysis are in contact with an oxidizing agent (manganese dioxide) and oxidized to CO_2, which is subsequently reduced to methane, the CH_4 concentration is then determined by a flame ionization detector. For a correct determination of the pyrolitic carbon, a laser, which continuously determines the reflectance or transmittance of the filter portion subjected to analysis, is used. The transmittance or reflectance of the filter varies depending on the pyrolitic carbon formation. The determination of the amount of EC, which is necessary to bring the transmittance or the reflectance to an initial value, makes possible the correction. However, it should be noted that the results of thermo-optical analysis are subject to various uncertainties. The main problems that occur in discriminating OC and EC are due to the pyrolytic carbon evaluation and to the identification of an optimal thermal protocol (times and temperatures of the different steps of heating) (Bae et al., 2009). The study of the chemical contributions that take part to the mass closure is not so easy. In fact, the reconstruction of the PM mass by chemical analysis is not always complete, mainly due to the large number of sources, the high spatial variability of the contributions and the occurrence of particular weather conditions. Despite the analytical techniques used are highly sensitive, not always the sum of the obtained values matches the total mass obtained by gravimetric analysis. For example, during periods characterized by high atmospheric stability, a significant increase in the concentration of PM secondary, especially ammonium nitrate is registered (Vecchi et al., 2004; Perrino et al., 2008). At the same time, an increase in the mass of PM considered "unknown" is observed. In circumstances of PM_{10} concentrations around 100 μ g/m^3, the percentage of ammonium nitrate can grow up to 30-35% of the total mass, while the unknown fraction can reach value up to 20%. Long-range transport of desert dust are also accompanied by an increase of the unknown PM mass. The common feature of these

two class of compounds is their hygroscopicity, suggesting that the water bound or adsorbed on the PM particles plays a very important role.

1.5 The role of the water in Particulate Matter

Water is present in the atmosphere as vapor or liquid, in the form of clouds, rain and fog; its concentration is very variable and mainly depends on the temperature. Most of the atmospheric particles are able to interact with water, undergoing changes of their original physical and chemical features. Particularly, this interaction affects particles' size distribution (Swietlicki et al.,1999), optical properties and residence time in the atmosphere (Sloane and Wolfe, 1997; Pilinis et al.,1995; Kreidenweis et al., 2001). Moreover, it is well-known that high values of relative humidity (RH) favors the occurrence of acid-base reactions that leads to the formation of the secondary inorganic salts, widely discussed in the first chapter (Baek et al., 2004; Squizzato et al., 2012). Inorganic salts are hygroscopic and can act as cloud condensation nuclei (CCN) that favor the formation of clouds and fogs. When the hygroscopic nuclei are numerous, water vapor rapidly condenses on them, leading to an increase in rainfalls over the cities, due to the particulate air pollution (Lutgens and Tarbuck, 2004). Finally, the amount of adsorbed water affects the solid-vapor equilibria of the secondary ammonium salts collected on the filters, a mechanism that is among the main responsible for sampling artifacts (Vecchi et al., 2009). Although in most cases the artifact is negative (loss of NH_4NO_3 due to release of NH_3 and HNO_3) (Chow et al., 2005; Yuc et al., 2006;), in the presence of very high humidity values, it becomes positive, as the formation of particulate NH_4NO_3 from gaseous NH_3 and HNO_3 is favored (Gysel et al., 2007; Khlystov et al., 2009; Hu et al., 2011). Of interest is also the contribution of water to the mass concentration of PM. The presence of considerable amounts of water in PM samples, in fact, causes an increase of PM mass concentration that might be responsible for the exceedances of the limit standards. It is worth noting that the knowledge of this contribution may be of interest also for a correct evaluation of the PM health effects: water is harmless, but it may cause a relevant variation of the aerodynamic diameter of the particles and thus of their ability to penetrate into the respiratory system. Moreover, in many papers attempting PM mass closure, the unidentified mass (difference between gravimetric determination and reconstruction from the single chemical analyses) is attributed to the presence of water and/or to the difficulty in determining an adequate conversion factors to calculate organic matter (OM) from the measurement of organic carbon (OC) (Balasubramanian et al., 2003; Harrison et al., 2003; Tsyro, 2005; Almeida et al., 2006; Sasaki and Sakamoto, 2006; Perrino et al., 2009; Perrone et al., 2012). In fact, water can exist within the PM as

bound or not-bonded water: the first being chemically bound to the crystalline structure of the inorganic salt. The only known species present in the atmospheric aerosols containing this kind of water is the Na_2SO_4. The not-bonded water is the water which condenses on the aerosol particles when the relative humidity atmospheric (RH) increases. Many papers in literature relate to the study of the interaction between water and atmospheric particles: in 1996 Yang e Cotton theoretically demonstrated that there is a relation between the relative humidity and the capability of a dry particle to absorb water. In 2011 Hu et al. studied the effects of RH on the size and hygroscopicity of NH_4Cl and NH_4NO_3. It was found that the evaporation of NH_4Cl is promoted by increasing the RH values and a similar trend was also observed for NH_4NO_3 particles less than 50 nm. The proposed mechanism suggests that, by increasing the RH, the equilibrium (1) is altered, converting $NH_3(g)$ e $HX(g)$ in NH_3*nH_2O e $HX*nH_2O$ (X is given by Cl^- or NO_3^-), making the evaporation of NH_4X (s) faster.

$$NH_4X\ (s) \rightleftharpoons NH_3(g) + HX(g) \qquad (1)$$

In spite of the relevant role played by water in the study of atmospheric PM, a quantitative determination of adsorbed water was attempted only in a few papers. Water content was generally determined by indirect methods, consisting of the differential determination of particle dimension (Dick et al., 2000; Hu et al., 2001; Rees et al., 2004; Stanier et al., 2004; Kitamori et al., 2009) or collected mass amount (Speer et al., 2003) before and after the exposure to controlled RH conditions. Water adsorption resulted to be relevant for fine particles, characterized by high surface area, and for particles containing water-soluble inorganic salts, mainly ammonium sulphate (Stanier et al., 2004; Kitamori et al., 2009), and hygroscopic organic species such as dicarboxylic acids (Ansari and Pandis, 2000; Dick et al., 2000; Decesari et al., 2001; Speer et al., 2003). In most of these papers, the instruments used to carry out the analysis are some particular analyzers, very expensive and quite complex to run and to manage and the analysis are carried out only on not-sampled aerosol. Moreover, these differential techniques evaluate only the amount of surface-adsorbed water and are not able to give information about further contributions due to structurally bound water.

1.5.1 Focus on Water and PM interaction

Thanks to the development and the optimization of a method for the determination of water in particulate matter (Canepari et al., 2013), in this work we applied the method to 24-h PM10 samples. In fact, we applied the same method to size-segregated particulate samples collected in different sites

and environmental conditions. For the first time, it has been possible to study the size distribution of PM-bound water, giving information about the chemical species it is bound to. This work allowed us to identify some environmental conditions that particularly favour the increase of the water content: atmospheric stability episodes and desert dust intrusions. A picture of the water content in urban PM is also given. The application of the method to size-segregated samples has revealed that water showed a typical mass size distribution in each one of the three environmental situations that were taken into consideration. A very similar size distribution was shown by the chemical PM components that prevailed during each event: ammonium nitrate in the case of atmospheric stability, crustal species in the case of desert dust, road-dust components in the case of urban sites. The shape of the tr-KF curve varied according to the size of the collected particles.Considering the size ranges that better characterize the event (fine fraction for atmospheric stability, *coarse* fraction for dust intrusion, bi-modal distribution for urban dust), this shape is coherent with the typical tr-KF shape shown by water bound to the chemical species that predominate in the same PM size range (ammonium nitrate, crustal species, secondary/combustion species - road dust components

*1.5.2 Mass size distribution of particle-bound water**

Introduction

Among the many scientific issues, regarding the chemical composition of atmospheric particulate matter (PM), of particular interest is the measurement of particle-bound water. On one side, in fact, we have the many effects water may exert on PM, which make its measurement a step forward in our knowledge of PM characteristics. Water may affect the size and thus the lifetime of atmospheric particles, their optical and chemical properties and their ability to penetrate into the respiratory tract (Swietlicki et al., 1999; Kreidenweis et al., 2001; Hu et al., 2011). Moreover, water may contribute, even significantly, to the mass concentration of PM, leading to possible exceedances of the regulatory limits. Finally, the increase in the aerosol dimensions due to water uptake may cause some particles to pass the cut-off of the sampling inlet, leading to a loss of PM mass during the sampling stage (Canepari et al., 2014). On the other side, however, many difficulties are encountered in identifying easy, reliable methods for its direct experimental determination. Only a few methods for determining the water content of PM have been reported in the scientific literature. Some of them do not involve any experimental determination: water can be empirically calculated from the chemical composition of PM (Harrison et al., 2003; Murillo et al., 2012) or theoretically determined from thermodynamic models (Tsyro, 2005; Hodas et al., 2014). However, the complexity of the physico-chemical characteristics of PM and the possibility for water to be bound to many chemical species, both inorganics and organics, makes it difficult to obtain a reliable estimate. Experimental indirect methods include the hygroscopic tandem differential mobility analyser (H-TDMA) and the Dry-Ambient Aerosol Size Spectrometer (DAASS), both based on the differential determination of particle dimension or mass amount before and after the exposure to different RH conditions (Speer et al., 1997; Dick et al., 2000; Stainer et al., 2004; Kitamori et al., 2009). Both methods are able to determine only the amount of water adsorbed on the aerosol surface and they are not able to give information about structurally-bound water. The direct analytical determination of water in atmospheric aerosols can be carried out by the Karl-Fisher (KF) method.

* Published on *Atmospheric Environment*

Canepari, S., Simonetti, G., & Perrino, C. (2017). Mass size distribution of particle-bound water. Atmospheric Environment, 165, 46-56. DOI: 10.1016/j.atmosenv.2017.06.034

This work was presented in poster form during the Congress PM2016 in Rome

This technique has been first applied to PM collected on filters by Ohta et al. (1998) and by Tsai et al. (2005), although the procedures they proposed were not suitable for routine measurements.

A step forward consisted in the use of a thermal ramp for the desorption of water from the PM samples, prior to the analysis by the coulometric KF technique (Canepari et al., 2013; Rogula-Kozłowska et al., 2017). The optimization of the thermal-ramp Karl-Fisher method (tr-KF) allowed the identification and quantification of different water contributes retained by the sample with different strength; these contributes have been shown to be associated to different chemical components in the aerosol (Canepari et al., 2013; Perrino et al., 2016).

The above method has been routinely applied to PM_{10} samples collected in different geographical areas and various environmental conditions. The results of these studies have shown that the concentration of water bound to PM_{10} is generally of the order of a few micrograms per cubic meter. However, in some environmental conditions, namely Saharan dust advection and very strong atmospheric stability leading to enhanced ammonium nitrate formation, water concentration may reach very high values (up to 30 $\mu g/m^3$) that cannot be neglected when the mass closure has to be obtained (Perrino et al., 2016). The present work is aimed at evaluating the mass size distribution of water in areas subjected to different environmental conditions by applying the tr-KF method to size-segregated PM samples. Information about the chemical components bound to water can be obtained by comparing the shape of the water curve obtained for each PM size fraction with the chemical composition of the same fraction.

Experimental

Sampling and analysis

Size-segregated PM samples were obtained by using two co-located Micro-Orifice Uniform Deposition Impactors (MOUDI) operating at the flow rate of 30 L min-1 and having stage cut-sizes of 0.18, 0.32, 0.56, 1.0, 1.8, 3.2, 5.6, 10 and 18 µm in aerodynamic diameter (AD) (mod. 110.R, MSP Corporation, U.S.A.); both impactors were equipped with Teflon membrane filters (TEFLO, 47 mm, 2.0 micron pore size, PALL Life Sciences). Filters from the two impactors were used to obtain the size distribution of water and of PM mass, inorganic ions and elements, respectively.

Daily collection of PM_{10} samples was carried out by using a dual channel beta attenuation automatic monitor (SWAM 5a Dual Channel Monitor, FAI Instruments, Fonte Nuova, Rome, IT) located side-by side to the MOUDI sampler. The two channels of the samplers were equipped with TEFLO membrane filters and quartz fiber filters (TISSUQUARTZ 2500QAT, 47 mm, PALL Life Sciences)

in order to obtain a complete chemical analysis of the samples (not reported in this paper). The automatic determination of PM_{10} mass concentration by the beta attenuation method was carried out on the channel employing Teflon filters. Additional daily sampling of PM_{10} on Teflon filters devoted to the determination of water was carried out by using a single-channel sampler (Skypost PM, Tecora, Mi, IT). Mass concentration on the MOUDI stages was determined gravimetrically by using an automated microbalance (1 μg sensitivity, mod. ME5, Sartorius AG, Goettingen, Germany). The procedure was as follows: - filters were equilibrated for two days at 20°C and 50% RH; - filters were weigthed; - filters were equilibrated again for two days at 20°C and 50% RH; - filters were analysed for water. The determination of water was carried out by the tr-KF method, using a 831 KF Coulometer (Metrohm AG, Herisau, CH) equipped with a programmable oven (874 Oven Sample Processor; Metrohm). The heating ramp was as follows: 5 min at 50 °C; from 50 °C to 120 °C at 14 °C min^{-1}; 5 min at 120 °C; from 120 °C to 180 °C at 12 °C min^{-1}; 2 min at 180 °C; from 180 °C to 250 °C at 14 °C min^{-1}; 20 min at 250 °C. This ramp has been previously optimized to obtain the selective desorption of different water contributes (Canepari et al., 2013). The KF curve of each sample (water vs. time) was obtained by subtracting the value of the operative blank to each point of the curve; the operative blank takes into account all the water contributes that do not pertain to the dust sample (humidity of air inside the vial, water adsorbed on the vial walls, humidity in the carrier gas, water content of the plastic vial cap). All samples show a peak in the first heating step (50°C) whose size has been found to depend on the storage and conditioning settings (Canepari et al., 2013). Although the tr-KF technique does not permit a control of the RH values, it is reasonable to infer that RH conditions lower than crystallization are reached in this first part of the thermal ramp. The peaks detected in the following heating steps, instead, are scarcely influenced by the storing and conditioning settings, they are structurally bound to particles (with increasing strength as far as the temperature increases) and they are characteristics of the chemical composition of the PM sample. It is worth noting that also the amount of this structurally bound water depends, at least in the case of ammonium salts, on the thermodynamic conditions encountered by the particle during her life-time (including also sampling and storage/conditioning phases) and on the deliquescence/crystallization cycle (Seinfeld and Pandis, 1998; Martin, 2000; Casati et al., 2015). However, the experimental conditions of our samplings (low time resolution) were not suitable for a reliable interpretation of the influence of RH values and hysteresis cycles on our results.

The limit of detection (LOD) and limit of quantification (LOQ) of the method are 7 μg and 25 μg respectively; values above LOQ show a repeatability of about 10%. Further details about the optimization of the tr-KF method are reported in Canepari et al. (2013).

The analyses of inorganic ions and elements on PM samples collected by the MOUDI impactor were carried out as follows: Teflon filters were extracted in acetate buffer; the solution was filtered and analyzed for its ionic content by ion chromatography (ICS1000, Dionex Co., CA, U.S.A.) and for the soluble fraction of elements (As, Ba, Be, Cd, Co, Cu, Fe, Li, Mg, Mn, Pb, Ni, Rb, S, Sb, Se, Sn, Sr, Ti, Tl, V) by inductively coupled plasma spectroscopy – mass detection (ICP-MS); solid residual was subjected to microwave-assisted acid digestion and analyzed by ICP-MS for the same elements (residual fraction; Canepari et al. 2006, 2010; Protano et al., 2016). This procedure allows to carry out both IC and ICP analyses on the same filter; moreover, the chemical fractionation of elements allows a relevant improvement in their performance as source tracers (Canepari et al., 2009). The rationale behind the choice of the extraction procedure is reported in Canepari et al. 2010.
Atmospheric stability was evaluated by using an automated monitor of natural radioactivity due to Radon progeny (PBL Mixing Monitor, FAI Instruments, Fonte Nuova, Rome - IT).

Field studies

The study was carried out during four Special Observation Periods (SOPs), performed in different geographical and environmental conditions. During each SOP, size-segregated PM samples were analysed for water, inorganic ions and soluble and residual fractions of elements. The analysis of water was carried out also on daily PM_{10} samples. The samples were stored inside plastic containers (Petri slides, Millipore) and kept at 5°C until the beginning of the analyses; all the analyses were completed within two months from the end of the sampling periods.
The first SOP was carried out from February 16th to March 1st, 2012; samples were taken in Cassana, a hamlet at 6 km from Ferrara, a medium-size city located in the Po Valley (Northern Italy) at a distance of about 50 Km from the Adriatic Sea (Google Earth co-ordinates: Lat. 44.848774° Long. 11.561354°). The sampling site was in a residential area close to a major industrial area; road traffic emission was mainly due to the highway, running at about 500 m. Due to the geographical position of the Po Valley area, long periods of atmospheric stability are frequently experienced during the winter, resulting in very high concentration of PM, notably of secondary pollutants (Perrino et al., 2014; Caserini et al., 2017).
The second SOP was carried out from February 13th to 26th, 2014, in the vicinity of Gela, a medium-size coastal city located on the southern coast of Sicily. The site is not directly influenced by traffic emission but it is very close to a major refinery plant (Google Earth co-ordinates: Lat. 37.062661°

Long. 14.283335°). During this SOP the chemical analysis of size-segregated samples and the tr-KF analysis of water on daily PM_{10} samples were not carried out.

The third SOP was carried out from May 16th to 27th, 2014, at the Research Area RM1 of the National Research Council of Italy in Montelibretti, (Central Italy), a peri-urban site at about 25 km from the city of Rome, close to a parking lot and at about 500 m from an highway (Google Earth co-ordinates: Lat. 42.105771° Long. 12.640080°).

The fourth SOP was carried out from December 3rd to 17th, 2014, at the Sapienza University of Rome, sited in the center of the city, 26 km from the Thyrrenian Sea (Google Earth co-ordinates: Lat. 41.902433° Long. 12.517505°). The site is characterised by heavy traffic, particularly during working days.

Results and Discussion

SOP 1 – atmospheric stability

The first period of SOP 1, from February 16th to 19th, was characterised by the occurrence of a long period of strong atmospheric stability. The average values of the main meteorological parameters during these 4 days (temperature: 3.8 °C; relative humidity: 70%; wind speed 1.6 m s^{-1}) were not particularly different from those recorded during the rest of the SOP (temperature: 8.0 °C; relative humidity: 62%; wind speed 2.5 m s^{-1}) and from those typical of the Po Valley (the Mateo data recorded during the whole SOP, kindly provided by the Regional Environmental Protection Agency of Emilia Romagna Region – ARPAER - are reported as Appendix A1). However, more detailed information about the intensity and time variations of atmospheric stability can be easily obtained by studying the time pattern of natural radioactivity due to Radon progeny . This method is based on two main points: *i*. the emission rate of Radon gas from the ground can be assumed to be constant on the time and space scale of our observations; *ii.* radioactive decay is the only transformation of Radon. As a consequence, the concentration of Radon progeny in the atmosphere is only driven by the mixing of the lower atmosphere and this parameter can be considered as a good tracer of the mixing propertied of the boundary layer. High values of natural radioactivity indicate atmospheric stability, a condition that facilitates the accumulation of atmospheric pollutants; low radioactivity values indicates good atmospheric mixing due to advection or convection. Details about this technique and the benefits that can be obtained for the interpretation of pollution events can be found in Kataoka et al. (2001), Perrino et al. (2001, 2008, 2014), Sesana et al. (2003), Vecchi et al. (2007), Chambers et al. (2015). The time pattern of natural radioactivity (1-h average) during the first SOP and during the

previous five days is compared with the daily mass concentration of PM_{10} in Figure 1. The five days preceding the SOP have been included to explain the evolution of the environmental conditions that led to the very high PM values recorded during the period 16th-19th. Starting from February 11th, natural radioactivity showed a progressive increase of night-time maxima, together with very high values of daytime minima. In the situation depicted by these data, the convective mixing of the air masses that generally occurs during daylight hours was extremely weak and insufficient to disperse pollutants both produced during the day and accumulated during the previous stable night.

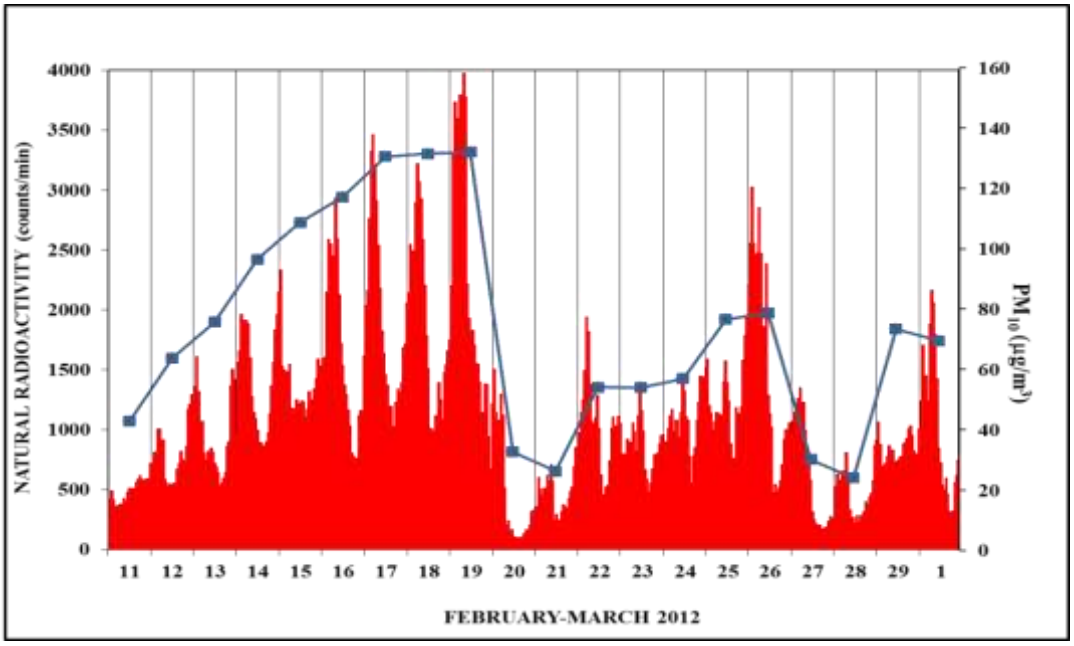

Figure 1: *Time pattern of natural radioactivity (1-h average, left y-axis) and daily PM_{10} concentration (right y-axis) during the first SOP and the previous five days.*

As a result, a gradual ageing of the air masses occurred, enhancing the formation of secondary pollutants (particularly, ammonium salts). PM_{10} concentration, in fact, shows a steady increase from the beginning of the event until February 19th. On the 20th, the wind speed rapidly increased up to about 10 m s^{-1} and the advection of fresh air masses caused an abrupt decrease of PM_{10} concentration from 132 to 33 µg/m^3. During the whole period, natural radioactivity very well matches the time pattern of PM_{10}, confirming that the atmospheric mixing was a main driving force in determining PM concentration (Perrino et al., 2014).

The water content of the daily PM_{10} samples collected during the first SOP is reported in the lower panel of Figure 2, together with PM_{10} mass concentration. The tr-KF analysis of water in the samples collected on February 19th and 24th are reported in the upper panels. The mass size distribution of

water during the same period is shown in the middle panel of Figure 3; the tr-KF analysis of water on stages 3.2-5.6 µm and 0.56-1.0 µm are reported in the upper panel. The graphs of the tr-KF analyses of all the daily PM_{10} filters and the size-segregated samples collected during this SOP are reported as Appendix A2. The data in Figure 2 show that a considerable amount of water was bound to particulate matter during the whole period and particularly during the first four, heavy stable days. Water concentration was up to 43 $\mu g/m^3$ (February 19th) and the water content of PM_{10} was from 10% to 33%. The scatter plot reported in the right corner of the graph, showing total water vs. PM_{10} mass, confirms that in atmospheric stability conditions the percentage of water in the dust sample increases with the increase of the collected mass, as already suggested in Perrino et al. (2013 and 2016). On February 19th (upper left graph), the shape of the tr-KF curve showed, in addition to surface water released during the first 300 s, only one peak, released between and 1450 and 1750 seconds, i.e. in the temperature range 180-250°. This shape is typical of a dust sample mainly constituted by ammonium nitrate. Almost identical shapes were obtained during the first three days of the SOP. It is worth noting that during winter stability conditions in the area of the Po Valley ammonium nitrate is by far the individual component at highest concentration in PM_{10} (Perrino et al., 2014). Furthermore, ammonium nitrate collected on filters has been shown to dissociate in the temperature range 180-250° (Perrino et al., 2012). On February 24th (upper right graph), taken as an example of the second part of the SOP, the shape of the tr-KF curve was more complex and included the same sharp peak, superimposed to a broader signal in the interval 1000–2000 s, plus additional smaller contributes. This shape is typical of samples including ammonium nitrate as well as other types of dust (Canepari et al., 2013). The mass size distribution of water during SOP 1 (Figure 3, middle panel) shows that most of the water was found in the range 0.32 – 1.8 µm (accumulation mode) with maximum in the range 0.56-1.0 µm, and that much smaller amounts were found in the coarse range, with relative maximum at 3.2-5.6 µm. Focusing on nitrate (lower panel, green bars), it is apparent that the size distributions of this species and of water in the fine range were almost identical; in the coarse range the contribution of nitrate was, instead, negligible. PM mass (lower panel, black line) was mostly distributed in the fine range, with maximum in the range 0.56-1.0 µm, but also showed a second mode in the coarse fraction, with a relative maximum at 3.2-5.6 µm. It is worth noting that the percentage of water with respect to PM was higher in the fine fraction (stage 0.56-1.0: 27% H_2O) than in the coarse fraction (stage 3.2-5.6: 18% H_2O). Appendix A3 reports the percentage of water (w/w) with respect to the PM mass amount during the four SOPs.

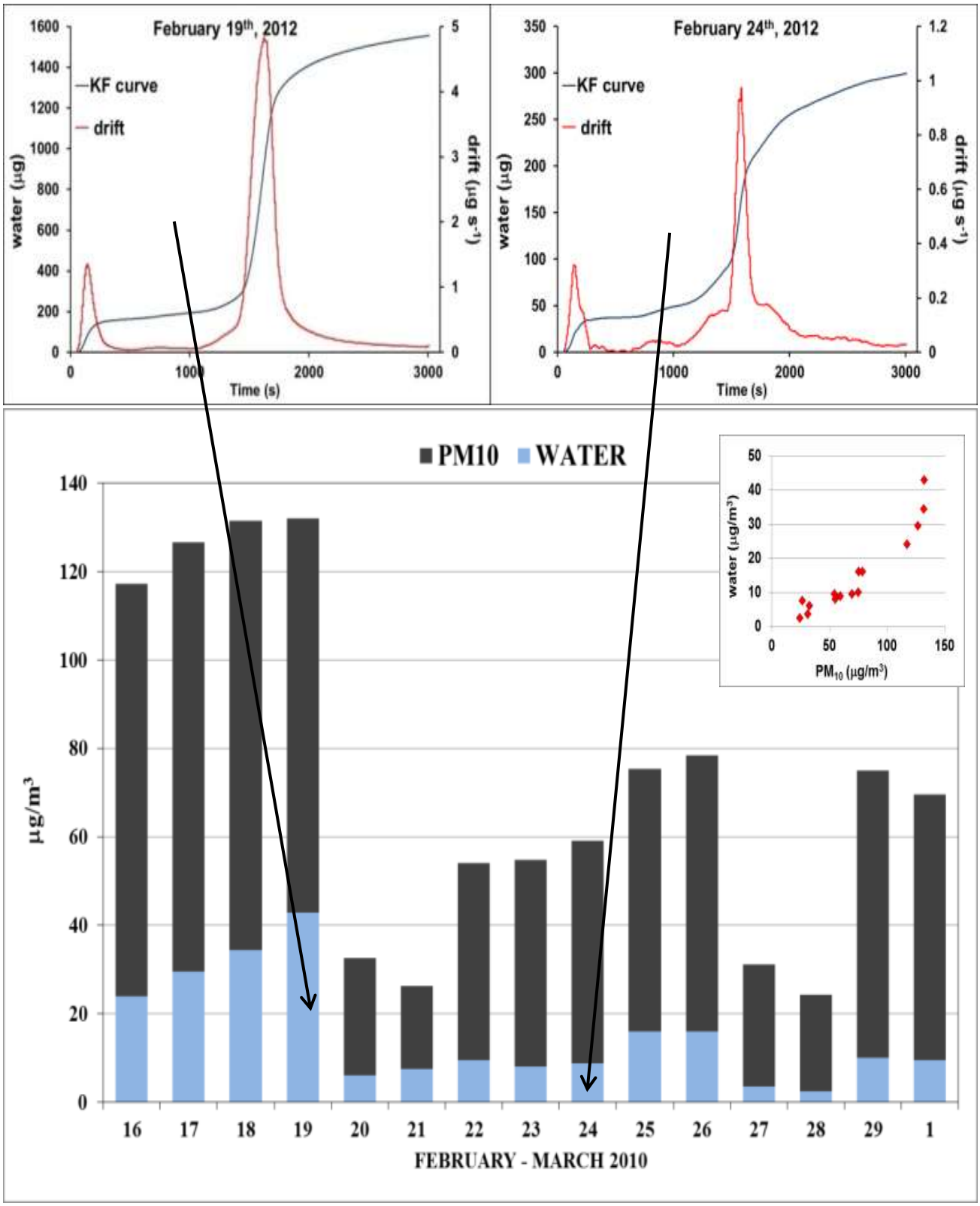

Figure 2: *Tr-KF profile of water on daily filters collected on February 19th and 24th (upper panels); time pattern and scatter plot of water concentration and mass concentration of daily PM_{10} samples during SOP 1 (lower panel).*

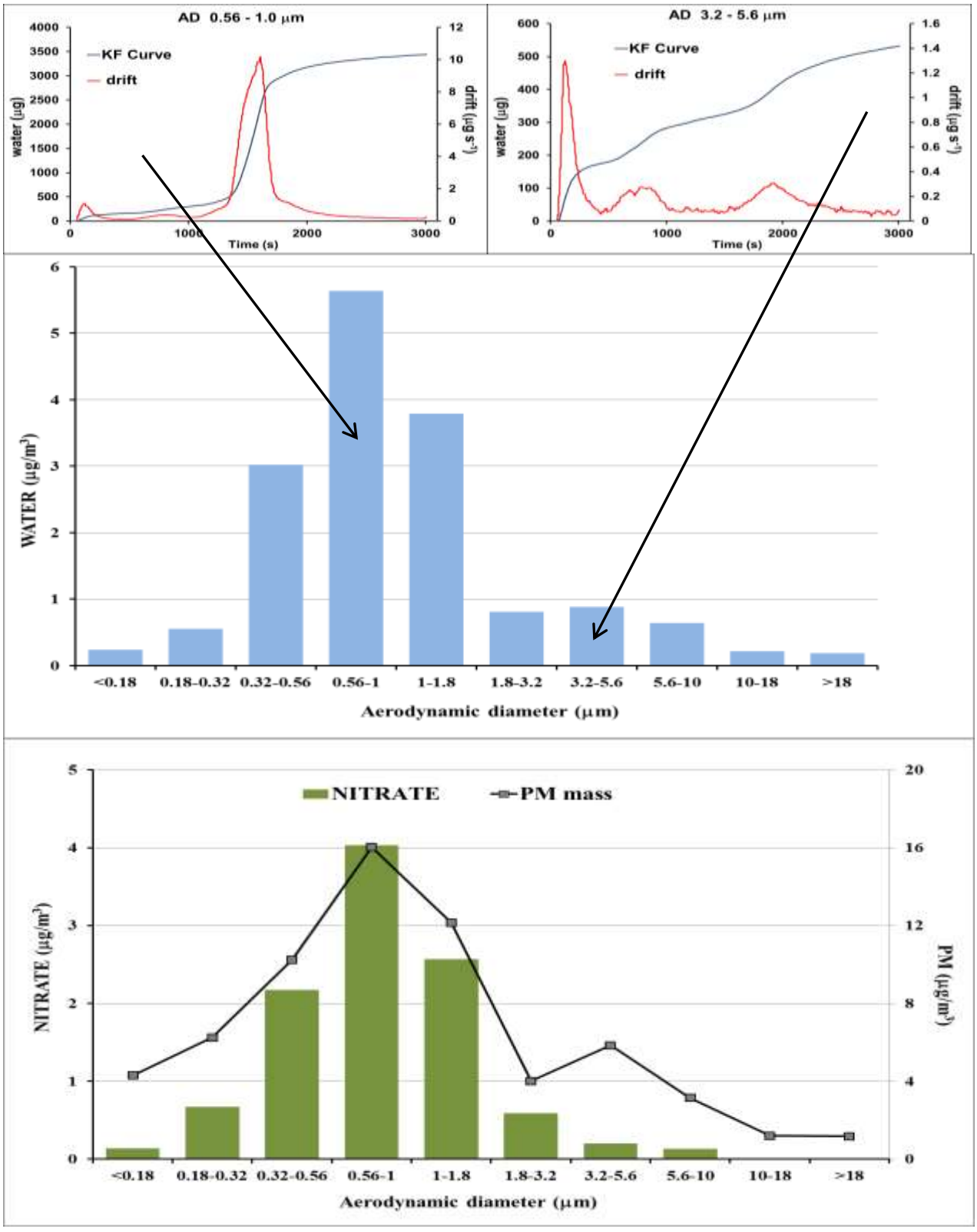

Figure 3: *Tr-KF profile of water in size-segregated PM samples having AD 0.56-1.0 µm and 3.2-5.6 µm (upper panels), mass size distribution of water (middle panel), of nitrate ion (lower panel, green bars) and of PM (lower panel, black line) during SOP 1.*

Very different shapes at the tr-KF analysis were obtained for the fine and the coarse fractions of PM. The upper left graph in Figure 3, which refers to PM in the size range 0.56-1.0, shows the same water peak (1450 - 1750 s) that was observed when analysing the daily PM_{10} samples (Figure 2) and that is characteristic of water bound to ammonium nitrate. The shape of the upper right graph (tr-KF analysis of PM in the size range 3.2-5.6), instead, includes a first peak between 500 and 1000 s, which has been shown to be characteristic of soil dust (Canepari et al., 2013; Perrino et al., 2016), and a second contribute that is released at about 1900 s. This more retained contribute is linked to PM components, still unidentified, included in the coarse fraction of the PM mass. In general, water in each size fraction shows a tr-KF shape that is coherent with the prevailing chemical composition of the same fraction.
It is worth noting that the tr-KF shapes of the daily PM_{10} samples shown in Figure 2 and in Appendix A2 included water contributes characteristic of both the fine and the coarse fractions. This is evident in the sample collected on February 24th, when ammonium nitrate did not prevail over the other PM components. Here, the contribution of water bound to ammonium nitrate is clearly visible but other, overlapped contributions are as well recognizable.

SOP 2 and SOP 3 – desert dust

During both SOP 2 (Sicily, winter 2014) and SOP 3 (Central Italy, spring 2014) Saharan dust intrusions were recorded. Figure 4 shows the surface concentration of dust as modelled by the Dust Regional Atmospheric Model (DREAM, available at http://www.bsc.es/projects/earthscience/BSC eDREAM/) during the two days when the maximum intensity of each event was forecasted (February 20th and May 23rd, respectively). It has been previously shown that during Saharan dust events the water content of PM_{10} may be considerably high and that this contribution is roughly proportional to the desert dust content of the sample (Perrino et al., 2016).
During both SOPs, a good atmospheric mixing occurred in the sampling areas and the mass concentration of PM was generally low. During SOP 2 the average concentration of PM_{10} was 25.5 $\mu g/m^3$, the Saharan dust intrusion lasted for about three days (February 19th – 21st) and the average PM_{10} concentrations during the dust events was 34.6 $\mu g/m^3$. During SOP 3 two desert dust intrusions were recorded, the first one from May 21st to 23rd and , the second one, of smaller intensity, on May 25th. The average concentration of PM_{10} was 27.1 $\mu g/m^3$ during the SOP and 42.4 $\mu g/m^3$ during the three days of the main dust event. The chemical composition of daily PM_{10} samples collected during SOP 3, including anions, cations, elements, elemental carbon, organic carbon and water, has been discussed in Perrino et al. (2016).

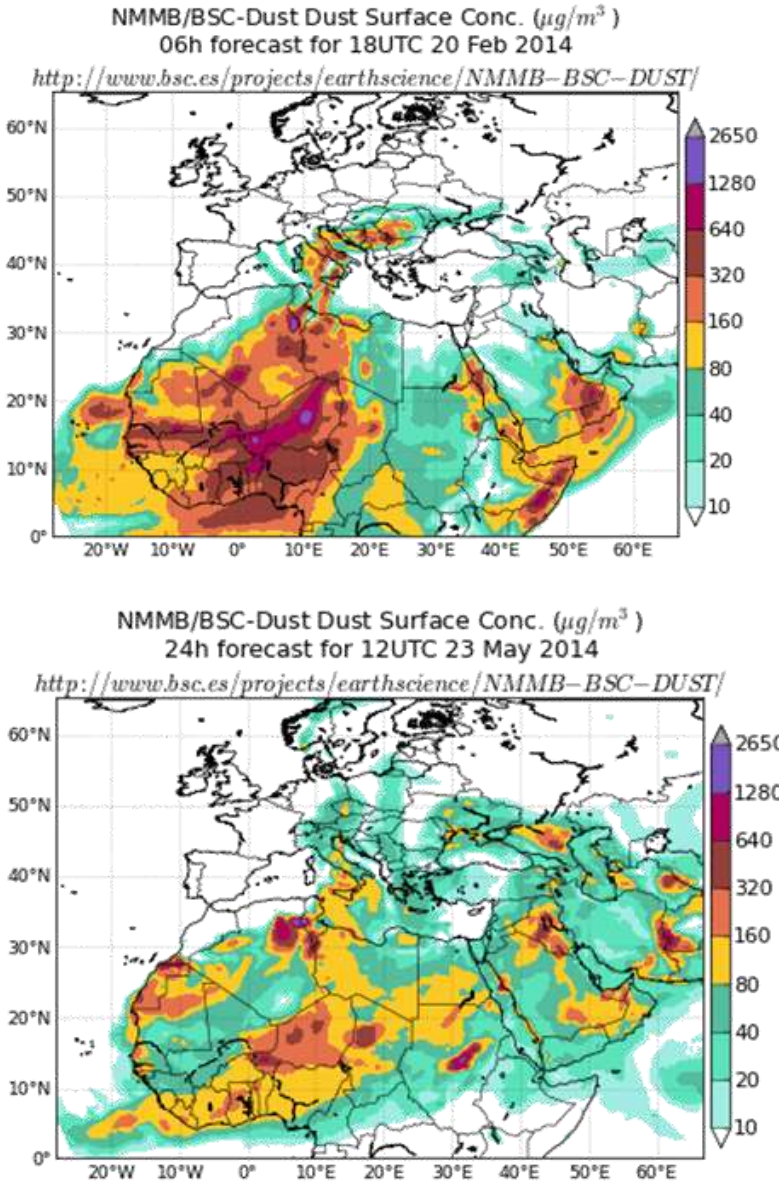

Figure 4: *Dust surface concentration as modelled by the Dust Regional Atmospheric Model (DREAM) on February 20th (SOP 2, upper panel) and May 23rd (SOP 3, lower panel).*

The mass size distribution of water during SOP2 and SOP3 is reported in Figure 5 (middle and lower panel, respectively). Although the data refer to different time periods and geographical areas, the size distributions of water in the two coarse fractions were exactly alike. The upper graphs of Figure 5 (tr-KF analysis of the stage 3.2-5.6 μm during SOP 2 and SOP 3, respectively) show that also the shapes of the tr-KF curves were very similar.

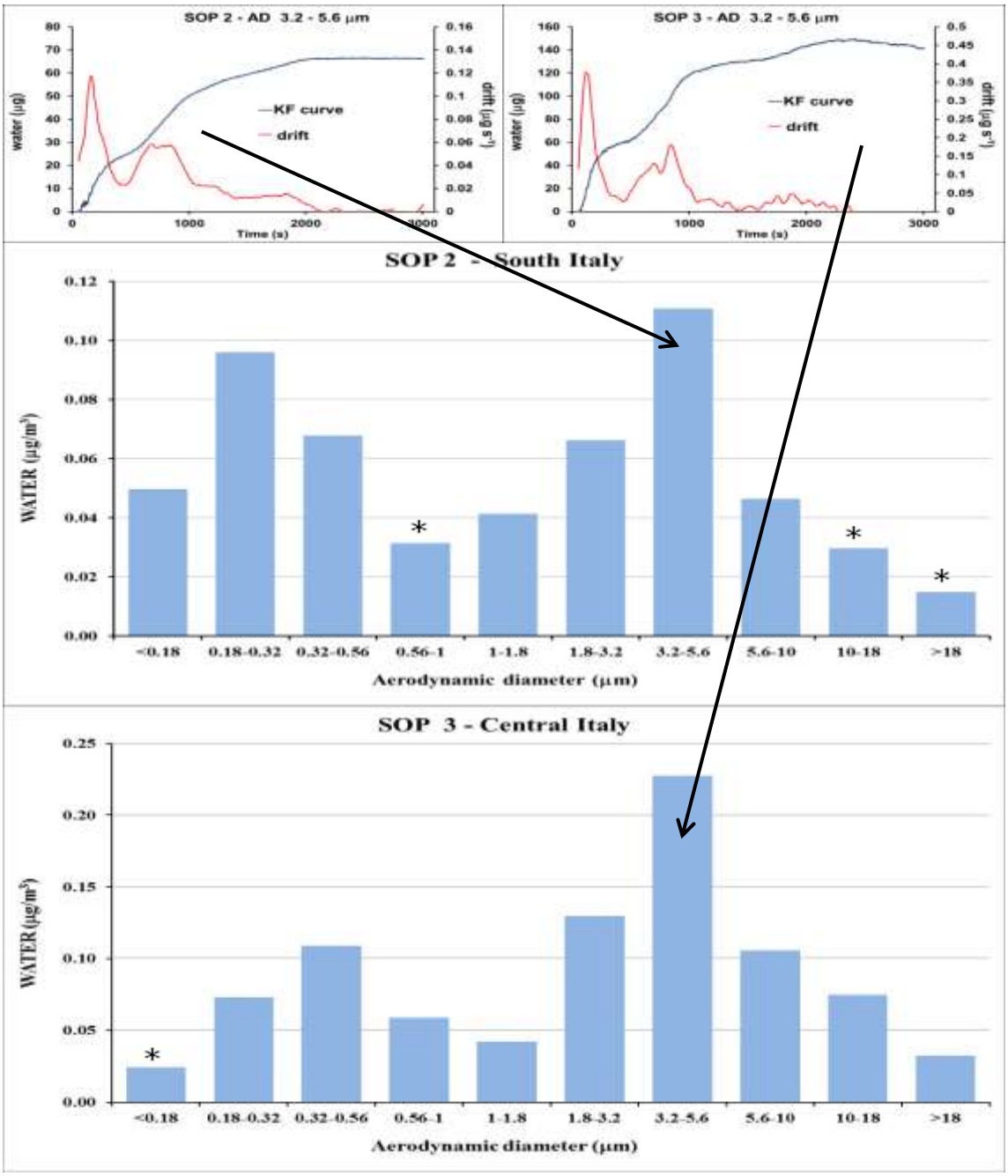

Figure 5: *Tr-KF profile of water in size-segregated PM samples having AD 3.2-5.6 µm during SOP 2 and SOP 3 (upper panels), mass size distribution of water during SOP 2 (middle panel) and SOP 3 (lower panel);* indicates values between LOD and LOQ.*

This shape (increase of the signal between 500 and 1250 s, corresponding to a temperature range of 100-180°C) has been previously shown to be characteristic of PM-bound water in the presence of desert dust events (Canepari et al., 2013; Perrino et al., 2016). The tr-KF analyses of water during SOP 2 are reported in Appendix A4. For comparison with water, the size distribution of the PM mass

(black line) and of manganese and magnesium (residual fractions, colour bars), which can be considered as reliable tracers of desert dust (Perrino et al., 2009; Diapouli et al., 2017), are reported in Figure 6 (SOP 3). As it can be seen, in the coarse fraction the size distribution of water and of manganese/magnesium are twin, and a good correspondence is also observed with PM mass. It can be concluded that also in the case of Saharan dust events, water shows the same mass distribution and the same tr-KF shape that is exhibited by the main components of PM (crustal species).

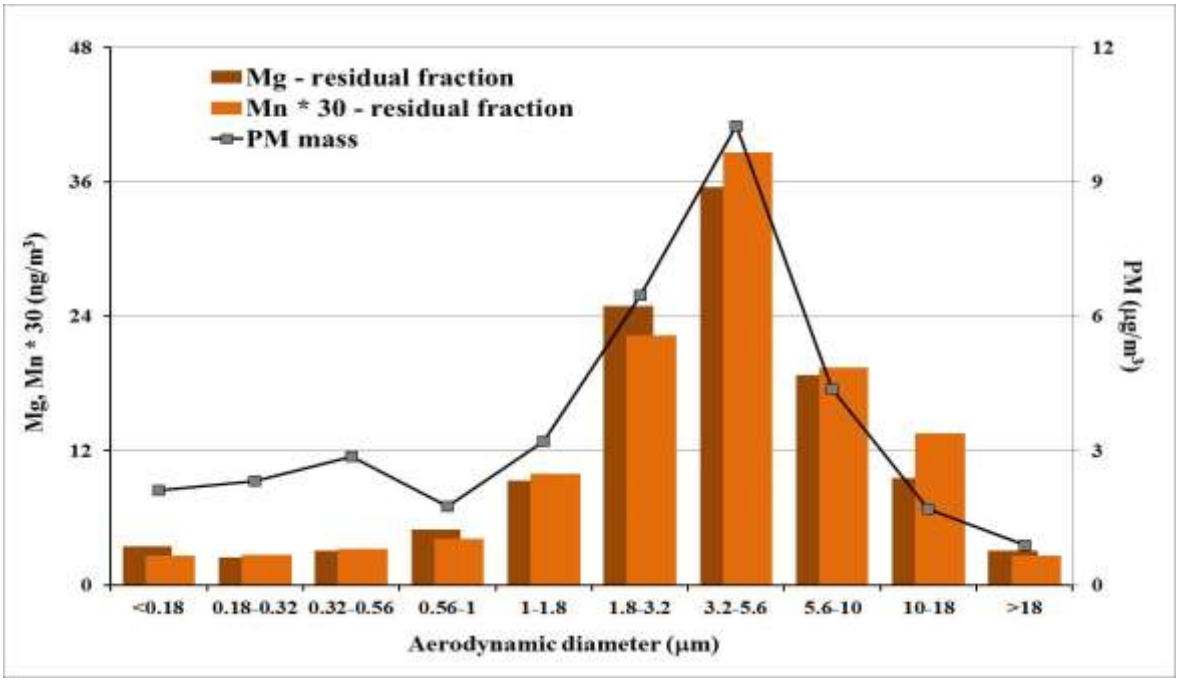

Figure 6: *Mass size distribution of the residual fraction of magnesium (brown bars) and manganese (orange bar) and of PM mass (black line) during SOP 3.*

One interesting point in the tr-KF shape of the fine fraction of PM in both SOP 2 and SOP 3 is that the peak in the temperature range corresponding to water bound to ammonium nitrate was negligible. This seems to indicate that during these periods nitrate was almost completely included in the coarse fraction of PM. The size distribution of nitrate confirms this hypothesis: the fine fraction was populated by ammonium and sulphate (maximum in the stage 0.32-0.56 µm) while nitrate was almost totally confined in the coarse fraction. The size distribution of nitrate, sulphate and ammonium during SOP 3 is reported in Appendix A5.

SOP 4 – urban site

During SOP 4, a typical winter period in Central Italy, days characterized by moderate atmospheric stability alternated with advection periods; PM_{10} concentration varied between 15 and 55 µg/m^3

(average value: 29.6 µg/m^3). During this period, no desert dust intrusions were recorded and the concentration of ammonium nitrate was relatively low. In these conditions, water bound to desert dust and to ammonium nitrate was also expected to be little. However, the daily concentration of water in PM_{10} was between 1.2 and 4.5 (average of the period 2.4 µg/m^3). The chemical composition, including water, of daily PM_{10} samples collected during SOP 4 has been discussed in Perrino et al. (2016). The mass size distribution of water during SOP4 is shown in Figure 7 (middle panel); individual tr-KF analyses are reported in Appendix A6. Also in this case, water showed a bi-modal distribution, with maxima of comparable size in the coarse mode (AD 3.2-5.6 µm) and in the fine mode (AD 0.32-0.56 µm). However, the tr-KF shape showed some differences with respect to those recorded during SOPs 1-3. The tr-KF analysis of the coarse fraction (Figure 7, upper right panel) shows two main peaks in the range 500-1000 e 1800-2300; the same shape had also been obtained when analysing the small coarse fraction collected during SOP 1, when the samplings were carried out not far from a highway (Figure 3). This shape seems to be related to re-suspension of non-exhaust traffic emission (brake, tyre, clutch and road surface wear). The fine fraction, instead (upper left panel), showed a signal increase in the range 1000-2000 s, which could be attributed to ammonium sulphate and/or to other unidentified PM component, likely generated by combustion or secondary formation processes. A similar shape is recognizable in the daily sample of February 24th (SOP 1) below the peak of ammonium nitrate-bound water.

Figure 7 (lower panel) also reports the size distribution of PM mass and of the residual fraction of iron, a reliable tracer of non-exhaust traffic emission (Farao et al., 2014). PM mass showed a bi-modal distribution with maxima in the same stages as water; also in this case the two maxima are of comparable height. The residual fraction of iron, instead, was comprised in the coarse fraction only; in this size range it showed the same pattern as water and PM mass.

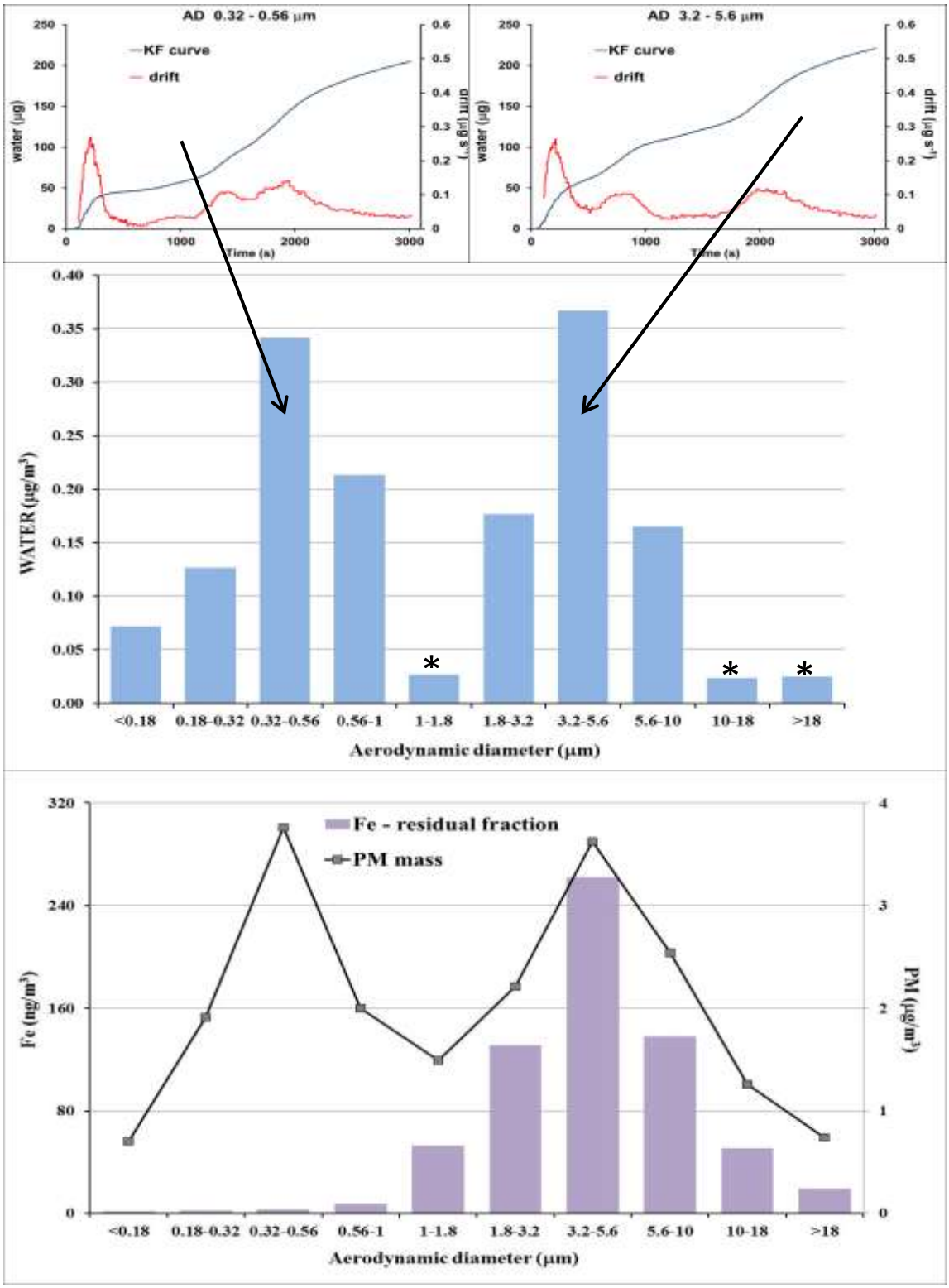

Figure 7: *Tr-KF profile of water in size-segregated PM samples having AD 0.32-0.56 µm and 3.2-5.6 µm (upper panels), mass size distribution of water (middle panel), of the residual fraction of iron (lower panel, violet bars) and of PM (lower panel, black line) during SOP 4;* indicates values between LOD and LOQ.*

Conclusions

The mass size distribution of water in atmospheric PM samples has been measured by means of the tr-KF method. PM samples were collected during Special Observation Periods characterized by different meteorological conditions and chemical PM composition.

During prolonged stability conditions, the chemical composition of PM was dominated by ammonium nitrate, water distribution was mainly in the fine size range and its size-distribution was very similar to that shown by nitrate. The shape of the tr-KF curve was also coherent with that of water bound to ammonium nitrate. Water concentration up to 43 $\mu g/m^3$ was measured in daily PM_{10} samples; in size-segregated samples water constituted about 30% of the fine fraction of PM.

During desert dust events, crustal species were the main PM components, water mass was distributed mainly in the coarse size range and its size-distribution was very similar to that shown by desert dust tracers. The shape of the tr-KF curve was characteristic of desert dust.

Urban areas showed a more complex picture: both PM mass and water exhibit a typical bi-modal size distribution. In the coarse mode the size distribution was similar to that of non-exhaust traffic-emission tracers and the tr-KF shape was also typical of coarse PM at traffic sites. In the fine mode, several sources probably contributed to the mass concentration of both PM and water. Accordingly, the shape of the tr-KF curve was more complex and revealed different overlapped contributes.

References

Abbas, Z., Steenari, B. M., & Lindqvist, O. (2001). A study of Cr (VI) in ashes from fluidized bed combustion of municipal solid waste: leaching, secondary reactions and the applicability of some speciation methods. *Waste Management*, *21*(8), 725-739.

Almeida, S. M., Pio, C. A., Freitas, M. C., Reis, M. A., & Trancoso, M. A. (2006). Source apportionment of atmospheric urban aerosol based on weekdays/weekend variability: evaluation of road re-suspended dust contribution. *Atmospheric Environment*, *40*(11), 2058-2067.

Ansari, A. S., & Pandis, S. N. (2000). Water absorption by secondary organic aerosol and its effect on inorganic aerosol behavior. *Environmental science & technology*, *34*(1), 71-77.

Barone, T. L., Lall, A. A., Zhu, Y., Yu, R. C., & Friedlander, S. K. (2006). Inertial deposition of nanoparticle chain aggregates: theory and comparison with impactor data for ultrafine atmospheric aerosols. *Journal of Nanoparticle Research*, *8*(5), 669-680.

Bae, M. S., Schauer, J. J., Turner, J. R., & Hopke, P. K. (2009). Seasonal variations of elemental carbon in urban aerosols as measured by two common thermal-optical carbon methods. *Science of the total Environment*, *407*(18), 5176-5183.

Baek, B. H., Aneja, V. P., & Tong, Q. (2004). Chemical coupling between ammonia, acid gases, and fine particles. *Environmental Pollution*, *129*(1), 89-98.

Balasubramanian, R., Qian, W. B., Decesari, S., Facchini, M. C., & Fuzzi, S. (2003). Comprehensive characterization of PM2. 5 aerosols in Singapore. *Journal of Geophysical Research: Atmospheres*, *108*(D16).

Birch, M. E., & Cary, R. A. (1996). Elemental carbon-based method for monitoring occupational exposures to particulate diesel exhaust. *Aerosol Science and Technology*, *25*(3), 221-241.

Canepari, S., Cardarelli, E., Giuliano, A., & Pietrodangelo, A. (2006). Determination of metals, metalloids and non-volatile ions in airborne particulate matter by a new two-step sequential leaching procedure: Part A: Experimental design and optimisation. *Talanta*, 69(3), 581-587.

Canepari, S., Cardarelli, E., Giuliano, A., & Pietrodangelo, A. (2006). Determination of metals, metalloids and non-volatile ions in airborne particulate matter by a new two-step sequential leaching procedure: Part A: Experimental design and optimisation. *Talanta*, *69*(3), 581-587.

Canepari, S., Pietrodangelo, A., Perrino, C., Astolfi, M. L., & Marzo, M. L. (2009). Enhancement of source traceability of atmospheric PM by elemental chemical fractionation. *Atmospheric Environment*, *43*(31), 4754-4765.

Canepari, S., Astolfi, M. L., Moretti, S., & Curini, R. (2010). Comparison of extracting solutions for elemental fractionation in airborne particulate matter. *Talanta*, *82*(2), 834-844.

Canepari, S., Farao, C., Marconi, E., Giovannelli, C., & Perrino, C. (2013). Qualitative and quantitative determination of water in airborne particulate matter. *Atmospheric Chemistry and Physics*, 13(3), 1193-1202.

Canepari, S., Astolfi, M. L., Farao, C., Maretto, M., Frasca, D., Marcoccia, M., & Perrino, C. (2014). Seasonal variations in the chemical composition of particulate matter: a case study in the Po Valley. Part II: concentration and solubility of micro-and trace-elements. *Environmental Science and Pollution Research*, *21*(6), 4010-4022.

Castro, L. M., Pio, C. A., Harrison, R. M., & Smith, D. J. T. (1999). Carbonaceous aerosol in urban and rural European atmospheres: estimation of secondary organic carbon concentrations. *Atmospheric Environment*, *33*(17), 2771-2781.

Casati, M., Rovelli, G., D'Angelo, L., Perrone, M., Sangiorgi, G., Bolzacchini, E., & Ferrero, L. (2015). Experimental measurements of particulate matter deliquescence and crystallization relative humidity: Application in heritage climatology. *Aerosol and Air Quality Research*, 15(2), 399-409.

Caserini, S., Giani, P., Cacciamani, C., Ozgen, S., & Lonati, G. (2017). Influence of climate change on the frequency of daytime temperature inversions and stagnation events in the Po Valley: historical trend and future projections. *Atmospheric Research*, *184*, 15-23.

CEN (1998). Air Quality. Determination of the PM_{10} fraction of suspended particulate matter – Reference method and field test procedure to demonstrate reference equivalence of measurement methods. Brussel (EN12341).

CEN (2005). Ambient air quality. Standard gravimetric measurement method for the determination of the PM2,5 mass fraction of suspended particulate matter (EN 14907).

Chambers, S. D., Williams, A. G., Crawford, J., & Griffiths, A. D. (2015). On the use of radon for quantifying the effects of atmospheric stability on urban emissions. *Atmospheric Chemistry and Physics*, *15*(3), 1175-1190.

Chan, Y. C., Simpson, R. W., Mctainsh, G. H., Vowles, P. D., Cohen, D. D., & Bailey, G. M. (1997). Characterisation of chemical species in PM2.5 and PM10 aerosols in Brisbane, Australia. *Atmospheric Environment*, *31*(22), 3773-3785.

Chow, J. C., Watson, J. G., Lowenthal, D. H., & Magliano, K. L. (2005). Loss of PM2. 5 nitrate from filter samples in central California. *Journal of the Air & Waste Management Association*, *55*(8), 1158-1168.

Cirillo, M.C. *Perché è difficile la riduzione degli inquinanti secondari* In "Qualità dell'ambiente urbano, XII Rapporto, edizione 2016 "Focus su Inquinamento atmosferico nelle aree urbane ed effetti sulla salute", ISPRA Stato dell'ambiente 68/2016, ISBN 978-88-448-0794-8

Decesari, S., Facchini, M. C., Matta, E., Lettini, F., Mircea, M., Fuzzi, S., Tagliavini, E.,& Putaud, J. P. (2001). Chemical features and seasonal variation of fine aerosol water-soluble organic compounds in the Po Valley, Italy. *Atmospheric Environment*, *35*(21), 3691-3699.

Diapouli, E., Manousakas, M. I., Vratolis, S., Vasilatou, V., Pateraki, S., Bairachtari, K. A., Querol, X., Amato, F., Alastuey, A., Karanasiou, A.A., Nava, S., Calzolai, G. Gianelle, V. L., Colombi, C., Alves, C., Custódio, D., Pio, C., Spyrou, C., Kallos, G.B., Eleftheriadis, K., & Lucarelli, F. (2017). AIRUSE-LIFE+: estimation of natural source contributions to urban ambient air PM_{10} and $PM_{2.5}$ concentrations in southern Europe–implications to compliance with limit values. *Atmospheric Chemistry and Physics*, *17*(5), 3673-3685.

Dick, W. D., Saxena, P., & McMurry, P. H. (2000). Estimation of water uptake by organic compounds in submicron aerosols measured during the Southeastern Aerosol and Visibility Study. *Journal of Geophysical Research: Atmospheres*, *105*(D1), 1471-1479.

EC (1997). Working Group on Particles. Position Paper on Ambient Air Pollution by Particulate Matter. http://europa.eu.int/comm.

EPA (1997) Reference Method for the Determination of Particulate Matter as PM_{10} in the Atmosphere. Federal Registrer, 62, No 138, Appendix M to part 50.

EPA (1999). Particulate Matter (PM2.5) Speciation Guidance (available at: http://www.epa.gov/ttn/amtic/files/ambient/pm25/).

Farao, C., Canepari, S., Perrino, C., & Harrison, R. M. (2014). Sources of PM in an industrial area: comparison between receptor model results and semiempirical calculations of source contributions. *Aerosol and Air Quality Research*, *14*(6), 1558-1572.

Ferm, M. (1979). Method for determination of atmospheric ammonia. *Atmospheric Environment (1967)*, *13*(10), 1385-1393.

Gelencsér, A., Hoffer, A., Molnár, A., Krivácsy, Z., Kiss, G., & Mészáros, E. (2000). Thermal behaviour of carbonaceous aerosol from a continental background site. *Atmospheric Environment*, *34*(5), 823-831.

Gysel, M., Crosier, J., Topping, D. O., Whitehead, J. D., Bower, K. N., Cubison, M. J., Williams P I, Flynn M J, McFiggans G B, & Coe, H. (2007). Closure study between chemical composition and hygroscopic growth of aerosol particles during TORCH2. *Atmospheric Chemistry and Physics*, *7*(24), 6131-6144.

Harrison, R. M., Jones, A. M., & Lawrence, R. G. (2003). A pragmatic mass closure model for airborne particulate matter at urban background and roadside sites. *Atmospheric Environment*, *37*(35), 4927-4933.

Harrison, R. M., & van Grieken, R. (Eds.). (1998). *Atmospheric particles* (Vol. 5). Chichester: Wiley.

Hering, S. V., Flagan, R. C., & Friedlander, S. K. (1978). Design and evaluation of new low-pressure impactor. I. *Environmental Science & Technology*, *12*(6), 667-673.

Heintzenberg, J., & Winkler, P. (1991). Elemental carbon in the atmosphere: challenges for the trace analyst. *Fresenius' journal of analytical chemistry*, *340*(9), 540-543.

Hodas, N., Sullivan, A. P., Skog, K., Keutsch, F. N., Collett Jr, J. L., Decesari, S., Facchini, M.C., Carlton, A.G., Laaksonen, A.,& Turpin, B. J. (2014). Aerosol liquid water driven by anthropogenic nitrate: Implications for lifetimes of water-soluble organic gases and potential for secondary organic aerosol formation. *Environmental science & technology*, *48*(19), 11127-11136.

Hu, D., Chen, J., Ye, X., Li, L., & Yang, X. (2011). Hygroscopicity and evaporation of ammonium chloride and ammonium nitrate: Relative humidity and size effects on the growth factor. *Atmospheric Environment*, *45*(14), 2349-2355.

John W (2001) Size Distribution Characteristics of Aerosols in: Baron, P. A., & Willeke, K. Aerosol Measurement – Wiley InterScience New York.

Kataoka, T., Yunoki, E., Shimizu, M., Mori, T., Tsukamoto, O., Ohashi, Y., Sahashi, K., Maitani, T., Miyashita, K., Iwata, T., Fujikawa, Y., Kudo, A., Shaw, R. H. & Kudo, A. (2001). A study of the atmospheric boundary layer using radon and air pollutants as tracers. *Boundary-layer meteorology*, *101*(2), 131-156.

Kleeman, M. J., & Cass, G. R. (1998). Source contributions to the size and composition distribution of urban particulate air pollution. *Atmospheric Environment*, *32*(16), 2803-2816.

Khlystov, A., Lin, M., Bolch, M. A., & Ma, Y. (2009). Investigation of the positive artifact formation during sampling semi-volatile aerosol using wet denuders. *Atmospheric Environment*, 43(2), 364-370.

Kitamori, Y., Mochida, M., & Kawamura, K. (2009). Assessment of the aerosol water content in urban atmospheric particles by the hygroscopic growth measurements in Sapporo, Japan. *Atmospheric Environment*, *43*(21), 3416-3423.

Kreidenweis, S. M., Remer, L. A., Bruintjes, R., & Dubovik, O. (2001). Smoke aerosol from biomass burning in Mexico: Hygroscopic smoke optical model. *Journal of Geophysical Research: Atmospheres*, *106*(D5), 4831-4844.

Lutgens, F. K. & Tarbuck, E. J., (2004). Earth Science 9th Edition (Chapter 18, Climate).

Manahan (2000), Chimica dell'ambiente, Editor: L Zoccolillo, Chapter 10, PICCIN.

Marcazzan, G. M., Vaccaro, S., Valli, G., & Vecchi, R. (2001). Characterisation of PM10 and PM2.5 particulate matter in the ambient air of Milan (Italy). *Atmospheric Environment*, *35*(27), 4639-4650.

Martin, S. T. (2000). Phase transitions of aqueous atmospheric particles. *Chemical Reviews*, *100*(9), 3403-3454.

Moore J W, Ramamoorthy S (1994), *Heavy Metals in Natural Waters*, Springer-Verlag, New York.

Murillo, J. H., Ramos, A. C., García, F. Á., Jiménez, S. B., Cárdenas, B., & Mizohata, A. (2012). Chemical composition of PM 2.5 particles in Salamanca, Guanajuato Mexico: source apportionment with receptor models. *Atmospheric research*, *107*, 31-41.

Ohta, S., Hori, M., Yamagata, S., & Murao, N. (1998). Chemical characterization of atmospheric fine particles in Sapporo with determination of water content. *Atmospheric Environment*, *32*(6), 1021-1025.

Pacyna J M (1999), *Source Inventories for Atmospheric Trace Metals* in: Harrison R M and Van Grieken R E, *Atmospheric Particles*, Vol 5.

Perrino, C., Pietrodangelo, A., & Febo, A. (2001). An atmospheric stability index based on radon progeny measurements for the evaluation of primary urban pollution. *Atmospheric Environment*, *35*(31), 5235-5244.

Perrino, C., Catrambone, M., & Pietrodangelo, A. (2008). Influence of atmospheric stability on the mass concentration and chemical composition of atmospheric particles: a case study in Rome, Italy. *Environment international*, *34*(5), 621-628.

Perrino, C., Canepari, S., Catrambone, M., Dalla Torre, S., Rantica, E., & Sargolini, T. (2009). Influence of natural events on the concentration and composition of atmospheric particulate matter. *Atmospheric Environment*, *43*(31), 4766-4779.

Perrino, C., Marconi, E., Tofful, L., Farao, C., Materazzi, S., & Canepari, S. (2012). Thermal stability of inorganic and organic compounds in atmospheric particulate matter. *Atmospheric environment*, *54*, 36-43.

Perrino, C., Canepari, S., & Catrambone, M. (2013). Comparing the performance of Teflon and quartz membrane filters collecting atmospheric PM: influence of atmospheric water. *Aerosol Air Qual. Res*, *13*, 137-147.

Perrino, C., Catrambone, M., Dalla Torre, S., Rantica, E., Sargolini, T., & Canepari, S. (2014). Seasonal variations in the chemical composition of particulate matter: a case study in the Po Valley. Part I: macro-components and mass closure. *Environmental Science and Pollution Research*, *21*(6), 3999-4009.

Perrino, C., Catrambone, M., Farao, C., & Canepari, S. (2016). Assessing the contribution of water to the mass closure of PM 10. *Atmospheric Environment*, *140*, 555-564.

Phongphiphat, A., Ryu, C., Finney, K. N., Sharifi, V. N., & Swithenbank, J. (2011). Ash deposit characterisation in a large-scale municipal waste-to-energy incineration plant. *Journal of hazardous materials*, *186*(1), 218-226.

Pilinis, C., Pandis, S. N., & Seinfeld, J. H. (1995). Sensitivity of direct climate forcing by atmospheric aerosols to aerosol size and composition. *Journal of Geophysical Research: Atmospheres*, *100*(D9), 18739-18754.

Protano, C., Astolfi, M. L., Canepari, S., & Vitali, M. (2016). Urinary levels of trace elements among primary school-aged children from Italy: The contribution of smoking habits of family members. *Science of the Total Environment*, *557*, 378-385.

Puxbaum H (1991), *Metal Compounds In The Atmosphere* in: Merian E (Edr), *Metals And Their Compounds In The Environment*, pp 257-286.

Querol X, Salvador P, Sanchez de la Campa A (2003), D.G. Environmental Quality and Evaluation, pp 424. (In Spanish with English summary).

Rees, S. L., Robinson, A. L., Khlystov, A., Stanier, C. O., & Pandis, S. N. (2004). Mass balance closure and the Federal Reference Method for PM 2.5 in Pittsburgh, Pennsylvania. *Atmospheric Environment*, *38*(20), 3305-3318.

Rogula-Kozłowska, W., Widziewicz, K., & Majewski, G. (2017). A simple method for determination of total water in PM 1 on quartz fiber filters. *Microchemical Journal*, *132*, 327-332.

Sasaki, K., & Sakamoto, K. (2006). Diurnal Characteristics of Suspended Particulate Matter and PM 2.5 in the Urban and Suburban Atmosphere of the Kanto Plain, Japan. *Water, Air, & Soil Pollution*, *171*(1), 29-47.

Seinfeld, J. H., & Pandis, S. N. (2006). *Atmospheric chemistry and physics: from air pollution to climate change*. John Wiley & Sons.

Sesana, L., Caprioli, E., & Marcazzan, G. M. (2003). Long period study of outdoor radon concentration in Milan and correlation between its temporal variations and dispersion properties of atmosphere. *Journal of Environmental Radioactivity*, *65*(2), 147-160.

Sloane C S and Wolfe G T (1997), *Aerosol Science and Technology*, 27:50–67.

Speer, R. E., Barnes, H. M., & Brown, R. (1997). An instrument for measuring the liquid water content of aerosols. *Aerosol Science and Technology*, *27*(1), 50-61.

Speer, R. E., Edney, E. O., & Kleindienst, T. E. (2003). Impact of organic compounds on the concentrations of liquid water in ambient PM 2.5. *Journal of aerosol science*, *34*(1), 63-77.

Squizzato, S., Masiol, M., Brunelli, A., Pistollato, S., Tarabotti, E., Rampazzo, G., & Pavoni, B. (2012). Factors determining the formation of secondary inorganic aerosol: a case study in the Po Valley (Italy). *Atmos. Chem. Phys. Discuss*, *12*, 16377-16406.

Stanier, C. O., Khlystov, A. Y., Chan, W. R., Mandiro, M., & Pandis, S. N. (2004). A Method for the In Situ Measurement of Fine Aerosol Water Content of Ambient Aerosols: The Dry-Ambient Aerosol Size Spectrometer (DAASS) Special Issue of Aerosol Science and Technology on Findings from the Fine Particulate Matter Supersites Program. *Aerosol Science and Technology*, *38*(S1), 215-228.

Swietlicki, E., Zhou, J., Berg, O. H., Martinsson, B. G., Frank, G., Cederfelt, S. I., Bower, K. N. Birmili, W., Wiedensohler, A., & Yuskiewicz, B. (1999). A closure study of sub-micrometer aerosol particle hygroscopic behaviour. *Atmospheric Research*, *50*(3), 205-240.

Tsyro, S. G. (2005). To what extent can aerosol water explain the discrepancy between model calculated and gravimetric PM 10 and PM 2.5?. *Atmospheric Chemistry and Physics*, *5*(2), 515-532.

Turpin, B. J., & Lim, H. J. (2001). Species contributions to PM2.5 mass concentrations: Revisiting common assumptions for estimating organic mass. *Aerosol Science & Technology*, *35*(1), 602-610.

Vecchi, R., Marcazzan, G., Valli, G., Ceriani, M., & Antoniazzi, C. (2004). The role of atmospheric dispersion in the seasonal variation of PM1 and PM2.5 concentration and composition in the urban area of Milan (Italy). *Atmospheric Environment*, *38*(27), 4437-4446.

Vecchi, R., Marcazzan, G., & Valli, G. (2007). A study on nighttime–daytime PM10 concentration and elemental composition in relation to atmospheric dispersion in the urban area of Milan (Italy). *Atmospheric Environment*, *41*(10), 2136-2144.

Vecchi, R., Valli, G., Fermo, P., D'Alessandro, A., Piazzalunga, A., & Bernardoni, V. (2009). Organic and inorganic sampling artefacts assessment. *Atmospheric Environment*, *43*(10), 1713-1720.

Viidanoja, J., Sillanpää, M., Laakia, J., Kerminen, V. M., Hillamo, R., Aarnio, P., & Koskentalo, T. (2002). Organic and black carbon in PM 2.5 and PM 10: 1 year of data from an urban site in Helsinki, Finland. *Atmospheric Environment*, *36*(19), 3183-3193.

Yang, S., Cotton, W. R., & Jensen, T. L. (1997). Feasibility of retrieving aerosol concentration in the atmospheric boundary layer using multitime lidar returns and visual range. *Journal of Atmospheric and Oceanic Technology*, *14*(5), 1064-1078.

Yu, X. Y., Lee, T., Ayres, B., Kreidenweis, S. M., Malm, W., & Collett, J. L. (2006). Loss of fine particle ammonium from denuded nylon filters. *Atmospheric Environment*, *40*(25), 4797-4807.

CHAPTER II: HIGH TIME RESOLVED ANALYSIS

2.1 Permanence, transport and removal mechanisms of PM in the atmosphere

Particles issued into or formed in the atmosphere are subject to transport in and removal from the atmosphere by different processes, which together determine the atmospheric lifetime of the particles. Particle size exerts strong control over residence time in the atmosphere and over particle dispersion and removal. For example, coarse particles are removed from the atmosphere by sedimentation and precipitation (the residence time for particles >20 μm is several hours while it is 2-4 days for 2-3 μm particles). Particles in the range of 0.1-1 μm (accumulation mode and larger Aitken mode particles) exhibit the longest lifetime in the atmosphere, ranging from days to a few weeks, so that they can be transported over long distances (~ several 1000 km). In addition, greater is the particle residence time, greater will be its possibility to incur in physical-chemical reactions occurring at particle surface, resulting in some changes of its original properties and residence time in atmosphere (EC 2004b). The most relevant physical phenomena acting on atmospheric lifetime of particulate matter are *diffusion* – which causes shifting of materials following their concentration gradient–, *sedimentation* – depending on gravitational force –, and the possible *resuspension* of soil-deposited particles, due to winds action and to prolonged lack of precipitations. Nucleation and coagulation are the most relevant chemical mechanisms of removal. In the first, over-saturation vapours condense to form particles in the liquid state, while the second process forms aggregates of larger particle due to collision or to interactions of electrostatic nature (Di Menno Di Bucchianico et al., 2002). Finally, meteorological parameters like speed and direction of winds, temperature, relative humidity, cloudiness and intensity of solar radiation strongly contribute to both transformation and transport of the particles in the atmosphere, being mainly responsible of the atmospheric distribution and concentrations of the different particle size fractions in a given area. In this optic, the study of the PM with high time resolved method is one of the modern challenges in environmental research in order to better understand all the parameter that affect the PM formation and the consequences of PM emission on the human health and environmental effect.

2.2 High-time resolution sampling and analysis of Particulate Matter

As mentioned, there are several parameters, as atmospheric transport and dilution processes, that change in few minutes/hours and daily samples are not able to tracking these rapid changes.

Particularly in the case of sporadic events, such as long-range transport from neighbouring countries or local occasional emissions, time-integrated measurements may lead to a loss of information about the behaviour of individual PM sources. Thanks to the optimization of new high time resolved instruments, it was possible to better insight on processes such as formation, transport, removal, deposition and chemical reactions in the atmosphere and monitoring local emission sources otherwise impossible to monitoring. Moreover, high-time resolved samplings can also give further information about source emissions. In fact, it is not that the emission sources impact on air quality with very high emission of elements or compounds during a few hours in a day, and the knowledge about the timing and intensity of specific episodes may be important to assess human exposure. Typically, statistical models for data analysis are used to identify the sources of PM (Principal Component Analysis, PCA, Positive Matrix Factorization and PMF). However, the use of these models requires the availability of large databases and the in-depth knowledge of the environmental behavior of chemical compounds used as tracers of individual emission sources. Therefore, sampling and analysis of the elements in the PM high temporal resolution would definitely be a valuable support to increase the information relative to the discrimination of contribution due to different local emission sources and to identify and characterize episodes of long- range transport. Moreover, these techniques do not involve sampling on filters and are thus free from the above sampling artifacts. These techniques are divided into physical and chemical methods. For the first category, we shall consider the optical particle counters, while for the second category we will focus our attention on three systems, the Semi-continuous Element in Aerosol Sampler (SEAS), the Aerosol Mass Spectrometer (AMS) and the Particle Into Liquid Sampler (PILS). The latter is object of the explanation of this technique.

Every parameter related to the variability of the atmospheric pollutants' concentrations, depends on the amount of the emitted pollutants, the distance from the sources, the physical condition of the medium in which they are dispersed and their formation processes that can affect both the mass and the volume of air in which this mass is present. It was studied an equation that explain the variation of the concentration C of a generic pollutant *i* with time *t*,

$$\frac{\partial C_i}{\partial t} = \alpha[\phi_i(t)] - \beta\{C_i\} + Adv + \sum F_i - \sum R_i - D_S$$

in which are taken into account both the factors affecting the mass and the volume. Factors affecting the mass are the primary emission – expressed by the source emission flow ($[\Phi_i(t)]$) –, the chemical-physical transformation and chemical removal processes – expressed respectively by F_i and R_i- and

the deposition- expressed by D_s. Volume variations are due to the advective phenomena expressed by *Adv* and the convective phenomena expressed by α and $\beta\{C_i\}$, which take into account respectively the stability conditions of the surface layer and the mixing processes. Given the complexity of the atmospheric processes responsible of these changes, a detailed interpretation of the relationship among the intensity of the sources, the formation processes and the meteo-climatic conditions requires sufficiently high temporal resolution measurements (Kidwell and Ondov,2004a).

2.3 High time resolved samplers

Many problems are linked to the PM sampling, mainly due to its heterogeneous composition and to the relatively low concentrations (few $\mu g/m^3$) in which it is present in the air. To perform a chemical characterization of PM it is necessary to collect a sufficient amount of dust to analyze it by using the conventional analytical techniques; sampled air volumes need then to be sufficiently high and this is usually obtained by long sampling times (usually 24 h). Unfortunately, in this case mach information is lost, due to the low temporal resolution, as during the sampling time some reactions among the particles occur and modify their original characteristics. To have a high temporal resolution some appropriate sampling devices have been developed in the last decades, able to carry out both the sampling and/or analyze of PM at time resolution of minutes or hours.

2.3.1 Particle optical-counters

The optical particle counters (OPC) is an instrument, which allows counting in real time the number of the particles by classifying them according to their size (in general, particles with a diameter greater than 0.05 μm). These devices are made up of a collimated source (a laser) that illuminates the volume in which the air flows. A photodetector, positioned at 90 degrees in respect to the axis of the laser beam, measures the light scattered of every single particles by refraction, reflection and diffraction (Figure 2.1). They can determine simultaneously both the number and the size of the particles by measuring respectively the number and the intensity of the pulses reaching the detector.
The intensity of the diffracted light in the various directions depends on the shape and size of the particles but not on their composition. This method has the advantage of providing an immediate measure of the number of particles present in the air in a given time and, since does not require a membrane, it can perform a continuous measurement. Then, it allows evaluating the temporal evolution of the particle size distributions.

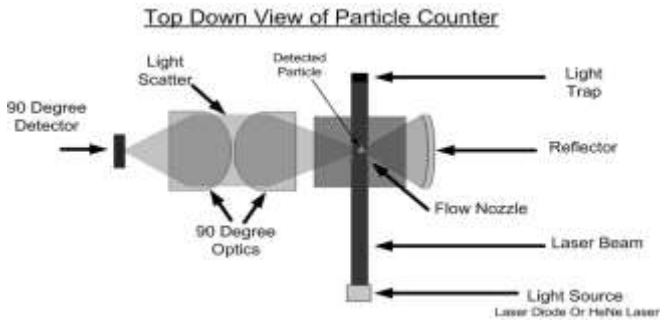

Figure. 2.1: *Scheme of a particle-optical counter.*

It should however be considered that it is not possible to determine the proper shape of the particle; the measure will be related only to the *optical equivalent diameter* that is the diameter of a spherical particle having the same optical behavior of the particle in question, which then spreads the light in the same way. This fact is very important when comparing dimensional data from different measurement techniques: it is not likely that the optical diameter corresponds to the actual diameter of the particle. It has been demonstrated that the particle shapes are far from a sphere and the particles' surfaces often show a high roughness. In addition, these devices calculate the mass concentration by giving a unit density to each particle. Actually, the density cannot be considered equal to 1 and constant for every particle so that very often the mass concentration value is quite different from the real one. Finally, the particles are counted per unit of volume. It has to be noted that the *fine* particles are much more numerous than the coarse ones, but they contribute much less to the total PM mass. Consequently, the optical-particle counters are very sensitive to the fine dust and very little sensitive to the coarse particles.

2.3.2 Semi-continuous Element in Aerosol Sampler (SEAS)

The SEAS device allows obtaining aqueous solutions from PM particles whit specific dimensions, by means of a specific cyclone that is located at the top of the instrument. It is substantially constituted by an aerosol concentrator coupled to an automated system for collecting samples collection into the vials (figure 2.2). By means of a peristaltic pump, deionized water is send to a heated chamber (100°C) to generate water vapor. The water vapor meets and reacts with the particles contained in the sampled airflow, producing the particle growth. A cooling system (up to 0.5°C) is placed after the heated chamber, leading to the condensation of the vapor and consequently to the formation of the sample solution. Then the solution is conveyed to the collection vials through a system of impactors.

Two impactors can be distinguished: the first impactor, *virtual*, reduces the intake flow (can be up to 190 L/min); the second impactor, *real*, guides the solution to the collection vials. An opening, in the proximity of the virtual impactor, connects the pump at the inlet of the airflow and aspires all those species (mostly atmospheric gas) that do not have the strength to reach the impactor. It was observed that with these system particles from 0.08 μm in diameter with a temporal resolution of up to 30 minutes may be sampled (Kidwell and Ondov, 2004b). To ensure a high aspiration flow the instrument generally works with a very powerful pump. This has two drawbacks:

1. Pump vibrations can damage the instrument;
2. The instrument needs of high amounts of power to work, so for field studies powerful energy generators are needed, difficult to transport and expensive (Pancras et al., 2005).

For these reasons it has been developed a more compact and easily transportable instrument, which operates at a lower flow (about 16 L/min), but, compared to SEAS, it is affected by lower analytical sensitivity due to the lower flow sampling.

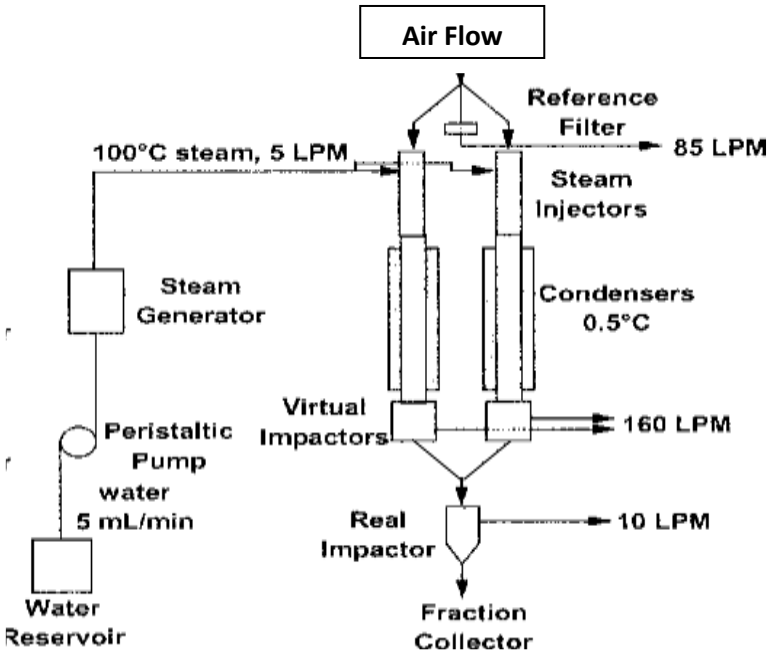

***Figure 2.2**: Schematic representation of a SEAS.*

2.3.3 Aerosol Mass Spectrometer (AMS)

The AMS is an instrument able to measure the size and chemical composition of the PM volatile and semi-volatile components with high temporal resolution (up to 1-10 seconds) (Jayne et al., 2000). It is a combination of a mass spectrometer with an atmospheric particulate sampler (Figure 2.3). The particles, whose diameter has been selected by a cyclone, are forced to enter into an orifice

(critical orifice) under the action of an aspiration pump. They are then sent in an aerodynamic lenses' system. This latter consists of a series of circular discs (separated by a distance of a few cm) which have a central hole. The diameter of the holes varies from the first (inlet hole) to the latter (outlet hole) of about 2-4 mm. The particles acquire a velocity dependent on their aerodynamic diameter. Smaller particles are more accelerated, while the larger particles, because of the greater inertia, acquire a lower speed. At the bottom of the lens system a particle separation based on their size occurs. A chopper, which is a rotating disc having two slots, selects the particles' beam to enter in a flight chamber (ToF).When the chopper is open all the particles can pass through, while when it is closed all the particles are blocked. By calculating the time spent by the particles to pass through the flight chamber, the aerodynamic diameter can be known. After the flight chamber, the particles go through a heated plate (up to 800° C) where there is the vaporization of non-refractory species and their ionization by electron impact. Therefore, only the organic species and most of the nitrate and sulphate salts are detected.

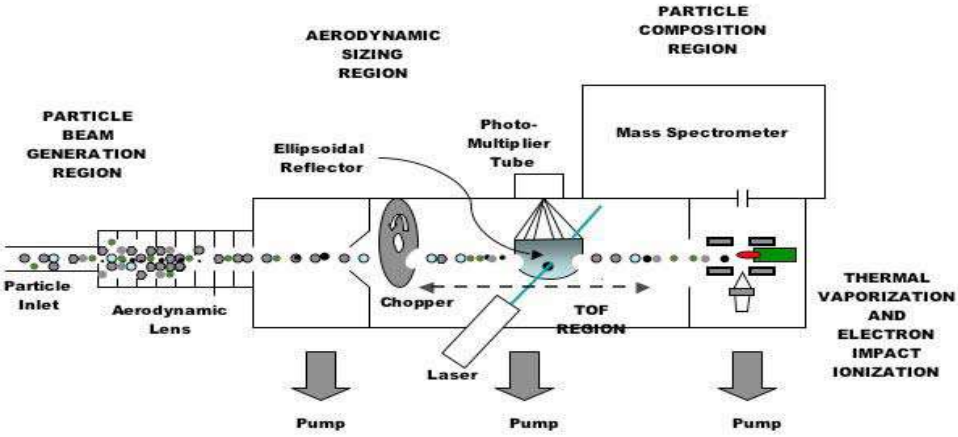

Figure 2.3: *Schematic representation of an AM.*

All the ionized species are finally sent to a mass spectrometer, which performs the chemical analysis, giving the chemical composition of every particle. This instrument can be transported by a mobile unit, but it is very expensive and also only experienced operators can handle the huge amount of provided data.

2.3.4 Particle Into Liquid Sampler (PILS)

The basic working principle of the PILS (Weber et al., 2001) is similar to the SEAS (described above). It allows obtaining samples of particulate (with selected diameter) in aqueous solutions, with high

temporal resolution. Several versions of this instrument have been proposed and the one used in the present work is the most recent one. In general, the complete system consists of three main components:

1. A zone of particle growth.
2. A zone of particle impact and collection of the solution.
3. A zone of direct connection to the instrument used for the analysis (in our case the ion chromatograph, IC).

The first two points will be described in the present paragraph, leaving the discussion of the last component in the following sections.

As it can be observed in Figure 2.4, the sampler consists of a vapor generator placed perpendicularly at the inlet of the sampled air flow, a central cylinder which acts as a growth chamber, and finally an impact structure (enlarged area of Figure 2.4) where the particles' impact are successively collected. The vapor, which is obtained by heating deionized water through a system of electrical resistances, meets the flow of sampled air (inlet by a vacuum pump at about 15 L/min) at the beginning of the conical structure. This happens for two reasons: to avoid the high temperature of the vapor that can change the structure and composition of the particulate, and to ensure that it works in oversaturation conditions. Oversaturated vapor is the vapor in a condition of unstable equilibrium, at a temperature lower than the one that would cause its condensation, but that does not condense because the condensation nuclei are absent (Weber et al., 2001). The conical structure, in fact, favors the expansion of the vapor flow, so that it cools. Moreover, the walls of the cone favor the condensation of the excess vapor that is sent to a drain (Douglas et al., 2003).

We must also point out that in order to maintain constant the supersaturated environment, the heating temperature must be constant and then a thermocouples' system checks the temperature value.

The sampled particulate instead, besides favoring the condensation (it is our condensation nucleus), move along the growth chamber up to the impact surface by an inertial push. The impact plate is made of quartz, which is continually "*washed*" by the collection solution. To make homogeneous the whole impact surface, a steel grid is applied around the quartz plate.

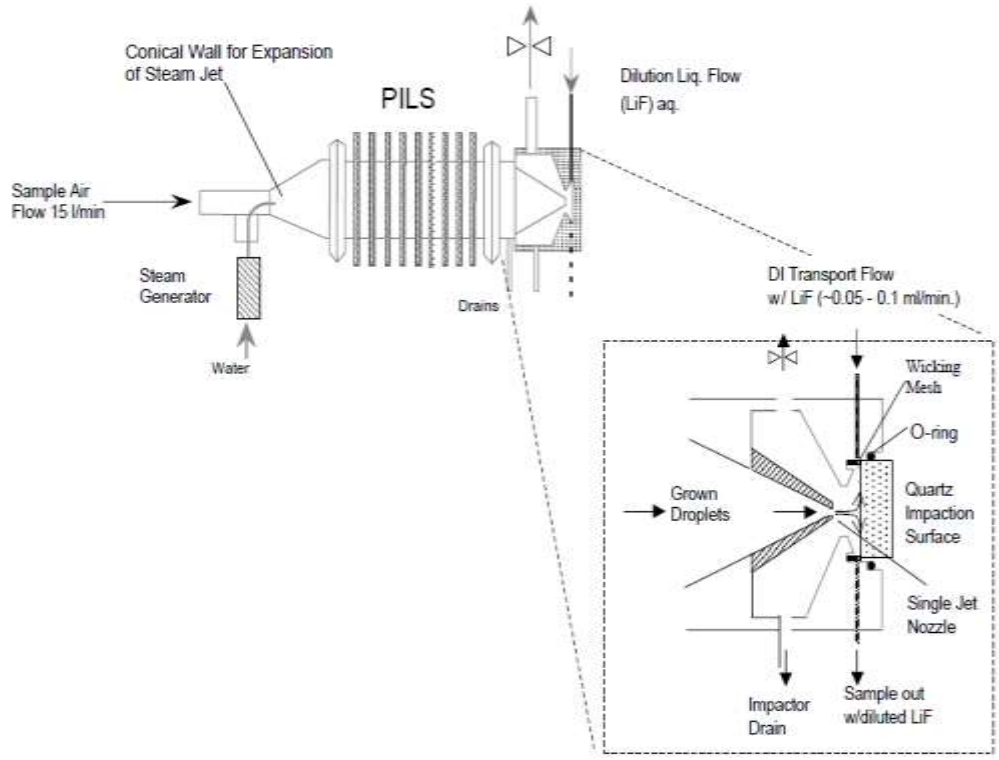

Figure 2.4: *Schematic representation of a PILS.*

2.4 Traceability of the sources using elemental chemical analysis

Elements in PM are often used as tracers of specific sources in source apportionment studies (in which ambient concentrations are apportioned to likely sources) (Almeida et al. 2006; Viana et al. 2008; Gielt et al. 2010; Argyropoulos 2012, 2013). Only by knowing, the relative strength of the individual emission sources it is possible to properly target the policies of reducing PM concentrations. In this field, the use of chemical tracers is extremely widespread. The identification of emissive sources of anthropogenic origin is possible, for example, by evaluating the relationship between natural abundance and relative abundance of certain elements, in particular areas (Pacyna et al., 1999). This assessment is diagnostic, because sources of anthropogenic origin are often responsible for the increase in concentration of trace metals in the atmosphere. Another method is the use of enrichment factors indicating the increase in concentration of a metal in aerosol relative to its natural abundance in certain reference materials, such as in rocks and soils (Junge et al., 1979).These factors may be related to the emission sources by means of transport models. The studies conducted over the last few years have allowed the creation of the first databases regarding the flow of metals in traces from natural sources. These studies show that more than 50% of Cr, Mn and V emissions, and metals such as Cu, Mo, Ni, Pb, Sb, Zn derive from soil dust. A high source of metal emissions are volcanic

emissions and forest fires, which are responsible for 40-50% of Cd and Hg and 20-40% of As, Cr, Cu, Ni, Pb and Sb in the total particulate matter of natural origin. In rural areas, the main PM component is organic and more than 60% of trace metals in wooded areas are due to biological emissions. Finally, for the contribution to the concentration of metals caused by anthropic sources, the landscape is more complex; the table shows an overall picture of the emissions caused by major anthropogenic sources (Pacyna et al., 1999)

Table 2.1: *Global emission of trace metals from anthropogenic sources (103 tonnes per year), n.f. = non ferrous*

Sorgente	As[b]	Cd[a]	Cu[a]	Ni[a]	Pb[a]	Se[c]	Zn[a]
Metalli minerali n.f.	0.013	0.002	0.8	-	8.2	0.005	1.6
Produzione primaria metalli n.f.	15.2	4.71	20.8	9.4	76.5	0.28	107
Produzione secondaria metalli n.f.	-	0.60	0.33	0.2	0.8	-	9.5
Produzione di acciaio e ferro	4.2	0.07	5.9	1.2	50	0.01	35
Applicazioni industriali	0.02	0.05	4.9	1.9	7.4	0.06	26
Combustione di carbone	0.55	0.06	4.7	0.7	14	0.68	15
Combustione olio e benzina	0.004	0.003	0.74	27	273	0.06	0.1
Combustione del legno	0.60	0.20	12	3.0	4.5	-	75
Incenerimento rifiuti	0.43	1.40	5.3	3.4	8.9	-	37
Produzione fertilizzanti	2.66	0.21	0.6	0.6	0.05	-	1.8
Altro	-	-	-	-	5.9	-	6.7
Totale	23.6	7.3	56	47	449	1.1	314

The databases (Table 2.1) show that combustion of fuels is the main anthropogenic emission source of metals in traces of Be, Co, Hg, Mo, Ni, Sb, Se, Sn e V and one of the most important for As, Cr, Cu, Mn e Zn. Mn and Cr, that are mainly emitted by the production processes of steel, wood and ferrous alloys. The presence of Pb is, on the other hand, due to the production of steel and fertilizer industry, Zn from the production of minerals. In this context, improving the selectivity of the source tracers can constitute the key step to solve the apportionment problem. Furthermore, an enhanced selectivity of the source tracers can be strictly necessary in areas characterized by frequent and severe atmosphere stability episodes, where the vertical diffusion of pollutants is impaired and the horizontal diffusion and the aging of the air masses cause a more and more homogeneous mixing of the emission products. Further improvements in the selectivity of elements as source tracers can be obtained by applying a chemical fractionation methodology based on their solubility (Fernandez Espinosa et al. 2002; Sillanpää et al. 2005; Al-Masri et al. 2006; Dutkiewicz et al. 2006; Canepari et al. 2008, 2009a, 2010). Elemental solubility, in fact, provides information about the chemical form in which the

element is released and this, on its turn, may be typical of its emission source. Moreover, biogeochemical cycles, environmental and health effects are strongly related to the chemico-physical behavior of the chemical species in which the elements are contained (Harrison and Yin 2000; Cho et al. 2009; Barrett et al. 2012). In the case of toxic elements, a reliable identification of their atmospheric sources and bioaccessibility is even more important, as inhalation is one of the most relevant route of exposure to these pollutants (Marmur et al. 2006; Reche et al. 2012). Although environmental studies reported in the scientific literature mostly concern the determination of total elemental concentration, in the last decades many different extracting procedures have been developed to study the solubility of elements, and thus their environmental mobility and bioaccessible fraction (Dos Santos et al. 2009; Limbeck et al. 2012; Armiento et al. 2013; Mukhtar and Limbeck, 2013). However, only a few studies concern the application of these procedures to intensive monitoring campaigns and include the interpretation of the results on the basis of the meteorological situation and the local emission framework, as this kind of methodologies require a lot of work both to carry out the chemical analysis and to elaborate and interpret the obtained data (Voutsa and Samara 2002; Heal et al. 2005; Birmili et al. 2006; Qureshi et al. 2006; Sato et al. 2008; Canepari et al. 2009a).

2.5 High time-resolution studies

PM is a very complex mixture of particles, whose dimension ranges from a few nanometres to tens of microns. It contains hundreds of chemical species, most of which still unidentified. In fact, many different sources, both natural and anthropic, release PM into the atmosphere. Although many studies revealed that several PM properties (chemical composition, particle dimension etc.) influence its health and environmental effects, there is no sufficient evidence that associates each property to specific outcomes (WHO, 2013). The new goal in the environmental research field concerns the study of the chemical composition of PM and the association of its effects on the environment and human health. In this optic, the development of new high-sensitivities methods able to help the study and the characterization of particular emissions process allowing to analyse a high number of tracers without requiring high amount of samples. In fact, the study of the PM chemical composition improves the selectivity of the source tracers and can constitute the key step to develop some emission reduction policies for the protection of both human health and environment. The main problem in the identification of elements able to trace individual sources is that they are not selective: it is known, in fact, that the same elements can be emitted from several different sources.

In subparagraph 2.5.1 it is reported the optimization of a new flowing system (FS), consisting in the on-line filtration and acidification of samples before their introduction in the Inductively Coupled Plasma Mass Spectrometer (ICP-MS), which allows the elemental analysis of PILS samples without any pretreatment to be performed. Thanks to this new FS method, the detection and quantification limits of the ICP-MS measurements were in fact significantly lowered, and are became compliant to the elemental concentrations of field samples. The optimized system was applied to field measurements by two operative configurations. In the first one we directly coupled PILS sampling line to the FS-ICP-MS and we obtained, by a very simple and quick experiment, the elemental profile of some relevant PM sources (cigarette, brushwood, pellet and incense combustion and road dust re-suspension). In the second one, we analysed off-line samples collected by PILS during some spot events in indoor and outdoor environments by FS-ICP-MS.

As already discussed, the use of high temporal-resolution methodology is crucial in the study of environmental PM concentrations, because the parameters that determine the temporal variability of the concentrations of the species present in the atmosphere are subject to variations in short time intervals, in the order of minutes or at most hours. It is therefore clear that the detailed interpretation of the relationship between source intensity, formation processes and weather-climatic parameters requires a use of high time-resolved measures and cannot be caught by the conventional 24-h filter measurements. These are precisely the reasons why, the work reported in subparagraph 2.5.2 describes a novel improvement of an existing instrument for the high-time-resolution measurement of inorganic ions in atmospheric particulate matter (Particle Into Liquid Sampler - Ion Chromatograph; PILS-IC). In the last few years, the development of time-resolved techniques for the chemical characterization of atmospheric particles has been attracting numerous research, as these techniques are essential for the comprehension of the complex physico-chemical behavior of atmospheric pollutants. However, this goal is generally obtained by complex and expensive instrumentation. With respect to the commercial instrument, our modified PILS-IC system allows one order of magnitude improvement in the detection and quantification limits of the measured species and assures higher time-coverage of the measurements (more than twenty-fold). These features make the device suitable for being used also in background sites and improve its ability in following fast variations in pollutants concentration and in obtaining a very good synchronization with the meteorological parameters. The proposed technical change is easily reproducible and has a very low cost, as it simply consists in the substitution of the sample loop of the IC injection valve with a pre-concentration cartridge. The analytical performances of the new system have been validated both in the laboratory and in the field, against two well-consolidated techniques (diffusion

denuder lines and Aerosol Mass Spectrometer). After the phase of laboratory optimization and validation of the pre-concentration system, the analyser was used and tested in an intensive campaign conducted at the Arnaldo Liberti detection station, located at the CNR centre during The European Monitoring Environment Program (EMEP). This program produces regularly reports on emissions, concentrations and depositions of atmospheric pollutants and monitors the quantity and relevance of critical crossings and threshold levels. Therefore, by comparing the results obtained from PILS with those relating to several different instrumentations used during the monitoring campaign (such as AMS and denuders lines) it was possible to validate the proposed method. The increased interest by environmental chemistry, in the study and the optimization of new high temporal resolved methods motivated me to deepen this application field. In fact, I have focused on an additional study (subparagraph 2.5.3) carried out by an innovative method (discussed in the last paper report in this chapter). This work was carried out in Los Angeles (California-USA) during my internship period in the Professor Constantine Sioutas Research Group. In this work the monitored site was a mixed urban site where ambient PM is largely impacted by vehicular emissions (Hasheminassab et al. 2014; Sowlat et al. 2016), as it is located 150 m downwind of a major freeway, i.e., I-110. It is also located approximately 3 km directly to the South of downtown Los Angeles, CA, and less than 2 km to the Southwest of another major freeway, i.e., the I-10. In this work it was developed a novel air sampling monitor for near-continuous (i.e., 2-h time resolution) measurement of iron (Fe), manganese (Mn), and chromium (Cr) concentrations in ambient coarse particulate matter (PM) (i.e., $PM_{10–2.5}$). The developed monitor consists of two modules: (1) the coarse PM collection module, utilizing two virtual impactors (VIs) connected to a modified BioSampler to collect ambient coarse PM into aqueous slurry samples; (2) the metal concentration measurement module, which quantifies the light absorption of colored complexes formed through the reactions between the soluble and solubilized target metals and pertinent analytical reagents in the collected slurries using a micro volume flow cell (MVFC) coupled with UV/VIS spectrophotometry. The developed monitor was deployed in the field for continuous ambient PM collection and measurements from January to April 2016 to evaluate its performance and reliability. Moreover, this monitor can be readily configured to measure the speciation (i.e., water-soluble portion as well as specific oxidation states) of those metal species. These unique abilities are essential tools in investigations of sources and atmospheric processes influencing the concentrations of the redox-active metals in coarse PM. Ambient coarse PM was collected in 2-h time intervals, resulting in 12 data points per day, and the concentrations of the target metals (i.e., Fe, Mn, and Cr) were subsequently measured using this system.

*2.5.1. Multi-elemental analysis of PM samples collected by Particle-Into-Liquid Sampler**

Introduction

Particulate matter (PM) is a mixture of solid particles and liquid droplets in the air (Knudsen and Rasmussen, 2012). It is largely recognised that human exposure to air pollution has severe consequences for human health such as diseases of the respiratory and cardiac systems (Pope and Dockery, 2006). Suspended particles vary in size, composition, and origin. The chemical composition, diameter, morphology, surface area, structure, electric charge, and solubility are important parameters for the characterisation of the behaviour of dust particles in the atmosphere. The most important parameters that influence the chemical and physical properties of PM are its source, mechanism of formation, emission process, and distance from the source. Several studies have shown that elementary analysis of particulate matter (PM) in the atmosphere helps understand the origin of the particles and characterize the emission sources. In this context, improving the selectivity of source tracers may be the key to developing emission reduction strategies for the protection of both human health and environment. The main problem in the identification of source tracers is that they are not selective i.e. the same elements can be emitted from several different sources (Querol et al., 2001; 2006; 2007a; Lee et al., 2003; Gotschi et al., 2005; Viana et al., 2007; Jeong et al., 2008). In light of this, development of highly sensitive methods for the study and characterisation of emissions from particular processes is required. Such methods allow simultaneous analysis of a large number of tracers without using a large sample amount. A number of studies on the temporal variability of the concentration of atmospheric pollutants on a 24-h sampling basis have been reported in literature (Kidwell and Ondov, 2004; Bukowiecki et al., 2005). The problem with this approach is that the obtained concentrations are mediated over a period (24 h) during which the strength of sources and the dilution capacity of the atmosphere are subject to wide variations. Information on the time-resolved variation of tracers in ambient air significantly facilitates the identification of pollution sources because it allows the decoupling of each time trend. Generally, the rate at which the strength of sources and the dilution capacity of the atmosphere changes influence the elemental composition of PM. Variations in emission rates, meteorological parameters, and atmospheric processes (Kidwell and Ondov, 2001) are fast (minutes to hours) and cannot be captured by conventional 24-h filter measurements. During the last few years, optimisation of the new high time-resolved monitoring systems has been an exciting challenge in atmospheric pollution research.

* Submitted to *Atmospheric Pollution Research* in August

Different techniques for optimisation have been proposed in literature. These include aerosol mass spectrometer (AMS), semi-continuous elements in aerosol sampler (SEAS), streaker sampler followed by analysis with proton-induced X-ray emission (PIXE), particle-into-liquid sampler (PILS), and bio-sampler with ambient metals monitor (Weber et al., 2001; Pancras et al., 2005; Li et al., 2015; Sowlat et al., 2016; Barnaba et al., 2017; Furger et al., 2017).

The operating principle of a PILS is to grow the sampled atmospheric particles by mixing them with supersaturated steam in a specific chamber, so that they can be collected by inertial impaction at the top of the impactor plate. The particles are continuously washed from the impactor plate by a water solution. PILS is generally used in combination with ion chromatography (PILS-IC) for on-line monitoring of water-soluble inorganic ions. However, it has also been used as a sampler for the analysis of other analytes (Hecobian et al., 2010; Timonen et al., 2010). The main limitation of this system is that samples are highly diluted by the wash solution, thus leading to a considerable increase in the detection limits. This does not allow the application of this system in areas with low concentration of pollutants (Wang et al., 2013; Perrino et al., 2015).

Despite the importance of time-resolved elemental analysis for source apportionment studies, only a few PILS applications involve elemental analysis. To our knowledge, there are two experimental PILS applications concerning elemental analysis. One involves the study of certain heavy metals (Zn, Cd, Pb, and Cu) using anodic stripping voltammetry (ASV) (Bogenschütz et al., technical report;) and the other involves measurement of water-soluble Fe (II) with a particle into liquid sampler (PILS) coupled to a liquid waveguide capillary cell (LWCC) and a UV/VIS spectrometer (Oakes et al., 2010).

In light of this, the aim of this study is to combine the sampling advantages of a PILS (high time-resolution and low costs) with the flexibility and sensitivity of inductively coupled plasma mass spectrometry (ICP-MS). This would help achieve simultaneous analysis of time-resolved pseudo-total (soluble in 1% HNO3 solution) concentrations of a large number of elements. The current paper describes the optimisation of a new flow system (FS) for introducing the samples collected with a PILS into the ICP-MS instrument. This system allows the PILS and ICP-MS to be directly coupled for the on-line analysis or the PILS samples collected off-line to be analysed by ICP-MS with an increased sensitivity. The optimised system was used to obtain elementary profiles of some specific indoor and outdoor sources, such as cigarette smoking, wood and incense combustion, and road dust resuspension (on-line measurements), and for short indoor and outdoor monitoring campaigns (off-line measurements).

Material and Methods

PILS

The PILS (ADI 2081, Metrohm AG, Herisau, Switzerland) consists of a vapour generator that is placed perpendicular to the entrance of the sampled air stream, a central cylinder that acts as an expansion chamber, and an impactor plate where particles are captured by inertial impaction and are subsequently washed with a wash solution before their collection. All the solutions entering and exiting the PILS were managed by a single eight-channel peristaltic pump (model 205S, Watson-Marlow Inc., Wilmington, MA, USA) running at a speed of 24 RPM. The operative flow rates were as specified in the PILS operating conditions manual. Water used for the collection of ambient PM and for system rinsing was purified by a water purification system (EMD Millipore, Billerica, MA, USA). It is important to note that the water solution introduced at the top of the impactor plate to transport the particles down to its base was spiked with 50 µg/L of LiBr (Merck KGaA, Darmstadt, Germany), which was used as an internal standard. The output flow rate (union of sample and acid lines) is 0.6 mL/min. Samples exiting the PILS were either collected in vials using a fraction collector (Varian SPS 5 Auto sampler) or connected to the ICP-MS instrument for on-line analysis, as described below.

Operatively, the blank values were obtained by placing a filter pack, comprised of one Teflon filter, one Nylon filter, and one paper filter, impregnated with H3PO3 solution at the inlet of the PILS. This filter pack was able to restrict the passage of particles and inorganic vapour (Perrino et al., 2015).

ICP-MS analysis

Samples collected by the PILS that are to be analysed by the conventional off-line procedure were mixed with 2% HNO_3 (obtained by diluting 65% HNO_3, Suprapur, LGC, Promochem) and filtered with a syringe filter (Millipore membrane, pore size: 0.45 µm) before analysis. ICP-MS conditions used for this analysis were as described in a previous study (Protano et al., 2016). Matrix-matched calibration was obtained by using yttrium (Y) (20 µg/L) as an internal standard. The instrument was calibrated for each element within a range of concentrations likely to be encountered in the field samples.

The new FS for sample introduction used for on-line and off-line field measurements is described below (section 2.5). In this case, the ICP-MS operating conditions were modified (Table 1) in order to achieve a fast instrumental response. In particular, the rinse time and stabilisation delay were set to zero, which is usually done when the ICP-MS instrument is used like a chromatographic detector.

In contrast to when the ICP-MS instrument is used as a detector, the replicates read times were maintained at 10 s in order to avoid reduction in the signal/background ratio.

Table1: *ICP-MS operating conditions used during FS-ICP-MS analysis*

Parameter			Value
	Flow Parameters (L/min)		
		Plasma Flow	18
		Auxiliary Flow	1.8
		Sheath Gas	0.18
		Nebulizer Flow	1.0
	Torch Alignment (mm)		
		Sampling Depth	7.0
	Other		
		RF power (kW)	1.4
		Pump Rate (rpm)	7.0
		Stabilization delay (s)	0
		Rinse time (s)	0
		Replicate read time (s)	10
	Ion Optics (volts)	First extraction lens	-1.0
		Second extraction lens	-180
		Third extraction lens	-205
		Corner Lens	240
		Mirrors lens left	34
		Mirrors lens right	28
		Mirror lens bottom	29
		Entrance lens	0.0
		Fringe Bias	-4.0
		Entrance plate	-4.0
		Pole Bias	0.0

Application to Sources Profile

The sources tested were individually simulated in a laboratory inside a Plexiglas box (volume: 1 m3) and the emissions were directly sampled and analysed by the coupled PILS-FS-ICP-MS system. Inside the Plexiglas box, we controlled the emission conditions as much as possible. We used a mechanical fan (Magic 12v 0.21a Cooling Fan, 2000 RPM) to maintain a homogeneous composition of air during the period of analysis and simulated the sources under controlled intensity and duration in order to avoid saturating the PILS. In addition, an optical particle counter (OPC; CON. TEC Engineering srl) was placed inside the box in order to estimate the PM mass concentration We characterised PM from five different emission sources: cigarette smoking, wood burning, pellet

burning, incense burning and resuspension of road dust (collected from the road surface at a traffic site in the centre of Rome located in Central Italy).

Application to outdoor and indoor monitoring campaigns

Air sampling with the PILS was performed at a peri-urban site, located about 40 km from Rome, Italy (42°9'52"N, 12°43'13"E), in a residential area bordering a small hamlet and a busy extra-urban road. The monitoring activities were performed during 12-29 March 2014. Short-term measurements were carried out during indoor (cleaning of pellet stoves or thermo-fireplaces) and outdoor (brushwood burning) spot events. The inside of the pellet stove was cleaned using a vacuum cleaner for about 10 min, while the thermo-fireplace was cleaned manually using a brush for about 5 min. For monitoring the brushwood burning event (outdoor event), the PILS was positioned 100 m away from the location of the spot event.

Samples were collected with a time resolution of 10 min, stored at 5 °C, and analysed by FS-ICP-MS without any further treatment. The OPC measurements (with a time resolution of 1 min) were taken during samplings.

RESULT AND DISCUSSION:

Optimization of the PILS/ICP-MS coupling and calibration

The elemental analysis of the solutions sampled by a PILS can be carried out by off-line ICP-MS analysis. However, due to the dilution of samples in the PILS concentration levels of most of the elements are too low to be detected. Furthermore, the use of ICP-MS requires the absence of suspended solids in the analysed solutions. For this reason, before the analysis of the total elemental concentration in PM, 24-h samples are usually pre-treated by microwave-assisted acid digestion.

The solution flowing from the PILS is a highly diluted solution containing very low amounts of suspended solids. In fact, elemental concentrations of samples collected by the PILS are about thirty times lower than those obtained in the present conventional elemental analyses of PM samples (flow rate: 2.3 m3/h; sampling duration: 24 h; indicative volume of the solution after acid digestion: 50 to 100 mL). The acid digestion step would dilute the samples further, leading to non-detectable concentration values for most of the elements. Furthermore, acid digestion does not achieve complete solubilisation of PM and therefore a successive filtration step is needed before introducing the samples into the ICP-MS instrument. Filtration often introduces high and variable blank values, which increases the limits of detection (LODs) and quantification (LOQs). To overcome these problems, we

created a new system (Figure 1) in which the acidification and filtration steps are performed on-line. As shown in Figure 1, the solution flowing from the PILS line or collected by the fraction collector (sample) is de-bubbled and mixed with an acid solution (2% HNO3) that is simultaneously aspirated by a peristaltic pump operating at 6 RPM (flow rate of the sample line and acid line is about 0.3 mL/min). The two solutions converge into a T-shaped junction with a dilution ratio of 1: 1. After this joint, the resulting solution (total flow rate of about 0.6 mL/min) is filtered on-line with a nitrocellulose filter and introduced into the ICP-MS nebuliser. In this configuration, we could determine the pseudo-total elemental concentration with low dilution and pre-treatment of the sample. The addition of 2% HNO3 does not achieve total digestion of the samples; however, pseudo-total elemental concentrations have been already successfully used for tracing emission sources (Canepari et al., 2009).

The new system needs an analytical control to verify the stability of the dilution ratio of the two convergent solutions (sample and acid solutions) in the T-shaped junction. The de-bubbler system present in the sample line splits the output solution into two different lines: the solution containing air bubbles is directed to the discharge unit and the solution without air bubbles is directed to the analysis unit. This causes certain variability in the sample flow rate and subsequently in the dilution ratio of the two solutions (sample and HNO3 solution). Two internal standards (ISs) were used to control and normalize the flow of the two lines; one of the IS was introduced into the PILS wash solution and the other was introduced into the HNO3 solution. Since the nebulising efficiency needs to be controlled during the introduction of samples into the ICP-MS torch a third IS was added (in the same concentration as the other two ISs) to both the PILS wash solution and the 2% HNO3 solution. Only those elements that are present in the samples at very low levels (< LODs), and therefore do not give rise to spectral interferences in ICP-MS, were considered as ISs. Beryllium (Be) and rhodium (Rh) were chosen as ISs to control the flow of the PILS and acid lines, respectively. Yttrium (Y) was chosen as an IS to control the ICP-MS nebulisation efficiency. The first two standards (Be and Rh) were used at a concentration of 50 μg/L and the last standard (Y) was used at a concentration of 20 μg/L. The signal from ICP-MS (c/s) was corrected by using Equation (1).

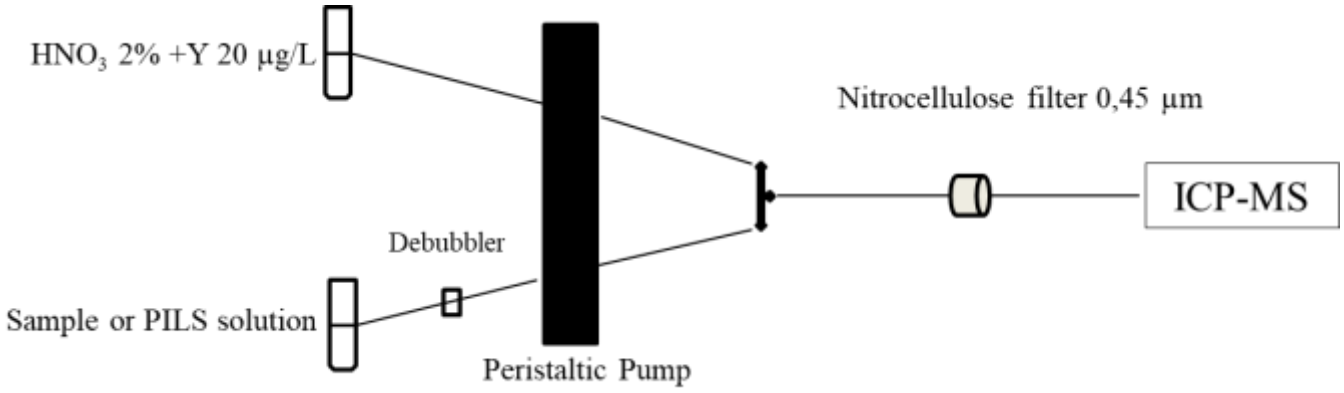

Figure 1: *Scheme of the flow system (FS) line for the introduction of samples into ICP-MS*

Only those elements that are present in the samples at very low levels (< LODs), and therefore do not give rise to spectral interferences in ICP-MS, were considered as ISs. Beryllium (Be) and rhodium (Rh) were chosen as ISs to control the flow of the PILS and acid lines, respectively. Yttrium (Y) was chosen as an IS to control the ICP-MS nebulisation efficiency. The first two standards (Be and Rh) were used at a concentration of 50 µg/L and the last standard (Y) was used at a concentration of 20 µg/L.

The signal from ICP-MS (c/s) was corrected by using Equation (1).

$$c/s_i' = c/s_i \frac{\frac{c}{s}Y_{sample}}{\frac{c}{s}Y_{black}} \frac{\frac{c}{s}Be}{\frac{c}{s}Rh} \quad (1)$$

where $\mathbf{c/s_i}$ is the uncorrected counts of the ith element/s, $\mathbf{c/s_{Ysample}}$ is the Y counts in the sample solution/s, $\mathbf{c/s_{Yblank}}$ is the Y counts in the blank solution/s, $\mathbf{c/s_{Be}}$ is the Be counts in the PILS wash solution/s, and $\mathbf{c/s_{Rh}}$ is the Rh counts in the nitric acid solution/s.

First, the counts/s of each element was/were multiplied by the ratio of the Y signal in single readings to the Y signal in the blank solution. Thus, we could correct the variability caused by possible inefficiencies in the nebulisation of the solution. The resulting counts/s can be further corrected in case the dilution ratio of the sample and acid solutions is altered (evidenced by the change in the Be and Rh signal ratio). The calibration curve of the system was plotted in the same FS mode. The first point of the curve, at concentration "0" corresponds to the blank signal and was acquired by introducing deionised water spiked with Y (20 µg/L) and Be (50 µg/L) into the first line of the system (Figure 2), and HNO_3 solution spiked with Y (20 µg/L), and Rh (50 µg/L) into the second line.

Subsequently, the deionised water solution was replaced by standard multi-element solutions of progressively increasing concentrations while maintaining same IS concentrations.

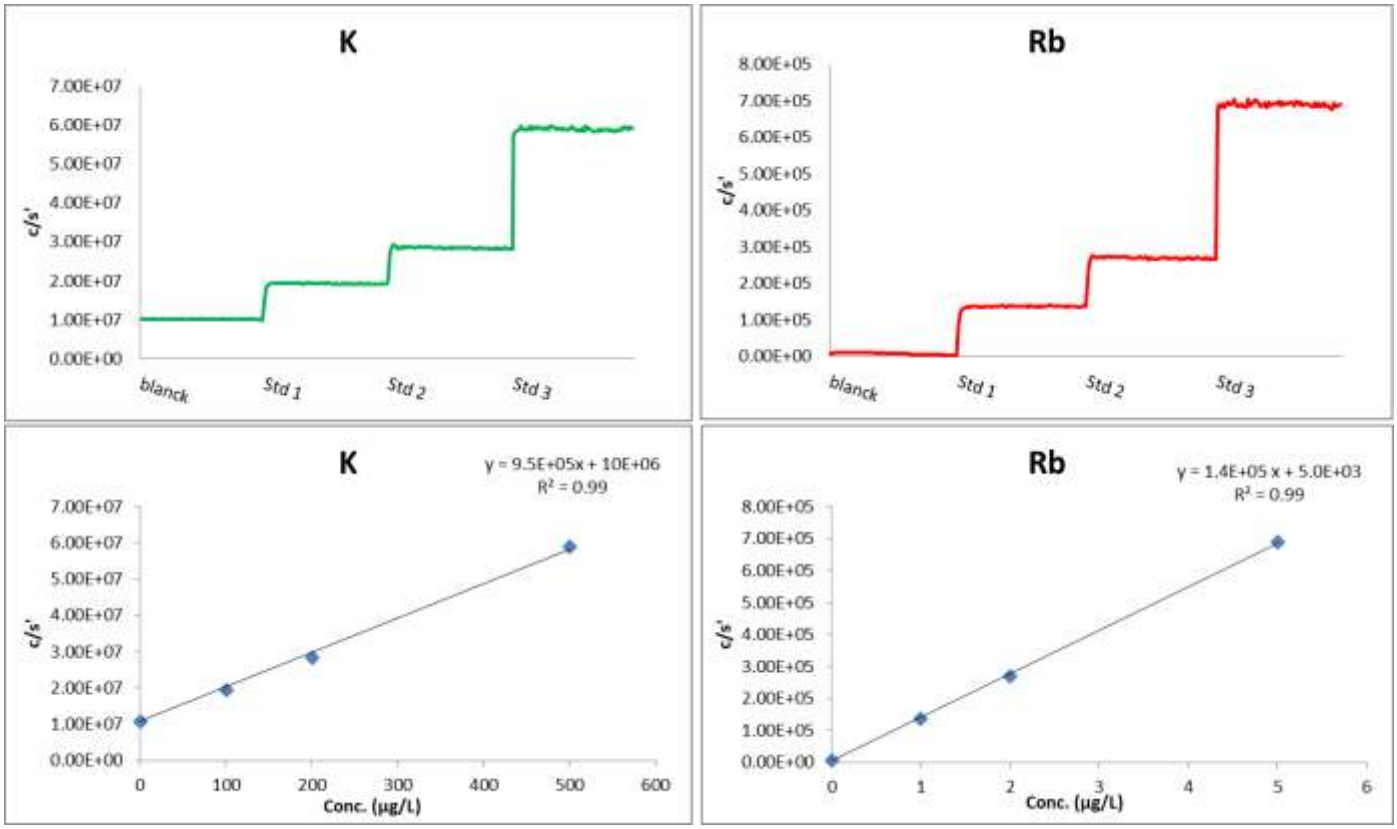

Figure 2: *ICP-MS instrumental signal of K and Rb and calibration curves.*

Figure 2 (upper panel) shows some of the ICP-MS signals obtained during calibration. As can be seen, the signal of the standard can be distinguished from the background noise for all the concentration ranges considered. The signals of the blank solution and standard solution were processed to eliminate transient points and mediate the central step values (50 points).

The calibration curves (Figure 2, lower panel) relative to the blank solution and the standard solution were plotted by taking the average values obtained for each concentration. As can be seen, the response linearity is very good for the explored concentration levels and R^2 values are between 0.97 and 1.00. The calibration step was repeated before each analysis.

Mass concentrations of different elements were calculated by considering the sampling rate of the PILS (13 L/min) and the flow rate of the PILS sample solution using Equation (2).

$$C_i = \frac{c_i}{W_{sol}} \frac{1}{W_{Air}} \quad (2)$$

where $\mathbf{C_i}$ (ng/m^3) is the ambient concentration of the ith element, $\mathbf{c_i}$ (µg/L) is the concentration of the ith element measured by FS-ICP-MS, $\mathbf{W}_{sol}$ (0.3 mL/min) is the flow rate of the solution at the inlet of FS-ICP-MS, and $\mathbf{W_{Air}}$ (m^3/min) is the airflow rate sampled by the PILS.

It is worth noting that on-line filtration reduces the variability of filtration blanks. Furthermore, since the working of the ICP-MS instrument is similar to a chromatographic detector, the limits of detection (LODs) and quantification (LOQs) of FS-ICP-MS can be calculated based only on the instrument's background noise, as in chromatographic analysis. The limit of detection (LOD) and limit of quantification (LOQ) for each element were calculated as three and ten times the background noise of the blank solution, respectively.

In Table 2, we report the LOD_S and LOQ_S of each element obtained by both conventional and FS measurements of the operative blanks. It can be seen that the results obtained with the new FS are significantly better than those obtained with the conventional off-line measurements and complies with the environmental monitoring criteria of most of the elements (Canepari et al., 2014).

Table 2: *LODs and LOQs (ng/m^3) for ICP-MS analysis of PILS samples obtianed by conventional measurements (off-line addition of HNO_3 and filtration) and by optimized flow system line.*

	On-line Coupling		**Off-Line measurements**	
	LOD ng/m^3	**LOQ ng/m^3**	**LOD ng/m^3**	**LOQ ng/m^3**
Li	0.2	0.5	0.5	2
Na	30	90	320	920
Mg	5	20	40	190
K	180	460	2000	3700
Ti	0.4	1	2	9
V	1.8	9	14	50
Cr	46	90	18	180
Mn	0.4	1	18	28
Co	0.1	0.3	0.5	0.9
Ni	0.9	2	14	37
Cu	3	9	14	32
Zn	14	46	180	1400
As	0.1	0.5	4	18
Rb	0.1	0.5	37	92
Sr	5	2	18	46
Zr	0.1	0.4	0.1	0.5
Mo	0.2	0.5	0.4	0.9
Cd	0.1	0.4	0.5	1
Sn	0.2	0.5	0.1	0.4
Sb	0.2	0.5	0.9	2
Te	0.1	0.5	0.3	0.9
Cs	0.0	0.1	0.1	0.2
Ba	3	9	9	37
Tl	0.0	0.2	0.1	0.4
Pb	0.3	0.9	14	40
Bi	0.1	0.4	0.2	0.5

Application of on-line PILS-FS-ICP-MS to identify the elemental source profiles.

The optimised FS was applied to determine the source profiles of five different sources, selected from among the indoor and outdoor PM sources of environmental interest.

Figure 3 shows the results obtained for cigarette smoking, one of the sources considered in this study. The upper panel of the figure reports PM10, PM2.5, and PM1 mass concentrations measured by the OPC, while the other two graphs (Figure 3, lower panels) show the results obtained using the optimised PILS-FS-ICP-MS system for two of the most common source tracers used for this type of source (Canepari et al., 2008, 2009, 2010). The OPC results show that almost all the emitted particles are in the fine mode, as expected for particles emitted from a combustion source. The source profiles of the two elements can be superposed to the source profiles obtained by the OPC. This confirms the good behaviour of these two elements as tracers.

In this study, PM samples from each source were analysed in triplicates. As can be seen in Figure 3, the repeatability of the optimised system is good. Several elements (Li, Na, Mg, Al, Mn, Zn, Sr, Cd, Sn, Sb, Tl, Cs, Tl, and Pb) were present in detectable concentrations in cigarette smoke and showed behaviour very similar that of K and Rb.

The elemental profiles were obtained as the mean value of the ratio of the concentration of each element analysed by the PILS-FS-ICP-MS coupled system to the mass concentration of PM10 estimated by the OPC. The results obtained for the selected PM sources are reported in Table 2. It can be noted that the obtained source profiles have good repeatability and include macro and microelements.

Each elemental profile was characterised by different elemental compositions depending on the type of source. The elemental profiles of cigarette smoking, pellet combustion, and brushwood combustion sources were characterised by very high concentrations of K. Relatively high concentrations of Rb and Li were also present, especially in cigarette smoke. Furthermore, it is important to note the presence of toxic elements such as Cd, Tl, Sn, and Pb in PM from all the sources tested. The combustion of incense also releases particles that are rich in K and Rb, even though its source profile was characterised by higher concentrations (almost twice the concentrations in cigarette smoke) of toxic elements such as, Cs, and Cd. The resuspension of road dust has a source profile that is completely different from that of the other sources; a predominance of elements that are usually present in greater quantity in the crust (Li, Al, Ti, Sr As, Co, Mn, V, Cr, and Zn) can be noted. However, the presence of Ni, Fe, and Pb confirms that this source profile is influenced by elements that are usually present in brake pads.

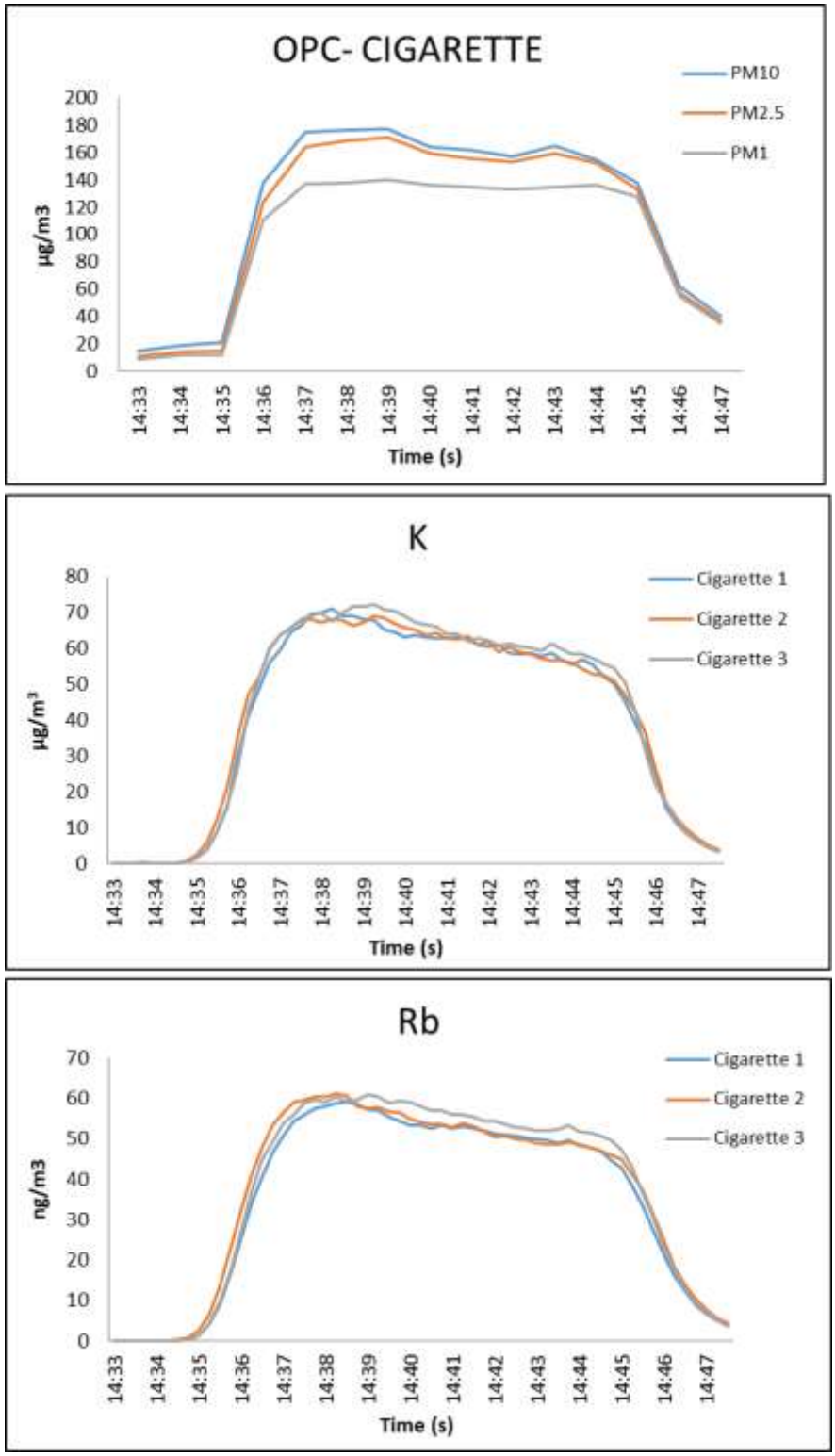

Figure 3: *OPC concentration of PM_{10}, $PM_{2,5}$, PM_1 (panel upper) and K and Rb concentration (panel lower) obtained during reproduction of smoke cigarette source with PILS/ICP-MS coupling.*

Table 3: Average and Standard Deviation of the five analysed sources

	Cigarette		**Incense**		**Pellet**		**Wood**		**Road Dust**	
mg/kg	Average	Dev. Std.	Average	Dev. Std.	Average	Dev. Std.	Average	Dev. Std.	Average	Dev. Std.
Li	39	1	*<LOD*	-	*<LOD*	-	6.2	0.1	6.0	0.2
Na	4900	110	2021	60	1500	3	6100	90	21000	390
Mg	190	10	86	7	90	1	150	3	2110	12
Al	96	2			200	6	160	1	378	2
K	238700	6700	99951	110	50900	656	111290	1500	5434	39
Ti	*<LOD*	-	*<LOD*	-	*<LOD*	-	*<LOD*	-	6.0	0.1
V	*<LOD*	-	*<LOD*	-	*<LOD*	-	*<LOD*	-	2.1	0.1
Cr	*<LOD*	-	*<LOD*	-	*<LOD*	-	*<LOD*	-	10	1
Mn	3.6	0.3	7.5	0.2	9.1	0.2	14	1	113	8
Co	*<LOD*	-	*<LOD*	-	*<LOD*	-	*<LOD*	-	7.3	0.2
Ni	*<LOD*	-	*<LOD*	-	*<LOD*	-	*<LOD*	-	30	3
Cu	14	0.1	*<LOD*	-	34	1	31	2	50	4
Zn	304	11	301	4	362	2	721	10	300	6
As	*<LOD*	-	30	1	*<LOD*	-	*<LOD*	-	3.0	0.2
Rb	229	24	548	35	95	2	625	6	10	1
Sr	2.3	0.1	*<LOD*	-	16	1	5.0	0.2	250	5
Zr	*<LOD*	-	*<LOD*	-	*<LOD*	-	*<LOD*	-	1.4	0.3
Mo	*<LOD*	-	2.5	0.1	0.79	0.01	*<LOD*	-	5.0	0.5
Cd	25	1	49	2	32	1	26	3	4.3	0.7
Sn	4.6	0.2	3.4	0.2	4.2	0.2	5.5	0.4	4.0	0.6
Sb	0.63	0.02	2.0	0.1	*<LOD*	-	*<LOD*	-	3.9	0.7
Te	4.9	0.1	*<LOD*	-	*<LOD*	-	*<LOD*	-	*<LOD*	-
Cs	1.2	0.1	18	2	1.2	0.3	40	1	0.21	0.05
Tl	3.1	0.1	8.7	0.3	1.5	0.2	8.2	0.2	0.041	0.003
Pb	10	1	13	2	51	3	40	1	3.0	0.1
Bi	*<LOD*	-	2.9	0.50	3.0	0.4	1.5	0.1	0.84	0.04

Application of off-line FS-ICP-MS to outdoor and indoor samples collected by PILS

The last part of this study concerns the application of the optimised system to indoor and outdoor monitoring campaigns of two houses located in a peri-urban area (near Rome, Italy). One of the houses used a pellet stove for heating while the other used a wood burning Thermo-fireplace. The pellet stove and Thermo-fireplace cleaning activities were monitored in the respective houses and the burning of brushwood was monitored in the outdoor environment of the two houses. These events of short duration were monitored by the PILS with a time-resolution of 10 min and was complemented by the OPC measurements. Air samples (both outside and inside the house) were collected before each monitored activity (by both the PILS and OPC) in the absence of spot sources (environmental background values).

Figure 4 shows the concentrations of PM and some elements (Rb, K, As, Cd, and Pb) measured during the considered indoor spot events (cleaning of the Thermo-fireplace and cleaning of the stove pellet) and outdoor spot event (agricultural waste burning). As can be noted in Figure 4, during the cleaning of the stove pellet, (ash and residues were removed by an ash cleaner without abatement filter) dust concentrations reached remarkably high values (exceeding 1000 μg/m3). The OPC result showed that the increase in the dust concentration was more marked in the PM10 fraction; however, this event also had a very marked effect on PM2.5 concentration (up to about 543 μg/m3), indicating that the pellet ashes remaining inside the stove also contain fine particles. Figure 4 shows a significant increase in K, Rb, Cd, As, and Pb concentrations during this event. The concentrations of other elements (Li, Ti, Mn, Cu, Sr, Mo, Sn, Sb, and Te) were characterised by similar time trends. These measurements suggest that the pellet stove cleaning event significantly influences the indoor air quality and releases particles containing many heavy metals.

The thermo-fireplace was cleaned by manually removing the residual ash. Increase in the PM10 concentration was observed (up to about 100 μg/m3). The increase was however much lower than that observed in the case of pellet stove cleaning. Consequently, the elemental analysis of PM sampled by the PILS showed a lower concentration of heavy metals. The most significant increase in elemental concentrations occurred for Mg, K, Mn, Rb, Sr, and Pb. Variation in the elemental profiles of these two indoor sources is probably due to the concentration of impurities contained in the fuel, which is evidently higher in pellets. It is also worth noting that in this case almost all the dust particles were confined in the coarse fraction (PM2.5 concentration was lower than 12.5 μg/m3).

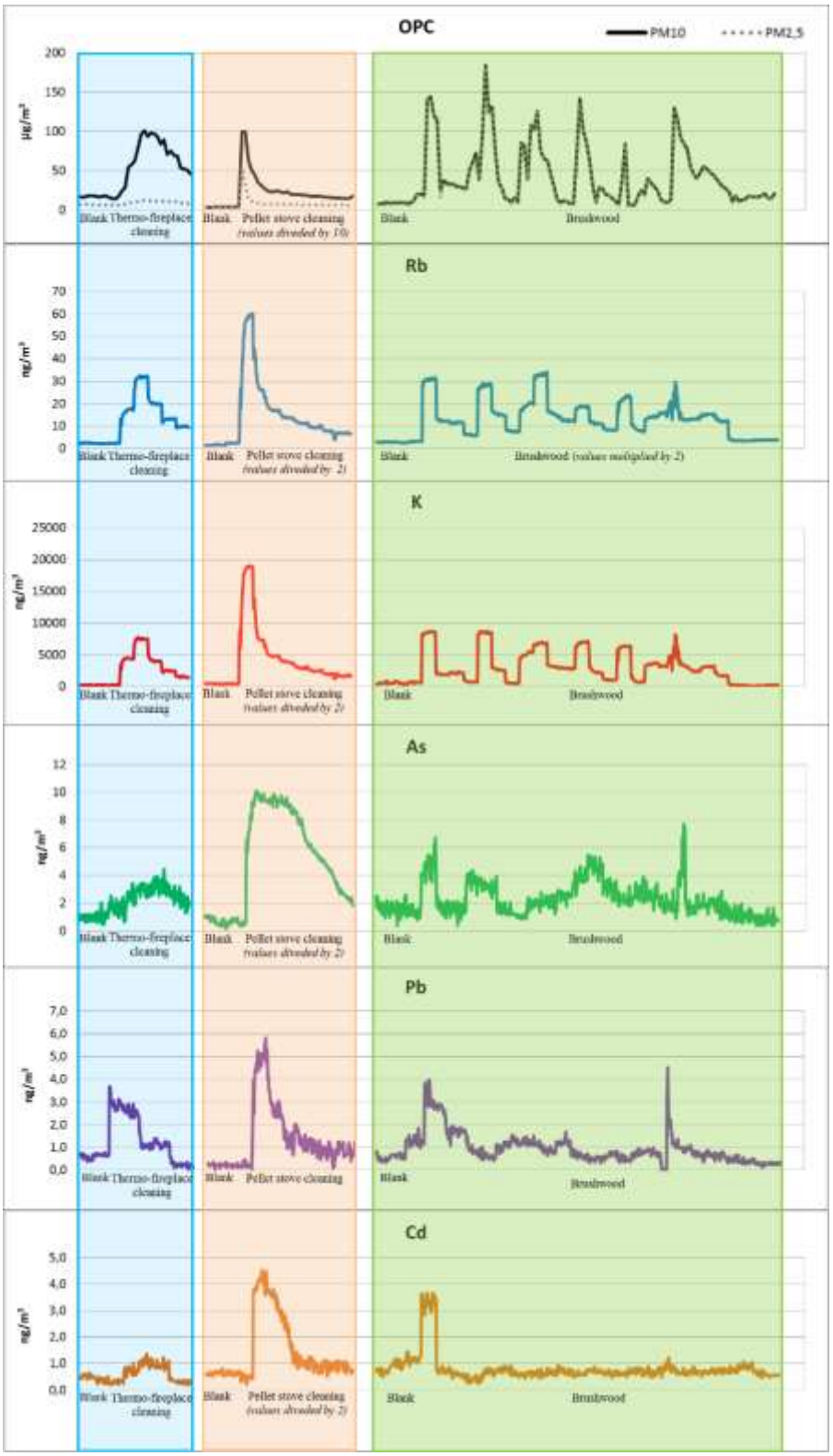

Figure 4: *Mass concentration of PM_{10} and $PM_{2,5}$ (OPC; 1 min time resolution) and of Rb, K, As, Pb and Cd (PILS collection and off-line FS-ICP-MS analysis; 10 min time resolution) measured during spot events in indoor and outdoor environments.*

Events of agricultural waste materials combustion (prunings, dry grass, etc.) that occurred in close proximity (about 30 m) of the houses were also monitored by the OPC and PILS. Despite to the easier dispersion of PM in the outdoor environment than in the indoor environment, the plume that was clearly detected by the OPC showed a series of PM2.5 concentration peaks when the monitored site was downwind of the fire. Elemental analysis of the samples collected by the PILS allowed concentration peaks of some elements to be as well detected during the passage of plumes. Concentrations of K and Rb were highly influenced by the burning of agricultural wastes; however, significant increases in As, Mn, Ni, Cu, Zn, Cd, Sr, and Pb concentrations were also registered. It is worth noting that the different trends in the elemental concentrations indicate a highly heterogeneous dust composition, which is reasonably influenced by the great variability in the composition of the burnt materials.

Conclusions

The optimised FS for on-line acidification and filtration of the samples collected by the PILS allows ICP-MS multi-elemental analysis with very low LODs and LOQs. The system may be easily assembled in any analytical laboratory and permits the simultaneous analysis of several elements in the samples collected by the PILS without any pre-concentration. Thus, it represents a cheap alternative for the time-resolved analysis of pseudo-total elemental concentrations in PM.

In this study, the FS was used to directly couple the PILS and ICP-MS instrument in order to obtain, by very simple and quick experiments, the elemental profiles of some indoor and outdoor sources of environmental interest, such as cigarette smoking, wood, pellet, and incense burning, and road dust resuspension.

Due to the great versatility of the PILS, which may be easily coupled with an auto-sampling system in order to collect samples for off-line analysis, the FS-ICP-MS system was also successfully applied for short-term indoor and outdoor monitoring campaigns. This allowed us to study indoor ambient air emissions of significant concentrations for different toxic elements such as, Cd, and Pb during the cleaning operation of technologically advanced domestic biomass burning systems (pellet stoves and thermo-fireplaces). It was also possible to assess the release of PM containing significant concentrations of toxic elements during the combustion of agricultural wastes, which is an illegal activity but frequently practiced in many rural areas.

*2.5.2 Improved time-resolved measurements of inorganic ions in Particulate Matter by PILS-IC integrated with a sample pre-concentration system**

INTRODUCTION

Measuring the chemical composition of atmospheric particulate matter (PM) at high time resolution is an exciting challenge in atmospheric pollution research. Time changes in PM concentration and composition depend on the variations in the pollutant mass amount released in the atmosphere as well as in the air volume available for its dispersion (mixing properties of the atmosphere). These variations are generally fast (minutes/hours) and cannot be caught by the traditional PM measurements, carried out on a 24-h sampling basis. Particularly in the case of sporadic events, such as long-range transport from neighboring countries or local occasional emissions, time-integrated measurements may lead to a loss of information about the behavior of individual PM sources. The identification of these events, in fact, requires a synchronization of PM composition data with meteorological data (mainly wind direction and velocity), that are easily available at high time frequency.(Wittig et al., 2004; Lee, et al., 2008; Gao, et al., 2011; Wu, et al., 2006). For a time-resolved determination of PM components it is generally possible to sample on filter media; by using this technique, the time resolution can reach 2-3 hours in moderately polluted atmospheres (Perrino, et al., 2010). However, this method is time-consuming and expensive; in addition, significant analytical uncertainties due to filter blanks may be introduced, particularly in the case of low concentrations. As regards the determination of soluble inorganic ions, an essential issue in studies about secondary pollution, the use of filters also favors the occurrence of sampling artifacts due to the interaction between gaseous and particulate species (e.g. nitric acid and sodium chloride) and to the volatilization of semi-volatile species (ammonium nitrate and ammonium chloride) (Tsai, et al., 1998; Chow, et al., 2005; Yu, et al., 2006; Vecchi et al., 2009). These sampling artifacts can be efficiently reduced by using diffusion lines, that is a number of diffusion denuders and a filter pack set in series, but the use of this technique increases laboratory work and analytical costs even more (Allegrini, et al., 1994; Perrino, et al., 2001).

*Published on *Aerosol Science and Technology* in 2015.

Perrino, Cinzia, et al. (2015). Improved Time-Resolved Measurements of Inorganic Ions in Particulate Matter by PILS-IC Integrated with a Sample Pre-Concentration System. *Aerosol Science and Technology* 49.7, 521-530. DOI: 10.1080/02786826.2015.1047821.

During the last decade several devices aimed to continuously collect and analyze atmospheric particles on a short time-scale (from seconds to few minutes) have been developed. These techniques do not involve sampling on filters and are thus free from the above sampling artifacts.

To name some, the steam-jet aerosol collector (SJAC, Khlystov, et al.,1995**)**, the aerosol mass spectrometer (AMS,) Jayne, et al., 2000; Allan, et al., 2003**)**, the flash volatilization nitrate monitor (R&P8400N, Stolzenburg, et al., 2000), the ambient ion monitor - ion chromatograph (AIM-IC, Markovic, et al., 2012**)**, the particle-into-liquid sampler coupled with ion chromatograph (PILS-IC, Weber, et al., 2001). PILS-IC is one of the most used device for on-line measurement of water-soluble inorganic ions in PM. Briefly, the air flow is denuded of gaseous species and aerosol particles are grown up in a saturated water vapor chamber up to form droplets that are collected by inertial impact on a collection plate. The plate is then washed by deionized water and the resulting solution is directly analyzed for anions and cations by two ion chromatographs, allowing the simultaneous analysis of Na^+, NH_4^+, K^+, Mg^{2+}, Ca^{2+}, Cl^- ,NO_2^-, NO_3^- and SO_4^{2-}, in about 15 minutes (Weber, et al., 2001 Orsini, et al., 2003). The analytical performances of the PILS-IC in its original set-up are affected by two main limitations. First, the dilution of the sample by the washing solution leads to high detection limits, which make the system unsuitable for low polluted areas (Wang, et al., 2013). Most important, the time coverage is low, as only the sample amount contained inside the loop at the time of the injection is analyzed, while the sample amount collected during the time of the analysis is discarded. Depending on the loop capacity, the time coverage is about 2-5 minutes per hour. We report here the optimization and the validation of a PILS-IC integrated with an automated pre-concentration system (pcPILS-IC) for the semi-continuous analysis of the inorganic ions in PM. In order to decrease the detection limits and increase the temporal coverage of the acquired data, the original instrument has been modified by adding two ion-exchange cartridges enriching the sample during the period of the IC analysis. The optimized system has been then used in the field during a short intensive measurement period organized in the framework of the EMEP program (Co-operative programme for monitoring and evaluation of the long-range transmission of the air pollutants in Europe) and conducted at a peri-urban site near Rome, Italy (Montelibretti, EMEP site IT01). In order to evaluate the analytical reliability of the modified PILS-IC, the results were compared with those obtained by two additional methods: an High-Resolution Time-of-Flight Aerosol Mass Spectrometer (HR-TOF-AMS) and a denuder-filter pack assembly (diffusion line), working at 5-min and 3-h time resolution, respectively.

EXPERIMENTAL

PILS-IC system

The schematic assembly of the PILS-IC used in this study is reported as Appendix (C1). Ambient air was sampled through a polyethylene cyclone with 2.5 µm cut-off at the flow rate of 15 L min^{-1}. In order to avoid the interference of gaseous species (HCl, HNO_2, HNO_3, SO_2, NH_3), two annular diffusion denuders were inserted in the sampling line, downstream of the cyclone. The denuders, made of pyrex glass, were 200 mm in length, 33 and 30 mm in outside and inside diameter, respectively. The first denuder, for the removal of acid gases, was coated with 1% Na_2CO_3 + 2% glycerine in ethanol-water solution (50:50); the second one, for the removal of ammonia, was coated with 1% H_3PO_4 in the same solution. At the operative flow rate, the removal efficiency of these annular denuder is better than 95% (Allegrini, et al., 1994; Allegrini, et al., 1987; Perrino, et al., 1990). Loading capacity of each denuder is above 1 mg, so they could be substituted every 3 days (Perrino, et al.,1999). Downstream of the denuder, the air sample entered the PILS (Metrohm AG, Herisau, Switzerland). In a condensation growth chamber, atmospheric particles were mixed with a supersaturated steam and grew into droplets large enough to be collected by an impactor. A water solution was introduced at the top of the impactor plate and transported the droplets down to its base, then through a system able to remove the air bubbles from the liquid stream and finally to the sampling loop of the IC system. The water solution was spiked with 50 µg/L of LiBr (© Merck KGaA, Darmstadt, Germany) used as internal standard. All the solutions entering and exiting the PILS were managed by a single 8-channel peristaltic pump (model 205S, Watson-Marlow Inc., Wilmington, MA, USA) run at a speed of 24 RPM; the operative flow rates are reported in Appendix (C2).
Cations were analyzed by a Dionex DX-120 equipped with an ION-PAC CS12A column; anions were determined by a Dionex ICS-1000 equipped with an ION-PAC AS12A column (Thermo Fisher Scientific Inc. Waltham, MA, USA) The eluent phases were methansulfonic acid 0.1M for cations and Na_2CO_3/$NaHCO_3$ 0.5M/0.5M for anions.

Pre-concentration system.

The connection between PILS and ICs is usually performed by two 6-way valves complemented with two capillaries (sample injection loops). In this work (Figure 1) the loops were replaced with two cartridges packed with ion-exchange resins (ION-PAC CG12A for cations and ION-PAC AG12A for anions, Thermo Fisher Scientific Inc., Waltham, MA, USA). During the *load* phase (configuration as in Figure 1a) the ions collected by the PILS were retained in the cartridges; during the *inject* phase

(configuration as in Figure 1b) the ions were eluted, in back-flush, and directly transported to the chromatographic column. The solutions used to elute the cartridges were the same used for the IC analysis. The automatic positioning of the valves in the *load* and *inject* configurations was managed by the Chromeleon 7.2 Chromatography Software (Thermo Scientific™ Dionex™ Chromeleon™ 7.2 Chromatography Data System).

The introduction of the pre-concentration cartridges made it possible to extend the *load* phase to include also the time duration of the analysis, so as to collect a significant sample amount that in the original setup of the PILS-IC would have been lost. In this configuration the sample is lost only during the *inject* phase, when the solution from the PILS is directed to the IC drains.

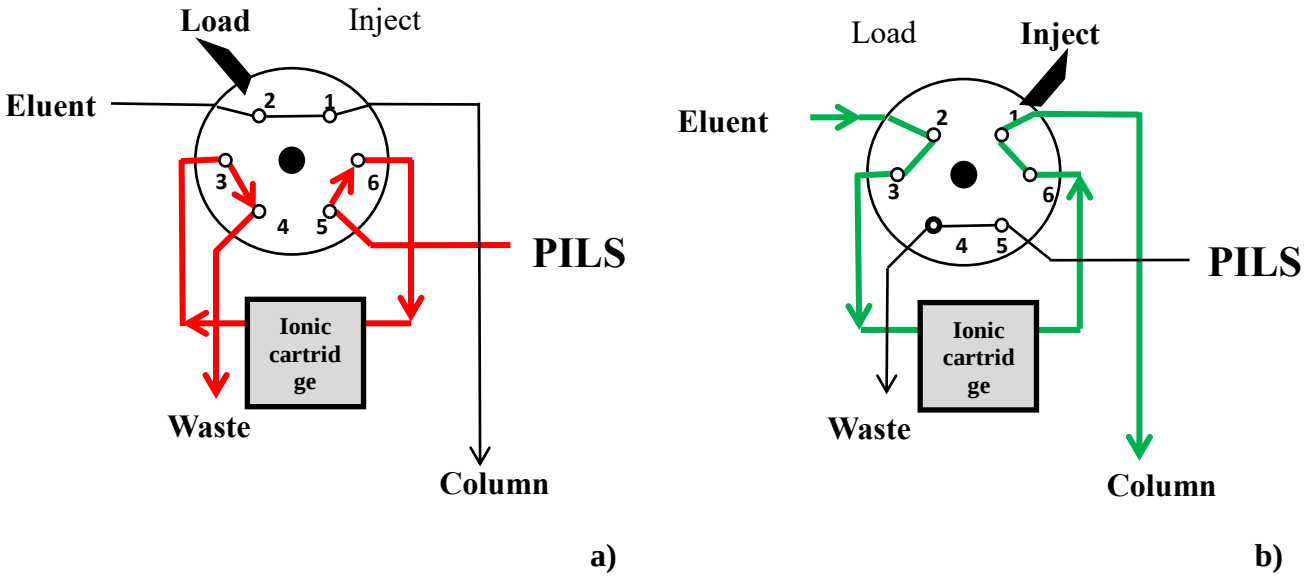

Figure 1: *Schematic diagram of the 6-way valve and of the cartridge used for sample pre-concentration and injection.*

The *load* time was set to 12 minutes, which was the minimum time needed to acquire a complete chromatogram for both anions and cations. The *inject* time was evaluated by connecting the loaded cartridges directly to the IC detector and by measuring the elution time of the resulting single broad peak. A quantitative (98%) elution of the ionic species from the cartridge was obtained after 3 min. In summary, the addition of the described pre-concentration system led to a significant gain in the measurement time coverage, which increased from 2 minutes per hour of the traditional PILS-IC (considering a sampling loop of 150 µL) to 48 minutes per hour of the pcPILS-IC.

Sampling site and additional instrumentations

The field performance of the pcPILS-IC was evaluated during one of the intensive measurement periods organized by the EMEP Task Force on Measurement and Modelling (http://www.nilu.no/projects/ccc/tfmm/index.html). Measurements were carried out from January 30th to February 10th, 2013 at the facilities of C.N.R. Institute of Atmospheric Pollution Research in Montelibretti, a peri-urban area about 25 km from Rome (EMEP site IT01, 42°06'13.2"N, 12°37'48.0"E, 48 m a.s.l.). Ancillary measurements included the main meteorological parameters (wind speed and direction, temperature, atmospheric pressure, relative humidity, rain amount) and the natural radioactivity due to the short-life beta-decay products of Radon, determined by means of an automated monitor operating over a 1-h time basis (PBL Mixing Monitor, FAI Instruments, Fonte Nuova, Rome, Italy). Natural radioactivity has been proved to be a reliable good proxy of the mixing properties of the lower boundary layer and a valuable tool for the interpretation of pollution events (Perrino, et al., 2001; Perrino, et al., 2009; Vecchi, et al.,2004; Canepari et al., 2014) In addition to pcPILS-IC, the measurement of inorganic ions was carried by two other systems working at high temporal resolution: a High-Resolution Time-of-Flight Aerosol Mass Spectrometer (HR-TOF-AMS, De Carlo, et al.,2006) and a diffusion line (diffusion denuders-filter pack assembly, Perrino, et al.,1990; Perrino, et al.,1999, Perrino, et al., 2001).The HR-TOF-AMS (Aerodyne Research Inc., Billerica, MA, USA) provides size-resolved chemical analysis of the non-refractory species (at 600°C, operating temperature of the vaporizer) in submicron particles (sulphate, nitrate, ammonium, non-sea-salt chloride and organics). The concentrations reported in this work were acquired by the HR-TOF-AMS, operating in "V" ion path modes (higher sensitivity, lower mass resolution), every 5 min. The characterization of the chemical speciation and of the size distribution were coupled by analysing the particle time-of-flight (Allan, et al.,2003). The AMS has a default collection efficiency of about 50% due to the transmission characteristics of the standard aerodynamic lens (Liu, et al., 2007). The experimental collection efficiency was estimated using the denuder results and applying the procedure described by Middlebrook and co-workers (Middlebrook, et al., 2012). All data were analysed using the standard AMS software SQUIRREL v1.53 within Igor Pro 6.2 (WaveMetrics Inc., Lake Oswego, OR, USA). The concentrations obtained by the AMS were corrected for the experimental collection efficiency and averaged over the pcPILS-IC sampling periods. Diffusion lines have been used at the EMEP station of Montelibretti since 1994 (http://www.nilu.no/projects/ccc/index.html). They are comprised of five annular denuders set in series: two coated with NaF (0.05% in ethanol-water solution 80:20), two with Na_2CO_3 and glycerol

(1% + 1% in ethanol-water solution 50:50), one with H_3PO_3 (1% in ethanol-water solution 80:20). The denuders are followed by a cyclone (cut size of 2.5 μm at the operative flow rate of 15 L min^{-1}) and by a filter pack comprised of one Teflon filter, one Nylon filter and one paper filter impregnated with the same H_3PO_3 solution used to coat the fifth denuder. This sampling line allows the determination of hydrochloric acid, nitric acid, nitrous acid, sulphur dioxide and ammonia in the gaseous phase, chloride, nitrite, nitrate, sulphate, ammonium, sodium, calcium, potassium and magnesium in the particulate phase (coarse and fine fractions). In particular, the configuration of the filter-pack is devised in order to take into account nitric acid, hydrochloric acid and ammonia possibly evolved from ammonium nitrate and ammonium chloride particles retained on the Teflon filter (HCl and HNO_3 are retained by the nylon filter, NH_3 is trapped by impregnated filter). The removal of the gaseous species on the denuders allows a correct discrimination between the gaseous and the particulate phases. Details about the rationale for the choice of the denuder coatings are reported in Perrino and coworkers (Perrino, et al.,1990). Diffusion lines are generally operated for 24 hours; for this inter-comparison with pcPILS-IC and HR-TOF-AMS during the first three days (January 30th – February 1st) the sampling duration was decreased to 3 hours, while the original 24-h sampling duration was kept for the rest of the period.

RESULTS and DISCUSSION

Optimization of the pcPILS-IC

The analytical performances of the pre-concentration cartridges were evaluated by performing cartridge breakthrough volume tests, cartridge recovery tests, calibration of the whole system.

Breakthrough volumes and recoveries

To calculate the breakthrough volumes of the pre-concentration cartridges (i.e. the volume of solution above which the ion is no more retained because of the saturation of the ion-exchange resin) standard solutions of anions (Cl^-, NO_2^-, NO_3^-, Br^-, SO_4^{2-}, 100 μg L^{-1}) and of cations (Li^+, Na^+, NH_4^+, K^+, Mg^{2+}, Ca^{2+}, 100 μg L^{-1}) were introduced by means of a peristaltic pump into the anionic and cationic cartridge, respectively. The outgoing solutions were collected in aliquots of 5 mL and analyzed by IC. The results are reported in Table 1. As the cartridges are functionally similar to the columns used for IC analyses, the species are released from the cartridges in the same order as the chromatographic elution. The breakthrough volumes varied from 30 mL (chloride) to 125 mL (bromide); Mg^{2+}, Ca^{2+}, NO_3^- and SO_4^{2-} were still retained in the cartridges after a volume of 250 mL. The loading capacity of the cartridges is satisfactory: considering the operative conditions of the pcPILS-IC and the ion

concentration usually found in the atmosphere, saturation phenomena resulting in analyte loss can be excluded for all ions (the loading capacity for Cl^-, the less retained species, is 3 µg, corresponding to an atmospheric concentration of 17 µg/m^3). Recovery tests were performed by using the same standard solutions. For each ion, the recovery was calculated as the ratio between the amount loaded into the cartridge and the amount eluted by the cartridge after 3 minutes, at the flow rate of 1.2 ml min^{-1} (operative conditions of the system). Per cent recoveries are reported in Table 1. Values above 95% were obtained for all the considered species, with a repeatability ranging from 2% to 12%.

Table 1. *Analytical performances of the pre-concentration cartridges (break-through volume, capacity and recovery percentage); Limit of Detection (LOD) and Limit of Quantification (LOQ) of the pc-PILS-IC and the PILS-IC (N=6).*

	Cartriges performances			**pcPILS**		**PILS**	
	Breakthrough (mL)	**Capacity (µg)**	**R ± SD (%)**	**LOD (µg/m^3)**	**LOQ (µg/m^3)**	**LOD (µg/m^3)**	**LOQ (µg/m^3)**
Br^-	120	12	99±4	-	-	-	-
Li^+	25	2.5	98±2	-	-	-	-
Cl^-	30	3.0	101±6	0.01	0.02	0.02	0.04
NO_2^-	65	6.5	97±4	0.001	0.002	0.01	0.03
NO_3^-	65	6.5	100±2	0.003	0.005	0.05	0.08
SO_4^{2-}	>250	>25	96±3	0.02	0.04	0.2	0.6
Na^+	50	5.0	98±2	0.01	0.01	0.02	0.03
NH_4^+	70	7.0	101±3	0.007	0.01	0.1	0.2
K^+	85	8.5	96±6	0.005	0.007	0.07	0.1
Mg^{2+}	>250	>25	99±8	0.01	0.02	0.1	0.3
Ca^{2+}	>250	>25	97±12	0.02	0.04	0.3	0.6

Calibration of the pcPILS-IC and calculation of the atmospheric concentration

The calibration of the system was carried out by introducing the standard solutions of anions and of cations directly into the 6-way valves equipped with the cartridges, by using a peristaltic pump. The amount (μg) of each ion retained by the cartridge (*load* phase) and then injected into the chromatographic system (*inject* phase) was calculated by measuring the solution volume eluted from the cartridge. The correlation between the injected amounts and the measured areas were linear for all the considered ions up to a concentration of 100 μg/L. In all cases Pearson coefficients were higher than 0.95.

In the field application of the pcPILS-IC, the sample collected by washing the impactor plate is partitioned into five lines: two of them are connected to the injection systems of the ICs, three are directed to the waste (see SC1). As the partitioning among these five lines cannot be accurately controlled, the sample volumes introduced into the two cartridges during the pre-concentration phase cannot be exactly determined. For this reason, to correctly calculate its air concentrations (*Ci*), the amount of each ion (*Qi*) obtained by the chromatogram has to be corrected by using an internal standard (LiBr). The correction factor was obtained as the ratio between the theoretical amount of the internal standard (Li^+ for cations, Br^- for anions) entering the impact plate during the pre-concentration time ($Q_{IS\text{-}in;}$ calculated by considering Li^+ and Br^- concentrations in the washing solution and its flow rate) and the amount of the same standard measured in each chromatographic run ($Q_{IS\text{-}out}$). This correction factor also takes into account the sample dilution caused by the water condensing on particles in the PILS growth chamber.

The atmospheric concentration (*Ci*, μg/m^3) was then calculated as:

$$C_i = \frac{Q_i}{V} * \frac{Q_{IS\ in}}{Q_{IS\ out}}$$

Where *V* is the air volume (m^3) sampled during the pre-concentration time.

It worth noting that this quantitative procedure introduces some uncertainty due to the progressive deterioration of the peristaltic tube supplying the LiBr solution to the impactor plate. This deterioration originates slight variations in the flow rate and then small differences between the theoretical value of $Q_{IS\text{-}in}$ (calculated by considering the initial flow rate) and its actual value. In this study this problem was managed through a close control and frequent substitution of the peristaltic tube. Anyway, it could be more efficiently solved by replacing the peristaltic pump with a more stable system.

LODs and LOQs

Detection and quantification limits (LODs and LOQs) of the pcPILS-IC were calculated by evaluating the blank values, according to the IUPAC definitions, or the background noise in case the blank values were not detectable (nitrite and nitrate). Operatively, the blank values were obtained by placing a clean filter-pack at the inlet of the system and carrying out the analysis with and without the pre-concentration unit. LODs and LOQs are reported in Table 1. In spite of the broadening of the peaks due to the presence of the pre-concentration cartridge, the values obtained by using the pcPILS-IC were 10-15 times lower than those obtained with the original setup of the PILS-IC. For Na^+ and Cl^- the improvement was lower because of the high blank values in the de-ionized water.

Comparison with denuder-filter pack and HR-TOF-AMS

The results obtained by the pcPILS-IC during the intensive measurement period were compared to the data obtained by a diffusion line and by a HR-TOF-AMS. The good performances of these two techniques have been well documented by comparison with side-by-side online instruments or with off-line filter methods.[2,16] To date, however, none of these systems by itself can be considered as a reliable reference method for the field validation of the pcPILS-IC. Diffusion lines are an effective method for the quantitative determination of inorganic ions without the artifacts due to the solid-vapor equilibrium of ammonium salts, but their typical time coverage (24 h) cannot be decreased below 2-3 hours because of the long analytical work they require and the non-negligible contribution of the blanks. On the other side, the HR-TOF-AMS allows high time-resolution measurements but its results have to be corrected for the collection efficiency.

In this work, we chose to compare the pcPILS-IC results averaged over 3 and over 24 hours with the data yielded by the diffusion lines, in order to evaluate the quantitative response of the pcPILS-IC. To evaluate its behavior at high time-frequency (15 min) we used the data yielded by the HR-TOF-AMS, averaged on the same time duration.

The linear regressions between the results obtained by the diffusion lines (24-h and 3-h) and the pcPILS-IC are reported as Appendix (C3). A good correlation was obtained for all ions (R^2>0.8). In all cases the slope was close to 1, showing a good quantitative agreement between the concentration values measured by the two techniques. Slightly worse results were obtained for chloride and sodium, probably due to the higher blank values of the diffusion denuders, typical of this species, and to a possible release of NaCl used as coating layer in the first two denuders of the diffusion line. Figure 2 shows the temporal pattern of NH_4^+, NO_3^- and SO_4 obtained during the whole intensive measurement

period by the pcPILS-IC and the HR-TOF-AMS. For all three ions the time variability of the measured concentrations were in very good agreement along the whole period (R^2>0.8), confirming the satisfactory performances of the pcPILS-IC in tracing even fine time variations in the concentration of ions.

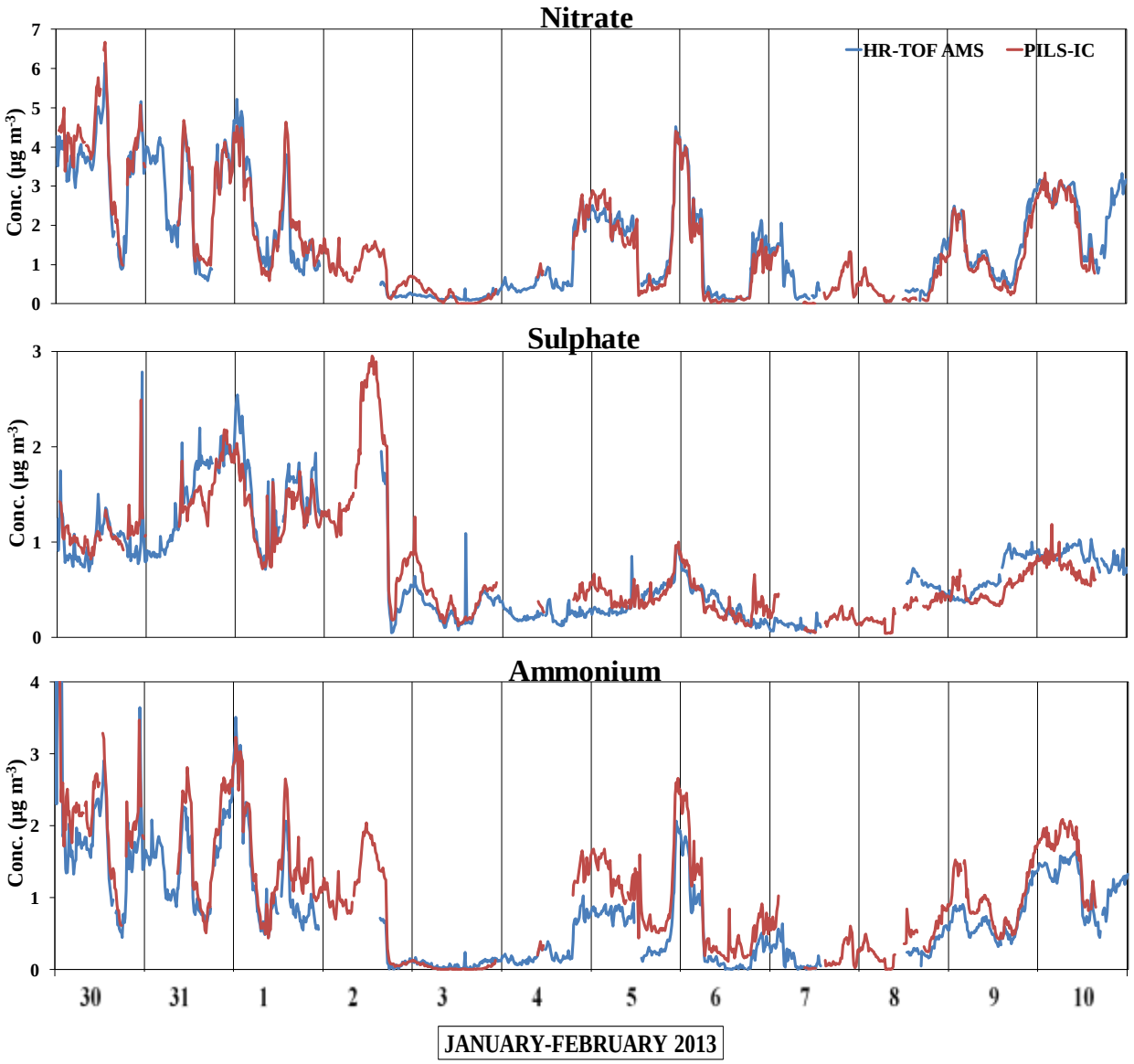

Figure 2: *Comparison of nitrate, sulphate and ammonium concentration as measured by the pcPILS-IC and by the HR-TOF-AMS*

Results of the monitoring campaign.

The ability of the pcPILS-IC to provide reliable data for the interpretation of rapidly changing atmospheric pollution events is discussed on the basis of the results obtained during the intensive field study (January 29th- February 10th). This period was characterized by climatic conditions typical

of the wintertime in Central Italy, with moderately low temperatures and very variable wind speed and direction. For an overall characterization of the period, we report the time pattern of natural radioactivity (Figure 3). This variable allows an overall evaluation of the mixing properties of the lower atmosphere: high values of natural radioactivity indicate a low air volume available for pollutant dispersion, low values indicates efficient atmospheric mixing (by advection or thermal convection, Perrino, et al., 2014; Farao, et al., 2014) Briefly, the typical day-night pattern of natural radioactivity during atmospheric stability periods consists in increasing values from sunset to early morning (nighttime stability) and decreasing values starting from sunrise, with a minimum during the warm hours, due to thermal convection. Atmospheric stability lasting for a number of consecutive days is generally responsible for a remarkable increase in the concentration of atmospheric pollutants, particularly of secondary species. During advection phenomena, instead, natural radioactivity keeps constant low values. The occurrence of advection is generally responsible for a fast change in the air quality that may improve or worsen according to origin of the incoming air masses.

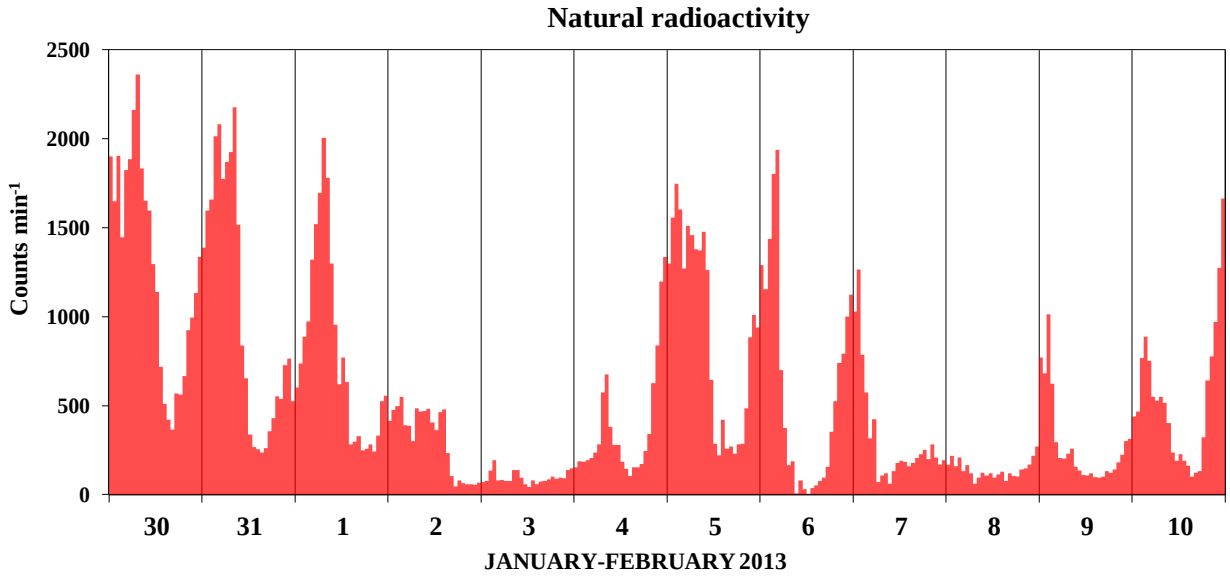

Figure 3. *Time pattern of natural radioactivity during the intensive measurement period.*

The study period can be ideally divided into three sub-periods. The first one, from the beginning of the study to February 1st, was characterised by fog and very stagnant conditions during the night, the early and the late morning. During these three days, especially during the first one, unusually high

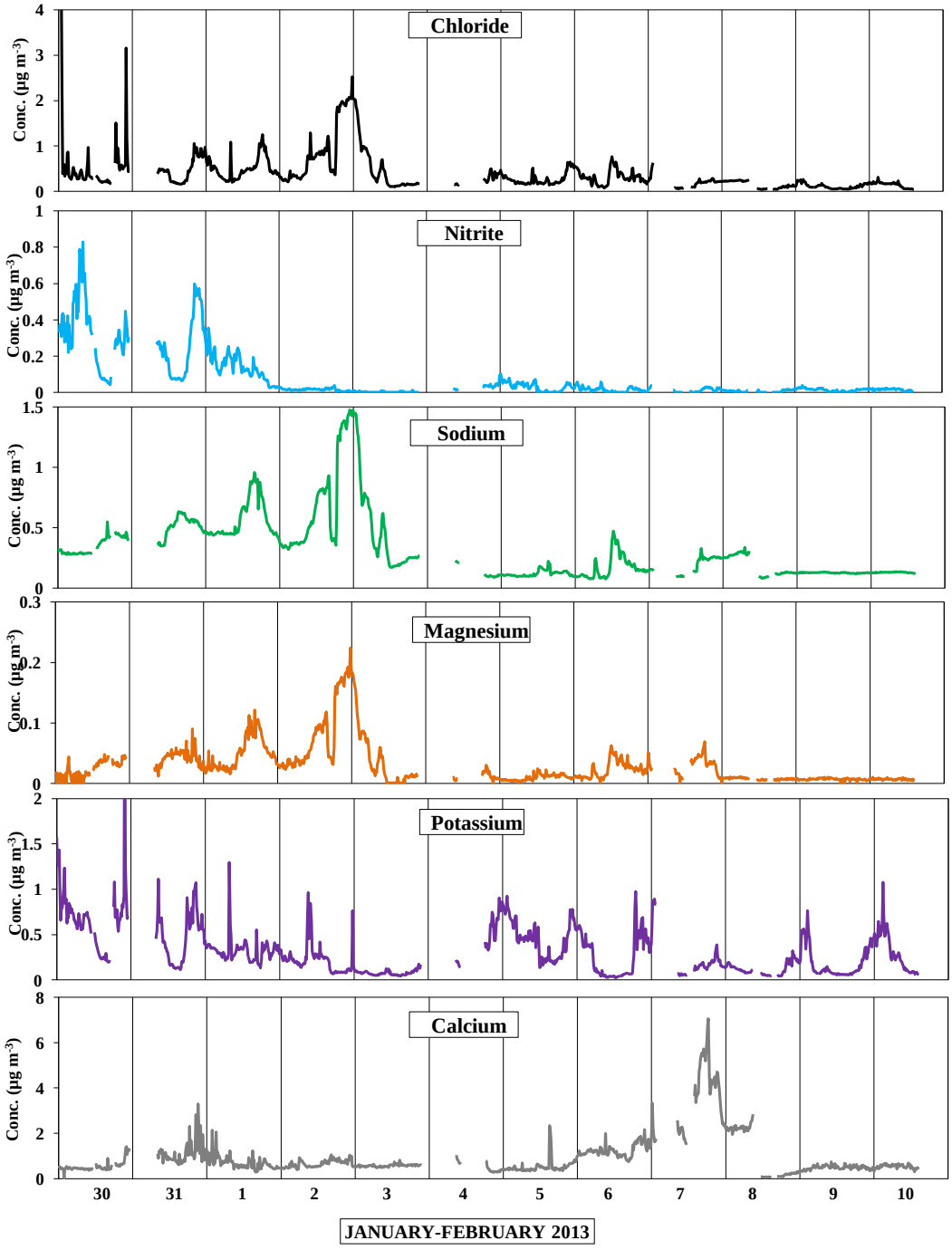

Figure 4. *Time patterns of chloride, nitrite, sodium, magnesium, potassium and calcium determined by the pcPILS-IC.*

values of natural radioactivity were measured during the late morning (until about noon); as a possible explanation, the presence of fog might have been delayed the atmospheric mixing produced by thermal convection. The following sub-period, from the afternoon of February1st to the afternoon of

February 4th, was characterised by advection (constantly low values of natural radioactivity), with wind gust up to 15 m s-1 and daily mean intensity up to 5.8 m s^{-1} on February 2nd. The rest of the study period was generally characterized by night-time stability (with the exception of the night between February 7th and 8th, when the wind increased again) and moderate atmospheric mixing during the day hours. The time patterns of the ion concentrations determined by the pcPILS-IC are reported in Figures 2 and 4. During the first sub-period the most noticeable feature was the simultaneous increase of ammonium and nitrate (R^2>0.86). The concentration of ammonium nitrate followed the pattern of natural radioactivity during the night and was particularly sensitive to the re-stabilization of the atmosphere during the morning hours. During the same days, the results of the pcPILS-IC showed an unusual increase in the concentration of particulate nitrite (up to 0.8 μg/m^3), possibly due to the dissolution of nitrous acid, generated during the night, into the fog droplets.

The second period was characterized by the simultaneous increase of sodium, chloride and magnesium, all tracer of sea-salt. As reported in Figure 5, which refers to February 2nd and 3rd, the concentration of the three sea-salt tracers increased between 9 a.m. and 4 p.m. of the first day, then abruptly decreased and finally increased again around 6 p.m., to keep high values all over the night. It is worth noting that the first of the two peaks was showed also by other ions, particularly by sulfate, while during the second event the concentration of all ions was very low except for the sea-salt tracers. The back trajectories of the air masses, calculated by the HYSPLIT Model (HYbrid Single-Particle Lagrangian Integrated Trajectory, access via NOAA ARL READY Website, http://www.arl.noaa.gov/HYSPLIT.php), reported as appendix (C4), show that the air masses followed two different trajectories: the first one, quite constant in direction until about 5 p.m., was originated from north Africa and travelled over the southern part of the Tyrrhenian Sea; the second one was originated from the area of France. The different origin of the air masses had a clear impact on the air quality at the receptor, as the air masses coming from North Africa were characterized by a poorer quality than those coming from the North, as already observed during a different field study by Perrino and coworkers. During the last part of the period, the time variations in the concentration of ions were driven by the mixing properties of the lower atmosphere. This is particularly true for nitrate, ammonium and potassium, which closely follows the time pattern of natural radioactivity.

In the case of potassium, the agreement with the natural radioactivity pattern indicates that the influence of the local sources was negligible and that diffuse sources were the main responsible for the time variation of its concentration.

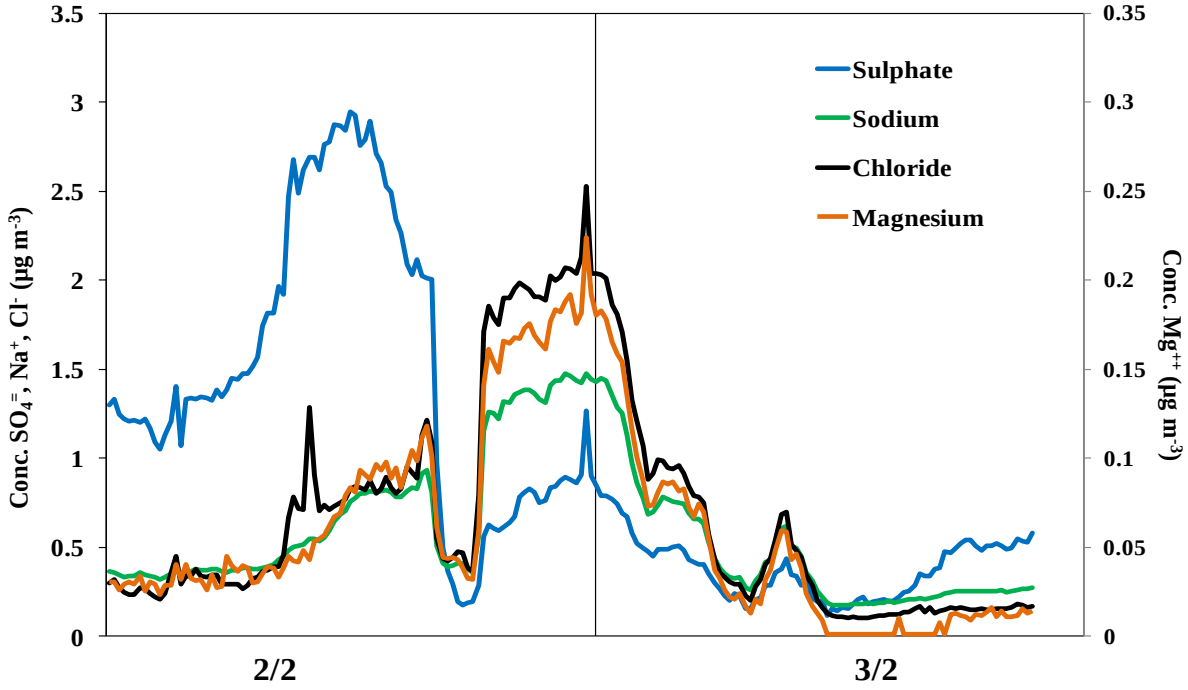

Figure 5. *Time pattern of $SO_4^{=}$, Na^+, Cl^- and Mg^{++} concentration during February 2nd and 3rd.*

As the main winter source of fine potassium is biomass burning, it is reasonable that the residential buildings in the area surrounding the sampling site were responsible for the concentration of this species at the receptor.

CONCLUSIONS

The addition of a pre-concentration step to a PILS-IC allowed a remarkable increase of the time coverage of this online technique (from 2 to 48 min per hour). At the operating conditions, the pre-concentration cartridges showed recoveries above 95% for all the ions and values of the breakthrough volumes high enough to exclude saturation phenomena. Detection limits were 10–15 times lower than those obtained by using the original PILS-IC setup. The modification of the PILS-IC into pc-PILC-IC is very cheap, as it only consists in the substitution of the injection loop of the IC with a commercial pre-concentration cartridge. Further advantages of the system are its flexibility, as its time resolution and sensitivity can be easily tuned by varying the cartridge loading time. A field inter-comparison with a diffusion line showed that the quantitative response of the pcPILS-IC is satisfactory; the very good greement with the time pattern of sulfate, nitrate, and ammonium measured by a HR-TOF-AMS demonstrated that the pcPILS-IC is able to trace fine time variations in the concentration of ions.The use of the modified instrument during a field campaign yielded very reliable results and allowed an accurate interpretation of the air quality variations during the study period.

*2.5.3 Development and field evaluation of an online monitor for near-continuous measurement of iron, manganese and chromium in coarse airborne particulate matter (PM)**

Introduction

The current body of epidemiological studies provides unequivocal evidence for the association between exposure to particulate matter (PM) and increased risk of cardiovascular, neurological as well as respiratory diseases, hospitalization, and premature death (Pope et al. 2002; Pope et al. 2004; Brunekreef and Forsberg 2005; Delfino et al. 2005; Dockery and Stone 2007; Perez et al. 2008; Delfino et al. 2010; Davis et al. 2013; Gauderman et al. 2015). It should be noted that most of these studies have linked the health end-points with PM mass concentrations of airborne PM, however, there is growing evidence highlighting the important role of the chemical composition of ambient PM, rather than simply the mass in driving the health outcomes (Claiborn et al. 2002; Verma et al. 2009). Redox-active transition metals, including iron (Fe), manganese (Mn), and chromium (Cr), are among the few chemical components of ambient PM that studies have documented an association with human health impacts, likely due to their ability to induce oxidative stress (e.g., via the generation of reactive oxygen species (ROS)), which usually occurs as a cascade of events that significantly increases the ROS concentration in the target cells and causes inflammatory responses in cells and tissues (Donaldson et al. 2003; Tao et al. 2003; Delfino et al. 2005; Peters et al. 2006; Li et al. 2009). Therefore, a focus of many recent studies has been on the evaluation of sources, transport, and chemical speciation of these redox-active trace metals (Putaud et al. 2004; Moreno et al. 2006; Pérez et al. 2008; Viana et al. 2008; Putaud et al. 2010; Harrison et al. 2012; Fang et al. 2015). Several studies have also examined the particle-size dependency of oxidative potential and relationship to chemical composition (Tao et al. 2003; Valavanidis et al. 2005; Ntziachristos et al. 2007; Ayres et al. 2008; Miljevic et al. 2010; Shafer et al. 2010; Charrier and Anastasio 2012).Nonetheless, the impact of individual chemical components of PM on the health end-points is still relatively poorly understood; therefore, the development of innovative PM measurement techniques capable of providing high-resolution of chemically-speciated data and their use in concurrent toxicological studies can drastically improve our current understanding of the main PM species driving these health effects (Karlsson et al. 1997; Weber et al. 2001; Wang et al. 2015).

* *Published on Aerosol Science and Technology in 2016:* Sowlat, M. H., Wang, D., Simonetti, G., Shafer, M. M., Schauer, J. J., & Sioutas, C. (2016). Development and field evaluation of an online monitor for near-continuous measurement of iron, manganese, and chromium in coarse airborne particulate matter (PM). *Aerosol Science and Technology*, 50(12), 1306-1319. *DOI:10.1080/02786826.2016.1221051*

These novel techniques will also help improve our understanding of the dynamics of atmospheric PM emission, dispersion, and fate through the provision of data with higher time resolution. In particular, the development of techniques/methods capable of measuring different forms of redox-active metals (i.e., different oxidation states as well as solubility characteristics) would be very important in studying aerosol toxicity. This is because the toxicity of PM-bound metals is significantly impacted by their solubility, with the water-soluble fraction of the redox-active metals better reflecting in many cases the bioavailable pool (Shi et al. 2003; Heal et al. 2005). Additionally, in most cases, the toxicity of these metals, *per se*, is dependent upon their oxidation state (Khlystov and Ma 2006; Majestic et al. 2006; Majestic et al. 2007). Recently, a novel online monitor was developed and successfully applied for the near-continuous measurement of $PM_{2.5}$-associated Fe, Mn, and Cr (Wang et al. 2016). The system comprised of two modules: 1) the PM collection module employing an aerosol-into-liquid collector; and 2) the chemical analysis module employing Micro Volume Flow Cell (MVFC) coupled with spectrophotometry. One of the critical advantages of the developed system over previously available technologies (e.g., aerosol time-of-flight mass spectrometry (ATOFMS) or X-ray-fluorescence (XRF) based technologies) is that it can measure these metals in both total or water-soluble forms, as well as in different oxidation states with a relatively high time resolution (i.e., 2 hr), which can provide crucial information on the biological pathways underlying the adverse health effects, which are mostly speciation-driven (Wang et al. 2016).There has been a variety of novel technologies developed to measure the on-line concentrations metals in the fine PM size fraction, including the particle-into-liquid sampler (PILS) (Weber et al. 2001); the Cooper Xact^{TM} 625 Monitoring System; the AMMS-100 Focused Photonics (Hangzhou), Inc., China; and the semi-continuous elements in aerosol system (SEAS) (Kidwell and Ondov 2001, 2004). Despite the recent development of these high time-resolution measurement methods for $PM_{2.5}$-bound elements, to the best of our knowledge, similar systems have not yet been developed for the measurement of redox-active metals in the coarse PM fraction ($PM_{10-2.5}$, i.e., particles with an aerodynamic diameter of between 2.5 μm and 10 μm) and, therefore, are highly needed. One of the factors hindering the development of such systems for coarse PM is the low solubility of these species in the coarse size range (Birmili et al. 2006; Wang et al. 2013), which limits the ability to accurately measure the total PM-bound concentration of the target metals. A large fraction of many of these metals and trace elements is partitioned in the coarse PM fraction (Allen et al. 2001), which further highlights the need for developing techniques capable of measuring coarse PM-bound redox-active metals with a high time-resolution. Such tools will be crucial in investigations of the health impacts induced by the coarse fraction of PM, as recent studies have indicated significant association between these metals

and the redox activity of coarse PM (Becker and Soukup 2003; Becker et al. 2005; Shafer et al. 2010; Cheung et al. 2011; Cheung et al. 2012; Wang et al. 2015). To address these needs, in the present study, we developed a new technique for near-continuous (i.e., a time resolution of 2 hr) measurement of three coarse PM-bound redox-active metals, namely Fe, Mn, and Cr. Following laboratory characterization, the system was operated in the field from January to April 2016 to assess its performance and reliability with minimum supervision over a relatively long period of time. Additionally, in order to check the validity of the results, the online-measured data were compared with those obtained by means of inductively coupled plasma mass spectrometry (ICP-MS) analysis conducted on filter samples collecting concurrently coarse PM through a parallel sampling system. Finally, in this paper, we present the results of four months of system deployment in the field, enabling us to explore the diurnal concentration profiles of these redox-active metals in ambient coarse PM.

Materials and methods

Reagents and standards

The water used for the collection of ambient coarse PM and system rinsing was produced by a Millipore A-10 water purification system (EMD Millipore, Billerica, MA). All the acids were trace metal grade (VWR). All the chemicals and reagents were prepared in polypropylene laboratory equipment, which were acid-washed (with either 4 M hydrochloric acid (HCl) or 4 M nitric acid (HNO_3) and water-rinsed before use. For Fe, a 1000 ppm stock solution was first prepared gravimetrically from $(NH_4)_2Fe(SO_4)_2$ (ACS) salt, and then diluted to obtained standard solutions in the range of 0-200 ppm. The Fe analytical reagent (i.e., Ferrozine) was prepared by addition of 133 mg of ferrozine (Sigma) to 50 mL of water that contained 65 µL of 4 M HCl (Rastogi et al., 2009). The Fe reducing agent (HA) was prepared by dissolving 19.3 mg of hydroxylamine hydrochloride (HA) solid (Sigma), with a purity of 99.9999%, in 50 mL of water (Majestic et al. 2006). One molar sodium hydroxide (NaOH) solution was prepared from reagent grade NaOH solid (AMRESCO) and was used for pH adjustment. For Mn, a 100 ppm stock solution was first prepared gravimetrically from $MnCl_2$ (ACS) salt, and then diluted to obtained standard solutions in the range of 0-100 ppm. The manganese analytical reagent (formaldoxime; FAD) was prepared by dissolving 20 g of HA in 450 ml of water, followed by the addition of 10 ml of 37% formaldehyde solution, and the solution was then made up to 500 ml with water. As with Fe, 1 M NaOH solution was used for pH adjustment. Both the Fe and Mn stock solutions were acidified to pHs below 1 using a 4 M HCl solution.

For Cr, a 100 ppm stock solution was first prepared gravimetrically from K_2CrO_7 (ACS) salt, and then diluted to obtained standard solutions in the range of 0-100 ppb. In the case of Cr, the stock solution was acidified using 4 M HNO_3. Additionally, in order to prepare the chromium analytical reagent (i.e., diphenylcarbazide, DPC), 167 mg of the reagent was dissolved into 100 ml of acetone. Afterwards, it was mixed with 1.67% H_2SO_4 solution at 1:1 volume ratio (Khlystov and Ma 2006). Finally, 0.143 ml of H_2O_2 was diluted to 100 ml of 0.1 M NaOH solution to prepare the 0.1% H_2O_2 solution.

System configuration

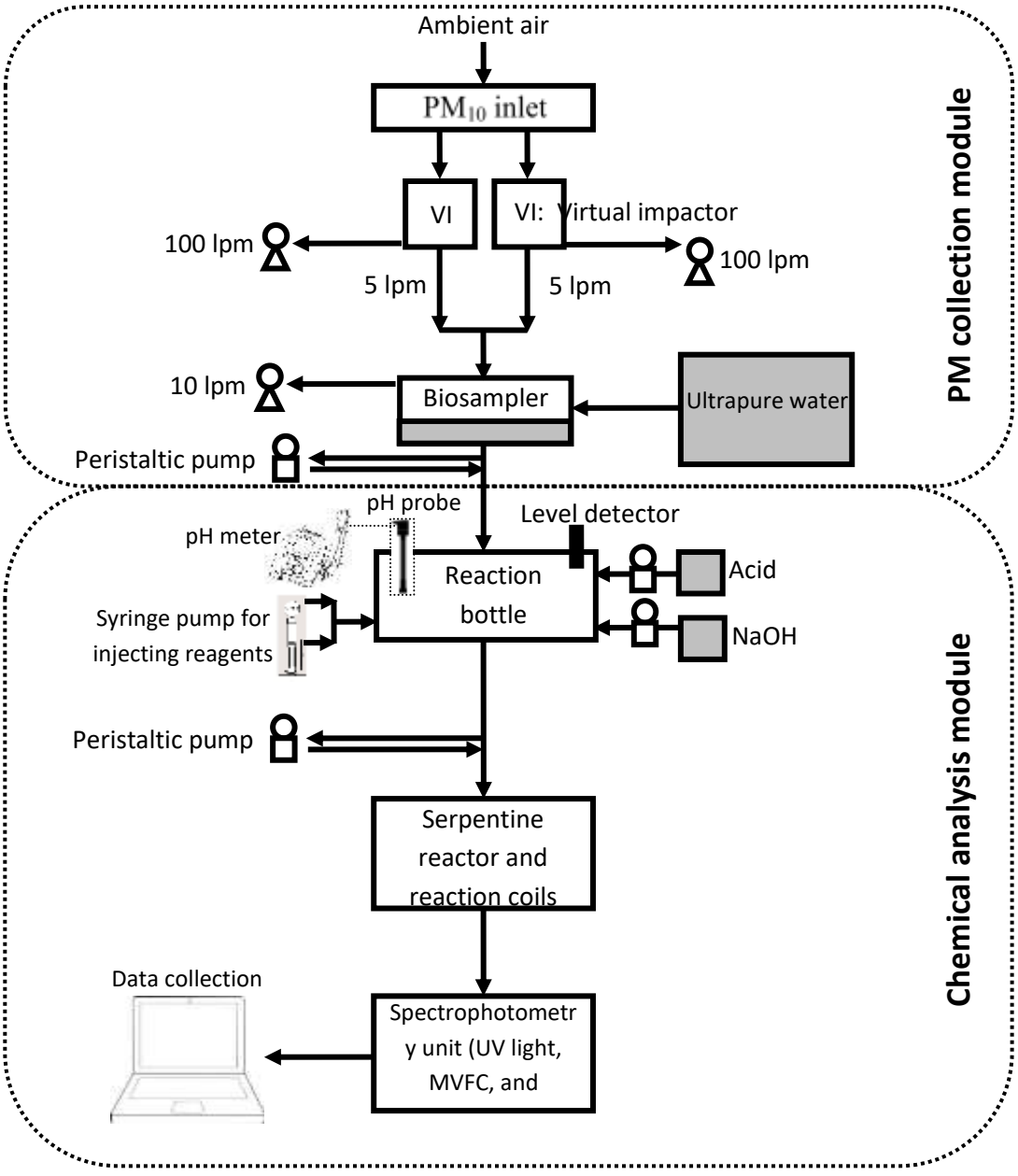

***Figure 1**: System schematic of the coarse PM metal monitor*

The system configuration is presented in Figure 1. The developed system comprises two modules: 1) the coarse PM collection module; and 2) the metal concentration measurement module. The coarse PM collection module utilizes two virtual impactors (VIs) connected in parallel, coupled with a modified BioSampler (i.e., liquid impinger) (BioSampler, SKC West, Inc., Fullerton, CA) technology, for which extensive details can be found elsewhere (Wang et al. 2015). Briefly, the air is drawn into two round nozzle VIs, each having a major flow rate of 100 L/min and a minor flow rate of 5 L/min. This total flow rate corresponds to a theoretical 50% cutpoint of 1.5 μm in aerodynamic diameter, concentrating airborne coarse PM into the VI's minor flow. As discussed in our earlier studies (Wang et al. 2015), although the theoretical cut point of the VIs is slightly lower than the traditional definition of the coarse PM size range (i.e., 2.5 μm), this cut point was selected to ensure that the entire size range of ambient coarse PM is concentrated by the maximum enrichment factor of about 20. The two minor flows are combined into a total flow rate of 10 L/min entering the modified BioSampler, in which particles are captured in 20 ml of ultrapure water to form a particle-liquid suspension. The collection efficiency of the BioSampler at that flow rate is near 100% for particles above 1.5 μm (Kim et al. 2001).

The second module, for which in-depth details can be found in (Wang et al. 2016), starts with the transferring of the aqueous sample into a capped bottle for chemical reactions. In this step, concentrated acids (i.e., 4 M HCl for Fe and Mn, and 4 M HNO_3 combined with 1% H_2O_2 for Cr) are added to the sample at a volume ratio of 1:20 (acid: sample). The addition of acids results in very low pH levels (i.e., around 0.5) to ensure that nearly all metal species are solubilized during the 10 min residence time of this step. The pH is then adjusted to 5-7 for Fe-ferrozine and 7-8.5 for Mn-FAD reactions by adding sufficient amounts of 1 M NaOH. It should be noted that no NaOH is added for Cr measurements, since the Cr-DPC reaction is optimal at pH=1. In the next step, oxidation/reduction agents (i.e., HA) are added to the sample solution to convert all different oxidation states of the target metals to a uniform state. Additionally, for Mn measurements, the ethylenediaminetetraacetic acid (EDTA, 0.08 N) solution was added to the sample at a volume ratio of 1% to eliminate any possible interference from Fe existing in the ambient coarse PM sample (Majestic et al. 2007). For Cr, however, no oxidation agent was added to the sample solution, mainly because all the Cr (III) was already converted to Cr (VI) due to the addition of H_2O_2. After a total residence time of 10 min in the serpentine reactor and then in the reaction coil, the sample is transferred to a 10-cm path-length, optical flow cell (60 μL internal volume) MVFC (FIA-ZSMA-ML-100-TEF, Ocean Optics, Inc., Dunedin, FL) for the spectrophotometry detection of the metals. The concentration of each metal was

determined at the wavelength with the highest level of absorption for the corresponding analytical reagent (i.e., ferrozine at 562 nm for Fe, FAD at 450 nm for Mn, and DPC at 540 nm for Cr), while a wavelength of 700 nm, at which there is effectively zero absorptivity for the analytical reagents, was selected to determine the background sample absorption. It should be noted that in the present study, the three target metals were not simultaneously measured, due mainly to limitations in the available equipment. Nonetheless, concurrent measurements can be easily implemented by splitting the concentrated slurry flow and using multiple spectrophotometry units in parallel. Additionally, in this study we focused on measuring the total concentrations of the three metals, however, as indicated in our previous work by Wang et al. (2016), the system configuration can be easily modified to measure water-soluble and different oxidation states of the target metals. The former can be achieved by removing the acid digestion step and using inserting an in-line liquid filtration unit (e.g., a 0.20 μm polypropylene syringe filter) to remove the water-insoluble fraction before the spectrophotometric measurement. The latter can be achieved by performing measurements with and without the addition of the oxidation and reduction reagents. For instance, the water-soluble Fe can be measured by omitting the HCl addition in the measurement sequence and filtration before the sample passes through the MVFC. Additionally, in order to measure Fe (II), the addition of the HA solution would be omitted from the procedure to prevent reducing Fe(III) to Fe(II). Furthermore, Fe (II) and total Fe can be measured using two distinct measurement lines, and the Fe(III) concentration can be easily calculated by subtracting Fe(II) concentration from that of total Fe. As illustrated by Wang et al. (2016), the same procedure can also be applied to Mn and Cr to measure water-soluble fraction and/or different oxidation states.

Field evaluation tests and continuous long-term operation

The developed system for the near-continuous measurement of Fe, Mn, and Cr in coarse PM was deployed at the Particle Instrumentation Unit (PIU), located on the University of Southern California's (USC) park campus, for field evaluation tests and continuous long-term run (i.e., approximately four months, from January to April 2016). As shown by previous studies performed at this location, this is a mixed urban site where ambient PM is largely impacted by vehicular emissions (Hasheminassab et al. 2014; Sowlat et al. 2016), as it is located 150 m downwind of a major freeway, i.e., I-110. It is also located approximately 3 km directly to the south of downtown Los Angeles, CA, and less than 2 km to the southwest of another major freeway, i.e., the I-10. Ambient coarse PM was collected in 2-hr time intervals, resulting in 12 data points per day, and the concentrations of the target metals (i.e., Fe, Mn, and Cr) were subsequently measured using the system described above. After each day of

sampling, the system was manually switched to measure the next metal species, therefore each metal was sampled every third day. Coarse PM sampling was done 6 days a week, starting on Tuesday and ending on the next Monday to incorporate weekend measurements as well. Every week, calibration and system maintenance was also performed on the day the system was stopped. Each metal was measured in two days per week. Additionally, the sequence of measuring these metals was changed every week to make sure that we capture the variations of metals concentrations during the week as well as during the weekends.

In addition, 5 time-integrated 24-hr filter samples were collected for each metal in parallel to the online measurements in order to compare the online concentrations to off-line measurements conducted on filters. For this purpose, another virtual impactor, with the same major and minor flow rates (i.e., 100 and 5 L/m, respectively) sampled in parallel with the on-line sampler. The air drawn by the minor flow of this virtual impactor was passed through 37-mm Teflon filters (Teflo, Pall Corp., Life Sciences, 1-µm pore, Ann Arbor, MI), which were held in a 37 mm air sampling cassette (Zefon International Inc., Ocala, FL). The filter samples were collected over a 24-hr interval to ensure that sufficient coarse PM mass was collected for the subsequent elemental analysis using an magnetic sector inductively coupled plasma mass spectrometry (SF-ICPMS) instrument. To directly compare the 2-hr online-measured data with those obtained from 24-hr filter samples, the online data were averaged over 24 hr. Concurrent to the measurements of the target metals using the developed technique, ambient coarse PM mass concentrations were continuously measured using a coarse particle mass monitor previously developed, for which extensive details can be found in (Misra et al. 2001). Briefly, the continuous coarse particle mass monitor (CCPM) consists of three major components, including a PM_{10} inlet, a round nozzle VI with a 2.5-µm cut point, and a standard tapered element oscillating microbalance (TEOM 1400A, Thermo Fisher Scientific, MA, USA) instrument. In this system, particles are drawn through the VI with a total flow rate of 50 L/min. Coarse particles are then concentrated into the minor flow of 2 L/min and drawn through the TEOM for continuous measurement of PM mass concentrations, while $PM_{2.5}$ were drawn into the major flow (48 L/min).

SF-ICPMS analysis of filter samples

Following acid digestion of the PM, the total elemental composition of the particulate matter (PM) collected on the 37mm Teflon filters was determined using magnetic sector inductively coupled plasma mass spectrometry (SF-ICPMS; Thermo-Finnigan Element 2) (Okuda et al. 2014). Filter membranes were placed in micro Teflon PFA digestion vessels and PM solubilized using a mixture of ultra-high-purity acids (1.0 mL of 16 M nitric acid, 0.25 mL of 12 M hydrochloric acid and

0.10 mL of hydrofluoric acid) in an automated microwave-aided digestion system (Milestone ETHOS+). This protocol effects a complete solubilization of all particle phases and element species. Digestates were diluted to 15 mL with high purity water (18 MΩ/cm^{-1}) in pre-cleaned low-density polyethylene (LDPE) bottles and then analyzed by SF-ICPMS. Forty-nine elements were quantified. Propagated analytical uncertainties were estimated from the uncertainties (square root of the sum of squares method) of the SF-ICPMS instrumental analysis, method blanks, and digestion recoveries. The latter correspond to the standard deviation of replicate analyses of National Institute of Standards and Technology (NIST) Standard Reference Materials (SRM). Six solid samples of three SRMs were digested and analyzed with every analytical batch of samples. Further details of these protocols can be found in previous publications (Zhang et al. 2008; Saffari et al. 2013; Okuda et al. 2014).

Results and Discussion

Calibration

For each metal, the measurement module (i.e., the spectrophotometry unit) of the developed system was calibrated using the dilution series prepared from the stock solution. Table 1 presents the results of the system calibration for each of the metals.

Table 1: *Results of the system calibration for each of the individual metals measured*

Element	Range	Calibration curve (units of slope: AU[a]/ppb)	R^2	Limit of Detection[b] (LOD) (ppb)	Limit of Detection[c] (LOD) (ng/m^3)
Fe	0-200 ppb	Y =0.0042x -0.0166	0.99	0.3	0.25
Mn	0-100 ppb	Y=0.0016x+0.0075	0.99	0.2	0.17
Cr	0-100 ppb	Y=0.0056x-0.0008	0.99	0.2	0.17

[a]*AU is absorbance unit*

[b]*The LOD was calculated as 3 times the standard deviation of the field method blanks (i.e., ultrapure water as a blank sample plus the pertinent reagents)*

[c]*Estimated based on a sampling flow rate of 200 L/min over a 2-hr collection time*

As presented in the table, the calibration results indicated robust linear associations between metal concentrations and absorbance level at the respective analytical wavelength - the R-square of the calibration curve was above 0.99 for all of the metals. Regression line slopes of 0.0042 (±0.0002)

(Abosorbance Unit (AU)/ppb), 0.0016 (±0.0001) (AU/ppb), and 0.0056 (±0.0004) (AU/ppb) for Fe, Mn, and Cr, respectively, confirm the high sensitivity of the long optical path spectrophotometric methods. It should be noted that system calibration was repeated multiple times during the sampling campaign as an additional quality assurance step to corroborate the validity of the on-line measurements. The limit of detection (LOD) for each metal was determined using the field method blanks prepared according to the following procedure: ultrapure water was first injected into the system and the relevant chemicals and reagents were added to the water as if this was an actual aerosol sample. Then, the blank sample was passed through the MVFC and the absorbance was measured. The LOD was estimated as 3 times the standard deviation of the field method blanks (Khlystov and Ma 2006; Majestic et al. 2007; Rastogi et al. 2009; Wang et al. 2016). According to the measurements and calculations mentioned above, the LODs were estimated to be 0.3 ppb (i.e., 0.25 ng/m^3), 0.2 ppb (i.e., 0.16 ng/m^3), and 0.2 ppb (i.e., 0.16 ng/m^3) for Fe, Mn, and Cr measurements (based on a flow rate of 200 L/min and a collection time of 2-hr), respectively. Our system has also high measurement sensitivity, demonstrated by the signal-to-noise (S/N) ratios of 231, 83, and 38 for Fe, Mn, and Cr, respectively, based on the average metal concentration levels observed in the current study.

Comparison between online-measured data with filter samples data

As noted earlier, time-integrated 24-hr filter samples were collected for each metal in parallel to the online measurements to verify the validity of the readings by the developed sampler. Figure 2 presents the linear regression and correlation between the total (i.e., soluble plus insoluble) concentrations of the metallic species measured by the developed monitor and those obtained from ICP-MS analysis of the off-line filter samples collected in parallel. For these samples, the ranges of total concentrations were 30-180 ng/m^3 for Fe, 5-27 ng/m^3 for Mn, and 2-14 ng/m^3 for Cr. As shown in the figure, very good agreement was observed between the total concentrations of the metallic species measured by the developed monitor and those obtained from the ICP-MS analysis performed on the collected filters, based on the slope of regression line (i.e., 0.86±0.05) and the R-square value (i.e., 0.96). This agreement based on total concentrations indicates that the ambient coarse PM has been effectively digested. Additionally, the average (±SD) online/filter concentration ratios were 0.83(±0.18), 0.93(±0.20), and 0.85(±0.11), respectively for Fe, Mn, and Cr. The approximately 10% lower on-line versus off-line filter-based concentrations could be attributed to the loss of particles (mostly the insoluble fraction) on the walls and bottom of the Biosampler, particle loss in the tubing and in the reaction vessel, and the likely resistance of a small fraction of the insoluble part of PM-bound metals to the acid digestion/solubilization procedure.

Previous studies have indicated that these metal species in the coarse PM fraction are largely (ranging between 60% and >90%) insoluble (Allen et al. 2001; Birmili et al. 2006; Wang et al. 2013; Shirmohammadi et al. 2015). Therefore, even though we did not directly measure the insoluble fraction of these metals in the collected samples, the very good agreement obtained between the online-measured data and offline filter samples corroborates the method's capability to efficiently digest/solubilize the insoluble fraction and accurately measure the total concentration of Fe, Mn, and Cr.

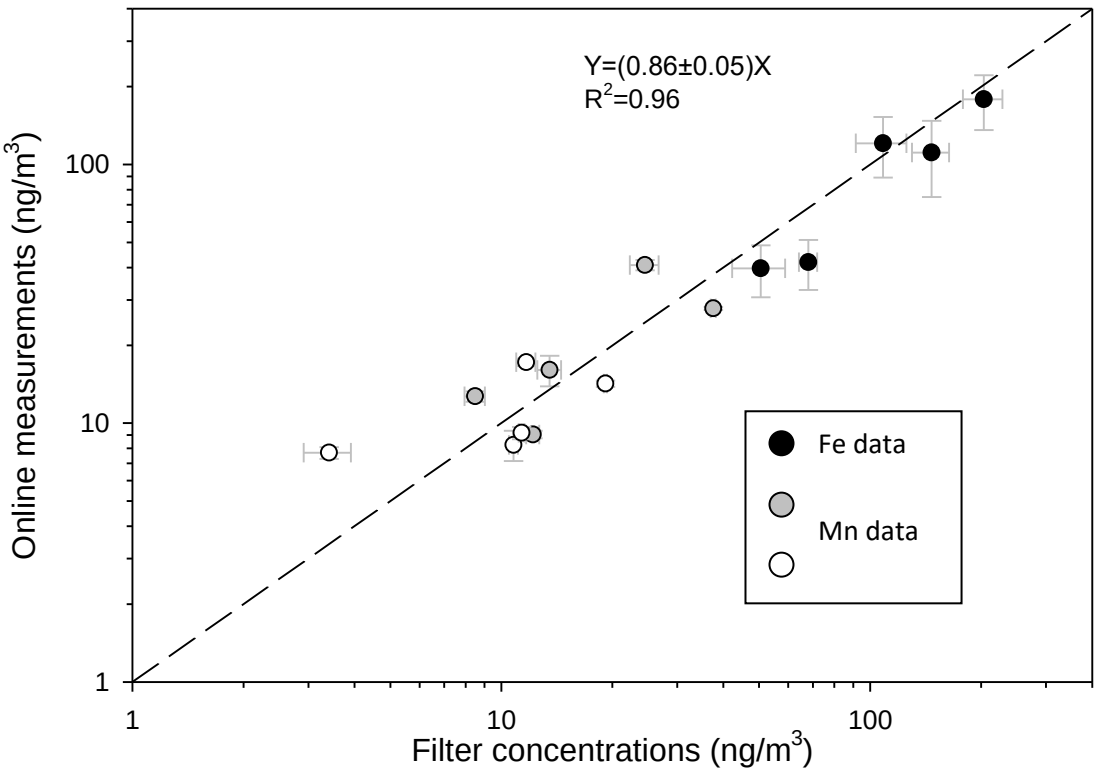

Figure 2: *Linear regression and correlation between the metal concentrations measured online with off-line concurrent measurements obtained using filter samplers. Error bars represent one standard deviation of multiple online (n = 12) and offline (n=3) measurements for each data point.*

Diurnal trends of Fe, Mn, and Cr in coarse PM concentrations and relationship to meteorological parameters in central Los Angeles

The developed monitor for online measurement of Fe, Mn, and Cr concentrations was deployed at the PIU site for an approximate four month period, from January to April 2016, to assess the long-term performance of the system. Table 2 presents the summary statistics of the online-measured concentrations of coarse PM-bound Fe, Mn, and Cr during the study period.

Table 2: *Summary statistics of the parameters collected over the entire study period*

Variables	Geometric Mean	Standard deviation	Minimum	Maximum
Fe (ng/m^3)	57.8	42.9	14.4	180.0
Mn (ng/m^3)	14.9	10.3	2.3	37.2
Cr (ng/m^3)	6.9	4.1	1.5	17.1
Wind speed (m/s)	1.9	1.2	0.9	8.5
Temperature (°C)	15.2	4.8	6.1	32.8
RH (%)	47.9	23.9	6.0	99.0
Coarse PM (µg/m^3)	11.6	8.9	1.20	55.1

This table also provides the mass concentration of coarse PM measured using the CCPM running concurrently with the metal monitor at the PIU. As shown in the table, the average coarse PM mass concentration was 11.6 (±9.0) µg/m^3 over the study period. The coarse PM Fe concentrations averaged 57.8 (±43.0) ng/m^3 (ranging from 14.4-180.0 ng/m^3) and were higher than those of Mn (i.e., 15.0 (±10.3) ng/m^3, ranging from 2.2-37.2 ng/m^3) and Cr (i.e., 6.9(±4.1) ng/m^3, ranging from 1.5-17.2 ng/m^3). In addition, The levels observed in the present study are in concert with those previously reported in central LA at the same sampling site (i.e., the PIU), both for particle mass concentrations and coarse PM-bound metals (Cheung et al. 2011; Cheung et al. 2012).

Data for meteorological parameters, including wind speed and direction, temperature, and relative humidity (RH) (Table 2) were acquired from the California Air Resources Board's (CARB) online database for the sampling site that is located in North Main St., downtown Los Angeles, which is located approximately 3 km northeast of our sampling site (i.e., the PIU). Figure 3(a-c) illustrates the average diurnal variation of meteorological parameters (i.e., temperature, wind speed, and RH) in the study area during our sampling campaign.

Figure 3(a-c): *The diurnal variation of meteorological parameters in the study location averaged over the study period; a) wind speed; b) temperature; and c) relative humidity. Error bars represent one standard error (SE) of the mean.*

a)

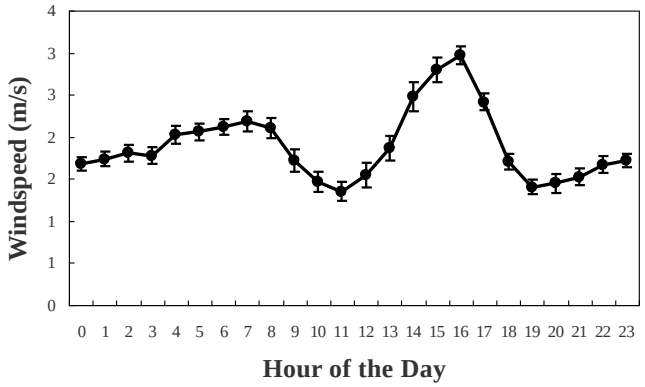

b)

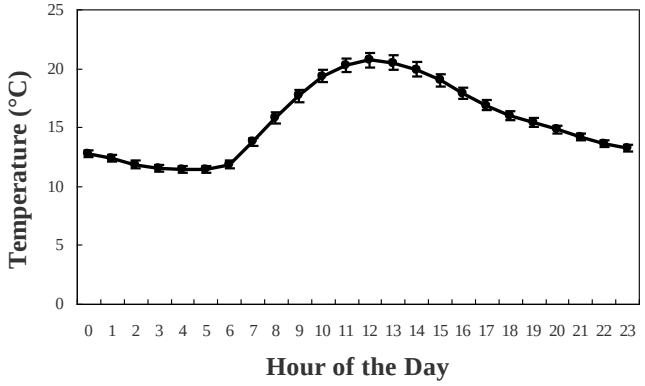

c)

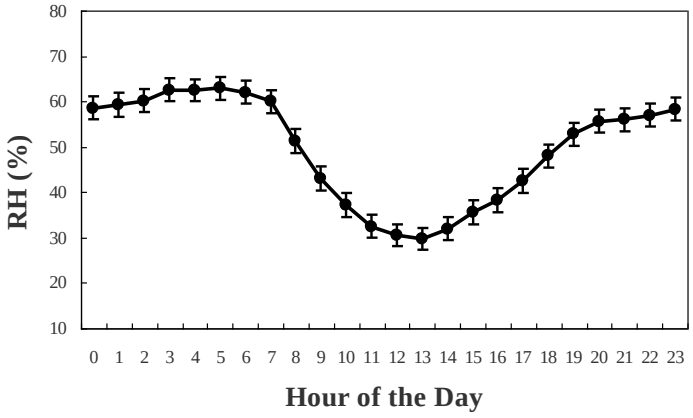

As shown in the figure, maximum temperatures (around 20 °C) were observed in the middle of the day, whereas RH (Figure 3(b)) peaked at night, reaching values up to 60%. The diurnal variations for wind speed (Figure 3(c)) exhibited a sharp peak (around 3 m/s) in the afternoon. These results are consistent with those reported previously in central Los Angeles (Cheung et al. 2011; Cheung et al. 2012).

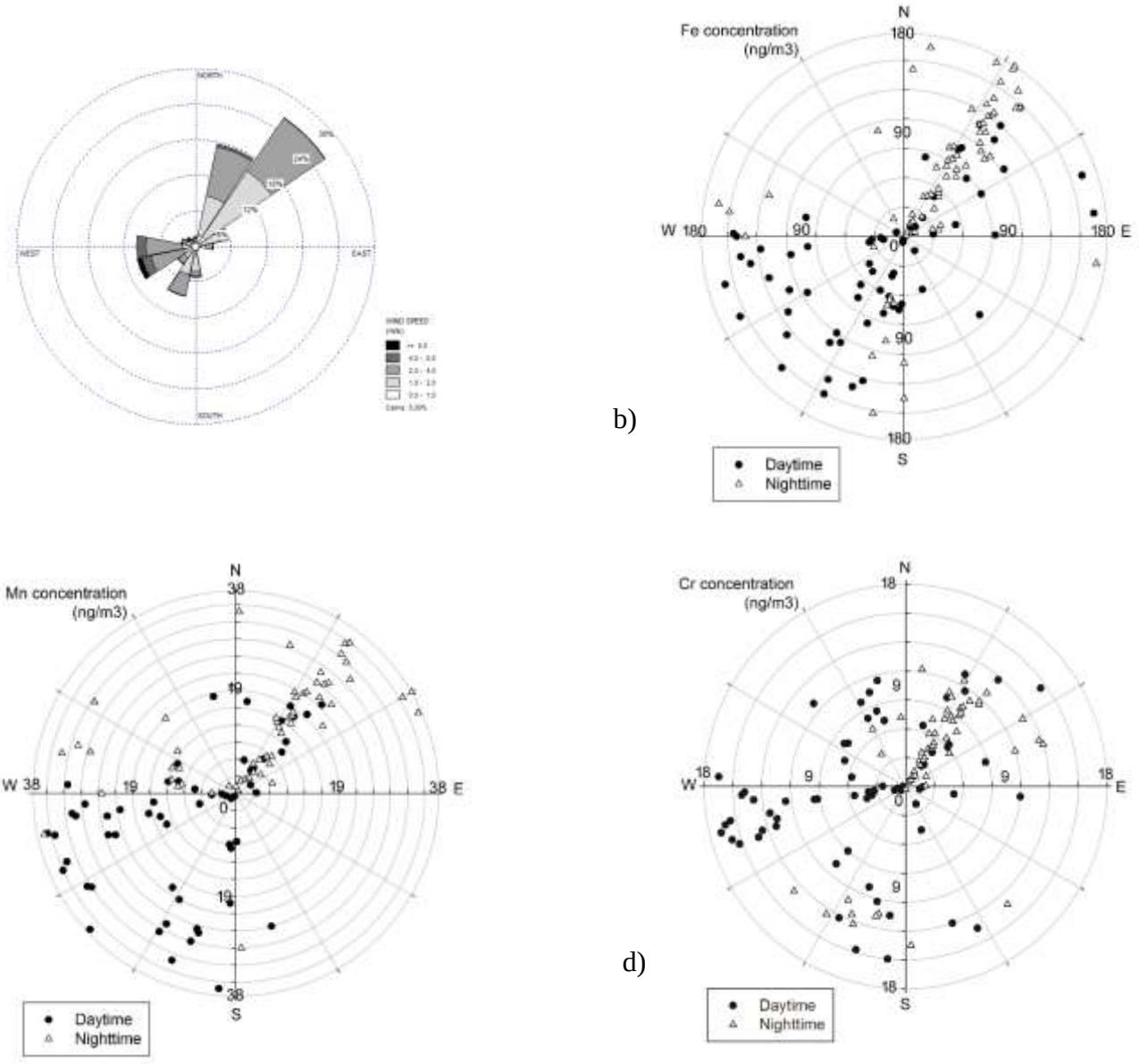

Figure 4(a-d): *Prevailing wind direction and speed (a) during the study period and its relationship with concentrations of Fe (b), Mn (c), and Cr (d).*

Figure 4(a) presents the wind rose in the sampling site, indicating the direction and speed of the prevailing wind in the study area during our campaign. As shown in the figure, the wind was most commonly blowing from the northeast (approximately 27% of the time), with the highest speeds ranging from 4 to 5 m/s. The second major wind direction during the sampling period was westerly and southwesterly winds, exhibiting even higher wind speeds (above 5 m/s).

Figures 4(b-d) present the concentrations of the metals in association with wind direction during the entire study period, presented separately for daytime and nighttime. As can be seen from the plots, for Fe and Mn, the highest concentrations (i.e., 150-200 ng/m^3 for Fe and 30-40 ng/m^3 for Mn) were observed during two distinct periods, i.e., westerly/southwesterly winds during the daytime, and northeasterly winds during the nighttime. Our sampling site is located approximately 150 m to the east of the I-110 freeway; it is also in close proximity (less than 2 km to the southwest) to the I-10 freeway. Therefore, the observed high Fe and Mn concentrations during daytime westerly winds and nighttime northeasterly winds can be associated with traffic emissions (i.e., road dust/resuspension soil) brought to the site by prevailing winds from these two major freeways. It is also noteworthy that, for both Fe and Mn, although high concentrations were observed during nighttime northeasterly winds, the average daytime concentrations during westerly and southwesterly winds (i.e., 89.5 (±30.0) ng/m^3 and 19.4 (±11.6) ng/m^3 for Fe and Mn, respectively) were higher than those during nighttime (i.e., 64.5 (±39.9) ng/m^3 and 13.6 (±8.7) ng/m^3 for Fe and Mn, respectively). In contrast to the Fe and Mn trends, as can be observed in Figure 4(d), the coarse PM Cr concentrations follow distinctly different trends that are suggestive of contributions of other potential local sources, including metal plating facilities using Cr-containing paints (Ospital et al. 2008; Propper et al. 2015), in addition to the road dust/resuspension soil noted earlier. Figure 5(a) illustrates the diurnal variations of the coarse PM mass concentrations in the sampling location during the study period. As can be seen in the figure, the PM mass concentration starts to sharply increase at 8 am and reaches a maximum at 11-am-noon, decreasing to slightly lower ranges until 6 pm, and then sharply decreases down to the lowest values of 8-10 µg/m^3 at nighttime. This trend clearly indicates the impact of meteorological conditions and traffic volume on CPM mass variations. As shown in Figures 3(a-c), during the midday period, we have the lowest RH and highest wind speed, both of which favor the resuspension of soil and road dust. This is also in agreement with the results from previous studies conducted in central LA at the same sampling site (Pakbin et al. 2010; Pakbin et al. 2011). The average diurnal variations of Fe concentrations are shown in Figure 5(b). The box represents the interquartile range (the bottom and top lines of the box representing the first and the third quartiles,

respectively). The line inside the box represents the median, while the whiskers above and below the box represent 95th and 5th percentiles.

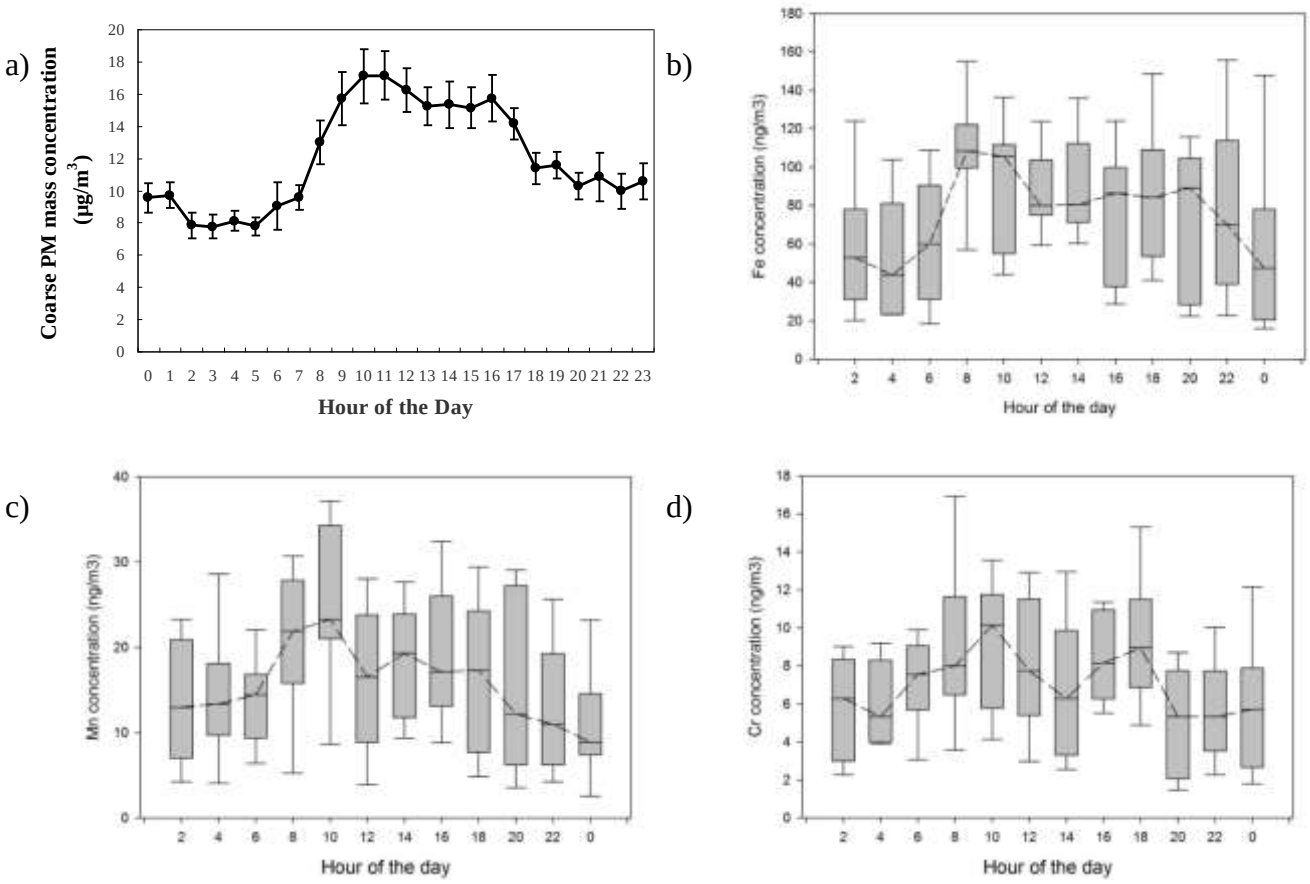

5(a-d): *Diurnal variations of the coarse PM mass concentrations and the online-measured metal concentrations averaged over the study period; a) coarse PM; b) Fe; c) Mn; and d) Cr. For panel a, the error bars represent one standard error (SE) of the mean. The box plots represent the interquartile range (the bottom and top lines of the box representing the first and the third quartiles, respectively). The line inside the box represents the median, while the whiskers above and below the box represent the 95th and 5th percentiles.*

As can be seen from the figure, two peaks were observed, one major peak during morning rush hours (8-10 am) and one minor peak during late afternoon/early evening hours (4-8 pm), bringing the average Fe concentration up to around 90 ng/m^3, compared to the lower values of around 40 ng/m^3 during other hours of the day. These two peaks illustrate the impact of traffic-related emissions (most likely resuspended dust, given the size range of the PM being measured in this study) on CPM levels at the sampling site. This trend was also observed in Figure 4(b), indicating high Fe concentrations during westerly and southwesterly winds, bringing atmospheric particles from the major freeway (i.e., I-110) located approximately 150 m to the west of our sampling site. There is also a smaller third

peak in concentration observed in the middle of the day (1-3 pm), which corresponds to maximum temperatures and wind speeds and minimum RHs, as shown in Figures 3(a-c). This peak can be attributed to southeasterly winds, which are most frequent in the middle of the day (Wang et al. 2015), particularly in the cold season (Dec – March, as in this sampling campaign). This finding is also consistent with those reported by Sowlat et al. (2016), observing very high contributions from the soil/road dust during high temperatures and wind speeds and very low RHs. Figure 5(c) shows the diurnal variations of Mn concentrations at the sampling location during the study period. As can be seen from the figure, the Mn concentrations peaked in the early morning (around 8-10 am), with an average concentration of 25 ng/m^3. As in the case of Fe concentrations, this peak can be attributed to the impact of traffic-related emissions (most likely resuspended dust) on CPM levels at the sampling site, which was also observed in Figure 3(c), indicating the highest Mn concentrations during westerly and southwesterly winds, which carried road dust particles from the major freeway (i.e., I-110) to our sampling site. In contrast to the Fe diurnal variations, we did not observe a second peak in late afternoon/early evening hours; however, the Mn concentrations remained relatively high during the daytime hours (slightly less than 20 ng/m^3), corresponding to maximum temperatures and wind speeds and minimum RHs, as shown in Figures 3(a-c), indicating the probable influence of the soil dust factor. This finding is in concert with previous studies performed in central Los Angeles, showing the major influence of soil dust on coarse PM-bound Mn concentrations (Pakbin et al. 2010; Pakbin et al. 2011; Cheung et al. 2012; Shrimohammadi et al. 2015). In other words, Mn is not dominated by mobile sources like Fe and more likely comes from soil. This is also confirmed by the results of the weekday/weekend analysis (Figure 7), which did not reveal any significant difference between Mn concentrations on weekdays compared to weekends. Figure 5(d) indicates the diurnal variations of measured concentrations of Cr during the study period. Two distinct peaks were observed, one during morning rush hours (around 9 am) and one during afternoon hours (3-5 pm), bringing the average Cr concentration up to around 12 ng/m^3, compared to the lower values of around 4-6 ng/m^3 during other hours of the day. Although these two peaks can be partly attributed to the impact of re-suspended road dust from 110 freeway, coarse PM-bound Cr may also be affected by other smaller local sources supported also by the association between Cr concentrations and wind direction data (Figure 4(d). Figures 6(a-c) illustrate the diurnal variations of Fe, Mn, and Cr mass fractions averaged over the entire study period. As shown in the figures, the diurnal trends for the mass fractions were almost similar to those of airborne concentrations for all three of the metals, exhibiting major peaks in early morning for all the metals and a second peak in late afternoon/early evening hours for Fe. However, it is apparent from the diurnal trends of the mass fractions of these

metals that the first peak occurs earlier in the morning (4-6 am versus 8-10 am), which is anti-correlated with coarse PM mass concentrations, implying the dilution of these metals by a less metal-enriched phase during morning rush hours.

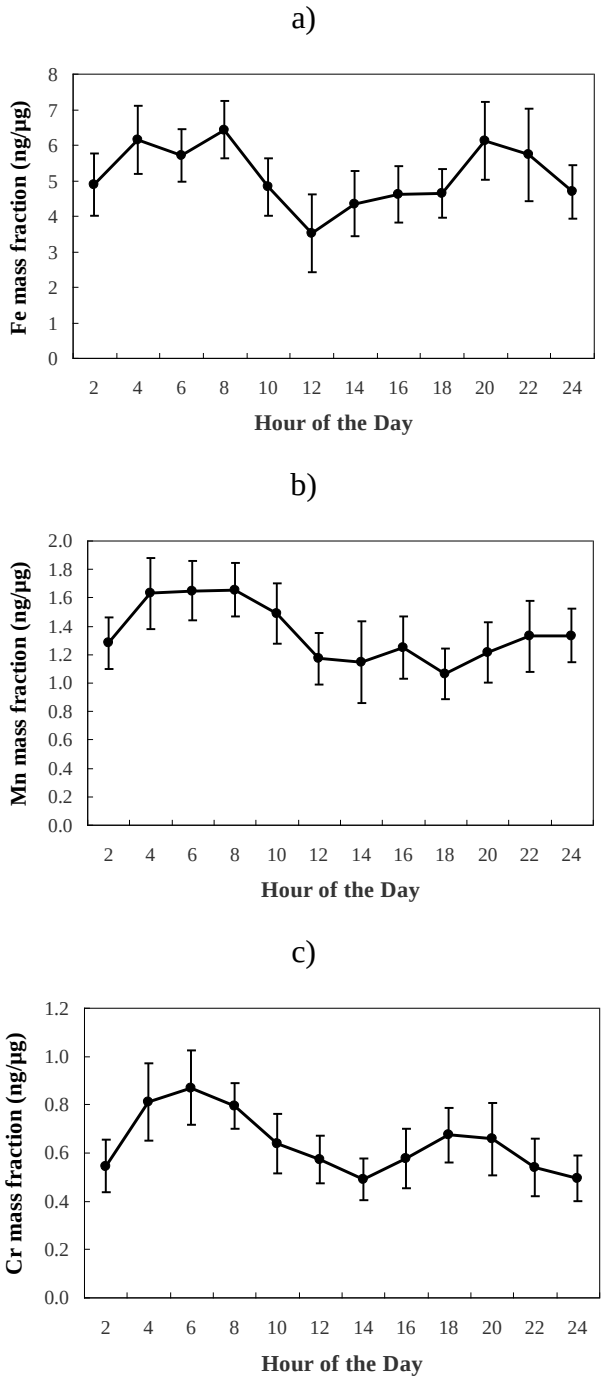

Figure 6(a-c): *Diurnal variations of the mass fractions of the online-measured metal concentrations averaged over the study period; a) Fe; b) Mn; c) Cr. Error bars represent one standard error (SE) of the mean.*

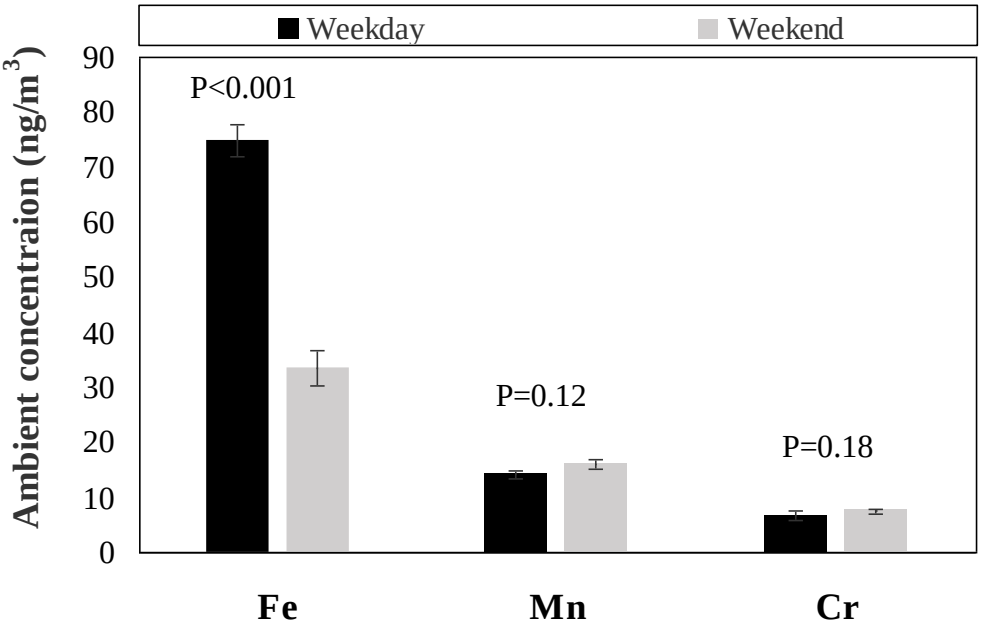

Figure 7: *Weekday-weekend analysis of the metallic species concentrations during the study period. The P-values shown on the graph correspond to independent samples T-test.*

Figure 7 presents a weekday/weekend analysis for Fe, Mn, and Cr concentrations at the sampling site over the entire study period. As can be seen from the figure, the concentration of Fe was significantly higher during the weekdays (about 75 ng/m^3) compared to the weekends (around 33 ng/m^3) (P<0.001), suggesting the major role of traffic in elevating Fe concentrations, which is consistent with the interpretation of the data in the metal rose plots as well as in the diurnal variation plots (Figures 5 and 6). However, the Mn and Cr concentrations were not statistically different (P>0.05) between the weekdays and weekends (averaging about 15 ng/m^3 for Mn and about 7 ng/m^3 for Cr).

Summary and conclusions

In this study, a novel monitor was developed for near-continuous measurement of Fe, Mn, and Cr concentrations in ambient coarse PM (i.e., $PM_{10-2.5}$) with a time resolution of 2 hr. This monitor consisted of two modules, the first one utilizing two VIs connected to a modified BioSampler (i.e., liquid impinger) to draw and concentrate coarse PM into slurry samples, and the second one utilizing a Micro Volume Flow Cell (MVFC) coupled with spectrophotometry to measure metal concentrations. Our results indicate that all major species of the target metals can be efficiently digested by directly collecting ambient coarse PM into aqueous slurries. The validity of the online measurements was investigated using parallel time integrated filter-collected data obtained from ICP-

MS analysis, which indicated very good agreement between the online measurements and parallel filters. The average concentrations of the three metals during the study period were 57.8 ng/m^3, 15.0 ng/m^3, and 6.9 ng/m^3 for Fe, Mn, and Cr, respectively, consistent with published data from the study site. Diurnal variations of these metals generally followed that of coarse PM mass concentrations, suggesting the influence of meteorological conditions and traffic sources on these metals in coarse PM. Results from the present study indicate that the developed monitor is capable of achieving measurements with high accuracy and reliability over long sampling periods with minimum supervision. These features, combined with the unique abilities of the system to measure water-soluble and different oxidation states of these metals make it a promising technology to achieve near-continuous measurements of metal concentrations in ambient coarse PM, enabling a better understanding of the atmospheric processes and sources involved in formation and transport of these redox-active metals in the coarse PM size range.

References

Allen, A. G., Nemitz, E., Shi, J. P., Harrison, R. M., & Greenwood, J. C. (2001). Size distributions of trace metals in atmospheric aerosols in the United Kingdom. *Atmospheric Environment*, *35*(27), 4581-4591.

Allan, J. D., Jimenez, J. L., Williams, P. I., Alfarra, M. R., Bower, K. N., Jayne, J. T., Coe, H., & Worsnop, D. R. (2003). Quantitative sampling using an Aerodyne aerosol mass spectrometer 1. Techniques of data interpretation and error analysis. *Journal of Geophysical Research: Atmospheres*, *108*(D3).

Al-Masri, M. S., Al-Kharfan, K., & Al-Shamali, K. (2006). Speciation of Pb, Cu and Zn determined by sequential extraction for identification of air pollution sources in Syria. *Atmospheric Environment*, *40*(4), 753-761.

Almeida, S. M., Pio, C. A., Freitas, M. C., Reis, M. A., & Trancoso, M. A. (2006). Source apportionment of atmospheric urban aerosol based on weekdays/weekend variability: evaluation of road re-suspended dust contribution. *Atmospheric Environment*, *40*(11), 2058-2067.

Argyropoulos, G., Manoli, E., Kouras, A., & Samara, C. (2012). Concentrations and source apportionment of PM 10 and associated major and trace elements in the Rhodes Island, Greece. *Science of the Total Environment*, *432*, 12-22.

Argyropoulos, G., Grigoratos, T., Voutsinas, M., & Samara, C. (2013). Concentrations and source apportionment of PM10 and associated elemental and ionic species in a lignite-burning power generation area of southern Greece. *Environmental Science and Pollution Research*, *20*(10), 7214-7230.

Allegrini, I., De Santis, F., Di Palo, V., Febo, A., Perrino, C., Possanzini, M., & Liberti, A. (1987). Annular denuder method for sampling reactive gases and aerosols in the atmosphere. *Science of the Total Environment*, *67*(1), 1-16.

Allegrini, I., Febo, A., Perrino, C., & Masia, P. (1994). Measurement of atmospheric nitric acid in gas phase and nitrate in particulate matter by means of annular denuders. *International Journal of Environmental Analytical Chemistry*, *54*(3), 183-201.

Armiento, G., Inglessis, M., Mazziotti Tagliani, S., Montereali, M. R., Nardi, E., Palleschi, S., Piga L, Sacco F, Silvestroni L., & Gianfagna, A. (2013). A comprehensive approach to the investigation of atmospheric particulate PM2. 5: preliminary results. *Periodico di Mineralogia*, *82*(1), 199-216.

Ayres, J. G., Borm, P., Cassee, F. R., Castranova, V., Donaldson, K., Ghio, A., Harrison, R. M.,

Hider, R., Kelly, F., Kooter, I. M.., & Marano, F. (2008). Evaluating the toxicity of airborne particulate matter and nanoparticles by measuring oxidative stress potential—a workshop report and consensus statement. *Inhalation toxicology*, *20*(1), 75-99.

Barrett, P. M., Resing, J. A., Buck, N. J., Buck, C. S., Landing, W. M., & Measures, C. I. (2012). The trace element composition of suspended particulate matter in the upper 1000m of the eastern North Atlantic Ocean: A16N. *Marine Chemistry*, *142*, 41-53.

Becker, S., & Soukup, J. (2003). Coarse (PM 2.5-10), Fine (PM 2.5), and ultrafine air pollution particles induce/increase immune costimulatory receptors on human blood-derived monocytes but not on alveolar macrophages. *Journal of Toxicology and Environmental Health Part A*, *66*(9), 847-859.

Becker, S., Mundandhara, S., Devlin, R. B., & Madden, M. (2005). Regulation of cytokine production in human alveolar macrophages and airway epithelial cells in response to ambient air pollution particles: further mechanistic studies. *Toxicology and applied pharmacology*, *207*(2), 269-275.

Birmili, W., Allen, A. G., Bary, F., & Harrison, R. M. (2006). Trace metal concentrations and water solubility in size-fractionated atmospheric particles and influence of road traffic. *Environmental Science & Technology*, *40*(4), 1144-1153.

Bogenschütz, G., Emmenegger, C., and Kalcher, M.: Semicontinuous determination of anions, cations, and heavy metals in aerosols using PILS-IC-VA G technical report: http://www.metrohm.com/com/Applications (search for 8.000.6086EN).

Brunekreef, B., & Forsberg, B. (2005). Epidemiological evidence of effects of coarse airborne particles on health. *European Respiratory Journal*, *26*(2), 309-318.

Bukowiecki, N., Hill, M., Gehrig, R., Zwicky, C. N., Lienemann, P., Hegedüs, F., Falkenberg, G., Weingartner, E., & Baltensperger, U. (2005). Trace metals in ambient air: hourly size-segregated mass concentrations determined by synchrotron-XRF. *Environmental science & technology*, *39*(15), 5754-5762.

Canepari, S., Perrino, C., Olivieri, F., & Astolfi, M. L. (2008). Characterisation of the traffic sources of PM through size-segregated sampling, sequential leaching and ICP analysis. *Atmospheric Environment*, *42*(35), 8161-8175.

Canepari, S., Pietrodangelo, A., Perrino, C., Astolfi, M. L., & Marzo, M. L. (2009). Enhancement of source traceability of atmospheric PM by elemental chemical fractionation. *Atmospheric Environment*, *43*(31), 4754-4765.

Canepari, S., Astolfi, M. L., Moretti, S., & Curini, R. (2010). Comparison of extracting solutions for elemental fractionation in airborne particulate matter. *Talanta*, *82*(2), 834-844.

Canepari, S., Astolfi, M. L., Farao, C., Maretto, M., Frasca, D., Marcoccia, M., & Perrino, C. (2014). Seasonal variations in the chemical composition of particulate matter: a case study in the Po Valley. Part II: concentration and solubility of micro-and trace elements. *Environmental Science and Pollution Research*, *21*(6), 4010-4022.

Charrier, J. G., & Anastasio, C. (2012). On dithiothreitol (DTT) as a measure of oxidative potential for ambient particles: evidence for the importance of soluble transition metals. *Atmospheric chemistry and physics (Print)*, *12*(5), 11317.

Cheung, K., Daher, N., Shafer, M. M., Ning, Z., Schauer, J. J., & Sioutas, C. (2011). Diurnal trends in coarse particulate matter composition in the Los Angeles Basin. *Journal of Environmental Monitoring*, *13*(11), 3277-3287.

Cheung, K., Shafer, M. M., Schauer, J. J., & Sioutas, C. (2012). Diurnal trends in oxidative potential of coarse particulate matter in the Los Angeles Basin and their relation to sources and chemical composition. *Environmental science & technology*, *46*(7), 3779-3787.

Cho, S. H., Tong, H., McGee, J. K., Baldauf, R. W., Krantz, Q. T., & Gilmour, M. I. (2009). Comparative toxicity of size-fractionated airborne particulate matter collected at different distances from an urban highway. *Environmental health perspectives*, *117*(11), 1682.

Chow, J. C., Watson, J. G., Lowenthal, D. H., & Magliano, K. L. (2005). Loss of PM2.5 nitrate from filter samples in central California. *Journal of the Air & Waste Management Association*, *55*(8), 1158-1168.

Claiborn, C. S., Larson, T., & Sheppard, L. (2002). Testing the metals hypothesis in Spokane, Washington. *Environmental Health Perspectives*, *110*(Suppl 4), 547.

Davis, D. A., Bortolato, M., Godar, S. C., Sander, T. K., Iwata, N., Pakbin, P., Shih, J.C., Berhane, K., McConnell, R., Sioutas, C., Morgan T.E., & Finch, C. E. (2013). Prenatal exposure to urban air nanoparticles in mice causes altered neuronal differentiation and depression-like responses. *PloS one*, *8*(5), e64128.

DeCarlo, P. F., Kimmel, J. R., Trimborn, A., Northway, M. J., Jayne, J. T., Aiken, A. C., Jimenez, J. L., Gonin, M., Fuhrer, K., Horvath, T., Docherty, K. S., & Worsnop, D. R. (2006). Field-deployable, high-resolution, time-of-flight aerosol mass spectrometer. *Analytical chemistry*, *78*(24), 8281-8289.

Delfino, R. J., Sioutas, C., & Malik, S. (2005). Potential role of ultrafine particles in associations between airborne particle mass and cardiovascular health. *Environmental health perspectives*, *113*(8), 934.

Delfino, R. J., Tjoa, T., Gillen, D. L., Staimer, N., Polidori, A., Arhami, M., Arhami, M., Jamner, L., Sioutas, C., & Longhurst, J. (2010). Traffic-related air pollution and blood pressure in elderly subjects with coronary artery disease. *Epidemiology (Cambridge, Mass.)*, *21*(3).

Di Menno Di Bucchianico A, Catrambone M, Perrino C, Passariello B, Quaresima S (2002), La valutazione del materiale particellare alla luce del DM 2/4/2002, Marina di Carrara 11/10/2002, Eventi di trasporto di sabbie sahariane nell'Italia centrale.

Dockery, D. W., & Stone, P. H. (2007). Cardiovascular risks from fine particulate air pollution.

Donaldson, K., Stone, V., Borm, P. J., Jimenez, L. A., Gilmour, P. S., Schins, R. P., Knaapen, A. M., Rahman, I., Faux, S. P., Brown, D. M., & MacNee, W. (2003). Oxidative stress and calcium signaling in the adverse effects of environmental particles (PM 10). *Free Radical Biology and Medicine*, *34*(11), 1369-1382.

Dos Santos, M., Gómez, D., Dawidowski, L., Gautier, E., & Smichowski, P. (2009). Determination of water-soluble and insoluble compounds in size classified airborne particulate matter. *Microchemical Journal*, *91*(1), 133-139.

Dutkiewicz, V. A., Qureshi, S., Husain, L., Schwab, J. J., & Demerjian, K. L. (2006). Elemental composition of PM 2.5 aerosols in Queens, New York: evaluation of sources of fine-particle mass. *Atmospheric Environment*, *40*, 347-359.

Espinosa, A. J. F., Rodríguez, M. T., de la Rosa, F. J. B., & Sánchez, J. C. J. (2002). A chemical speciation of trace metals for fine urban particles. *Atmospheric Environment*, *36*(5), 773-780.

Farao, C., Canepari, S., Perrino, C., & Harrison, R. M. (2014). Sources of PM in an industrial area: comparison between receptor model results and semiempirical calculations of source contributions. *Aerosol and Air Quality Research*, *14*(6), 1558-1572.

Fang, T., Verma, V., Bates, J. T., Abrams, J., Klein, M., Strickland, M. J., Sarnat, S. E., Chang, H. H., Mulholland, J. A., Tolbert, P. E. & Russell, A. G. (2015). Oxidative potential of ambient water-soluble PM 2.5 measured by Dithiothreitol (DTT) and Ascorbic Acid (AA) assays in the southeastern United States: contrasts in sources and health associations. *Atmospheric Chemistry & Physics Discussions*, *15*(21) 30609-30644.

Gao, X.; Yang, L.; Cheng, S.; Gao, R.; Zhou, Y.; Xue, L.; Shou, Y.; Wang, J.; Wang, X.; Nie, W.; Wang, W. & Xu, P. (2011). Semi-continuous measurement of water-soluble ions in PM 2.5 in Jinan, China: temporal variations and source apportionments. *Atmospheric Environment*, *45*(33), 6048-6056.

Gauderman, W. J., Urman, R., Avol, E., Berhane, K., McConnell, R., Rappaport, E., Chang, R., Lurmann, F., & Gilliland, F. (2015). Association of improved air quality with lung development in children. *New England Journal of Medicine*, *372*(10), 905-913.

Gietl, J. K., Lawrence, R., Thorpe, A. J., & Harrison, R. M. (2010). Identification of brake wear particles and derivation of a quantitative tracer for brake dust at a major road. *Atmospheric Environment*, *44*(2), 141-146.

Götschi, T., Hazenkamp-von Arx, M. E., Heinrich, J., Bono, R., Burney, P., Forsberg, B., & Sunyer, J. (2005). Elemental composition and reflectance of ambient fine particles at 21 European locations. *Atmospheric Environment*, *39*(32), 5947-5958.

Harrison, R. M., Jones, A. M., Gietl, J., Yin, J., & Green, D. C. (2012). Estimation of the contributions of brake dust, tire wear, and resuspension to nonexhaust traffic particles derived from atmospheric measurements. *Environmental science & technology*, *46*(12), 6523-6529.

Harrison, R. M., & Yin, J. (2000). Particulate matter in the atmosphere: which particle properties are important for its effects on health?. *Science of the total environment*, *249*(1), 85-101.

Hasheminassab, S., Pakbin, P., Delfino, R. J., Schauer, J. J., & Sioutas, C. (2014). Diurnal and seasonal trends in the apparent density of ambient fine and coarse particles in Los Angeles. *Environmental Pollution*, *187*, 1-9.

Hecobian, A., Zhang, X., Zheng, M., Frank, N., Edgerton, E. S., & Weber, R. J.(2010) Water-Soluble Organic Aerosol material and the light-absorption characteristics of aqueous extracts measured over the Southeastern United States. *Atmospheric Chemistry and Physics*, 10, 5965–5977,

Heal M.R., Hibbs L.R., Agius R.M., &Beverland I.J. (2005) Total and water-soluble content of urban background PM10, PM2.5 and black smoke in Edinburg, UK. *Atmospheric Environment*, 39, 1417-1430.

Jayne, J.T.; Leard, D.C.; Zhang, X.F.; Davidovits, P.; Smith, K.A.; Kolb, C.E.; & Worsnop, D.R. (2000) Development of an Aerosol Mass Spectrometer for Size and Composition Analysis of Submicron Particles. *Aerosol science & technology*, 33, 49–70.

Hueglin, C., Gehrig, R., Baltensperger, U., Gysel, M., Monn, C. and Vonmont, H. (2005) Chemical Characterisation of PM2.5, PM10 and Coarse Particles at Urban, Near-City and Rural Sites in Switzerland. *Atmospheric Environment*, 39, 637-651.

Jeong, C.H., Evans, G.J., Dann, T., Graham, M., Herod, D. Dabek-Zlotorzynska, E. Mathieu, D., Ding, L., Wang, D. "Influence of biomass burning on wintertime fine particulate matter: Source contribution at a valley site rural in British Columbia*" Atmospheric Environment.*, 42(16) 3684-3699 (2008) doi: 10.1016/j.atmosenv.2008.01.006

Knudsen, H., and Rasmussen, N.: Particulate Matter: Sources, Emission Rates and Health Effects, Chapter 1, *Nova Science Publishers*, New York, pp 330, 2012.

Karlsson, A., Irgum, K., & Hansson, H. C. (1997). Single-stage flowing liquid film impactor for continuous on-line particle analysis. *Journal of Aerosol Science*, *28*(8), 1539-1551.

Khlystov, A., Wyers, G. P., & Slanina, J. (1995). The steam-jet aerosol collector. *Atmospheric Environment.* 29, 2229–2234.

Khlystov, A., Zhang, Q., Jimenez, J. L., Stanier, C., Pandis, S. N., Canagaratna, M. R., et al. (2005). In situ Concentration of Semi-Volatile Aerosol Using Water-Condensation Technology. *Journal of Aerosol Science,* 36:866–880.

Khlystov A, & Ma Y. (2006). An On-line Instrument for Mobile measurement of the spatial variability of Hexavalent and Trivalent Chromium in Urban Air. *Atmospheric Environment*. 40, 8088–8093.

Kidwell, C. B., and Ondov, J. M. (2001). Development and Evaluation of a Prototype System for Collecting Sub-Hourly Ambient Aerosol for Chemical Analysis. *Aerosol Science Technology*. 35,596–601

Kidwell, Christopher B., Ondov J. M. (2004). Elemental analysis of sub-hourly ambient aerosol collections. *Aerosol Science & Technology.* 38: 205-218

Kidwell, C. B., & Ondov, J. M. (2004). Elemental analysis of sub-hourly ambient aerosol collections. *Aerosol Science and Technology*, *38*(3), 205-218.

Kim, S., Jaques, P. A., Chang, M., Froines, J. R., Sioutas, C. (2001). Versatile aerosol concentration enrichment system (VACES) for simultaneous in vivo and in vitro evaluation of toxic effects of ultrafine, fine and coarse ambient particles Part I: Development and laboratory characterization. *Journal of Aerosol Science.* 32:1281-1297.

Lee, P. K. H., Brook, J. R., Dabek-Zlotorzynska, E. & Mabury, S. A. (2003). Identification of the major sources contributing to PM2.5 observed in Toronto. *Environmental Science & Technology.* 37**,** 4831–4840, doi: 10.1021/es026473i.

Lee, T., Yu, X.-Y., Kreidenweis, S.M., Malm, W.C., & Collett, J.L. (2008). Semi-continuous measurement of PM2.5 ionic composition at several rural locations in the United States. *Atmospheric Environment*. 42, 6655–6669

Li, N., Wang, M., Bramble, L. A., Schmitz, D. A., Schauer, J. J., Sioutas, C., Harkema, J. R.,& Nel, A. E. (2009). The adjuvant effect of ambient particulate matter is closely reflected by the particulate oxidant potential. *Environmental. Health Perspectives*.117:1116-1123.

Li, Y. J., Lee, B. P., Su, L., Fung, J. C. H., & Chan, C. K.(2015). Seasonal characteristics of fine particulate matter (PM) based on high-resolution time-of-flight aerosol mass spectrometric (HR-ToF-AMS) measurements at the HKUST Supersite in Hong Kong. *Atmospheric Chemistry and Physics*. 15, 37-53, https://doi.org/10.5194/acp-15-37-2015.

Limbeck, A., Wagner, C., Lendl, B., & Mukhtar, A. (2012). Determination of water-soluble trace metals in airborne particulate matter using a dynamic extraction procedure with on-line inductively coupled plasma optical emission spectrometric detection. *Analytica chimica acta*, *750*, 111-119.

Liu, P. S., Deng, R., Smith, K. A., Williams, L. R., Jayne, J. T., Canagaratna, M. R., Moore, K., Onasch, T. B., Worsnop, D. R., & Deshler, T. (2007). Transmission efficiency of an aerodynamic focusing lens system: Comparison of model calculations and laboratory measurements for the Aerodyne Aerosol Mass Spectrometer. *Aerosol Science and Technology*, *41*(8), 721-733.

Markovic, M. Z., VandenBoer, T. C., & Murphy, J. G. (2012). Characterization and optimization of an online system for the simultaneous measurement of atmospheric water-soluble constituents in the gas and particle phases. *Journal of Environmental Monitoring*, *14*(7), 1872-1884.

Marmur, A., Park, S. K., Mulholland, J. A., Tolbert, P. E., & Russell, A. G. (2006). Source apportionment of PM 2.5 in the southeastern United States using receptor and emissions-based models: Conceptual differences and implications for time-series health studies. *Atmospheric Environment*, *40*(14), 2533-2551.

Middlebrook, A. M., Bahreini, R., Jimenez, J. L., & Canagaratna, M. R. (2012). Evaluation of composition-dependent collection efficiencies for the aerodyne aerosol mass spectrometer using field data. *Aerosol Science and Technology*, *46*(3), 258-271.

Majestic, B. J., Schauer, J. J., Shafer, M. M., Turner, J. R., Fine, P. M., Singh, M., & Sioutas, C. (2006). Development of a wet-chemical method for the speciation of iron in atmospheric aerosols. *Environmental science & technology*, *40*(7), 2346-2351.

Majestic, B. J., Schauer, J. J., & Shafer, M. M. (2007). Development of a manganese speciation method for atmospheric aerosols in biologically and environmentally relevant fluids. *Aerosol Science and Technology*, *41*(10), 925-933

Miljevic, B., Fairfull-Smith, K. E., Bottle, S. E., & Ristovski, Z. D. (2010). The application of profluorescent nitroxides to detect reactive oxygen species derived from combustion-generated particulate matter: Cigarette smoke–A case study. *Atmospheric Environment*, *44*(18), 2224-2230.

Misra, C., Geller, M. D., Shah, P., Sioutas, C., & Solomon, P. A. (2001). Development and Evaluation of a Continuous Coarse (PM10–PM25) Particle Monitor. *Journal of the Air*

Moreno, T., Querol, X., Alastuey, A., Viana, M., Salvador, P., De la Campa, A. S., Artiñano, B., De la Rosa, J., & Gibbons, W. (2006). Variations in atmospheric PM trace metal content in Spanish towns: illustrating the chemical complexity of the inorganic urban aerosol cocktail. *Atmospheric Environment*, *40*(35), 6791-6803.

Mukhtar, A., & Limbeck, A. (2013). Recent developments in assessment of bio-accessible trace metal fractions in airborne particulate matter: A review. *Analytica chimica acta*, *774*, 11-25.

Ntziachristos, L., Froines, J. R., Cho, A. K., & Sioutas, C. (2007). Relationship between redox activity and chemical speciation of size-fractionated particulate matter. *Particle and fibre toxicology*, *4*(1), 5.

Orsini, D. A., Ma, Y., Sullivan, A., Sierau, B., Baumann, K., & Weber, R. J. (2003). Refinements to the particle-into-liquid sampler (PILS) for ground and airborne measurements of water-soluble aerosol composition. *Atmospheric Environment*, *37*(9), 1243-1259.

Oakes, M., Rastogi, N., Majestic, B. J., Shafer, M., Schauer, J. J., Edgerton, E. S., & Weber, R. J. (2010). Characterization of soluble iron in urban aerosols using near-real time data. *Journal of Geophysical Research: Atmospheres*, *115*(D15).

Ospital, J., Cassmassi, J., & Chico, T. (2008). Multiple Air Toxics Exposure Study in the South Coast Air Basin (MATES III). *South Coast Air Quality Management District, Diamond Bar, CA*.

Pacyna J M (1999), *Source Inventories for Atmospheric Trace Metals* in: Harrison R M and Van Grieken R E, *Atmospheric Particles*, Vol 5.

Pancras, J. P., Ondov, J. M., & Zeisler, R. (2005). Multi-element electrothermal AAS determination of 11 marker elements in fine ambient aerosol slurry samples collected with SEAS-II. *Analytica chimica acta.* 538(1), 303-312.

Pant, P., & Harrison, R. M. (2013). Estimation of the contribution of road traffic emissions to particulate matter concentrations from field measurements: a review. *Atmospheric Environment*, *77*, 78-97.

Pakbin, P., Hudda, N., Cheung, K. L., Moore, K. F., & Sioutas, C. (2010). Spatial and temporal variability of coarse (PM10− 2.5) particulate matter concentrations in the Los Angeles area. *Aerosol Science and Technology*, *44*(7), 514-525.

Pakbin, P., Ning, Z., Shafer, M. M., Schauer, J. J., & Sioutas, C. (2011). Seasonal and spatial coarse particle elemental concentrations in the Los Angeles area. *Aerosol Science and Technology*, *45*(8), 949-963.

Perez, L., Tobias, A., Querol, X., Künzli, N., Pey, J., Alastuey, A., Viana, M., Valero, N., González-Cabré, M., & Sunyer, J. (2008). Coarse particles from Saharan dust and daily mortality. *Epidemiology*, *19*(6), 800-807.

Pérez, N., Pey, J., Querol, X., Alastuey, A., López, J. M., & Viana, M. (2008). Partitioning of major and trace components in PM 10–PM 2.5–PM 1 at an urban site in Southern Europe. *Atmospheric Environment*, *42*(8), 1677-1691.

Perrino, C., De Santis, F., & Febo, A. (1990). Criteria for the choice of a denuder sampling technique devoted to the measurement of atmospheric nirous and nitric acids. *Atmospheric Environment. Part A. General Topics*, *24*(3), 617-626

Perrino, C., & Gherardi, M. (1999). Optimization of the coating layer for the measurement of ammonia by diffusion denuders. *Atmospheric Environment*, *33*(28), 4579-4587.

Perrino, C., Ramirez, D., & Allegrini, I. (2001). Monitoring acidic air pollutants near Rome by means of diffusion lines: development of a specific quality control procedure. *Atmospheric Environment*, *35*(2), 331-341.

Perrino, C., Pietrodangelo, A., & Febo, A. (2001). An atmospheric stability index based on radon progeny measurements for the evaluation of primary urban pollution. *Atmospheric Environment*, *35*(31), 5235-5244.

Perrino, C., Canepari, S., Catrambone, M., Dalla Torre, S., Rantica, E., & Sargolini, T. (2009). Influence of natural events on the concentration and composition of atmospheric particulate matter. *Atmospheric Environment*, *43*(31), 4766-4779.

Perrino, C., Canepari, S., Pappalardo, S., & Marconi, E. (2010). Time-resolved measurements of water-soluble ions and elements in atmospheric particulate matter for the characterization of local and long-range transport events. *Chemosphere*, *80*(11), 1291-1300.

Perrino, C., Catrambone, M., Dalla Torre, S., Rantica, E., Sargolini, T., & Canepari, S. (2014). Seasonal variations in the chemical composition of particulate matter: a case study in the Po Valley. Part I: macro-components and mass closure. *Environmental Science and Pollution Research*, *21*(6), 3999-4009.

Perrino, C., Catrambone, M., Farao, C., Salzano, R., Esposito, G., Giusto, M., Montagnoli, M., Marini, A., Brinoni, M., Simonetti, G., & Canepari, S. (2015). Improved Time-Resolved Measurements of Inorganic Ions in Particulate Matter by PILS-IC Integrated with a Sample Pre-Concentration System. *Aerosol Science and Technology*, *49*(7), 521-530.

Peters, A., Veronesi, B., Calderón-Garcidueñas, L., Gehr, P., Chen, L. C., Geiser, M., Reed, W., Rothen-Rutishauser, B., Schürch, S., & Schulz, H. (2006). Translocation and potential neurological effects of fine and ultrafine particles a critical update. Particle and fibre toxicology, 3(1), 13.

Pope III, C. A., Burnett, R. T., Thun, M. J., Calle, E. E., Krewski, D., Ito, K., & Thurston, G. D. (2002). Lung cancer, cardiopulmonary mortality, and long-term exposure to fine particulate air pollution. *Jama*, *287*(9), 1132-1141.

Pope, C. A., Burnett, R. T., Thurston, G. D., Thun, M. J., Calle, E. E., Krewski, D., & Godleski, J. J. (2004). Cardiovascular mortality and long-term exposure to particulate air pollution. *Circulation*, *109*(1), 71-77.

Pope III, C. A., & Dockery, D. W. (2006). Health effects of fine particulate air pollution: lines that connect. *Journal of the air & waste management association*, *56*(6), 709-742.

Protano, C., Astolfi, M. L., Canepari, S., & Vitali, M. (2016). Urinary levels of trace elements among primary school-aged children from Italy: The contribution of smoking habits of family members. *Science of the Total Environment*, *557*, 378-385.

Propper, R., Wong, P., Bui, S., Austin, J., Vance, W., Alvarado, Á., Croes, B., & Luo, D. (2015). Ambient and emission trends of toxic air contaminants in California. *Environmental science & technology*, *49*(19), 11329-11339.

Putaud, J. P., Raes, F., Van Dingenen, R., Brüggemann, E., Facchini, M. C., Decesari, S., Fuzzi, S., Gehrig, R., Hüglin, C., Laj, P. & Lorbeer, G. (2004). A European aerosol phenomenology—2: chemical characteristics of particulate matter at kerbside, urban, rural and background sites in Europe. *Atmospheric environment*, *38*(16), 2579-2595.

Putaud, J. P., Van Dingenen, R., Alastuey, A., Bauer, H., Birmili, W., Cyrys, J., Flentje, H., Fuzzi, S., Gehrig, R., & Harrison, R. M. (2010). A European aerosol phenomenology–3: Physical and chemical characteristics of particulate matter from 60 rural, urban, and kerbside sites across Europe. *Atmospheric Environment*, *44*(10), 1308-1320.

Querol, X., Alastuey, A., Rodriguez, S., Plana, F., Ruiz, C. R., Cots, N., Massague, G. & Puig, O. (2001). PM10 and PM2. 5 source apportionment in the Barcelona Metropolitan area, Catalonia, Spain. *Atmospheric Environment*, *35*(36), 6407-6419.

Querol, X., Zhuang, X., Alastuey, A., Viana, M., Lv, W., Wang, Y., López, A., Zhu, Z., Wei, H., & Xu, S. (2006). Speciation and sources of atmospheric aerosols in a highly industrialised emerging mega-city in Central China. *Journal of Environmental Monitoring*, *8*(10), 1049-1059.

Querol, X., Minguillón, M. C., Alastuey, A., Monfort, E., Mantilla, E., Sanz, M. J., Sanz, F., Roig, A., Renau, A., Felis, C., Artíñano, B., & Miró, J. V. (2007). Impact of the implementation of PM abatement technology on the ambient air levels of metals in a highly industrialised area. *Atmospheric Environment*, *41*(5), 1026-1040.

Qureshi, S., Dutkiewicz, V. A., Khan, A. R., Swami, K., Yang, K. X., Husain, L., Schwab J.J. & Demerjian, K. L. (2006). Elemental composition of PM 2.5 aerosols in Queens, New York: solubility and temporal trends. *Atmospheric Environment*, *40*, 238-251.

Saffari, A., Daher, N., Shafer, M. M., Schauer, J. J., & Sioutas, C. (2013). Seasonal and spatial variation of trace elements and metals in quasi-ultrafine (PM 0.25) particles in the Los Angeles metropolitan area and characterization of their sources. *Environmental pollution*, *181*, 14-23.

Sato, K., Tamura, T., & Furuta, N. (2008). Partitioning between soluble and insoluble fractions of major and trace elements in size-classified airborne particulate matter collected in Tokyo. *Journal of Environmental Monitoring*, *10*(2), 211-218.

Shafer, M. M., Perkins, D. A., Antkiewicz, D. S., Stone, E. A., Quraishi, T. A., & Schauer, J. J. (2010). Reactive oxygen species activity and chemical speciation of size-fractionated atmospheric particulate matter from Lahore, Pakistan: an important role for transition metals. *Journal of Environmental Monitoring*, *12*(3), 704-715.

Shi, T., Schins, R. P., Knaapen, A. M., Kuhlbusch, T., Pitz, M., Heinrich, J., & Borm, P. J. (2003). Hydroxyl radical generation by electron paramagnetic resonance as a new method to monitor ambient particulate matter composition. *Journal of Environmental Monitoring*, *5*(4), 550-556.

Shirmohammadi, F., Hasheminassab, S., Wang, D., Saffari, A., Schauer, J. J., Shafer, M. M., Delfino, R.J., & Sioutas, C. (2015). Oxidative potential of coarse particulate matter (PM 10–2.5) and its relation to water solubility and sources of trace elements and metals in the Los Angeles Basin. *Environmental Science: Processes & Impacts*, *17*(12), 2110-2121.

Sillanpää, M., Saarikoski, S., Hillamo, R., Pennanen, A., Makkonen, U., Spolnik, Z., Van Grieken R, Koskentalo T, & Salonen, R. O. (2005). Chemical composition, mass size distribution and source analysis of long-range transported wildfire smokes in Helsinki. *Science of the Total Environment*, *350*(1), 119-135.

Sowlat, M. H., Hasheminassab, S., & Sioutas, C. (2016). Source apportionment of ambient particle number concentrations in central Los Angeles using positive matrix factorization (PMF). *Atmospheric Chemistry and Physics*, *16*(8), 4849-4866.

Stolzenburg, M. R., & Hering, S. V. (2000). Method for the automated measurement of fine particle nitrate in the atmosphere. *Environmental science & technology*, *34*(5), 907-914.

Tao, F., Gonzalez-Flecha, B., & Kobzik, L. (2003). Reactive oxygen species in pulmonary inflammation by ambient particulates. *Free Radical Biology and Medicine*, *35*(4), 327-340.

Tsai, C. J., & Perng, S. N. (1998). Artifacts of ionic species for hi-vol PM 10 and PM 10 dichotomous samplers. *Atmospheric Environment*, *32*(9), 1605-1613.

Timonen, H., Aurela, M., Carbone, S., Saarnio, K., Saarikoski, S., Mäkelä, T., Kulmala, M., Kerminen, V. M., Worsnop, D.R., & Hillamo, R. (2010). High time-resolution chemical characterization of the

water-soluble fraction of ambient aerosols with PILS-TOC-IC and AMS. *Atmospheric Measurement Techniques*, *3*(4), 1063-1074.

Rastogi, N., Oakes, M. M., Schauer, J. J., Shafer, M. M., Majestic, B. J., & Weber, R. J. (2009). New technique for online measurement of water-soluble Fe (II) in atmospheric aerosols. *Environmental science & technology*, *43*(7), 2425-2430.

Reche, C., Moreno, T., Amato, F., Viana, M., van Drooge, B. L., Chuang, H. C., Bérubé K, Jones T, Alastuey A,& Querol, X. (2012). A multidisciplinary approach to characterise exposure risk and toxicological effects of PM 10 and PM 2.5 samples in urban environments. *Ecotoxicology and environmental safety*, *78*, 327-335.

Valavanidis, A., Fiotakis, K., Bakeas, E., & Vlahogianni, T. (2005). Electron paramagnetic resonance study of the generation of reactive oxygen species catalysed by transition metals and quinoid redox cycling by inhalable ambient particulate matter. *Redox Report*, *10*(1), 37-51.

Vecchi, R., Marcazzan, G., Valli, G., Ceriani, M., & Antoniazzi, C. (2004). The role of atmospheric dispersion in the seasonal variation of PM1 and PM2.5 concentration and composition in the urban area of Milan (Italy). *Atmospheric Environment*, *38*(27), 4437-4446.

Vecchi, R., Valli, G., Fermo, P., D'Alessandro, A., Piazzalunga, A., & Bernardoni, V. (2009). Organic and inorganic sampling artefacts assessment. *Atmospheric Environment*, *43*(10), 1713-1720.

Verma, V., Polidori, A., Schauer, J. J., Shafer, M. M., Cassee, F. R., & Sioutas, C. (2009). Physicochemical and toxicological profiles of particulate matter in Los Angeles during the October 2007 southern California wildfires. *Environmental science & technology*, *43*(3), 954-960.

Viana, M., Querol, X., Götschi, T., Alastuey, A., Sunyer, J., Forsberg, B., Heinrich, J., Norback, D., Payo, F., Maldonado, J.A. & Künzli, N. (2007). Source apportionment of ambient PM 2.5 at five Spanish centres of the European community respiratory health survey (ECRHS II). *Atmospheric Environment*, *41*(7), 1395-1406.

Viana, M., Kuhlbusch, T. A. J., Querol, X., Alastuey, A., Harrison, R. M., Hopke, P. K., Winiwarter, W., Vallius, M., Szidat, S., Prévôt, A. S. H. & Hueglin, C. (2008). Source apportionment of particulate matter in Europe: a review of methods and results. *Journal of aerosol science*, *39*(10), 827-849.

Voutsa, D., & Samara, C. (2002). Labile and bioaccessible fractions of heavy metals in the airborne particulate matter from urban and industrial areas. *Atmospheric Environment*, *36*(22), 3583-3590.

Wang, D., Pakbin, P., Saffari, A., Shafer, M. M., Schauer, J. J., & Sioutas, C. (2013). Development and evaluation of a high-volume aerosol-into-liquid collector for fine and ultrafine particulate matter. *Aerosol Science and Technology*, *47*(11), 1226-1238.

Wang, D., Pakbin, P., Shafer, M. M., Antkiewicz, D., Schauer, J. J., & Sioutas, C. (2013). Macrophage reactive oxygen species activity of water-soluble and water-insoluble fractions of ambient coarse, PM 2.5 and ultrafine particulate matter (PM) in Los Angeles. *Atmospheric environment*, *77*, 301-310.

Wang, D., Shafer, M. M., Schauer, J. J., & Sioutas, C. (2015). A new technique for online measurement of total and water-soluble copper (Cu) in coarse particulate matter (PM). *Environmental Pollution*, *199*, 227-234.

Wang, D., Sowlat, M. H., Shafer, M. M., Schauer, J. J., & Sioutas, C. (2016). Development and evaluation of a novel monitor for online measurement of iron, manganese, and chromium in ambient particulate matter (PM). *Science of the Total Environment*, *565*, 123-131.

Weber, R. J., Orsini, D., Daun, Y., Lee, Y. N., Klotz, P. J., & Brechtel, F. (2001). A particle-into-liquid collector for rapid measurement of aerosol bulk chemical composition. *Aerosol Science & Technology*, *35*(3), 718-727.

Wittig, A. E., Takahama, S., Khlystov, A. Y., Pandis, S. N., Hering, S., Kirby, B., & Davidson, C. (2004). Semi-continuous PM 2.5 inorganic composition measurements during the Pittsburgh air quality study. *Atmospheric Environment*, 38(20), 3201-3213.

Wu, W.S., Wang, T. (2007). On the performance of a semi-continuous PM2.5 sulphate and nitrate instrument under high loadings of particulate and sulphur dioxide. *Atmospheric Environment* 41, 5442–5451

Yu, X. Y., Lee, T., Ayres, B., Kreidenweis, S. M., Malm, W., & Collett, J. L. (2006). Loss of fine particle ammonium from denuded nylon filters. *Atmospheric Environment*, *40*(25), 4797-4807.

Zhang, Y., Schauer, J. J., Shafer, M. M., Hannigan, M. P., Dutton, S. J. (2008). Source apportionment of in-vitro reactive oxygen species bioassay activity from atmospheric particulate matter. *Environmental Science & Technology,* 42:6502-7509.

CHAPTER III: Health and Environmental Effects of Particulate Matter (PM)

In recent years, the air pollution is attracting increased attention from institutions and research groups. In particular, the environmental problem of PM is one of the most difficult to solve, because of its heterogeneous and variable composition, and because of all the chemical physical factors that influence it. However, recent environmental studies are focusing their attention on the development of monitoring systems in urban, rural and remote areas and on the possibility to determine the chemical form and concentration of the species present in the atmosphere. To this purpose, information about concentration and chemical forms may be useful to study and explain the possible cause-effect relationships between harmful pollutants and human health (Hlavay et al., 2001, Ricci and Cirillo, 1985).

3.1 Effects on human health.

The human population is subject to air pollution exposure because particulate matter is considered an integral part of the air we breathe. International institutions think that the dangerousness of PM are essentially based on the mass concentration and particle size fractions. This approach can show different aspect of environmental impact and toxicity; in addiction, we have to take into account that the only determination of the total concentration do not provide any information about the bioavailability of the species and their interaction with the human organism. For instance, the metals' toxicity is closely related to the oxidation state in which they are present. An element can be beneficial or toxic depending on its oxidation and this represents a great limitation, as it is well known that the different chemical physical forms in which a substance is present, e.g. Cr (III) can be an essential element for the metabolism of glucose, while Cr (VI) is carcinogenic. The oxidation state can also affect the absorption and elimination time of an element. The ion Fe (II) is soluble in physiological conditions, it diffuses freely through the membranes, while the Fe (III) does not easily enter into the cells, and is more subject to hydrolysis in biological systems. Moreover, the mobility of an element depends on many other factors, such as solubility, pH and ionic strength. For example, Cr is not soluble in neutral water solutions, but may become soluble at a more basic pH values (Goodarzi and Huggins, 2001). However, these substances undergo transformation, interconversion and degradation processes, affected by the environmental conditions; giving rise to products with physical chemical properties and toxicity different from those of the originating compounds. At present, only few chemical species present in the atmosphere are normed:

• The Italian Dlgs 60/2002 contains the limit values and alert thresholds for NO_2, NO_x, SO_2, CO, PM_{10}, Benzene, Pb (Dlgs 60/2002).

• The Dlgs 261/2002 establishes target values for As, Cd, Ni, Hg and Benzo (a) pyrene (Dlgs 261/2002). The gaseous NO_x and SO_2 are irritating and pungent. They form oxidizing and corrosive acids in the atmosphere. These acids form secondary salts, as previously discussed, which, because of the small size, penetrate into the respiratory system reaching the pulmonary alveoli and causing chronic respiratory diseases such as asthma, bronchitis and emphysema.Among these, the carbon monoxide is quickly adsorbed in the pulmonary alveoli; the benzo (a) pyrene is highly soluble and can cross the membrane very easily. In addition, the Polycyclic Aromatic Hydrocarbon (PAHs) as well as benzene have been classified by the IARC (International Agency for Research on Cancer) as possible or probable human carcinogens.

3.2 Effects on climate and environment

The PM absorbs and/or reflects the sunlight radiations as a function of the particle size and chemical composition: on one hand, particles reflect sunlight, leading to a cooling of the earth surface;on the other hand, hey have a role in the absorption of terrestrial infrared radiations, contributing positively to the global heating. The light attenuation is mainly caused by the particles of secondary origin belonging to the ultrafine fraction, while the particles of the accumulation mode involve the light dispersion and cause a reduced visibility. The light absorption is directly related to the chemical composition of the particles. For example, the carbonaceous substances absorb strongly the solar radiation (Barry and Chorley, 1992). PM also acts on the environment through acid rains.

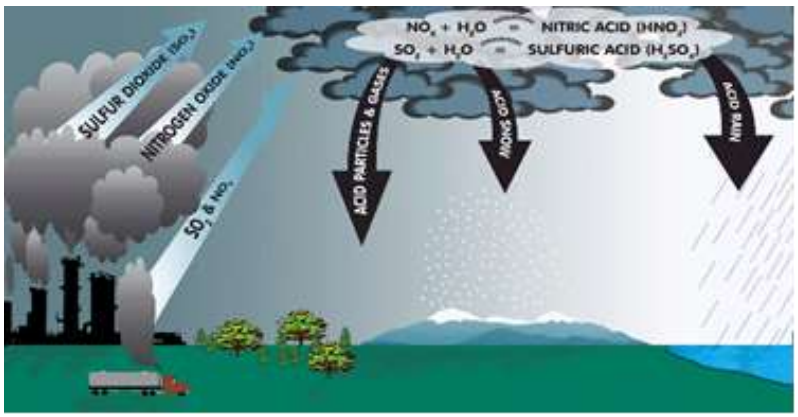

Figure 3.1: *Acid Deposition Large Graphic (http://www.dec.ny.gov/chemical/41293.html)*

This phenomenon is caused mainly by atmospheric gaseous components (SO_2, SO_3, NO_x and CO_2) coming from combustion and industrial activities in general. These gases can be transformed in a few days in acid (H_2SO_4, HNO_3, HNO_2) by means of reactions with H_2O or OH radical, giving rise to acid precipitations (figure 3.1). The fallout on the ground of acid pollutants occurs through wet or dry deposition. The first one is the most known and occurs in the form of rain, snow, acid fog. The dry deposition consists of the fallout on the soil of acidic substances in the form of gas or microscopic particles (Morselli, 1991). These phenomena can cause an alteration of the chemical composition of the groundwater, lakes, rivers and seawaters. In addition, the vegetation also is affected by acid rains causing plants' weakening and resulting in a rapid decline of some forests. Moreover, the action of acid rain is clearly visible on the monuments (historic buildings, metal statues, etc.) by action of corrosion or by the removal mechanical of materials, previously made friable and soluble. In the limestone monuments, sulphuric acid (H_2SO_4) present in the acid depositions turns the calcium carbonate ($CaCO_3$) into calcium sulphate ($CaSO_4$), which is easily washed away by rainwater. Even metals are considerably corroded by acid rain and in particular by the sulphuric and nitric acid, which have a strong oxidizing power, e.g. acid precipitation determines the formation of a typical green layer on copper or bronze monuments, due to copper salts (Morseli, 1991).

3.3 Regulations concerning PM emissions

The standards concerning air quality are constantly evolving because of the increasing need to protect both resources and human health and to assure a sustainable development for the next generations. During the last decades, the Italian situation has profoundly changed: most of the emissions are due to particulate matter and nitrogen oxides resulting from the natural gas combustion and to carbon monoxide from road traffic. As a result, air pollution today mainly interests the urban areas and industrial centers. The vehicular traffic is the main cause of air pollution in urban areas, in which very often the high concentrations of pollutants accumulate, due to the unfavorable atmospheric conditions. A key role is played by the European Union (EU), which has established new regulations to ensure a significant reduction of the ambient concentrations of pollutants. The Italian Dlgs 60/2002 (transposition of the European Directive 1999/30/CE), sets the daily limit value for PM_{10} to 50 $\mu g/m^3$ not to be exceeded more than 35 times a year, while 40 $\mu g/m^3$ is the yearly average value. In 2008 the EU adopted a new directive 2008/50/CE, transposed in Italy as Dlgs 155/2010, promoting further studies in the air quality field and recognizing, for the first time, the limits of the only PM mass concentration determination. In particular, it introduced the measurement of the $PM_{2.5}$ mass

concentration, considered potentially more dangerous to human health, while the limit values for PM_{10} have remained unaltered. Furthermore, it establishes the obligation to measure the concentration of some specific components (reported in table 3.1), useful to allow the differentiation among the background, local and regional contributions. Unlike the previous one, this legislation requires the chemical characterization of samples, necessary to understand the mechanisms of formation of secondary particles. This also allows to differentiate the emission sources and to separate the contributions due to some special climatic phenomena (transport of natural dust from the desert, or transport of dust from the neighboring Countries), through the combination of the chemical analysis and the statistical models. Finally, this Directive allows deducting the exceedances attributable to the phenomena just mentioned above and it establishes some exceptions to the sampling sites that are subject to particular weather conditions, such as the Po Valley.

Table 3.1*: Species to be measured in PM according to the Directive 2008/50/CE.*

Anions	**Cations**	**C-containing compounds**
SO_4^{2-},Cl^-, NO_3^-	Ca^{2+},NH^{4+},Na^+,K^+, Mg^{2+}	Elemental Carbon (EC) Organic Carbon (OC)

3.4 Oxidative Stress

Numerous epidemiological studies have shown a correlation between increased cardiorespiratory disease outbreaks and exposure to atmospheric particulate matter; this is one of the mechanisms related to these effects concerning the generation of oxidative stress (Brook et al., 2010).

Oxidative stress arises when there is an imbalance between the level of reactive oxygen species (ROS) or free radicals, and the biological system's natural antioxidant defence. ROS can be generated directly on PM's surface or indirectly when cells interact with PM. ROS can damage membrane lipids, proteins, and DNA, which can result in cell death via either necrotic or apoptotic processes. Elevated levels of oxidative stress lead to inflammatory response via activation of various transcription factors and stimulation of cytokine production. The right balance between oxidizing and antioxidant substances is essential to maintain unaltered physiological functions; for example, proteins are susceptible to variation of redox species in intracellular transduction processes. Oxidative

phosphorylation processes and mitochondrial electron transport are the basis of ROS formation in cells by generating superoxide ion (O_2^-), hydroxyl radical hydroxide and hydrogen peroxide (H_2O_2). These molecules are able to interact with DNA, lipids and proteins creating physiological alterations. In particular, the superoxide ion, produced at the mitochondrial level, reacts with the sulfhydric centres of some enzymes and is converted into hydrogen peroxide by the superoxide dismutase enzyme. Hydrogen peroxide can also react with metals by reacting Fenton producing the hydroxyl radical (Schwarze et al., 2006; Vidrio et al., 2008).

$$Fe^{2+} + H_2O_2 \rightarrow Fe^{3+} + OH\cdot + OH^-$$
$$Fe^{3+} + H_2O_2 \rightarrow Fe^{2+} + OOH\cdot + H^+$$

Some enzymes such as superoxide dismutase, catalase and glutathione peroxidase (GPX) (Brook et al., 2010) and antioxidant molecules such as vitamins, flavonoids, carotenoids, uric acid and glutathione provide antioxidant defences in the body. If these are not enough to avoid oxidative action, the cell may suffer damage to the membrane phospholipids, causing the loss of selective transport function. In addition, alterations in genetic expression can be caused by damage to nucleic acids and proteins by oxidation of cysteine groups with loss of protein structure. Several studies indicates that the chemical composition, surface area and other characteristics of PM are potentially more closely linked to the induction of toxic responses (Kelly et al., 2012; Borm et al., 2007; Nel et al., 2005). As it is known, transition metals such as iron (Fe), copper (Cu), vanadium (V), and nickel (Ni) have been implicated as potential mediators of PM-related respiratory inflammation and associated with mortality and increased hospital admissions (Kelly et al., 2012; Cassee et al., 2013). Especially Fe and Cu are considered important in PM induced formation of ROS through the Fenton reaction (Schwarze, et al 2006; Vidrio et al., 2008). Furthermore, elemental carbon (EC, also called black carbon or soot) and organic carbon (OC) constitute a large part of particle mass and have been associated with mortality and hospital admissions in epidemiological studies. (Kelly et al., 2012; Janssen, et al., 2011; World Health Organization. REVIHAAP project: final technical report, 2013). The OC fraction of PM includes compounds such as polycyclic aromatic hydrocarbons (PAHs) and quinones. Quinones especially have the ability to catalyse production of ROS (i.e. hydrogen peroxide) by undergoing redox recycling and reducing oxygen to produce superoxide radicals (Chung et al., 2006). Finally, the role of secondary organic aerosols (SOA), which are formed after photochemical oxidation of volatile organic precursors, is still unclear as presently it is difficult to distinguish between the toxicity of primary and secondary organic aerosols (Cassee, et al., 2013). Thanks to the

study of the chemical composition of the particles and the measurement of oxidative potential (OP) we would be able to obtain important information, capable of linking the chemical species to the possible toxicological mechanisms

3.5 Oxidative potential assays

To assess the particles' OP, several acellular assays have been developed. These assays reflect the chemical properties of PM, which are responsible for the induction of oxidative stress under biological conditions. An overview of different acellular OP assays is shown in Table 3.2.

Table 3.2 Overview of available acellular assays to assess the oxidative potential of PM.

Assay	Methodology/principle
Depletion of antioxidants	Depletion of antioxidants in a synthetic respiratory tract lining fluid (RTFL) consisting of single or composite solutions of ascorbate acid, reduced glutathione, uric acid, measured by reverse phase high pressure liquid chromatography (HPLC) or spectrophotometer (Mudway et al., 2004; Stoeger et al., 2008).
Consumption of dithiothreitol (DTT)	Based on the ability of PM to transfer electrons from DTT to oxygen, generating superoxides (Cho et al., 2005).
Fluorescent probes	Based on the principle that a fluorescent product is generated when a nonfluorescent probe molecule reacts with ROS: • p-hydroxyphenylacetic acid (POHPAA) with horseradish peroxidase enzyme to detect hydroperoxides (Hasson et al., 2003). • DCFH probe which gets oxidized in the presence of ROS and horseradish peroxidase (Hung et al., 2001). • BPEAnit: probe based on trapping of ROS by profluorescent nitroxides (Miljevic et al., 2010). • CRAT: chemiluminogenic compounds, where certain acridium esters are sensitive to superoxides (Zomer et al., 2011).
Formation of hydroxyl radical	• Based on the reaction of salicylic acid with hydroxyl radical to form dihydroxybenzoate

	(DHBA), measured by HPLC (DiStefano et al., 2009). • Measures OH-radical production by adding dimethylsulfoxide (DMSO), quantified fluorometrically (Alaghmand et al., 2007). • Electron paramagnetic/spin resonance (EPR/ESR): Measures the formation of the hydroxyl (•OH) radical in PM suspensions in the presence of hydrogen peroxide and 5,5-dimethyl-1-pyrroline-N-oxide (DMPO) as a specific spin-trap (Shi et al., 2003).
Glyceraldehyde-3- Phosphate dehydrogenase (GAPDH) in activation	Based on the reaction between an electrophile and a reactive thiolate in GAPDH (Shinyashiki et al., 2008).

In my PhD work, I focused my attention on three different methods present in literature for the determination of oxidative potential. The choice can be justified through a careful evaluation of different important factors, as the literature knowledge, the ease of reproduction of the three methods, and the possibility to include the OP assay in the analytical procedure already used in our laboratory, which allows a quite detailed chemical characterization on a single PM sample. OP assays choose were: dithiothreitol (DTT), 2′,7′-dichlorofluorescin (DCFH) and acid ascorbic (AA).

3.5.1. 1,4-Ditiotreitolo (DTT)

The 1,4-ditiotreitolo (DTT, $HSCH_2CH(OH)CH(OH)CH_2SH$) is a strong reducing agent, commonly used as an acellular method for measuring the oxidative potential induced by atmospheric particulate matter (Verma et al., 2011; Cho et al., 2005). The assay is based on the measurement of the DTT depletion due to components present in the PM filter extracts; this procedure measures the ability of soluble PM components to transfer electrons to DTT producing radical superoxides, and then other ROSs, such as hydrogen peroxide and radical hydroxide.

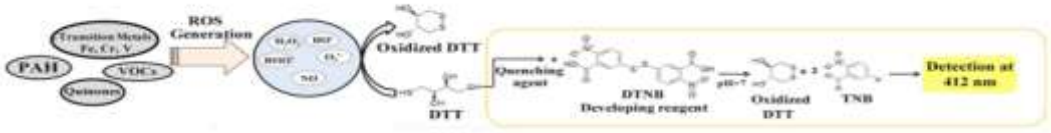

Figure 3.2: *Representative scheme of the reaction mechanism between DTT and ROS and subsequent quantification of depletion*

Although it is a widely used method, there is little information in the literature about the specific substances that can oxidize DTT. In general, correlation studies between the PM composition and DTT depletion were performed to determine the individual species. Some studies have been conducted by making known additions of copper or iron in order to detect possible correlation with metals and oxidation of DTT. Such experiments did not show an increase in antioxidant depletion, so it was thought that the method was not sensitive to metals (Verma et al., 2011). In contrast, it has been shown that the major substances responsible for oxidation of DTT are carbon species, elemental carbon, the WSOC and the IPA (Verma et al., 2011; Cho et al., 2005). In particular, Kumagai et al. (2002) demonstrated that quinone 9,10 phenanthrachinone can effectively catalyse the transfer of electrons from DTT to oxygen, generating superoxides, as shown in Figure 3.3. Although several works seem to indicate that the method is specific to organic substances, recent studies have shown its affinity for some metals, especially for Cu and Mn. Recent studies also demonstrated a correlation between metals and DTT, probably due to a covariance between metals and carbonaceous species (Ntziachristos et al., 2007).

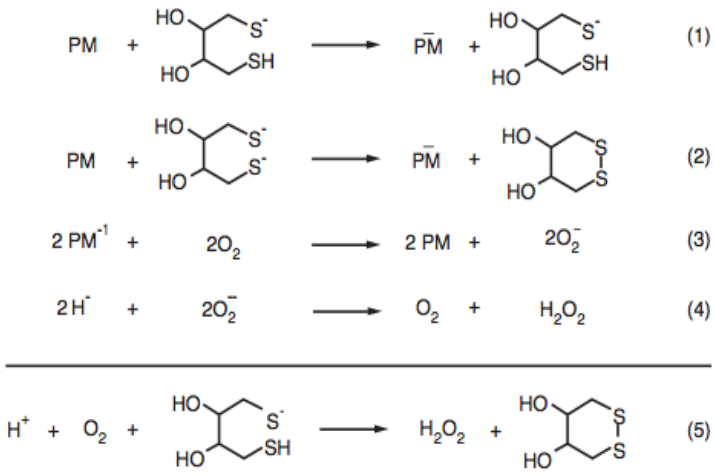

Figure 3.3: *Chemical reaction between DTT and oxygen, with PM as a catalyst*

3.5.2. 2,7-Diclorodiidrofluoresceina (DCFH)

The 2,7-dichlorodihydrofluorescein method is widely used to measure the oxidative potential of atmospheric particulate matter. It is based on the oxidation of DCFH, a non-fluorescent reagent, to DCF, a fluorescent compound, in the presence of ROS and horseradish peroxidase (HRP), a redox enzyme that primarily reacts with hydrogen peroxide and organic hydroperoxides.

In general, as mentioned above, the reaction mechanism involves two stages: in the first step, PM reacts with the enzyme, in the second the DCFH is oxidized to the DCF fluorescent compound, the

concentration of which is proportional to the concentration of the ROS. The product is detected by fluorescence. The diagram below (figure 3.4) shows the reaction pattern between DCFH /HRP with peroxides: in the cycle a) it is shown the initial reaction of H_2O_2 with the HRP enzyme followed by the DCFH reaction that lead to the formation of DCF fluorescence product. In cycle b) is reported the reaction of HRP with the oxygen which generate DCF. The fluorescence intensity is measured, and then converted into hydrogen peroxide equivalents, which is used as an indicator of the ROS reactivity by calibration of the instrument performed with H_2O_2 standard (Wang et al., 2012).

For a proper evaluation of the final fluorescence measurement, it must be considered that a concentration of the nmol of H_2O_2 in deionized water is constantly present and it is in equilibrium with the dissolved oxygen; as a consequence there is a background signal not due to the presence of ROS.

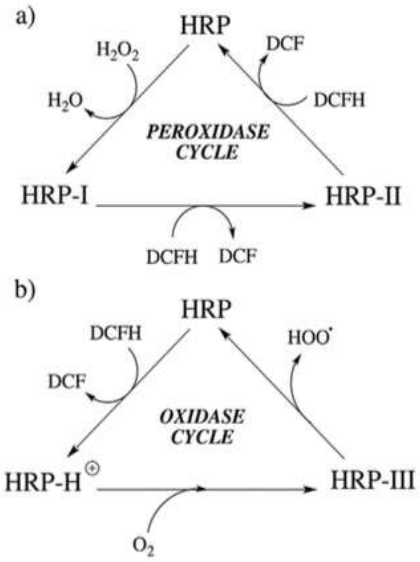

Figure 3.4: *DCFH-DA: Fluorescent compound formation from ROS*

(Berglund et al., 2002)

Additionally, dissolved oxygen can interact with HRP to oxidize DCFH to DCF, as shown in Figure 3.3. Both of these background signals must be eliminated by subtracting the value obtained from background at the fluorescence value measured in the presence of PM samples. And besides, to reduce the background signal of H_2O_2 and to prevent photo-oxidation of DCFH, the procedure must be performed in the dark. In order to reduce these signals, previous studies have foreseen the use of metal catalysts such as MnO to remove H_2O_2, but it was seen that hydrogen peroxide concentrations were rapidly regenerated, so today it is used the blank subtraction to clear the background signals. Originally, this method was used to detect picomol concentrations of hydrogen peroxide and only in

the recent years it has been applied to determine the formation of ROS in biological cells. Today is one of the most common methods used for ROS measurement in PM (Venkatachari et al., 2005).
ROSs are generally quantified by off-line techniques in extracts of airborne particulate filters by detecting fluorescence. Due to the high ROS reactivity, off-line methods may be unworkable as some species may degrade over time during sampling and during laboratory activity. Recent studies present online methods for measuring ROS with DCFH to reduce time and possible degradation of compounds. For example, in Wang et al., 2012 have developed an on-line method for determining ROS by DCFH.

3.5.3 Ascorbic acid (AA)

The ascorbic acid method for measuring oxidative potential induced by PM consists of a simplified reproduction of the respiratory tract fluid (RTFL). RTFL is a fluid thin layer rich in enzymes, proteins and small molecules such as vitamin E and C and is able to minimize respiratory tract diseases thanks to a high antioxidant power. In vitro and in vivo studies have shown that ascorbic acid, uric acid and glucose peroxide present in RTFL are consumed following the exposure of ozone, nitrogen dioxide and particulate matter (Zielinski et al., 1999; Mudwayet al., 2004), making ineffective the natural antioxidant defences, and generating oxidative stress. Ascorbic acid is thus a physiological antioxidant that prevents oxidation of lipids and proteins and a variation in the concentration of this molecule in RTLF may be determinant in the generation of adverse effects on human health.
For example, in Kelly et al. (2012), it has been shown that asthmatic patients exhibit a significant decrease in ascorbic acid concentration in the respiratory tract.

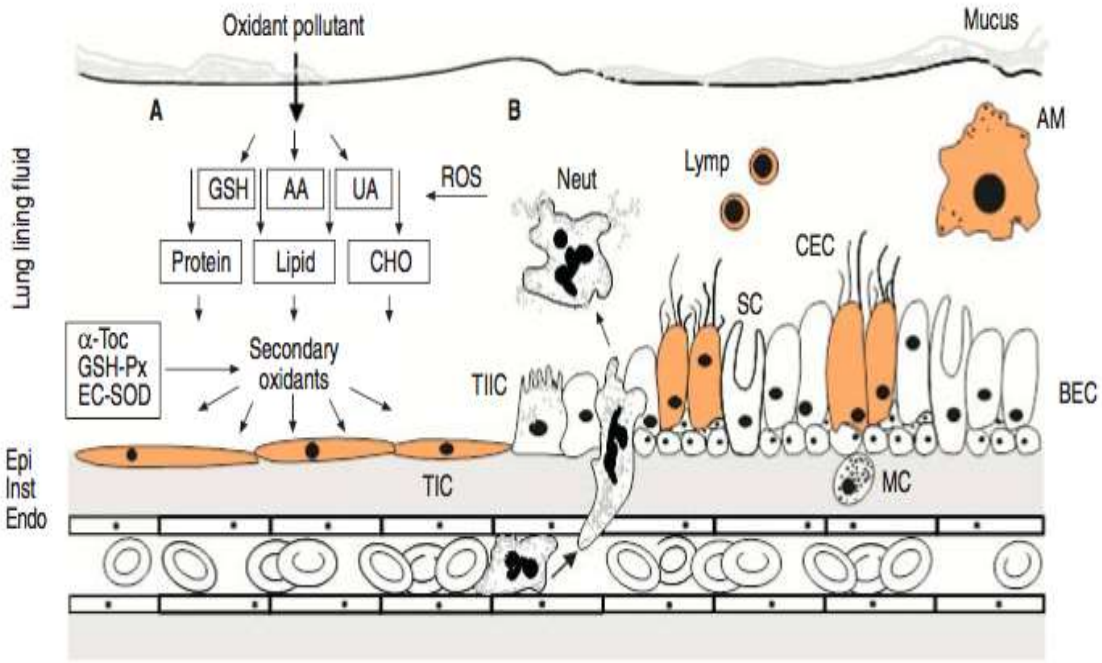

Figure 3.5: *Mechanism of toxicity caused by oxidants present in the lung.*
A: biochemical events; B: cellular events. UA: urate; GSH: glutathione (reduced); CHO: carbohydrates; A-Toc: α-tocopherol; GSH-Px: glutathione peroxidase; EC-SOD: extracellular superoxide dismutase; Epi: epithelial cell; Ist: interstitium; Endo: endothelial cell; Neutral: neutrophil; Lymphocytes; AM: alveolar macrophage; MC: mast cell; TIC: epithelial cell type 1; TIIC: epithelial cell type II; CEC: cherry epithelial cell; BEC: bronchial epithelial cell; SC: secretion cell. Air pollution and the elderly: oxidant/antioxidant issues worth consideration, F.J. Kelly, C. Dunster, I. Mudway)

The use of ascorbic acid as an antioxidant in samples of PM filter extracts represents the interaction caused by the inoculation of particulate material with biological antioxidants, which generates an imbalance of reducing and oxidizing substances, with consequent increase in oxidative stress. The experimental method consists in the measure of the depletion time of ascorbic acid by UV-VIS detection. The decrease in concentration of the antioxidant corresponds to the capacity of reactive species present in PM to catalyse the transfer of electrons from AA to oxygen, generating oxidative potential. Numerous studies have shown that ascorbic acid is mainly related to the redox activity of transition metals, but recent applications show further affinity for organic compounds, especially for quinones (Mudwayet al., 2004).

3.6 Oxidative potential studies

The exploration of the relationship that link the chemical composition of PM with the toxicity for human health is the topic of this chapter. The use of acellular methods for the assessment of the oxidative potential of atmospheric particulate matter has been receiving great scientific attention in

recent years. These methods, considered as predictors of the ability of dust to generate oxidative stress, are typically applied only to the water-soluble fraction of particulate matter (PM). This fraction is considered the most responsible for the effects on health. However, some in vitro studies indicate that the water insoluble fraction also plays an active role in generating oxidative stress (Marcoccia et al., 2017). In subchapter 3.6.1 it is showed the first application of the three different methods for measuring oxidative potential (dithiothreitol (DTT), ascorbic acid and the 2′,7′-dichlorofluorescin (DCFH) assays) to understand the existing correlations between OP and PM generated by specific emission sources. In fact, each method was applied to the soluble and insoluble fractions of some kinds of dust that make significant environmental contributions to PM (i.e. NIST1648a, brake dust, coke, road dust, Saharan dust, soil, ash pellet). The obtained values were interpreted based on the chemical composition of the two solubility fractions. The study showed that the three methods respond differently to the individual chemical components of the PM and that the oxidative potential measured in the insoluble fraction of the dusts is comparable to (or even higher than) that measured in the soluble fraction.

Thanks to these preliminary results, we decided to validate the three acellular assays selected by the analysis of real sample pairs (subchapter 3.6.2). Despite the numerous contributions to uncertainty (sampling, extraction, analysis) and the very small quantities analysed (around 1 mg), the good regression parameters obtained in this evaluation (slope; intercept; Pearson's coefficient) confirmed the good analytic repeatability of the three OP assays. Moreover, we decided to apply the PO assays to field monitoring campaigns carried out in two different areas of Italy: one located in a highly trafficked urban site in Rome, Italy, and the second one situated in an industrial area in the town of Ferrara in the middle of the Po valley. Due to the different chemical composition of the atmospheric particulate in the two areas, it was possible to deepen the relationship between the chemical composition and the response of the three different assays.

Following the results of this two monitoring campaigns, we focused our attention on the relationship that link the size distribution of PM particles with oxidative potential results. The study of the particles' dimensional fraction allows obtaining more information about their origin and formation. It is common knowledge that there is a significant correlation between the size fraction and the contribution due to PM pollution sources in different monitoring areas. In fact, changes of chemical composition, emission sources and meteorological condition could contribute to different health effects. For this reason in the subchapter 3.6.3 we decided to monitor in the same geographical areas (Ferrara and Rome) size-segregated PM samples, obtained by using a co-located Micro-Orifice Uniform Deposition Impactors (MOUDI) equipped with Teflon membrane filters in order to obtain

samples with cut-sizes of 0.18, 0.32, 0.56, 1.0, 1.8, 3.2, 5.6, 10 and 18 µm in aerodynamic diameter (AD) (mod. 110.R, MSP). This work shows significant results in the study of the OP in relation with size distribution particles. In fact, through the study of the relationship that links different locations, with different contributing sources and different size fraction to OP analysis, we can confirm the affinity of the three methods for different chemical and dimensional components.

Finally, in the last period of my PhD work I have taken part in a project about "Carbonaceous Aerosol in Rome and Environs (CARE)", in collaboration with some of the most important Italian research institutions. The experiment was carried out in a downtown in Rome in February 2017. In this monitoring campaign, spatially resolved measurements with high time resolution of Black and elemental carbon (EC), organic carbon (OC), water soluble organic carbon (WSOC) and BrC, major components of nor-refractory PM1 (NH_4^+ , SO_4^{2-} , NO_3^- , Chl), and particle size distribution from 0.008 to 10 *m*m were carried out. The aim of this project was to provide baseline levels of carbonaceous aerosols for the Mediterranean urban area of Rome reducing the assessment uncertainties of aerosol optical, chemical and microphysical properties, and to address future research directions. Furthermore, during this last work (subchapter 3.6.4) I have been involved in the determination of the oxidative potential, sampled by high time resolved sampler, PILS, and subsequently analysed by DCFH assay. The first results showed a relationship between BC and the oxidative stress, explaining significantly different values associated to road traffic and biomass burning aerosols.

*3.6.1 Oxidative potential of selected particulate matter components**

Introduction

Several epidemiological studies have established a consistent association between particulate matter (PM) concentrations and increased morbidity and mortality due to respiratory and cardiovascular diseases (Brunekreef et al., 2002; Brook, et al., 2010; Hoek et al., 2013). Furthermore, various experimental studies have provided a plausible correlation between the PM oxidative capacity and its toxicity (Brook et al., 2010; Donaldson et al., 2003; Nel, 2005; Shi et al., 2003a; Shi et al., 2003b; Zielinski et al., 1999; Kelly and Fussell, 2012). Toxicological studies documented the ability of the inhaled PM to cause oxidative stress by inducing pro-inflammatory effects in the nose, lungs, and cardiovascular system (Donaldson et al., 2003; Ning et al., 2003; Sheesley et al., 2003). Oxidative stress occurs when there is an imbalance between the level of reactive oxygen species (ROS, or free radicals) and the natural antioxidant defence of the biological system. The ROS class includes families of free radicals, ions, and other oxygenated molecules (such as organic and inorganic peroxides). Their formation in cells occurs through the reduction of oxygen from biological reducing agents such as nicotinamide adenine dinucleotide (NADH) and nicotinamide adenine dinucleotide phosphate (NADPH). Electron transfer enzymes and redox active chemical species, of both organic and inorganic nature, facilitate these processes (Donaldson et al., 2001; Ning et al., 2003). It is now commonly thought that ROS can damage lipids, proteins, and membrane DNA and can also cause cell death by necrotic or apoptotic processes. However, the relationships between the toxicological mechanisms and the physico-chemical properties of PM are still largely unknown and need further research. In the literature, several methods are mentioned that are used to measure the so-called aerosol oxidative potential (PO). The objective of these acellular assays is to provide a proxy of the oxidative capability of PM samples. Among the most commonly used methods are the dithiothreitol (DTT), the ascorbic acid (AA) and the 2′,7′-dichlorofluorescin (DCFH) assays. DTT is considered a chemical surrogate of the cellular reductants (such as NADH or NADPH) which reduce O_2 to superoxide anion (O^-_2) and induce oxidative stress (Kumagai et al., 2002). The AA used in the assay is a physiological antioxidant that prevents the oxidation of lipids and proteins (Valko et al., 2005).

* *Submitted to Atmosperic Enviroment* in Setember

The DDT and AA assays involve the controlled incubation of the anti-oxidant (DTT or AA) in aqueous extracts of PM under controlled conditions (T = 37 °C and pH 7.4) and the measurement of its depletion over time (by following the decrease of absorbance at the wavelengths of 412 and 265 nm, respectively) (Cho et al., 2005; Fang et al., 2016). The antioxidant loss rate represents the ability of the aerosol redox-active species to transfer electrons from DTT or AA to oxygen.

The DCFH assay was formerly developed for the in vitro determination of ROS in biological cells (Keston and Brandt, 1965; Lebel et al., 1992; Wang and Joseph, 1999; Halliwell and Whiteman, 2004), but in recent years it has been adapted and applied as an acellular method. In this assay, the non-fluorescent DCFH is oxidized to the fluorescent dichlorofluorescein (DCF) by ROS in the presence of horseradish peroxidase (HRP). The fluorescence of the DCF formed can easily be measured at the excitation and emission wavelengths of 485 and 530 nm, respectively (Hung and Wang, 2001; Venkatachari et al., 2005; Venkatachari et al., 2007).

Although these methods are frequently applied to predict PM biological effects, there is still a gap of knowledge about the relationship that links PM chemical composition and the oxidative potential results obtained using these assays (Perrone et al., 2016; Chirizzi et al., 2017).

In this work, we used AA, DTT, and DCFH assays for the determination of the PO of seven types of dust coming from various emission sources and characterized by very different chemical compositions. The aim was to better investigate the roles of the single components of PM in the generation of PO. Besides the certified material NIST1648 (urban dust; UD), we considered some of the major PM components. Soil (S) is the major natural component of PM while road dust (RD) is a complex mixture of natural soil with particles formed by mechanical abrasion of vehicle components (brakes, tires) and by deposition of road surfaces (asphalt). The contribution of road dust to PM is mainly due to resuspension caused by vehicular traffic, which is particularly relevant in urban areas (Canepari et al., 2008; Pant and Harrison, 2013). Brake dust (BD), produced by brake pad linings, is the part of RD containing the highest concentration of heavy metals and other toxic elements (Thorpe and Harrison 2008; Canepari et al., 2010). Saharan dust (SD) constitutes a major contribution to PM in the Mediterranean area after events of long-range transport from North Africa; These events are usually responsible for high PM_{10} concentrations and have been recently considered potentially harmful to human health (Canepari et al., 2008; Pant and Harrison, 2013; Goudie, 2014). Pellet ash (PA) is one of the few components of PM of which the contribution has increased in recent years. This is because of the growing proliferation of pellet stoves for domestic heating. Several studies have recognized the damage caused by this emission source, which contains toxins such as polycyclic aromatic hydrocarbons and toxic elements (De Oliveira Alves et al., 2011). Finally, coke (C) was

chosen because it contains very high concentrations of organic toxin species, which have been considered responsible for genotoxic and oxidative stress effects (Taioli et al., 2007; Vernile et al., 2013). In most literature studies, the PO assays are applied only to the soluble fraction of PM samples. In a few recent studies, however, there is evidence that the role of the insoluble fraction of PM in generating oxidative stress is not negligible (Knaapen et al., 2002; Yi et al., 2014; Marcoccia et al., 2017). In this work, we applied the three assays to both the soluble and insoluble fractions of the dusts, in order to deepen understanding of the relationship between the solubility of the chemical species and the PO.

Experiments

Dust collection

The dust samples were collected in different and very specific areas. The soil dust (S) was sampled in rural areas around the city of Rome, within a radius of 20 km. Road dust (RD) was obtained by collecting the dust deposited on the road surface at several traffic sites in the centre of Rome (Central Italy). The brake dust (BD) was collected from the brake linings of three different cars. Saharan dust (SD) was collected in Algeria, in the north of the Sahara Desert. The ash produced by pellet burning (PA) was collected inside the hood of a domestic pellet stove and coke (C) was collected near a refinery plant, on the ground near a coal park. All the dust samples were homogenized and sieved (50 μm, Giuliani, Torino, Italy) before use with the exception of SD, which was sieved at 100 μm. In addition to the above dust samples, the certified material NIST1648a was used as the urban dust (UD) sample. More details about the collection of these dust samples are given in Pietrodangelo et al. (2013) and in Marcoccia et al. (2017).

Dust chemical characterization

Macro-elements, soluble and insoluble fractions of micro-elements, elemental carbon (EC), water soluble and total organic content (WSOC and OC, respectively) and inorganic ions were determined in all the examined dusts. Major elements (Al, Si, Fe, Ca, Cr, and Ti) were determined using x-ray fluorescence (XRF; X-Lab2000, Spectro Analytical Instruments, Kleve-D; 3 g of sample and 4 g of extra-pure wax were pressed to obtain a tablet). The quantification of soluble inorganic ions (Ca^{2+}, Cl^-, NO_2^-, NO_3^- and SO_4^{2-}) was performed by ion chromatography (ICS1000; Dionex Co., Sunnyvale, CA, USA) after extraction in deionized water. Inductively coupled plasma mass spectroscopy (ICP-MS; Bruker 820, Bremen, Germany) was used for the determination of As, B, Cd, Ce, Co, Cs, Cu, La, Mn, Mo, Ni, Pb, Rb, Sb, Se, Sn, Sr, Tl, V, Zn, and Zr in their soluble (after water extraction of

samples) and insoluble (after microwave assisted digestion of the residual by 2:1 HNO_3/H_2O_2 mixture) fractions. ICP-MS analysis of Al, Si, Ti, Fe and Cr was performed only on the soluble fraction, due to the low efficiency of the acid digestion for these elements. A collisional reaction interface (CRI), alimented by 30 mL min^{-1} helium and 35 mL min^{-1} hydrogen (SOL Spa, Monza, Italy), was used to reduce the polyatomic interference of ^{75}As, ^{51}V, ^{52}Cr, and ^{55}Mn. The thermo-optical analyser (ECOC analyser, Sunset Laboratory, OR, USA; NIOSH-QUARTZ temperature protocol) was used for the determination of the total organic and elemental carbon. Further details about the experimental procedures of these analyses are reported elsewhere (Canepari et al., 2009; Perrino et al., 2009). Water-soluble organic carbon (WSOC) was analysed by TOC-VCSH (Shimadzu) using the NPOC (non-purgeable organic carbon) procedure (Sanna Saarikosk at al., 2007). Before the instrumental analysis of WSOC, samples were extracted in 20 mL of Milli–Q water and subjected to mechanical agitation for 20 min. Solutions were then filtered through nitrocellulose (Millipore, pore size 0.45 μm) after which 100 μL of chloride acid (10 M) was added.

Oxidative potential assays

Next, exactly 50 mg of each dust was weighed (Analytical Balance Gibertini Elettronica E505, sensitivity of 0.01 mg) and then extracted by mechanical agitation (20 min) in 50 mL of Milli-Q water. Subsequently the solutions were centrifuged (30 min at 10,000 r/min and 25 °C; ALC Multispeed refrigerated centrifuge PK131R) in order to separate the soluble and the insoluble fractions. The soluble part was further filtered through a nitrocellulose filter (MF-Merck membrane, pore size 0.45 μm) before the application of the three OP assays. The insoluble part was re-suspended in 50 mL of water and again analysed for OP by the same procedures used for the soluble fraction. The suspensions were filtered (NC 0.45 μm) just prior to each instrumental analysis. For each sample, six replicates were performed.

DTT procedure

According to the method of Fang et al. (2016), five aliquots (0.7 mL) of the soluble or residual fractions were mixed with 0.2 mL of phosphate buffer (1 M) and with 0.1 mL of DTT 1 mM; then incubated at 37 ° C in a thermostatic bath (HAAKE DC3 Fisons). At regular intervals (0, 5, 10, 15 and 20 min), 1 mL of trichloroacetic acid 10% was added to one of the aliquots to stop the reaction. Then, 1 mL of each solution was mixed with 2 mL of Tris-buffer (0.08M, containing EDTA 4 mM) and with 50 μL of 5,50-dithiobis-2-nitrobenzoic acid (DTNB) 0.2 mM. After 5 min, the absorbance of the solutions was measured at 412 nm by UV-Vis spectrophotometry (UV-Vis; Varian Cary 50

UV-VIS Spectrometer). An operative blank was always measured in parallel. OP^{DTT} was calculated as DTT consumption rate per unit of PM mass as follows:

$$\sigma DTT = -\sigma Abs \times \frac{N_0}{Abs_0};\ \ OP^{DTT} = \frac{\sigma DTT_s - \sigma DTT_b}{\frac{V_a}{V_e} \times m_{dust}}$$

where σAbs is the slope of absorbance (412–700 nm) vs. time (min^{-1}); Abs_0 is the initial absorbance calculated from the intercept of the linear regression of absorbance vs. time; N_0 is the initial number of moles of DTT added in the reaction (100 nmol); σDTT_s and σDTT_b are the rate of DTT consumption for sample and for operative blank (nmol min^{-1}); V_e and V_a are the extraction volume (50 mL) and actual sample volume added to the reaction vial (0.7 mL), respectively; m_{dust} is the weighted amount of dust (μg) and OP^{DTT} represents the mass normalized DTT activity, in units of nmol $min^{-1}\mu g^{-1}$.

2.3.2 DCFH procedure

The DCFH procedure was adapted from Huang et al. (2016). By keeping all the reagents in the dark, a weighed amount (about 5 mg) of 2′,7′-Dichlorofluorescin diacetate was dissolved in 5 mL of ethanol and mixed with 20 mL of 0.01M NaOH in order to favour de-acetalisation. The 5 μM DCFH solution so obtained was then kept in the dark at room temperature for 30 min before use. The HRP solution (0.5 units/mL) was prepared by dissolving the proper weight of commercial product (Type VI, essentially salt-free, lyophilized powder, ≥250 units/mg solid) in 1 L of phosphate buffer 25 mM at pH 7.4. It was incubated at 37 °C for 15 min before use. Aliquots of 5 mL of the HRP solution were mixed with 1.5 mL of sample (soluble or residual fraction) and with 125 μL of the DCFH solution. The mixture was then kept at 37 °C for 15 min and transferred by a peristaltic pump (1 mL min^{-1}) to a fluorescence detector (Jasco FP-920) for the measurement of the emitted radiation at 530 nm (excitation wavelength 427 nm). A calibration curve was obtained daily using standard H_2O_2 solutions (5×10^{-6}, 1×10^{-7}, 2×10^{-7}, 5×10^{-7} and 1×10^{-6} M) instead of the sample. The OP values (OP^{DCFH}; nmol H_2O_2 μg^{-1}) were obtained using the calibration curve to convert the obtained fluorescence intensity into H_2O_2 equivalents.

AA procedure

According to the method of Fang et al. (2016), 2.4 mL of sample (soluble or residual fraction) were mixed with 0.3 mL of 0.5 mM phosphate buffer at pH 7.4 with 100 μL of 2 mM ascorbic acid and

the mixture was kept at 37 °C. The absorbance variation at 265 nm was then followed for 20 min by UV-Vis spectroscopy. OP^{AA} was calculated as the AA consumption rate per mass unit (nmol min^{-1} μg^{-1}) by the following equations:

$$\sigma AA = -\sigma Abs \times \frac{N_0}{Abs_0};\ \ OP^{AA} = \frac{\sigma AA_s - \sigma AA_b}{\frac{V_a}{V_e} \times m_{dust}}$$

where σAbs is the slope of the absorbance measured for blanks vs. time (min^{-1}); Abs_0 is the initial absorbance calculated from the intercept of the linear regression of absorbance vs. time; N_0 is the number of AA moles added in the reaction vial (200 nmol); σAA_s and σAA_b are the rate of AA consumption for the sample and for the blank, respectively (nmol min^{-1}); V_e and V_a are the extraction volume (50 mL) and sample volume added to the reaction vial (2.4 mL), respectively, and m_{dust} is the amount of weighted dust (μg).

Statistical elaboration

Multivariate statistical computations were performed using statistical software (R-3.0Gui, 32-bit) for Windows (R-project for statistical computing). Multivariate analyses were done on the OP assay results (DTT, DCFH and AA) and on the data obtained by the chemical characterization of the dusts (EC, WSOC, OC, Al, Si, Fe, Ca, Cr, Ti, As, B, Cd, Ce, Co, Cs, Cu, La, Mn, Mo, Ni, Pb, Rb, Sb, Se, Sn, Sr, Tl, V, Zn, Zr Ca^{2+}, Cl^-, NO_2^-, NO_3^- and SO_4^{2-}). Soluble and insoluble fractions of the dusts were examined separately. The matrix of the data was transformed by performing column mean centering and row and column autoscaling. These operations served to correct multiplicative variations of the data caused by the sample preparation and presentation, or due to the different scaling and units of the variables analysed. Then, principal component analysis (PCA) of the data was performed in order to confirm the correlations between the OP assay results and the chemical characteristics of the dusts.

Results and discussion

Chemical composition of the dusts

Tables 1 and 2 report the concentrations of the analysed chemical species in the soluble and insoluble (respectively) fractions of the selected dusts. Because of analytical hindrances, the concentration of some species in the insoluble fraction was not directly measured in the insoluble dusts that remained after the water extraction. In particular, Al, Si, Fe, Ti and Cr concentrations were calculated by

subtracting the value obtained by ICP-MS (soluble fraction) from the value obtained by XRF. Similarly, the concentration of the insoluble fraction of Ca was obtained as the difference between their total concentration measured by XRF and the concentration of Ca^{2+} ion measured by IC, while the insoluble organic content (WIOC) was obtained by subtracting WSOC from OC. As expected, the chemical composition of the two fractions differed significantly among the dusts. For all the dusts, the insoluble fraction contained more than 50% of the total determined concentration. In the coke sample only 2% of the measured components were present as soluble species, while in the NIST, soil and pellet ash samples; the overall percentage of soluble species was of about 40%. Soluble species represented about 10–15 % of the total measured concentration in brake dust, road dust and Saharan dust. More specifically, most of the elements that are typically associated with the geo-crustal component (Al, Si, Ti and Cr) are almost completely contained in the insoluble fraction, independent from the dust considered. Among the crustal elements, only Ca had a solubility percentage of about 50%. Fe, Mn and Cu are often indicated as redox-active elements (Mates et al., 1999). Fe is a major component of brake dust (about 20% of the total mass) and its concentration is, as a consequence, also relatively high in the other dusts influenced by vehicular traffic (NIST and Road dust; about 40 and 60 g/kg, respectively). Its solubility is low and the soluble fraction of Fe is of about 6 g/kg in brake dust and NIST, and 0.5 g/kg in road dust. Cu was also present in significant concentrations in brake dust; its total concentration was distributed between 4.2 g/kg of insoluble species and 0.7 g/kg of soluble species. Mn was also present in the selected dusts mainly as insoluble species (solubility percentages lower than 25% for all the dusts, with the exception of NIST in which the soluble fraction was about 45%). The Mn concentration was very high in the pellet ash: about 2 g/kg in the soluble fraction and almost 18 g/kg in the insoluble fraction. In all the other dusts, the total Mn concentration was lower than 1.5 g/kg. The remaining elements, including toxic elements such as Ni, Cd, Pb and As, were distributed very differently between the soluble and insoluble fraction. Their overall concentration as soluble species was higher than 2 g/kg in NIST, brake dust and pellet ash (3.9, 2.3 and 2.0 g/kg, respectively) and lower than 1 g/kg in the other dusts (0.1, 0.9, 0.4 and 0.2 g/kg in coke, road dust, Saharan dust and soil, respectively). Their total concentration as insoluble species was about 6 g/kg in NIST and brake dust, about 2 g/kg in road dust and pellet ash, 1.2 g/kg in coke and less than 1 g/kg in soil and Saharan dust (0.6 and 0.1, respectively). It is worth noting that Pb was present at very high concentration (6.5 g/kg, with a solubility percentage of 37%) in NIST, in urban dust collected before unleaded fuels were adopted. Inorganic oxygenated ions (SO_4^{2-}, NO_3^- and NO_2^-) were present in PM almost exclusively as soluble salts. They were the predominant species in the

soluble fraction of NIST (sulphate: 154 g/kg; nitrate: 47 g/kg) and were also present in significant concentrations in pellet ash and Saharan dust (overall concentrations: 46 and 28 g/kg, respectively). Elemental carbon is an insoluble component that may play a key role in the redox equilibria, due to its adsorption and catalytic properties. It accounts for more than 30% of the coke sample and its concentrations are significant also in pellet ash and NIST, as combustion residue, and in brake dust, where it is probably present as a filling component. Organic carbon is a major component in both the soluble and the insoluble fractions of all the dust, with the sole exception of the Saharan dust. WSOC in PM was generally composed of a mixture of high-molecular-weight carboxylic, keto/carbonyl, amino/imino and nitro multifunctional organic compounds, as well as of smaller organic molecules such as anhydrides, sugars and keto- and α,ω-dicarboxylic acids (Graham et al., 2002; Cappiello et al., 2003; Fuzzi et al., 2006; Duarte et al., 2007; Ding et al., 2008). Most of these compounds could participate to create redox equilibria. Pellet ash and NIST contained a significant mass fraction of WSOC (about 2%). Although determination of the speciation of OC was not attempted in this work, it can be reasonably hypothesized that the WSOC is mainly constituted by oxygenated species secondary organic aerosol (SOA) formation in NIST (Miyazaki et al., 2009) and by degradation products of cellulose (such as levoglucosan) in pellet ash (Simoneit et al., 1999).

Oxidative potential of the soluble fraction

In Figure 1 are shown the results obtained by the application of the three OP assays to the soluble fraction of dusts (s-OP). All the assays gave very different results among the selected dusts As largely expected and as already evidenced in other studies, the chemical composition is a key factor in determining the redox behaviour of the samples (Perrone at al., 2006; Chirizzi et al., 2017). However, very significant differences were also observed in the relative sensitivity of the three assays toward the same dust. The DCFH assay was the least selective method and led to appreciable s-OP values for all the considered dusts. Road dust, of which the chemical composition in the soluble fraction was not particularly rich in inorganic and organic species, provided the highest s-OP^{DCFH} values. Similarly, high s-OP^{DCFH} values were measured for coke and Saharan dust, which contained the lowest overall concentration of soluble species.

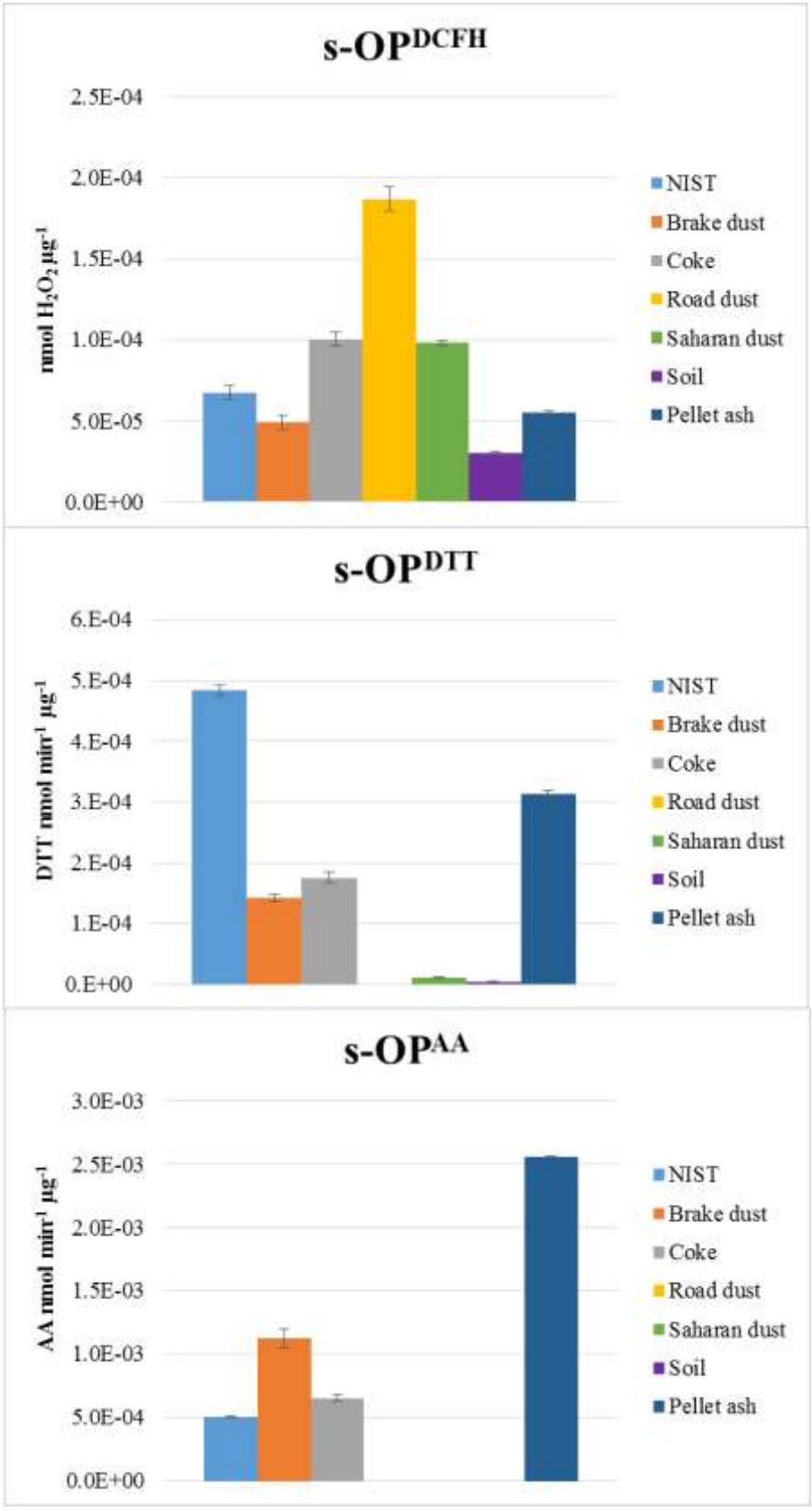

Figure 1: *Oxidative potentials measured in the soluble fraction of dusts*

The DTT assay furnished completely different results: the highest s-OP^{DTT} values were obtained for pellet ash and NIST, which contained the highest overall soluble species concentration. In particular, with respect to the other considered samples, pellet ash and NIST were characterized by very high WSOC concentrations. Brake dust and coke, which also contained relevant WSOC concentrations, provided significant values of s-OP^{DTT}; while very low s-OP^{DTT} values were measured in the other considered samples. These results are in agreement with those of previous studies (Cho et al., 2005; Fang et al., 2016) which indicate that soluble organic compounds contain species able to catalyse ROS generation by various reactions. These reactions lead to the formation of superoxide radicals that are probably responsible for the generation of oxidative potential.

The AA assay was particularly sensitive toward pellet ash, but significant s-OP^{AA} values were measured also in brake dust, NIST and coke.

Thanks to the principal component analysis (PCA) of the data obtained, the correlations between the OP assay results and the chemical characteristics of the dusts were confirmed. The high variability of the data obtained for each dust, provided statistically significant results. From Fig. 3 we observe that the variables examined separated the first two principal components (PC1 and PC2) of the loading plot, which explains 69.7% of the total explored variance. Variables were grouped in three main clusters, each one characterized by the presence of one PO assay.

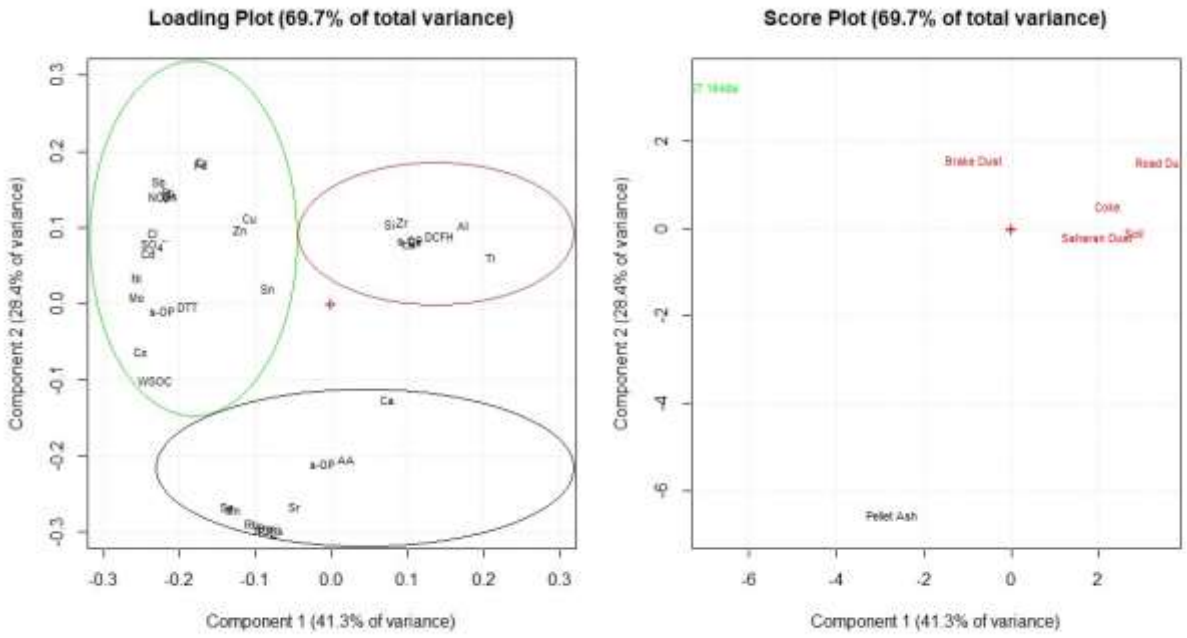

Figure 3: *Principal component analysis of OP assays' results and chemical characteristics of dusts' soluble fraction*

The lower part of the loading plot shows s-OP^{AA}, as well as Mn, Sr, Rb, Se, P and Ca, which were present at high concentration in the pellet ash (shown in the lower part of the score plot). Hence, we can confirm that the acid ascorbic assay is sensitive toward the pellet ash because it responds to high concentrations of water soluble fractions of Mn, Sr, Rb, Se, P and Ca. The same goes for DCFH and DTT. The position occupied by s-OP^{DCFH}, which is near those of Si, Zr, Ce, Al, La and Ti (to the right of centre) confirms that the DCFH assay is sensitive towards soil, coke, road dust and Saharan dust because it responds to water soluble fractions of the crustal components of PM (typically characterized by elements such as Ti, Al and Si). Finally, Figure 3 shows that the DTT assay is influenced by several parameters including Mo, Ni, Cl^-, SO_4^{2-}, Cd and WSOC, which are in the same part of the loading plot of s-OP^{DTT}. These variables allow for hypothesizing the sensitivity of the DTT assay toward the combustive and secondary compounds of PM. The multivariate statistical elaboration of the data confirmed that the three assays have a selective affinity towards different chemical compounds and that they are non-interchangeable.

Oxidative potential of the insoluble fraction

The OP values related to the insoluble fraction (i-OP) of dusts, as specified in the experimental section, were obtained by applying the assays to suspensions of the insoluble part of the dusts that remained after water extraction. To our knowledge, this procedure has never been used in previous studies and undoubtedly, the obtained results are hardly indicative of the ability of dusts of generating ROS in living organisms. However, it has to be considered that the direct contact of solid particles with cells may occur in the respiratory tract and that PM from combustion processes contain nanoparticles that are thought to be able to enter organisms (Canepari et al., 2010). Moreover, once inside the solid particles could then establish in vivo redox equilibria, although by mechanisms that are still largely unknown. The obtained i-OP results are reported in Figure 2. As can be noted, the i-OP values are generally much higher than the s-OP ones (in most cases, one magnitude order or more). This result confirms the possible role of the insoluble PM components in the generation of oxidative stress, already hypothesised in a few works (Marcoccia et al., 2017, Zou et al., 2016; Knaapen et al., 2002). Pellet ash provided the highest i-OP^{DCFH} and i-OP^{DTT} values. It is noteworthy that for this dust, i-OP^{DTT} was more than 20-fold s-OP^{DTT}, and i-OP^{DCFH} more than 10-fold s-OP^{DCFH}.

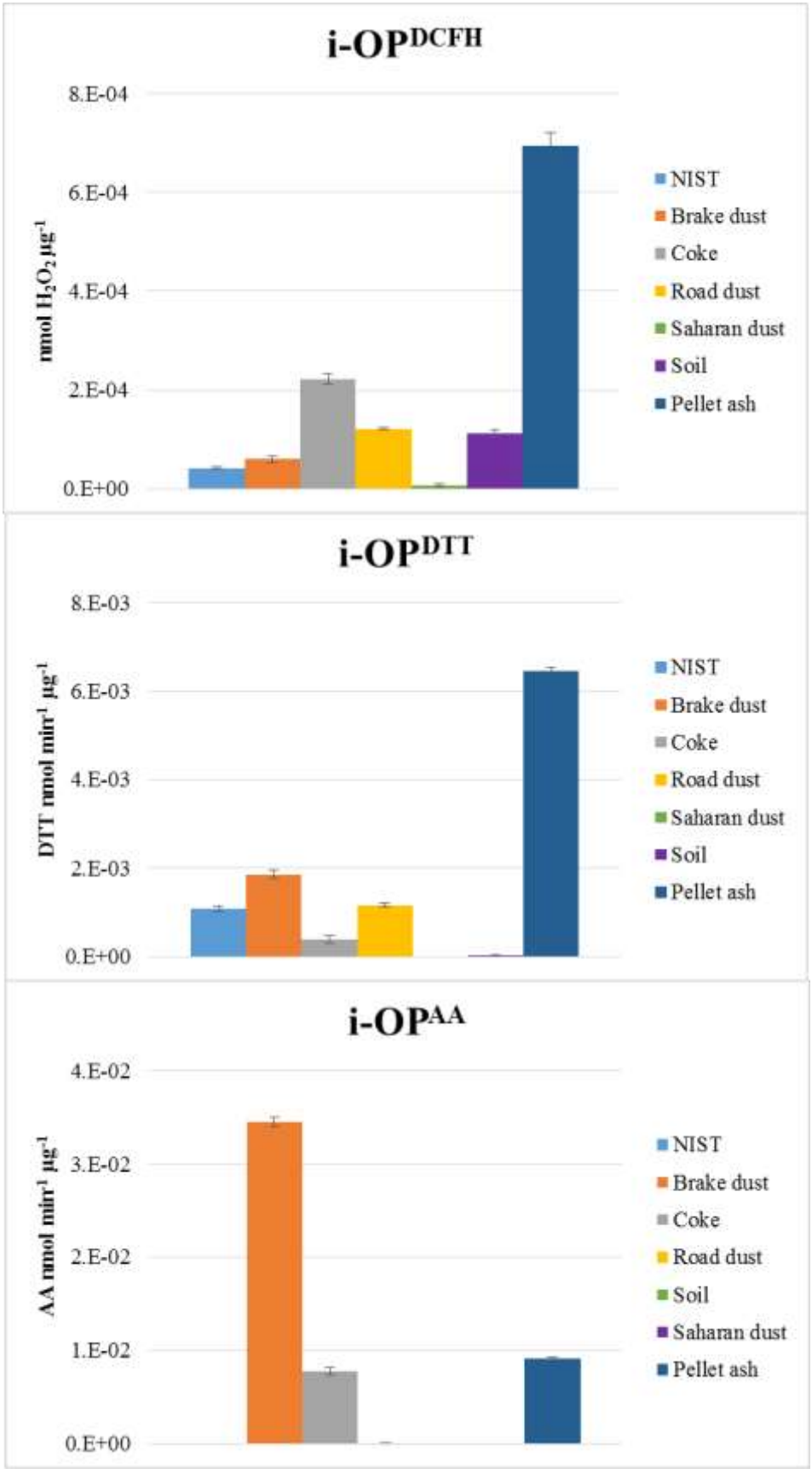

***Figure 2**: Oxidative potentials measured in the insoluble fraction of dusts*

This result suggests that emissions due to domestic biomass burning, of which the contribution to PM has increased in the last year (Reche et al., 2012), may be particularly harmful for human health and environment. It is also interesting to note that, in the insoluble fraction, by using the DCFH and DTT assays, the only dust that exhibited low i-OP was the soil, and that the relative sensitivity of these two assays towards the dusts considered was quite similar. The AA assay, also regarding the insoluble fraction, showed instead very different behaviour: the i-OP^{AA} values were in fact particularly high (more than 30-fold the s-OP^{AA}) for the brake dust and significant for pellet ash and coke only.

A completely different behaviour was observed when the dataset relative to the insoluble fraction of dusts was elaborated using multivariate statistical analyses. From the principal component analysis of the OP assay results and the chemical characteristics of the dust insoluble fractions, no specific clusters were individuated in the loading plot or in the score plot (Appendix D1). Therefore, for these data it was not possible to reliably correlate the three methods with the different specific chemical species of each dust. The correlations in this case were much lower and difficult to interpret, probably because there were many hydrophobic species in these samples that had not been analysed in this work. The presence of a great number of components that affect the total variability makes the study of the residual parts very interesting. Pursuing this study by analysing more insoluble chemical species, could provide new elements of correlation and more information about the mechanisms involved in these three methods.

Conclusions

The oxidative potential of the selected dusts obtained by the three assays indicated that most of the PM components are potentially able to induce oxidative stress in living organisms. However, because different mechanisms are involved in generating ROS, no one assay, applied singly, is able to successfully predict the overall capacity of PM for causing oxidative stress.

The soluble and insoluble fractions of each dust were separately analysed. In the soluble fraction, the DTT assay showed high sensitivity towards pellet ash and road dust, and seemed to be influenced mainly by the organic compounds of PM, including water-soluble organic carbon (WSOC). On the other hand, the ascorbic acid assay is more sensitive to dusts rich in metals and metalloids, such as brake dusts and pellet ash. The DCFH assay showed a certain affinity to organic (chemical) species, but seemed to be less selective then the other assays. Thanks to multivariate statistical computations of the data obtained, it was possible to confirm the correlations between the OP assay results and the chemical characteristics of the soluble fraction of the dust.

The insoluble fraction of all the dusts provided noteworthy contributions to the oxidative potential. Although the three OP assays showed different sensitivity to the selected dusts, all of them indicated OP values higher in the insoluble fraction than in the soluble one. Knowledge of the chemical species responsible for this contribution, and of the mechanisms involved in the redox activities of the solid components, needs to be deepened.

Future studies should be focused toward achieving a deeper understanding of the relationships between acellular OP assay results and the in vivo biological effects of the dusts produced by individual sources.

Table 1: Chemical composition of the soluble fraction (mean and standard deviation; six replicates)

			NIST1648a	Brake dust	Coke	Road dust	Saharan dust	Soil	Ash pellet
Technique	**UoM**		**Mean** ± *SD*	**Mean** ± *SD*	**Mean** ± *SD*	**Mean** ± *SD*	**Mean** ± *SD*	**Mean** ± *SD*	**Mean** ± *SD*
ICP-MS	g/Kg	**Al**	**0.28** ± *0.04*	**0.162** ± *0.003*	**0.9** ± *0.1*	**1.76** ± *0.03*	**0.4** ± *0.1*	**0.69** ± *0.01*	**0.097** ± *0.002*
ICP-MS	mg/Kg	**As**	**81** ± *3*	**1.13** ± *0.05*	**0.60** ± *0.03*	**2.1** ± *0.1*	**1.1** ± *0.1*	**7.9** ± *0.6*	**2.9** ± *0.3*
ICP-MS	mg/Kg	**B**	**19.0** ± *0.4*	**8.5** ± *0.2*	**2.8** ± *0.8*	**1.7** ± *0.0*	**11.0** ± *0.6*	**0.4** ± *0.1*	**590** ± *30*
IC	g/Kg	**Ca**	**9.6** ± *0.2*	**27.9** ± *0.4*	**1.29** ± *0.02*	**48** ± *1*	**17.1** ± *0.3*	**139** ± *2*	**74** ± *1*
ICP-MS	mg/Kg	**Cd**	**48** ± *4*	**0.30** ± *0.02*	**0.02** ± *0.01*	**0.07** ± *0.01*	**0.12** ± *0.01*	**0.019** ± *0.001*	**13** ± *1*
ICP-MS	mg/Kg	**Ce**	**0.180** ± *0.001*	**0.106** ± *0.005*	**0.022** ± *0.005*	**2.2** ± *0.1*	**0.16** ± *0.01*	**0.30** ± *0.03*	**0.041** ± *0.002*
IC	mg/Kg	**Cl**	**4540** ± *80*	**660** ± *8*	**19** ± *4*	**190** ± *20*	**1220** ± *30*	**41** ± *7*	**1090** ± *60*
ICP-MS	mg/Kg	**Co**	**5.40** ± *0.01*	**1.06** ± *0.00*	**0.05** ± *0.00*	**0.62** ± *0.01*	**0.18** ± *0.01*	**0.24** ± *0.01*	**4.3** ± *0.3*
ICP-MS	mg/Kg	**Cr**	**28.0** ± *0.4*	**24.7** ± *0.4*	**0.83** ± *0.01*	**13.7** ± *0.2*	**4.0** ± *0.1*	**3.8** ± *0.1*	**4.6** ± *0.1*
ICP-MS	mg/Kg	**Cs**	**0.003** ± *0.001*	**0.210** ± *0.001*	**0.010** ± *0.003*	**0.212** ± *0.003*	**0.020** ± *0.002*	**0.28** ± *0.02*	**2.7** ± *0.2*
ICP-MS	mg/Kg	**Cu**	**275** ± *1*	**765** ± *2*	**13** ± *2*	**9** ± *1*	**3** ± *4*	**1.2** ± *0.1*	**37** ± *6*
ICP-MS	g/Kg	**Fe**	**5.9** ± *0.1*	**6.4** ± *0.1*	**1.0** ± *0.3*	**0.46** ± *0.01*	**0.24** ± *0.01*	**0.43** ± *0.01*	**0.02** ± *0.02*
ICP-MS	mg/Kg	**La**	**0.160** ± *0.002*	**0.067** ± *0.001*	**0.011** ± *0.006*	**1.585** ± *0.004*	**0.111** ± *0.002*	**0.17** ± *0.02*	**0.062** ± *0.004*
ICP-MS	mg/Kg	**Mn**	**340** ± *1*	**119.7** ± *0.3*	**6.4** ± *0.1*	**29.7** ± *0.1*	**6.2** ± *0.1*	**25** ± *1*	**1751** ± *24*
ICP-MS	mg/Kg	**Mo**	**5.70** ± *0.01*	**3.80** ± *0.01*	**0.827** ± *0.003*	**0.038** ± *0.002*	**0.009** ± *0.001*	**0.053** ± *0.005*	**3.6** ± *0.2*
ICP-MS	mg/Kg	**Ni**	**20.0** ± *0.4*	**3.97** ± *0.01*	**1.88** ± *0.04*	**1.15** ± *0.03*	**0.8** ± *0.1*	**1.6** ± *0.1*	**9** ± *1*
ICP-MS	mg/Kg	**Pb**	**2424** ± *9*	**5.94** ± *0.02*	**9.85** ± *0.1*	**5.36** ± *0.04*	**2.5** ± *0.2*	**0.54** ± *0.05*	**0.42** ± *0.02*
ICP-MS	mg/Kg	**Rb**	**26.4** ± *0.5*	**5.6** ± *0.1*	**0.6** ± *0.1*	**0.68** ± *0.05*	**6.4** ± *0.5*	**0.8** ± *0.1*	**310** ± *26*
ICP-MS	mg/Kg	**Sb**	**26.0** ± *0.1*	**13.9** ± *0.4*	**0.16** ± *0.03*	**0.047** ± *0.003*	**0.415** ± *0.001*	**0.002** ± *0.001*	**1.6** ± *0.2*
ICP-MS	mg/Kg	**Se**	**5.7** ± *0.2*	**0.27** ± *0.01*	**0.37** ± *0.01*	**0.44** ± *0.01*	**1.2** ± *0.1*	**0.15** ± *0.01*	**23** ± *8*
ICP-MS	g/kg	**Si**	**1.41** ± *0.03*	**0.52** ± *0.02*	**0.4** ± *0.1*	**5.2** ± *0.1*	**1.48** ± *0.01*	**0.32** ± *0.02*	**0.39** ± *0.01*
ICP-MS	mg/Kg	**Sn**	**0.310** ± *0.005*	**1.62** ± *0.03*	**0.130** ± *0.002*	**0.056** ± *0.002*	**0.002** ± *0.001*	**0.09** ± *0.01*	**0.46** ± *0.04*
ICP-MS	mg/Kg	**Sr**	**125** ± *4*	**98** ± *3*	**4** ± *3*	**164** ± *2*	**350** ± *10*	**150** ± *10*	**542** ± *29*
ICP-MS	mg/Kg	**Ti**	**1.20** ± *0.02*	**0.98** ± *0.02*	**13** ± *1*	**7.6** ± *0.1*	**8.6** ± *0.1*	**13.1** ± *0.2*	**0.061** ± *0.001*
ICP-MS	mg/Kg	**Tl**	**0.008** ± *0.002*	**0.04** ± *0.01*	**0.002** ± *0.001*	**0.026** ± *0.001*	**0.03** ± *0.01*	**0.014** ± *0.002*	**1.05** ± *0.05*
ICP-MS	mg/Kg	**V**	**89** ± *3*	**1.29** ± *0.04*	**1.08** ± *0.01*	**2.14** ± *0.01*	**0.84** ± *0.03*	**1.2** ± *0.1*	**3.7** ± *0.4*
ICP-MS	mg/Kg	**Zn**	**1023** ± *56*	**2120** ± *8*	**100** ± *5*	**673** ± *18*	**7** ± *2*	**18** ± *3*	**525** ± *27*
ICP-MS	mg/Kg	**Zr**	**0.270** ± *0.002*	**2.31** ± *0.01*	**0.018** ± *0.001*	**4.83** ± *0.03*	**0.007** ± *0.001*	**0.58** ± *0.02*	**0.07** ± *0.01*
IC	g/Kg	**NO_2^-**	**<0.1**	**<0.1**	**<0.1**	**<0.1**	**<0.1**	**<0.1**	**6.5** ± *0.3*
IC	g/Kg	**NO_3^-**	**47** ± *2*	**4.0** ± *0.4*	**<0.1**	**<0.1**	**<0.1**	**<0.1**	**2.2** ± *0.3*
IC	g/Kg	**SO_4^{--}**	**154** ± *4*	**5.9** ± *0.2*	**<0.1**	**<0.1**	**28.0** ± *1.0*	**0.9** ± *0.2*	**37** ± *1*
TOC	g/Kg	**WSOC**	**22** ± *1*	**5.7** ± *0.1*	**9.5** ± *0.2*	**2.1** ± *0.1*	**0.53** ± *0.02*	**0.3** ± *0.1*	**22** ± *1*

Table 2: Chemical composition of the insoluble fraction (mean and standard deviation; six replicates)

			NIST1648a		Brake dust		Coke		Road dust		Saharan dust		Soil		Ash pellet	
Technique	**UoM**		**Mean**	± *SD*	**Mean**	± *SD*	**Mean**	± *SD*	**Mean**	± *SD*	**Mean**	± *SD*	**Mean**	± *SD*	**Mean**	± *SD*
XRF/ICP-MS	g/Kg	**Al**	**34***	± *1*	**14.7**	± *0.4*	**12**	± *2*	**70**	± *2*	**69**	± *2*	**9.7**	± *0.2*	**6.1**	± *0.1*
ICP-MS	mg/Kg	**As**	**35.0**	± *0.2*	**18.0**	± *0.1*	**0.52**	± *0.04*	**1.6**	± *0.2*	**0.3**	± *0.1*	**87**	± *10*	**2.3**	± *0.3*
ICP-MS	mg/Kg	**B**	**44**	± *2*	**23.1**	± *0.8*	**0.7**	± *0.3*	**48.2**	± *0.8*	**2.2**	± *0.2*	**1.2**	± *0.3*	**235**	± *18*
XRF/IC	g/Kg	**Ca**	**53***	± *1*	**12.9**	± *0.3*	**1.38**	± *0.03*	**29**	± *1*	**15**	± *1*	**131**	± *3*	**74**	± *2*
ICP-MS	mg/Kg	**Cd**	**26**	± *3*	**0.73**	± *0.08*	**0.05**	± *0.04*	**0.28**	± *0.03*	**0.76**	± *0.07*	**0.072**	± *0.002*	**20**	± *3*
ICP-MS	mg/Kg	**Ce**	**546**	± *4*	**26.2**	± *0.2*	**0.3**	± *0.1*	**109**	± *5*	**1.0**	± *0.1*	**10**	± *1*	**9**	± *1*
XRF/IC	mg/Kg	**Cl**	**-**		**-**		**1.0**	± *0.3*	**-**		**100**	± *4*	**-**		**-**	
ICP-MS	mg/Kg	**Co**	**13.0**	± *0.4*	**13.9**	± *0.5*	**1.02**	± *0.04*	**10.8**	± *0.3*	**0.55**	± *0.02*	**1.6**	± *0.1*	**9**	± *1*
XRF/ICP-MS	mg/Kg	**Cr**	**374***	± *9*	**3083**	± *74*	**9.6**	± *0.2*	**57**	± *1*	**48**	± *1*	**36**	± *1*	**20.4**	± *0.5*
ICP-MS	mg/Kg	**Cs**	**1.70**	± *0.02*	**2.99**	± *0.03*	**0.04**	± *0.01*	**20.90**	± *0.04*	**0.005**	± *0.001*	**2.5**	± *0.3*	**0.43**	± *0.05*
ICP-MS	mg/Kg	**Cu**	**336**	± *1*	**4286**	± *17*	**43**	± *11*	**71**	± *14*	**10**	± *18*	**13**	± *1*	**204**	± *53*
XRF/ICP-MS	g/Kg	**Fe**	**33***	± *1*	**198**	± *5*	**16**	± *4*	**59**	± *1*	**40.7**	± *0.3*	**3.5**	± *0.1*	**3.7**	± *0.1*
ICP-MS	mg/Kg	**La**	**32**	± *1*	**12.7**	± *0.2*	**0.3**	± *0.2*	**54.4**	± *0.2*	**26.5**	± *0.1*	**5**	± *1*	**5.5**	± *0.6*
ICP-MS	mg/Kg	**Mn**	**450**	± *2*	**1093**	± *4*	**40**	± *1*	**475**	± *2*	**22.5**	± *0.4*	**96**	± *4*	**17869**	± *364*
ICP-MS	mg/Kg	**Mo**	**8.30**	± *0.03*	**171**	± *1*	**75.5**	± *0.1*	**0.83**	± *0.05*	**0.15**	± *0.02*	**0.65**	± *0.09*	**1.2**	± *0.1*
ICP-MS	mg/Kg	**Ni**	**61.0**	± *0.2*	**108**	± *3*	**355**	± *1*	**14.2**	± *0.1*	**5.1**	± *1.0*	**9**	± *1*	**28**	± *4*
ICP-MS	mg/Kg	**Pb**	**4127**	± *22*	**677**	± *4*	**8.9**	± *0.1*	**67.0**	± *0.7*	**0.010**	± *0.002*	**11**	± *2*	**55**	± *5*
ICP-MS	mg/Kg	**Rb**	**26**	± *1*	**27**	± *1*	**0.5**	± *0.1*	**240**	± *3*	**1.1**	± *0.1*	**10**	± *2*	**31**	± *4*
ICP-MS	mg/Kg	**Sb**	**23.4**	± *0.1*	**292**	± *1*	**4.07**	± *0.01*	**0.204**	± *0.002*	**2.08**	± *0.01*	**0.4**	± *0.1*	**1.7**	± *0.3*
ICP-MS	mg/Kg	**Se**	**20**	± *1*	**9.0**	± *0.4*	**9.0**	± *0.2*	**3.1**	± *0.1*	**0.37**	± *0.03*	**11**	± *2*	**0.02**	± *0.01*
XRF/ICP-MS	g/Kg	**Si**	**128***	± *4*	**26**	± *1*	**21**	± *1*	**173**	± *5*	**228**	± *2*	**16**	± *1*	**6.5**	± *0.3*
ICP-MS	mg/Kg	**Sn**	**55.0**	± *0.1*	**1419**	± *3*	**14.7**	± *0.3*	**1.97**	± *0.01*	**0.02**	± *0.01*	**2.7**	± *0.5*	**21**	± *3*
ICP-MS	mg/Kg	**Sr**	**90**	± *4*	**159**	± *7*	**6**	± *7*	**674**	± *11*	**2.7**	± *0.1*	**375**	± *36*	**717**	± *57*
XRF/ICP-MS	mg/Kg	**Ti**	**3900***	± *94*	**526**	± *13*	**894**	± *21*	**3835**	± *92*	**4532**	± *109*	**241**	± *6*	**18.9**	± *0.5*
ICP-MS	mg/Kg	**Tl**	**1.9**	± *0.5*	**0.3**	± *0.1*	**0.03**	± *0.01*	**1.30**	± *0.01*	**0.004**	± *0.002*	**0.11**	± *0.03*	**0.9**	± *0.1*
ICP-MS	mg/Kg	**V**	**38**	± *2*	**7.6**	± *0.4*	**557**	± *1*	**118**	± *4*	**4.9**	± *0.3*	**10**	± *1*	**8**	± *1*
ICP-MS	mg/Kg	**Zn**	**1200**	± *7*	**3197**	± *18*	**160**	± *12*	**318**	± *12*	**40**	± *18*	**86**	± *21*	**1157**	± *91*
ICP-MS	mg/Kg	**Zr**	**28.0**	± *0.3*	**87**	± *1*	**11.1**	± *0.1*	**89**	± *1*	**9.4**	± *0.1*	**12**	± *1*	**10**	± *2*
ECOC	g/Kg	**EC**	**23.0**	± *2.0*	**17**	± *1*	**310**	± *15*	**0.07**	± *0.01*	**<0.001**		**<0.001**		**44**	± *4*
ECOC/TOC	g/Kg	**WIOC**	**83**	± *4*	**30**	± *3*	**146**	± *5*	**12**	± *1*	**0.10**	± *0.02*	**41**	± *3*	**4**	± *1*

* certificate values of the reference material were used instead of XRF values, due to the low available amount of dust.

*3.6.2 Chemical composition and oxidative potential of PM in two geographic areas in Italy**

Introduction

In the last years, several studies highlighted the important role of the urban airborne particulate matter (PM) in the increase of morbidity and mortality due to cardiopulmonary diseases, related to inflammatory processes and genotoxic effects (Dockery et al.,1993; Pope et al., 2002; Simoni et al.,2015). In this optic, the study of the PM-induced toxicity represents a very important field, in the evaluation of the most harmful components involved. The epidemiological studies present in literature link the adverse health effects to the exposure of coarse particulate matter (PM with aerodynamic diameter 2.5 μm; Brunekreef and Forsberg (2005) and focus on the importance of understanding the mechanisms by which PM exert its role in generating asthma, chronic obstructive pulmonary disease (COPD), cardiac and respiratory hospital admissions (Brunekreef and Forsberg 2005; Burnett et al. 1997, 1999; Chen et al. 2004; Sheppard et al. 1999).

One of the most broadly accepted mechanism consists of the induction of oxidative stress in airway epithelial cells and macrophages due to the generation of reactive oxygen species (ROS) by the interaction of PM with cellular systems (Cho et al., 2005; Nel, 2005). Typically, ROS are formed in cells through the reduction of oxygen by biological reducing, with the catalytic assistance of electron transfer enzymes and redox active chemical species [Li Net al., 2003; Sigaud et al., 2005). For this reason, the study of the PM chemical composition is needed to improve the knowledge of the relationship between the chemical species and the formation of ROS. The presence of transition metals is thought to be particularly relevant, as they may support, by chemical reaction like Fenton reactions, the formation of strong oxidizing species (hydrogen peroxide, superoxide radical, peroxy radical, hydroxyl radical, hypochlorous acid and other organic hydroperoxides). The water-soluble fraction of metals is generally considered to play a fundamental role in the ROS generation. [(Knaapen et al., 2002; Cheung et al., 2012) The oxidative potential (OP), which consists in the a-cellular measure of the capacity of PM to oxidize target molecules, has been proposed as a proxy of the biological oxidative response to PM and it could give more reliable information on health effect than the PM mass concentration (Borm et al., 2007). Oxidative potential is also an attractive measure because it integrates important biological propriety properties, like surface and chemical composition (Yang, A. X. 2015).

** Paper in preparation*

In literature several *cell-test* and *a-cellular test* for measuring OP have been reported and applied to investigate the oxidative stress activity of PM; these studies have shown that each assay has a different sensitivities towards the ROS generating compounds (Cho et al., 2005;Charrier and Anastasio, 2012; Sauvain et al., 2013; Yang et al.,2014). Among the assays used to assess OP, the dithiothreitol (DTT), the ascorbic acid (AA) and the 2′,7′-dichlorofluorescin (DCFH) assays are the most diffused in the literature studies (Cho et al., 2005; Fang et al., 2016; Landreman et al., 2008). The dithiothreitol (DTT) assay measures the ability of redox active compounds to transfer electrons from DTT to oxygen (Cho et al., 2005; Steenhof et al.,2011). The rate of DTT consumption represents the capacity of PM of generating superoxide radicals and is therefore an indicator of oxidative potential (Cho et al., 2005, Li et al., 2003; Ayres et al., 2008). The 2,7-dichlorofluorescenin (DCFH) assay is a fluorescence method that measures PM-related ROS like hydrogen peroxide (H_2O_2); DCFH is oxidized to fluorescent dichlorofluorescein (DCF) by ROS in the presence of the enzyme horseradish peroxidase (HRP) (Huang et al. 2005; Venkatachari et al. 2007; See et al. 2007; Venkatachari et al. 2005; Venkatachari and Hopke 2008). This assay was originally developed to detect p-mole levels of H_2O_2 and is widely applied for the determination of ROS formation also in biological cells (Cathcart et al. 1983; Lebel et al. 1992; Keston and Brandt 1965; Wang and Joseph 1999; Halliwell and Whiteman 2004). The third considered assay is based on the ability of PM to deplete the antioxidant ascorbic acid(AA); the ascorbate solution used in this assay represents a simplified version of the synthetic respiratory tract lining fluid (RTFL) (Zielinski et al.,1999; Mudway et al., 1998).

In the last years several studies regarded the study of the possible relations between chemical components and OPs values; however, the knowledge in this field still presents some important gaps (Janssen et al., 2014; Charrier et al., 2015; Yang et al., 2015; Perrone et al., 2016; Chirizzi et al., 2017). In this work the three PO assays were adapted to be included in a multi-parametric procedure previously optimized in our laboratories that allows the determination of macro-elements (Al, Si, Fe, Na, Mg, Cl), inorganic ions (Cl^-, NO_3^-, SO_4^{2-} Na^+, NH_4^+, Mg^{2+}, Ca^{2+}) and micro- and trace- elements in their soluble and insoluble fraction ((Canepari et al., 2006 a,b; Canepari et al., 2009)) to be performed on a single 24h PM sample. The analytical integrated procedure was then applied to two field-monitoring campaigns: the first campaign was carried out at an urban traffic site in Rome (central Italy), while the second campaign was carried out at site located in the proximity of the industrial areas of Ferrara (Po valley; north Italy). These sites have been chosen because of the presence of different emission sources and climatic conditions in the two geographical areas, which reflects in a very different PM chemical composition of samples collected at the two sites. These differences will be fully debated. Eventually, in order to have more relevant information about these

processes, we applied the Focused Principal Component Analysis (FPCA) analysis with the aim to correlate the chemical parameters (i.e. elements, anions and cations) determined in samples of PM2.5 and PM10 collected in the cities of Ferrara and Rome with the indicators of oxidative potential (OP) (i.e. AA, DCFH and DTT). These additional findings and their implications with the atmospheric environment will be fully discussed.

Material and method:

Sample Collection

Samples of PM_{10} and $PM_{2.5}$ were collected during the period 17 February – 17 March on a daily basis at a residential site (C 44°50′N 11°33′E) in the sub-urban area of Ferrara, a city with about 132,000 inhabitants located in the eastern Po Valley. A complete description of the monitored area is described in Perrino et al., 2014. The sampling site is influenced by several PM sources: the urban area, the highway A13, and a major industrial area containing a power plant, an urban waste incinerator and many small and medium size enterprises (SMEs). Mass concentration was measured daily, by means of dual channel beta attenuation automatic monitors (SWAM 5a Dual Channel Monitor – FAI Instruments, Fonte Nuova, Rome - IT) configured with PM_{10} and $PM_{2.5}$ heads compliant with the EN 12341 (PM_{10}) and EN14907 ($PM_{2.5}$) standards. The sampler was equipped with Teflon membrane filters (TEFLON, 47 mm, 2.0-micron pore size, PALL Life Sciences). A dual channel samplers (HYDRA Dual Sampler, FAI Instruments, Fonte Nuova, Rome - IT) were placed at the site in order to collect daily PM_{10} and $PM_{2.5}$ samples also on quartz fibre filters (TISSUQUARTZ 2500QAT, 47 mm, PALL Life Sciences). At the traffic site (about 50 meter from the nearest road) located in Rome (Central Italy,41◦54’03.69’’N, 12◦30’44.93’’E) only PM_{10} samples were collected. This site is characterized by heavy traffic, particularly during working days. A HYDRA dual sampler equipped with two independent PM_{10} sampling heads compliant with EN 12341 was used in this monitoring campaign to simultaneously collect pairs of PM_{10} samples. Samplings were performed during two periods. Samples collected during the first period (20-29/12/2016) were used to evaluate the repeatability of OP assays; in this case, both the sampler lines were equipped with Teflon membranes. Samples collected during the second sampling period (16-30 march, 2017) were instead submitted to chemical characterization and OP assays. In this case, the two sampler lines were equipped with Teflon and Quartz membranes, respectively. PM mass concentration was determined gravimetrically, by weighting the Teflon membranes (conditioned for 48 at 20°C and 50% RH) before and after samplings. In figure 1 the map of the two monitored sites is reported.

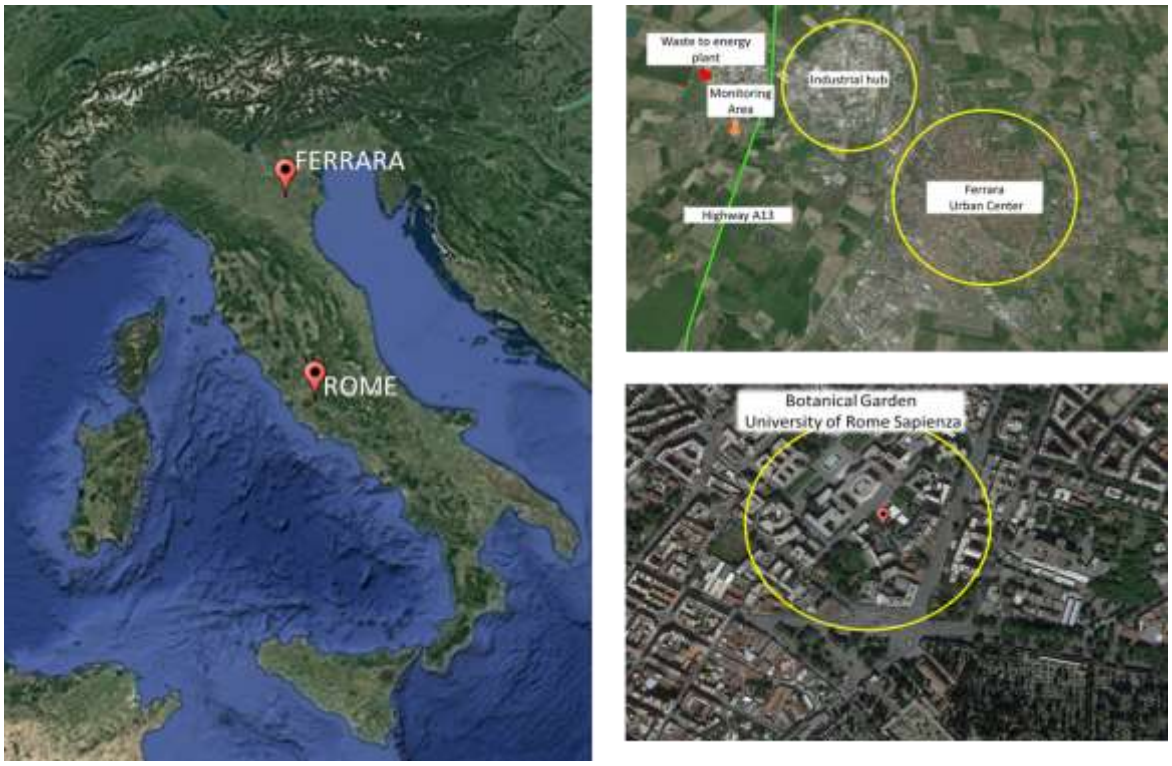

Figure 1: *Map of the two sampling sites. Rome and Ferrara*

Chemical Analysis

The Teflon and quartz filters, collected during the two monitoring campaign, were used for the chemical determination of several components. The Quartz filters were used for the analysis of Organic Carbon (OC) and Elemental Carbon (EC) by means of a thermo-optical analyser (OCEC Carbon Aerosol Analyser, Sunset Laboratory, OR-U.S.A; NIOSH-QUARTZ temperature protocol). The Teflon filters were used for the analysis of elements and inorganic ions following a modified version of the method reported in Canepari *et al.* (2009a). Breefly, the macro-elements Al, Fe K, Mg, Ca, Ti, S and Si were analysed by non-destructive energy-dispersive X-Ray fluorescence (EPD-XRF, X-Lab 2000, SPECTRO); subsequently each filter was extracted in 10 mL of deionized water by using a mechanical shaker (Falc Instrument F205G-2/40RPM) for agitation and filtered on nitrocellulose membranes (NC Millipore, pore size 0.45 μm). With respect to the previously optimized method, we used water instead of acetate buffer and avoided the use of ultrasound-assisted extraction; acetate buffer may in fact interfere in the OP determinations and ultrasounds may generate ROS species. For example, Miljevic et al. (2014) reported that simple sonication of pure water lead to the formation of detectable levels of hydroxyl radicals, that playing key roles as oxidants in the atmosphere. The obtained solution was divided in aliquots. The first aliquot (2 mL) was analysed for anions (Cl^-, NO_3^-, SO_4^{2-}) and cations (Na^+, NH_4^+, Mg^{2+}, Ca^{2+}) by using Ion Chromatography (DX 100, DIONEX Co.,

CA-USA). A second aliquot was analysed for the extractable fraction of the elements (Li, Be, B, Na, Mg, Al, Si, P, K, Ca, Ti, V, Cr, Mn, Fe, Co, Ni, Cu, Zn, Ga, As, Se, Rb, Sr, Zr, Nb, Mo, Cd, Sn, Sb, Te, Cs, Ba, La, Ce, W, Tl, Pb, Bi and U) by inductively coupled plasma with mass spectrometer detection (ICP-MS: Bruker 820, equipped with a reaction cell, CRI, and a 400 μL/min MicroMist nebulizer). Another aliquot (1 mL, successively diluted to 5 mL with deionized water) , was used for the determination of water soluble organic carbon (WSOC) by Total Organic Carbon Analyser (TOC-VCSH, Shimadzu) WSOC was determined by the Non-Purgeable Organic Carbon (NPOC) method, which measures non-volatile OC present in the sample Inorganic carbon (carbonates, hydrogen carbonates and dissolved carbon dioxide) In the NPOC method the samples was acidified with 1% acid (Timonen, et al., 2008). The remaining solution was used for the OP assays. The residual dust on Teflon and NC filter was digested in a mix of HNO_3 and H_2O_2 (2:1) by using a microwave oven (Milestone Ethos Touch Control with HPR 1000/6S rotor) and the mineralized fraction was then analysed by ICP-MS for its insoluble elemental content. The recovery percentage and repeatability of the analytical procedure was previously validated using certified material (NIST1648) and real samples (Canepari *et al*., 2006a, 2006b). Thanks to this procedure, it was possible to obtain a complete inorganic characterization of PM in a single sample

Oxidative potential assays

0.7 mLs of water extract were incubated with DTT (Sigma, Zwijndrecht). The reaction was stopped at designated time (0, 5, 10, 15, 20 min), by adding 1 mL of trichloroacetic acid 10%. 1 mL of each solution was then mixed with 2 mL of Tris-buffer (0.08M, containing EDTA 4 mM) and with 50 μL of 0.2 mM. 5,50-dithiobis-2-nitrobenzoic acid (DTNB, Sigma, Zwijndrecht). The absorbance at 412 nm was recorded; the results are expressed as nmol DTT min^{-1} per sampled volume (m^3) or per mg of PM. Domestic oil burning furnace (DOFA, obtained from US EPA, RTP, NC) with a fixed concentration was used as a positive control and ultrapure water as a negative control.

AA analysis was performed according to the protocol by Mudway et al. (2011) and Fang et al., (2016) Briefly, PM extracts are incubated in the spectrophotometer (spectra MAX 190: Molecular Devices, Sunnyvale, USA) for 10 min at 37 °C. After adding ascorbate acid, the absorption at 265 nm is measured at designated time (0, 5, 10, 15, 20 min). The maximum depletion rate of ascorbic acid is determined by linear regression of the linear section data, plotted as absorbance against time. The results are expressed as the AA consumption rate per mass unit (nmol min^{-1}) depletion per sampled volume or per mg of PM. Domestic oil burning furnace (DOFA obtained from US EPA, RTP, NC) with a fixed concentration was used as a positive control and ultrapure water as a negative control.

The DCFH-DA solutions were prepared by dissolving 4.873 mg of the reagent in 5mL of CH_3CH_2OH in the dark. Then, 20 mL NaOH 0.01M were added to favour the de-acetalization reaction; the solution was then kept in the dark at room temperature for 30 minutes before use. The HRP solution (0.5 units/mL) was prepared by dissolving proper weighted amount of the commercial product (Type VI, essentially salt-free, lyophilized powder, ≥250 units/mg solid) in 1L of 25 mM phosphate buffer at pH 7.4 and incubated at 37 ° C for 15 minutes. Sample's water extracts (1.5 mL) and 5 µM DCFH (125 µL) were added to 5 mL of the buffered HRP solution and the solution was kept at 37°C for 15 min. The intensity of the fluorescence radiation at 530 nm was then measured by a Fluorescence detector (Jasco FP-920; excitation wavelength: 427 nm). The calibration curve was obtained daily by standard H_2O_2 solutions (5x10-6, 1×10-7, 2×10-7, 5x10-7, 1x10-6 M) and the measured fluorescence intensity was converted into equivalent H_2O_2 concentrations (Venkatachari, et al., 2005). Further experimental details about OP assays are given in Simonetti et al., 2017 submitted in Atmospheric Environment.

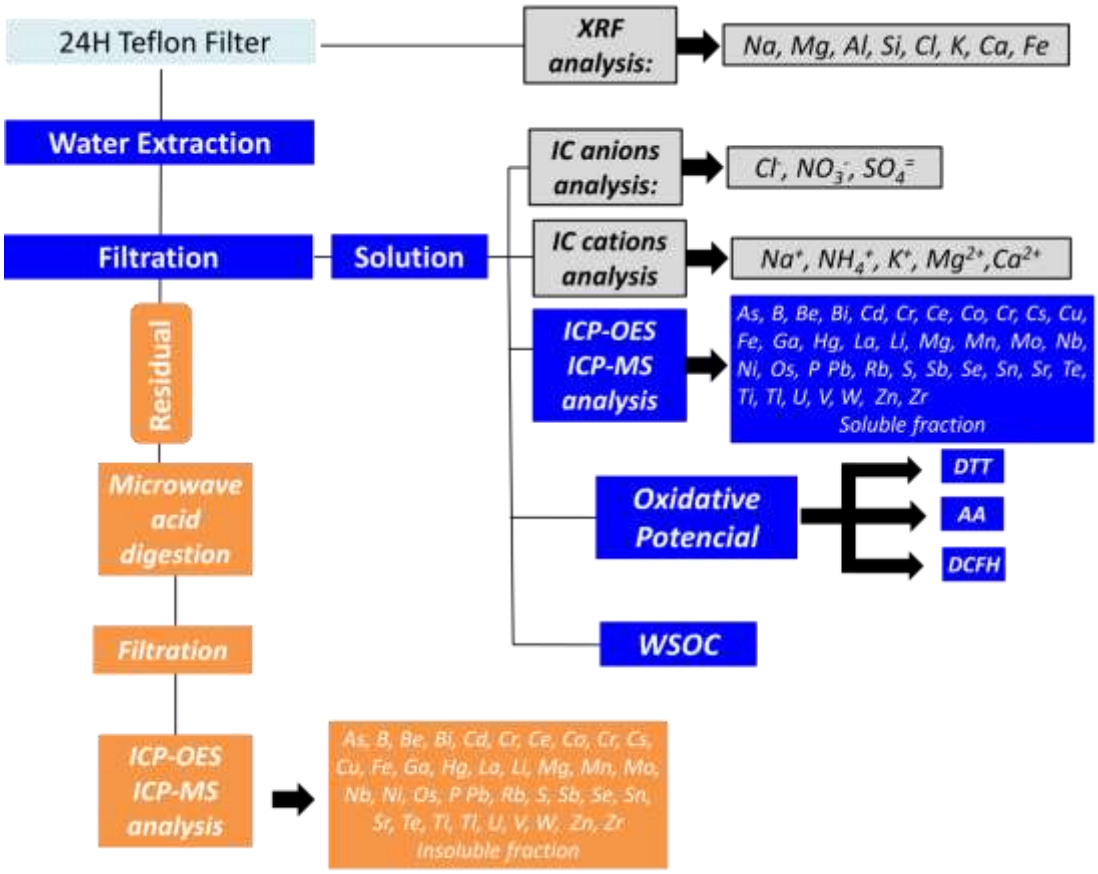

Figure 2: *Sequence of the chemical analysis performed on Teflon filters.*

Statistical elaborations

Several statistical methods can be applied for data analysis in environmental studies (Conti et al. 2005; 2007). As known, the Principal Component Analysis (PCA) is a statistic technique belonging to the so-called ‘‘unsupervised pattern recognition methods,’’ useful for performing exploratory data analysis when there is no preliminary knowledge about the distribution and structure of the data to be analyzed (Brereton 1990; Conti et al. 2010). In this study, we applied the Focused PCA (FPCA) (Falissard, 1999) in order to test the possible correlation between the OP indicators (i.e. AA, DHCF and DTT) with the analyzed chemical parameters [elements, anions and cations (n=45)] in the $PM_{2.5}$ and PM_{10} samples collected in the Ferrara and Rome sites.

In the FPCA, data representation is close to a PCA, but contrary to PCA, correlations between the dependent variable (i.e. AA, DHCF and DTT) and the other variables (i.e. chemical parameters determined in $PM_{2.5}$ and PM_{10} samples) are represented faithfully. The relationships between no dependent variables are interpreted like in a PCA: correlated variables are close or diametrically opposite (for negative correlations), independent variables make a right angle with the origin. The focus on the dependent variable leads formally to a partialisation of the correlations between the no dependent variables by the dependent variable (Falissard, 1999; 2012). FPCA presents correlations in graphic format as concentric circles, those of smaller radius representing stronger correlations. The center of these circles (target) contains the variable of interest, which directs the analysis. Negative and positive correlations are differentiated in the graph by use of different colors. The interpretation of points in an FPCA graph is as follows:

(1) Variables inside the red circle are significantly correlated to the dependent variable with $p<0.05$; (2) Green variables are positively correlated to the dependent variable; (3) yellow variables are negatively correlated. Data analysis was performed using the software R version 3.1.2 (2014 The R Foundation for Statistical Computing) and the packages Ade4 (Dray et al. 2007) and psy (Falissard, 1999; 2012).

In particular, in the Ferrara site, by using FPCA (Falissard, 1999) we tested the correlations between the analyzed chemical parameters with the OP indicators (i.e. AA, DHCF and DTT) in the PM 2.5 samples. Subsequently, with the aim to gain more reliable information about the PM10 – OP correlations in the two selected sites we used the t Student test with the Bonferroni correction of the type I error ($p<0.001$) applied to verify the chemical parameters that discriminate the sites of Rome and Ferrara for the PM10 samples. Then, FPCA was only applied to the chemical parameters that showed no significant differences between Rome and Ferrara sites.

Result and Discussion

Evaluation of the assays repeatability

Limits of detection (LODs) and of quantification (LOQs) were calculated by following the IUPAC (International Union of Pure and Applied Chemistry) indications as three times and ten times the standard deviation of the blank, respectively (10 replicates). One of the main problems in the validation of analytical methods for PM characterization is the absence of representative reference materials. Pairs of equivalent field samples were then used for method's validation.

Figure 3 shows the scatter plot of the results obtained from each real samples pair.

To assess the repeatability of the complete method, we applied the procedure defined in UNI EN14902 [23], using 10 pairs of equivalent real samples, analysed in random order. Relative repeatability, Rrel, of the set of filters pairs A and B, was calculated as follows

$$r_{rel} = \frac{r}{\overline{X}} * 100 \quad ; \quad r = \sqrt{\frac{\sum_{i=1}^{N} (m_{iA} - m_{iB})^2}{2N}} \quad ; \quad \overline{X} = \frac{\sum_{i=1}^{N} (m_{iA} + m_{iB})}{2N}$$

Where m_{iA} and m_{iB} are the masses of the analyte measured on the i-th pair of filters A and B. To confirm, the repeatability of our method, we also calculated coefficient of linear regression (R2) between results from the A and the B filters. This procedure enabled us to assess the robustness of our results with respect to the environmental variability of real samples. Table 1, summarizes the results calculated for each OP assay.

Table 1: *Values of the R^2 and Rrel intercept and slope obtained from the graphs in Figure 3 and relative LOD and LOQ of each methods*

	R^2	**X**	**B**	**R_{REL}%**	**LOD**	**LOQ**
DCFH	0.97	1.1	0.00030	2.5	0.7 nMH_20_2	8 nMH_20_2
DTT	0.95	1.05	-0.17	4.4	0.09 $nMmin^{-1}$	0.3 $nMmin^{-1}$
AA	0.91	1.01	0.12	7.6	0.2 $nMmin^{-1}$	0.8 $nMmin^{-1}$

As showed in table 1, the regression parameters (slope; intercept; Pearson's coefficient) confirm the good analytic repeatability, also considering the numerous contributions to uncertainty (sampling, extraction, analysis) and the very small analysed quantities (around 1 mg).

Figure 3 show a different trends for each PO assays in response to the same PM samples confirming the non-inter-changeability of the three methods. In figure 3 is also shown how interesting and singular results were obtained with the DCFH assay; most of the determined values are negative or, better, lower than the value measured in blank sample. In fact, the fluorescence value (instrumental signal) is positive and perfectly appreciated, as demonstrated by the good repeatability of the measurement. However, the value obtained in the presence of dust samples is lower than the value of blank (deionized water). For this reason, when the samples fluorescence data were inserted into the calibration curve, the concentration values expressed by equivalent of H_2O_2 result to be negative. To explain this phenomenon, which has also occurred in most of the analyzed PM samples, we have considered different hypotheses. A first hypothesis is the possible presence of reducing reagent species that compete with oxidizing species, decreasing the OP signal. This hypothesis could be confirmed by some preliminary tests, in which a signal reduction was observed by adding bromide (oxidizer as is well known) to the solution containing PM samples.

A further explanation could be the existence of one or more substances capable of inhibiting the enzyme, slowing the reaction between ROS and HRP and blocking the formation of the fluorescent compound. Obviously, these results will require future investigations in order to understand more clearly the nature of the negative values of oxidative potential.

Despite the DCFH method presents negative values, the results are particularly repeatable and for this reason we decided, in this paper, to continue the analysis of PM filters.

Evaluation of the macro-sources

The mean concentration, 10 and 90 ° percentile of PM mass concentration and of the measured PM macro components are reported in appendix E1; the reported data concern the results obtained by the XRF, IC, WSOC and EC/OC analysis of $PM_{2.5}$ and PM_{10} samples collected at the Ferrara site and of PM_{10} samples collected at the Rome site. These results were elaborated as fully described in Perrino et al., 2014 to estimate the intensity of the main ubiquitous PM macro-sources: soil, sea, secondary inorganics, vehicular emission and organic matter (OM; including secondary OC, biomass burning and other primary sources such as bioaerosol).

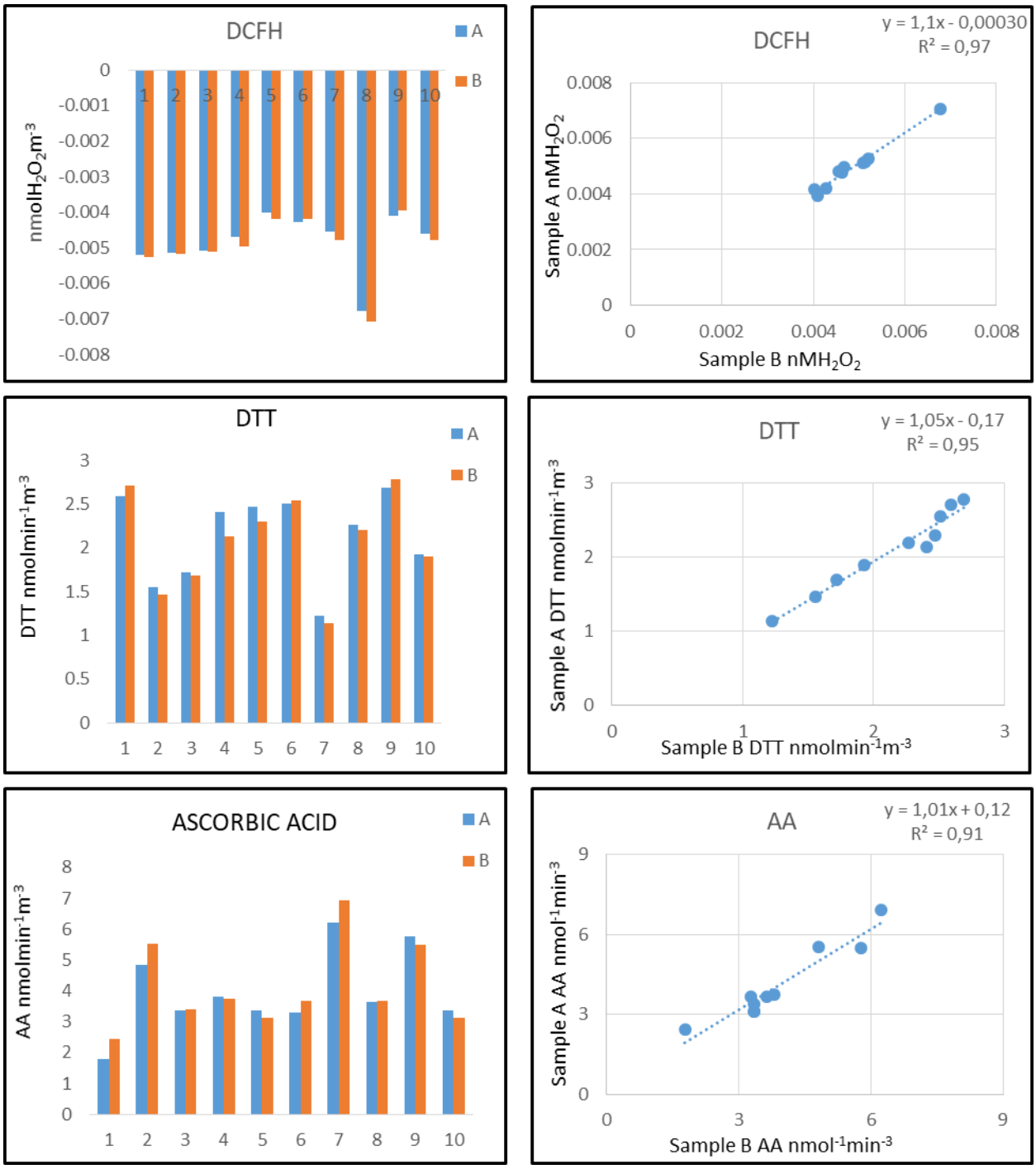

Figure 3: *PO results obtained on 10 pairs of filters with the three DCFH, DTT and AA methods*

Figure 4 shows the daily variation in the strength of the main PM_{10} and $PM_{2.5}$ macro-sources in Ferrara and of PM_{10} in Rome during the monitored periods. The Ferrara area, located in the Po Valley, is particularly problematic for the atmospheric monitoring, because of it is characterized by climatic and weather conditions that often lead to the intensive foggy phenomena favouring the accumulation of the secondary species. In fact, the Po Valley is characterized by particular climatic conditions, such

as poor mixing of the air and poor ventilation, which lead to the accumulation of the atmospheric pollutants. This situation get worse by the persistence of a high relative humidity, which acts as a promoter of the condensation and, therefore, the retention of the pollutants. This is due to its geomorphological structure situated among high mountains opened only on the eastern side, which partially obstruct the winds and favour the accumulation of high humidity in the air. Furthermore, this region is highly populated and industrialized and Ferrara is the major area of industrial development and one of the first petrochemical sites in Italy (Perrino et al., 2013a). These features make the Po Valley one of the most polluted areas in Europe and the fourth area most polluted in the world. In the area of Ferrara, in fact, particularly during the winter, the formation of organic and inorganic secondary species is favoured by the occurrence of frequent and long-lasting atmospheric stability conditions (Matta et al., 2003), contributing to more than 70% of PM composition. It is worth noting that during the whole monitoring campaign particles were almost completely confined in the fine fraction of PM, with a ratio $PM_{2.5}/PM_{10}$ ranging from 0.49 to 0.95. This condition, which is quite characteristic during the winter season in the Po Valley, indicates the clear dominance of particles formed by secondary or combustion processes. It is worth noting that in Po Valley during winter, biomass burning is typically responsible for roughly half of the total organic matter (Perrino et al., 2014). As showed in figure 4, it is evident that inorganic secondary species and organic matter are predominant during the first 6 days of the observation period, characterized by low wind intensity and high relative humidity (see appendix E1) whereas in the following days, when the meteo-climatic conditions favoured the pollutants dilution, the macro-source composition was much more balanced. The influence of meteorological condition on the PM composition may be easily appreciated by comparing the sources strength in two opposite conditions. On February 17nd, the day of the campaign that presented the maximum PM mass concentration (PM_{10} = 68 µg/m^3; $PM_{2.5}$ = 59 µg/m^3), the secondary inorganic species accounted for 53% of the PM_{10} mass and for 60% of the $PM_{2.5}$ mass, while the soil concentration did not exceed 11% of PM_{10} and 4% of $PM_{2.5}$. Conversely, on March 5th, the day with the lowest PM concentration (PM_{10} = around 6 µg/m^3; $PM_{2.5}$ = 3 µg/m^3), the main macro-source was the organic matter (49 % of PM_{10} and 57 % of $PM_{2.5}$) and secondary inorganic species accounted for less than 9% of the PM_{10} mass and for less than 10 % in $PM_{2.5}$, while natural sources, as a whole, were responsible for 35% of the PM_{10} mass and of 20 % of the $PM_{2.5}$ mass.

The urban area of Rome is characterized by less severe meteo-climatic conditions: periods of persistent atmospheric stability are quite infrequent and relative humidity is lower than in the Po Valley. Consequently, much lower concentrations of secondary formation species is usually much lower than in Po Valley (Perrino et al., 2008; Perrino et al., 2009). On the other hand, the sampling

site is located in the city center, at about 50 m from a busy road and a higher contribute from traffic-related sources is expected (Canepari et al., 2008). Furthermore, Rome is situated at a relatively short distance (about 30 Km) from the Tyrrhenian Sea and episodes of sea salt transport are quite frequent. As shown in figure 4 (lower panel), these difference resulted in a very different relative strength of the main sources. At the Rome site, the main sources were much more distributed and none of them were prevalent on the other in the whole monitored period. As an average, soil (that includes resuspension dust due to vehicular traffic) represents 24 % of the PM_{10} mass, while secondary inorganics accounts for 24 %, OM for 31%, sea salt for 9% and combustive vehicular emission for 12 %. A sea-salt transport event was registered on March 20th and 21st, but, in general, the inter-day variability of the concentrations measured in Rome during the monitored period was moderate.

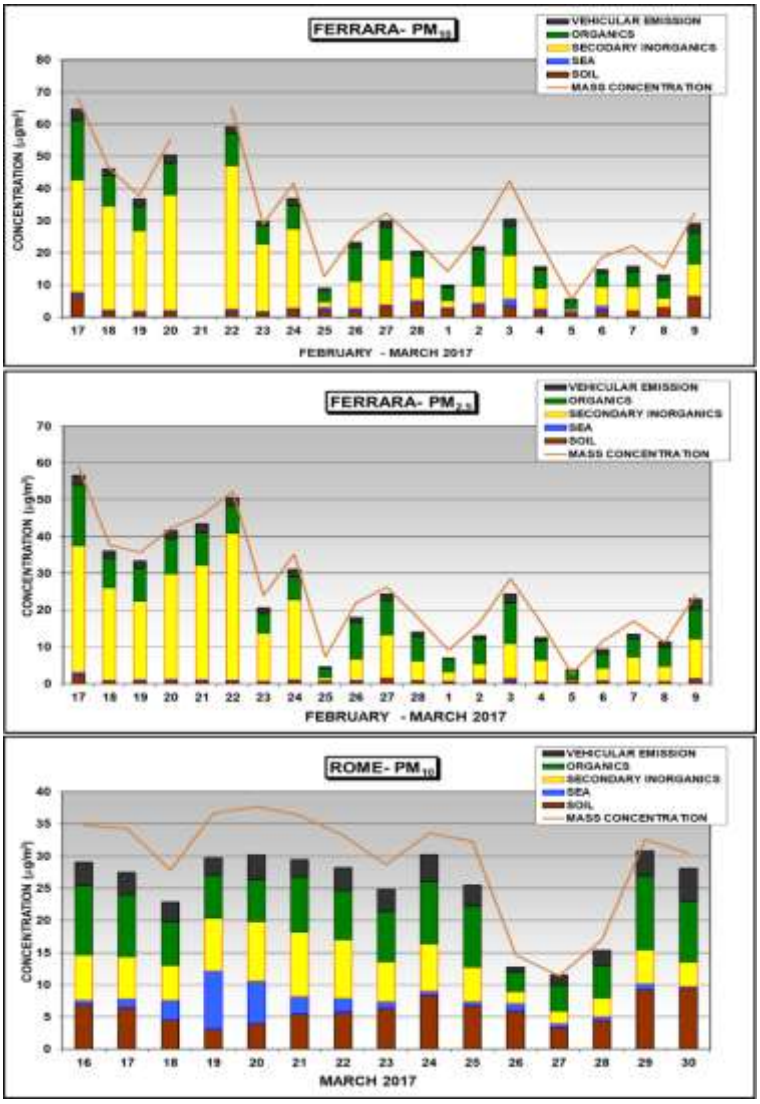

Figure 4: *Daily variation of the chemical composition of PM_{10} and $PM_{2,5}$ at site C in Ferrara during February-March 2017 campaign (upper graph) and PM10 in Rome during March campaign (lower graph).*

Oxidative potencial results

ROMA **FERRARA**

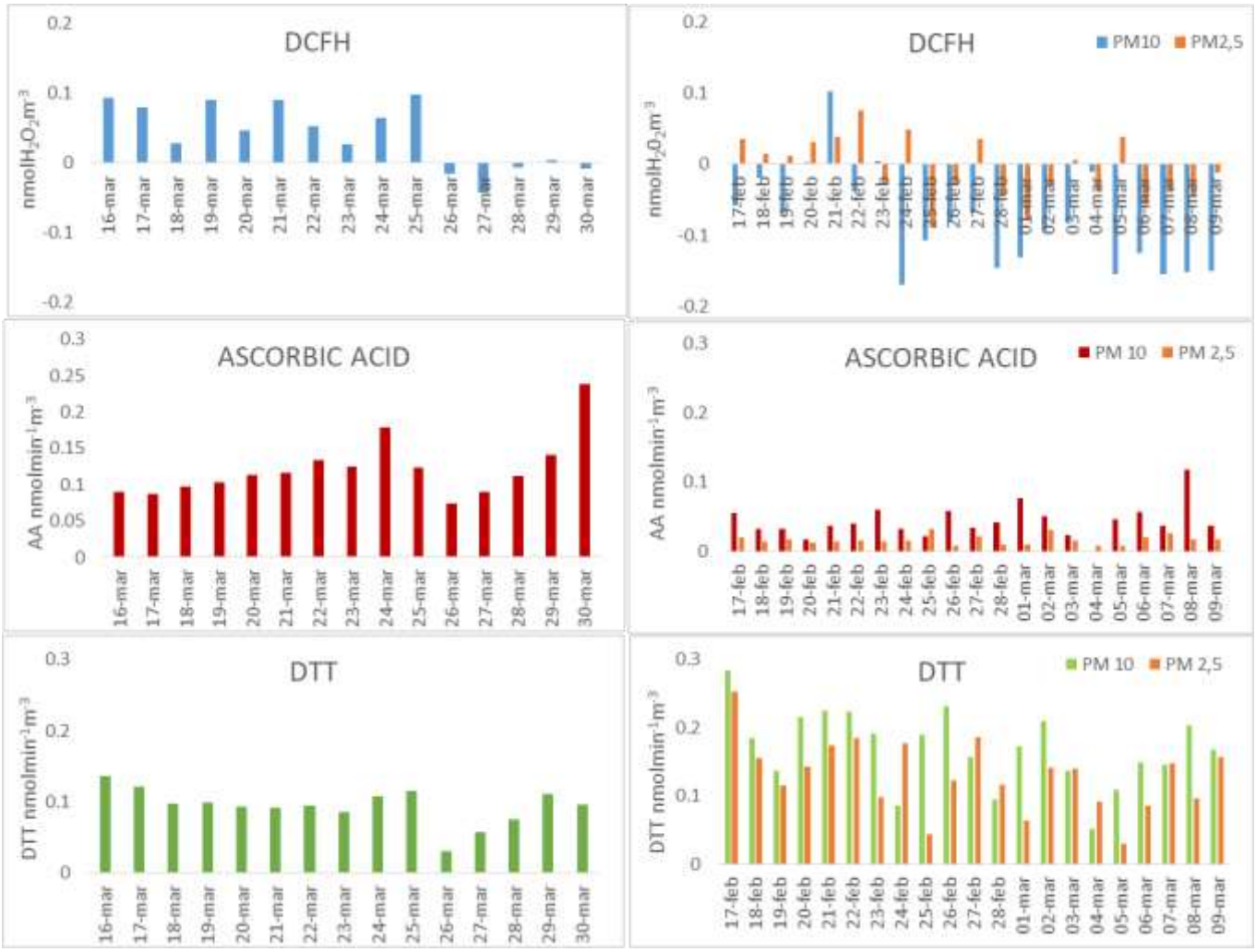

Figure 5: *Comparison of oxidative potential values obtained by the three DCFH, DTT and AA methods for the monitoring campaign of Rome (left) and Ferrara (right)*

The three OP assays were applied to all the sampled filters. The results are shown in figure 5 (Rome: left panels; Ferrara: right panels); in accordance with previous results (Simonetti et al., submitted to Atmospheric Environment; Janssen et al., 2014), each OP assay showed a different trend, confirming the non-interchangeability of each methods. A further consideration is that the OPs inter-day variability was not particularly high and not easily correlated to the PM chemical composition. The DCFH assays, also in this field application, presented negative values, especially at the Ferrara site,

confirming the unexpected behaviour already evidenced in the case of paired samples used for calculating the method repeatability.

The comparison between the results obtained in the two different areas indicated that considerably higher values of oxidative potential measured by DCFH assay (OP^{DCFH}) during in Rome than in Ferrara, at least during the first days of the campaign, despite the PM mass concentrations of in Ferrara was higher than that recorded in Rome. Therefore, it is evident that the results of the assay does not depend on the PM's total concentration, but is strongly linked to the chemical composition of the dust. It is important to underline that in most of the studies present in the literature, the health effects due to PM are evaluated only by considering the mass concentration of the dust; more extensive studies would be needed to give a deeper knowledge of the environmental and health damage caused by the PM, which can be obtained also through an intense application of OP assays.

The results obtained for the AA and DTT assays (OP^{AA} and OP^{DTT}, respectively) allowed some features to be evidenced.

OP^{AA} were in fact significantly higher in Rome than in Ferrara, probably due to the reactivity of ascorbic acid toward the crustal components, whose concentration is much higher in Rome, due to road dust resuspension phenomena caused by vehicular traffic (Fang et al., 2016). Figure 4 also shows that at the Ferrara site OP^{AA} values in PM_{10} are much higher than $PM_{2.5}$ ones (mean value of the ratio (OP^{AA}) $PM_{2.5}$/(OP^{AA})PM_{10} equal to 0.73); this results is again consistent with the high sensitivity of the AA assay towards soil components, which are usually confined in the coarse fraction of PM.

OP^{DTT} values are instead higher at the Ferrara site; furthermore, values in $PM_{2.5}$ are on average 98% of those observed in PM_{10}. In agreement to results reported in previous studies (Boogaard et al., 2012; Charrier and Anastasio, 2012). The DTT assay seems to be more sensitive to the components present in the fine fraction of PM.

Focused PCA analysis

PM 2.5 Ferrara site

For the FPCA analysis, we have considered only the concentration of chemical species that are present in the soluble fraction of samples (the same species tested for OP assays). In Table 2 are reported the mean concentrations, 10 and 90 ° percentiles of the parameters included in the statistics. The total chemical parameters' concentrations are reported in appendix E2.

Table 2: *data obtained by the soluble fraction analysis of $PM_{2.5}$ and PM_{10} samples collected at the Ferrara site and of PM_{10} samples collected at the Rome site*

	PM_{10} - FERRARA				**$PM_{2.5}$ - FERRARA**				**PM_{10} - ROME**			
	Soluble Fraction (ng/m^3)				**Soluble Fraction (ng/m^3)**				**Soluble Fraction (ng/m^3)**			
	average	**median**	**10%**	**90%**	**average**	**median**	**10%**	**90%**	**average**	**median**	**10%**	**90%**
Li	0.097	0.094	0.057	0.13	0.074	0.065	0.037	0.12	0.083	0.085	0.045	0.12
Be	0.00084	0.00066	0.00019	0.0018	0.00030	0.00032	0.000048	0.00063	0.00417	0.00475	0.001196	0.00608
B	5.1	4.1	1.4	10	4.7	4.1	1.6	9.9	3.5	3.5	2.1	4.8
Na	331	248	98	580	89	68	35	161	600	272	8	1856
Mg	62	62	33	89	16	16	7.4	25	104	71	44	217
Al	6.3	4.8	1.8	12	3.1	2.4	1.3	5.2	11	12	3.0	16
Si	19	17	8.0	26	13	12	10	16	-	-	-	-
P	7.8	7.5	3.6	13	3.7	3.5	0.91	6.6	-	-	-	-
K	241	237	139	358	214	210	118	349	-	-	-	-
Ca	399	346	218	645	86	80	53	130	647.8	603.80	517.62	862.3
Ti	0.11	0.10	0.031	0.24	0.062	0.054	0.019	0.13	0.14	0.15	0.074	0.19
V	1.1	0.60	0.21	2.6	1.0	0.59	0.19	2.5	1.4	1.4	0.44	2.8
Cr	0.28	0.24	0.083	0.49	0.22	0.21	0.051	0.40	0	0	0.0	0
Mn	3.9	3.3	1.8	5.8	1.9	1.6	0.65	3.4	3.9	4.02	2.29	5.3
Fe	28	20	5.5	61	16	12	2.5	32	25.93	27.83	8.784	38.39
Co	0.032	0.029	0.013	0.051	0.015	0.013	0.0059	0.025	0.059	0.065	0.0322	0.075
Ni	0.58	0.48	0.18	1.1	0.46	0.31	0.13	0.92	0.91	0.91	0.33	1.4
Cu	5.0	4.8	2.0	7.8	1.8	1.9	0.73	2.7	14	15	5.9	18
Zn	29	25	10	48	22	19	8.2	39	20	21	12	26
Ga	0.0092	0.0073	0.0018	0.020	0.011	0.0083	0.0022	0.024	0.008	0.0075	0.0040	0.012
As	0.44	0.41	0.15	0.75	0.41	0.35	0.11	0.72	0.24	0.23	0.15	0.34
Se	0.50	0.47	0.24	0.71	0.43	0.43	0.19	0.60	0.38	0.39	0.14	0.59
Rb	0.53	0.50	0.27	0.83	0.49	0.47	0.24	0.82	0.98	0.99	0.29	1.71
Sr	1.2	1.0	0.58	2.0	0.28	0.27	0.17	0.37	2.67	2.73	1.79	3.32
Zr	0.059	0.033	0.0064	0.15	0.042	0.022	0.0049	0.076	0.081	0.078	0.0209	0.113
Nb	0.0025	0.0011	0.000032	0.0046	0.0015	0.0006	0.00012	0.0039	0.0024	0.0029	0.00099	0.0037
Mo	0.48	0.41	0.13	0.81	0.41	0.32	0.10	0.73	0.39	0.24	0.12	0.91
Cd	0.16	0.13	0.048	0.30	0.15	0.12	0.049	0.30	0.15	0.16	0.052	0.24
Sn	0.30	0.23	0.060	0.57	0.20	0.13	0.038	0.43	0.18	0.16	0.086	0.29
Sb	0.74	0.65	0.31	1.2	0.62	0.63	0.26	0.96	0.87	0.88	0.36	1.31
Te	0.0032	0.0028	0.00080	0.0066	0.0037	0.0035	0.00083	0.0075	0.0029	0.0026	0.00059	0.0048
Cs	0.016	0.014	0.0065	0.030	0.014	0.013	0.0060	0.022	0.0303	0.0282	0.01451	0.0464
Ba	1.7	1.4	0.77	2.7	0.71	0.66	0.38	1.0	4.1	4.2	1.90	5.9
La	0.0079	0.0069	0.0029	0.013	0.0049	0.0046	0.0031	0.0068	0.0167	0.0173	0.0085	0.0221
Ce	0.015	0.012	0.0055	0.027	0.010	0.0092	0.0059	0.014	0.035	0.0375	0.0191	0.045
W	0.037	0.031	0.010	0.069	0.028	0.022	0.0071	0.052	0.019	0.016	0.0102	0.033
Hg	0.0	0.0	0.0	0.0	0.0	0.0	0.0	0.0	0.0	0.0	0.0	0.0
Tl	0.018	0.017	0.0053	0.031	0.016	0.016	0.0050	0.026	0.060	0.049	0.0240	0.102
Pb	1.4	1.1	0.34	2.6	1.6	1.4	0.56	2.8	0.7	0.7	0.25	1.1
Bi	0.033	0.025	0.0068	0.064	0.030	0.024	0.0058	0.063	0.017	0.019	0.0074	0.024
U	0.0027	0.0021	0.00076	0.0053	0.0017	0.0013	0.0006	0.0032	0.0	0.0	0.0	0.0
S	0.0	0.0	0.0	0.0	0.0	0.0	0.0	0.0	1643	1532	804	2338

Figures 1 A-C show the FPCA results were the correlation between the analyzed chemical parameters with the OP indicators (i.e. AA, DHCF and DTT) in the $PM_{2.5}$ samples is reported.

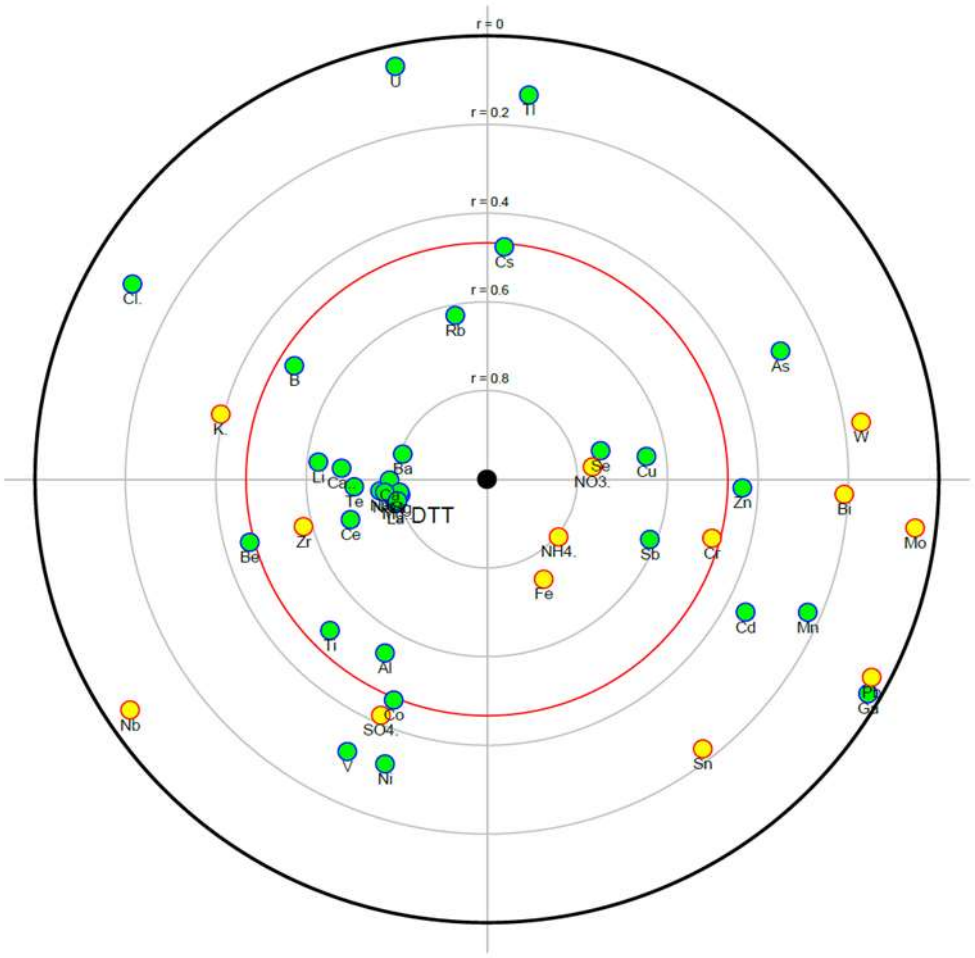

Figure 1 A): *Focus PCA between chemical analysis parameters of $PM_{2,5}$ filters and DTT assays results*

Figure A, DTT as dependent variable and the chemical parameters as no dependent variables.
First, we observe that the correlation between a relevant group of chemical parameters is significant and positively correlated (i.e. Ca, La, Ba, Na,) while Cr, Zr, Fe, NH_4^+, NO_3^- are significantly and negatively correlated with DTT. Moreover, a group of elements is positively correlated among them (Ca, La, Ba, Li, Mg). Second, the correlations between DTT and other elements (i.e. Zn, As, Cd, Ga, U Cl^-, V, Ni, Tl) are not significant and positive (they are outside of the red circle with green color). Some parameters in particular (i.e. K, SO_4^{2-}), resulted no significant and negatively correlated with DTT.

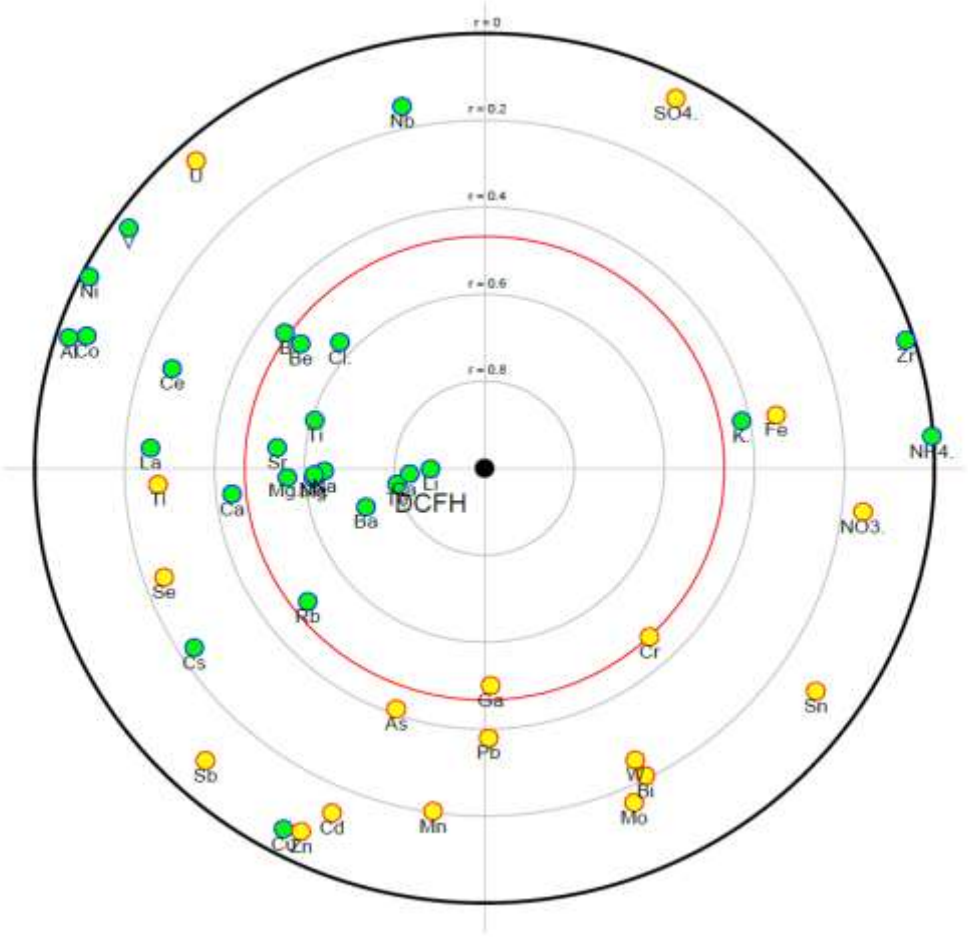

Figure 1 B): *Focus PCA between chemical analysis parameters of $PM_{2,5}$ filters and DCFH assays results*

Figure B, DCFH as dependent variable and the chemical parameters as no dependent variables. Here we observe that the correlation between DCFH and Li, Ca and Te is positive and highly significant. There are other significant and positive correlations with other elements (see inside red circle). Instead, only Ga showed significant and negative correlation with DCFH while other elements (i.e. As, Pb, Fe and others) resulted to be no significant with a negative correlation with DCFH.

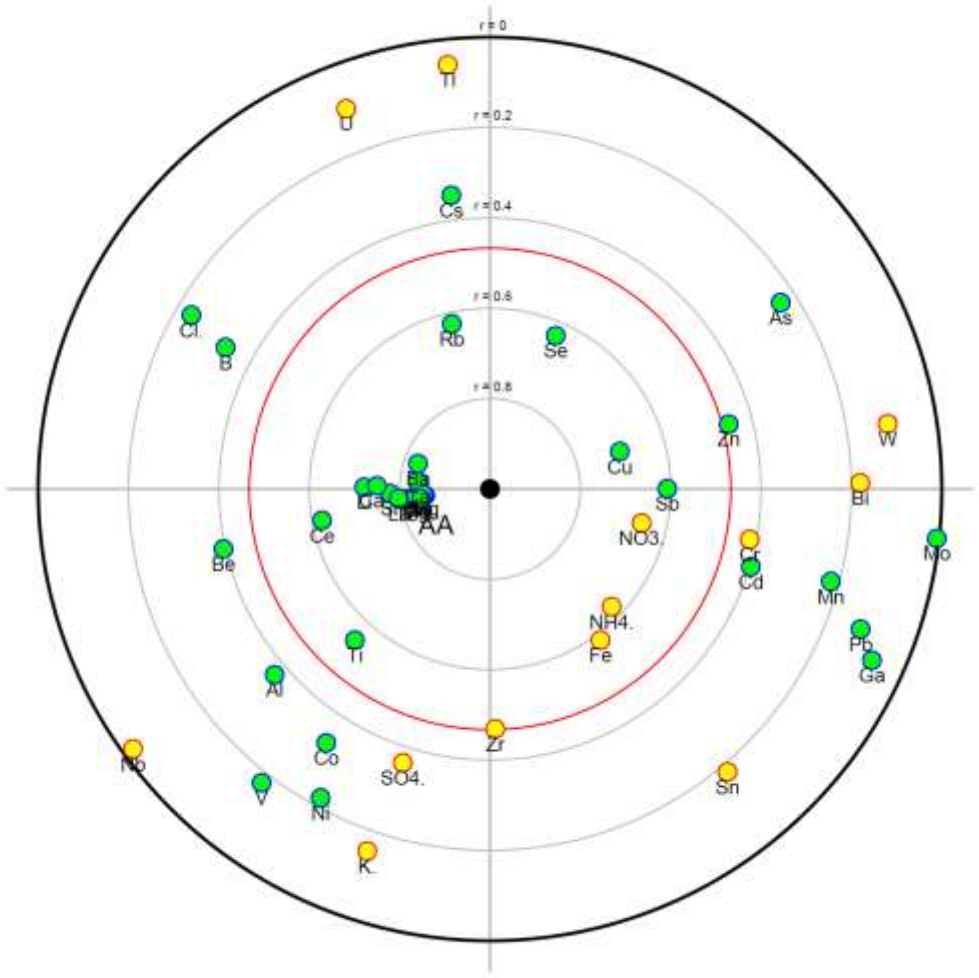

Figure 1 C): *Focus PCA between chemical analysis parameters of $PM_{2,5}$ filters and AAassays results*

Figure C, AA as dependent variable and the chemical parameters as no dependent variables. The results of AA assay are very similar to those reported for DTT-PM 2.5 assay. A relevant group of chemical parameters is significant and positively correlated (i.e. Ca, La, Ba, Na,) with AA, and they are also positively correlated among them. Moreover, Fe, NH_4^+, NO_3^- are significantly and negatively correlated with AA (similar to DTT). Cd, Mn, Pb and Ga resulted to be no significant with a positive correlation with AA. These results are similar to those reported for DTT with the exception of Pb that resulted to be no significant and negatively correlated. Comparing these methods in this kind of studies ($PM_{2.5}$-OP), these results seem better support the hypothesis that a more reliable response is obtained by using AA and DTT OP methods instead of DCFH.

PM 10: Ferrara and Rome sites

Table 2 shows the results of the t Student test with the Bonferroni correction of the type I error ($p<0.001$) applied to verify the chemical parameters (elements, cations and anions) that discriminate the sites of Roma and Ferrara for the PM10 samples. Be, Al, Ca, Ti, Cr, Co, Cu, Rb, Sr, Cs, Ba, La, Ce, W, Tl, Pb, Bi, NO_3-, Ca^{2+} are the variables that showed a significant effect due to the sampling areas (Roma/Ferrara). Then, these chemical parameters (n=19) had to be eliminated from the data set of the multivariate analysis. We then applied FPCA to the other 26 parameters that showed no significant differences between the two selected sampling areas (i.e. Li, B, Na, Mg, V, Mn, Fe, Ni, Zn, Ga, As, Se, Zr, Nb, Mo, Cd, Sn, Sb, Te, U, Cl^-, SO_4^{2-}, Na^+, NH_4^+, K^+, Mg^{2+}). The results of this study are reported in Figures 2 D-E-F.

Table 2: *T Student test results with the Bonferroni correction of the type I error ($p<0.001$) applied to chemical parameters of PM_{10} samples collected in Roma and Ferrara monitoring campaigns.*

Parameter	T	gdl	p	Parameter	T	gdl	p
Li	2.4	25	n.s.	**Mo**	0.78	27	n.s.
Be	-8.08	15	p<0.001	**Cd**	0.48	29	n.s.
B	-0.56	29	n.s.	**Sn**	2.61	31	n.s.
Na	-0.26	28	n.s.	**Sb**	-2.81	23	n.s.
Mg	-1.75	29	n.s.	**Te**	-0.27	19	n.s.
Al	-4.18	29	p<0.001	**Cs**	-5.29	22	p<0.001
Ca	-4.4	28	p<0.001	**Ba**	-8.14	17	p<0.001
Ti	-4.44	34	p<0.001	**La**	-8.93	33	p<0.001
V	-0.57	33	n.s.	**Ce**	-9.79	33	p<0.001
Cr	7.19	32	p<0.001	**W**	3.86	33	p<0.001
Mn	-0.88	34	n.s.	**Tl**	-4.24	15	p<0.001
Fe	-0.56	33	n.s.	**Pb**	4.57	29	p<0.001
Co	-7.76	29	p<0.001	**Bi**	4.32	26	p<0.001
Ni	-2.45	34	n.s.	**U**	-1.37	34	n.s.
Cu	-10.58	16	p<0.001	**Cl^-**	-1.19	20	n.s.
Zn	3.39	27	n.s.	**NO_3^-**	5.71	24	p<0.001
Ga	-1.34	22	n.s.	**SO_4^{2-}**	-3.32	34	n.s.
As	2.63	21	n.s.	**Na^+**	-3.33	17	n.s.
Se	2.93	33	n.s.	**NH_4^+**	-3.36	21	n.s.
Rb	15.04	20	p<0.001	**K^+**	-3.26	24	n.s.
Sr	-6.69	33	p<0.001	**Mg^{2+}**	-2.83	21	n.s.
Zr	-2.21	31	n.s.	**Ca^{2+}**	-6.65	23	p<0.001
Nb	-0.49	21	n.s.	**Bonferroni correction: p'=0.05/45=0.001**			

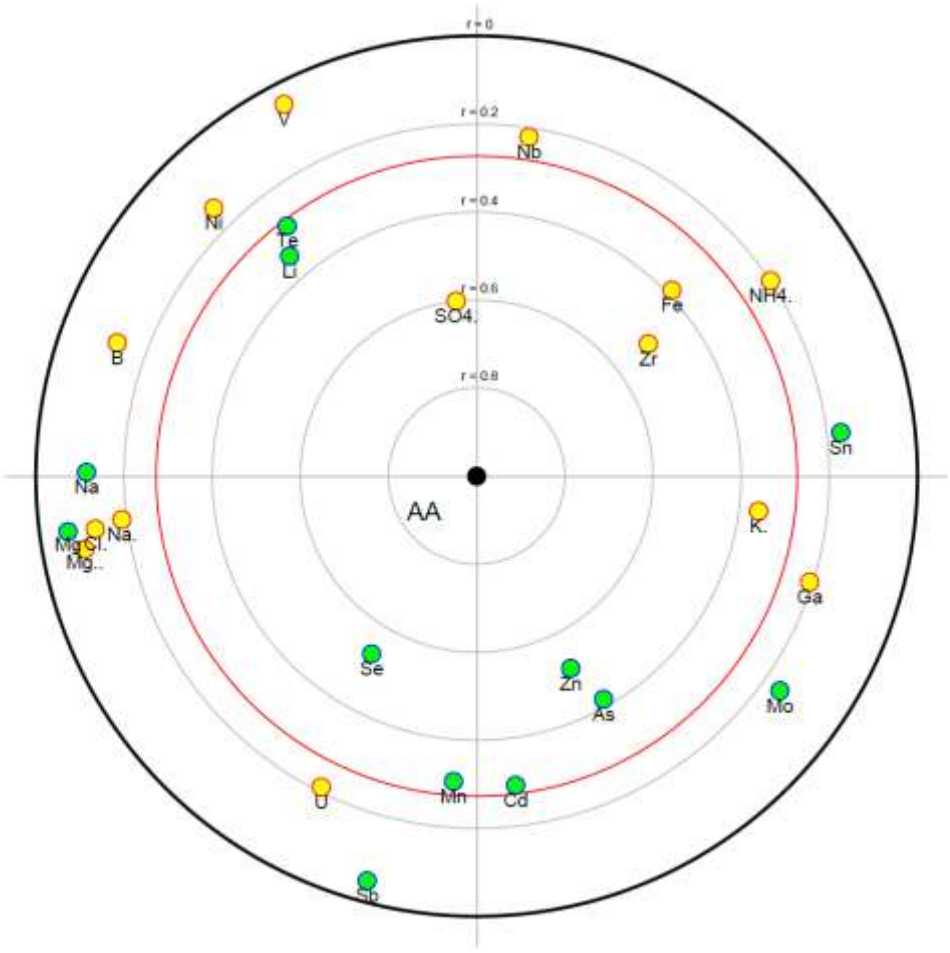

Figure 2 D): *Focus PCA between chemical analysis parameters of PM_{10} filters and AA assays results*

Figure D, DTT as dependent variable and the chemical parameters as no dependent variables. Here we observe that the correlation of Se, Zn, Te, Li, As, Cd and B with DTT is significant and positive while SO_4^{2-}, Zr and Fe are significant and negatively correlated with DTT. Te and Li are positively correlated among them.

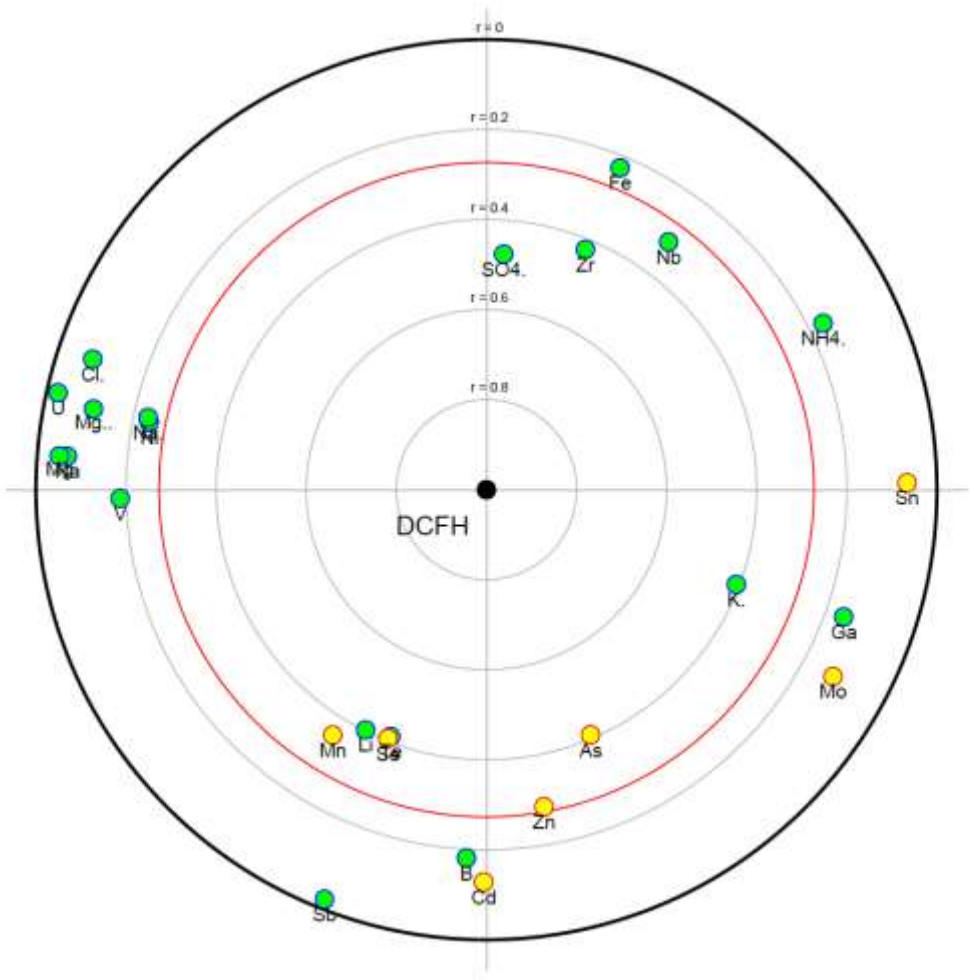

Figure 2 E): *Focus PCA between chemical analysis parameters of PM_{10} filters and DCFH assays results*

Figure E, DCFH as dependent variable and the chemical parameters as no dependent variables. SO_4^{2-}, Zr, Nb, K, Li, Te are significant e positively correlated with the DCFH, while Mn, Se, As are significant but negatively correlated with DCFH. These results are in contrast with DTT and AA assays where SO_4^{2-}, Zr and Fe resulted to be significant and negatively correlated

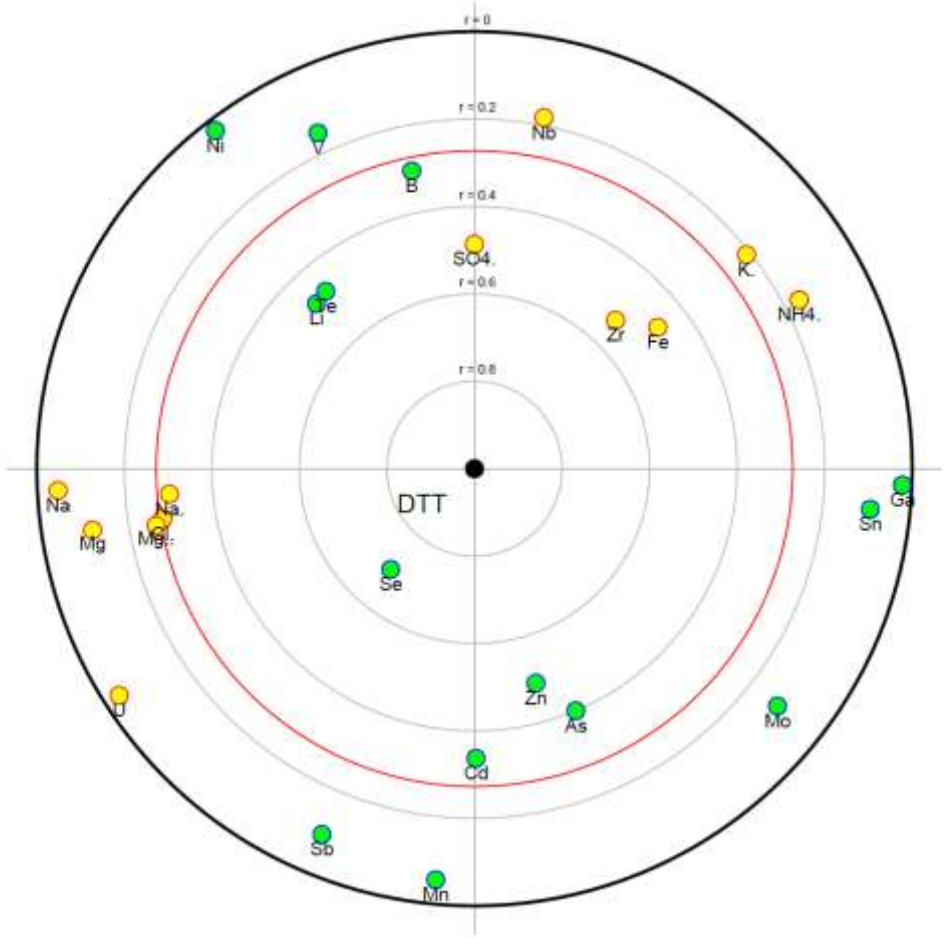

Figure 2 F): *Focus PCA between chemical analysis parameters of PM_{10} filters and DTT assays results*

Figure F, AA as dependent variable and the chemical parameters as no dependent variables. The results of AA assay are similar to those reported for DTT-PM 10 assay. In fact SO4, Zr , Fe and K are significant and negatively correlated with DTT. Similarly to DTT assay, Se, Zn, As and Cd are significant e positively correlated with AA. A group of parameters Na^+, Cl^- and Mg^{2+} are not significant and are negatively correlated with AA while Na and Mg are not significant and are positively correlated with AA.

Even if there are some differences, the results here reported for the PM_{10} assays generally agree with those of the $PM_{2.5}$. They better support the hypothesis that a more reliable response is obtained by using AA and DTT OP methods instead of DCFH.

*3.6.3 Dimensional distribution of particulate matter's oxidative potential**

INTRODUCTION:

As well known, the size rages of atmospheric particles (PM) is closely related to emission sources and health effects. The study of the dimensional distribution of PM and of its chemical components provides relevant information about its origin and formation processes (Kelly et al., 2012). Coarse PM is in fact generally originated from resuspension processes or mechanical shearing and may contain bioaerosols, such as pollen and spores. Conversely, fine PM are generally formed by fuel combustion, biomass burning and secondary particles, resulting from atmospheric transformations of gaseous precursors (Brunekreef & Forsberg, 2005; Sarnat et al., 2010; Shridhar et al., 2010). Furthermore, the particles dimensional distribution gives information about the ageing phenomena of dusts, which depends on climatic conditions and on distance of sources from the sampling site. During their permanence in the atmosphere, smaller particles tend in fact to increase their size by condensation and/or aggregation phenomena, while larger diameter particles tend to reduce their dimension by abrasion (Di Menno Di Bucchianico et al., 2002; Manahan 2000). Fine particles are more subjected to ageing phenomena and easily diffuse in vast geographic areas, while coarse particles tend to settle on the soil quite near the emission or formation zones, due to their higher mass and lower diffusion coefficients (Mahowald, et al., 2014). The particle size also influences the ability of particles to penetrate in the respiratory tract, thus influencing their harmfulness (Xing et al., 2016; Kelly et al., 2012). Several epidemiological studies evidenced an association between ambient air PM size and health effects (Ntziachristos, et al., 2007; Stephanie et al., 2011 Steenhof et al. 2011). Ultrafine particles (particles with diameters lower than about 100 nm) may be more toxic and biologically active than larger particles (Li et al., 2003;Oberdörster et al., 2001); fine PM has been most closely associated with excess cardiovascular mortality (Dockery et al., 1993; Pope et al., 2002, 2004), lung cancer (Turner et al., 2011) and cardiac arrhythmias (Peters et al., 2000), and it is important to underline that this effects vary with sampling location, season and size fraction (Zanobetti & Schwartz, 2009). Coarse PM has been instead associated mainly with respiratory disease (Host et al., 2008; Lin et al., 2005) and cardiopulmonary morbidity, (Malig & Ostro, 2009), although some research studies were not able to identify any clear associations with health effects (Chen et al., 2011; Peng et al., 2008; Puett et al., 2009).

** Paper in preparation*

The dependence of health effects upon dust chemical composition (which is directly correlated to its emission sources) is attracting a large number of studies in the last years. The mechanisms of PM related health effects are still difficult to understand; an hypothesis is the possible association between health effects and oxidative stress, which consists in the formation of reactive oxygen species (ROS) able to damage membrane lipids, proteins, and DNA, and to cause a change in the redox status of the cell (Squadrito et al., 2001). An important metric used in the literature to study the biological responses to PM exposures is the oxidative potential (OP; Borm et al., 2007). The OP is defined as a measure of the capacity of PM to oxidize target molecules; it integrates various biologically relevant properties, including size, surface and chemical composition. There is a growing number of studies in literature concerning the study of possible acellular and cellular OP assay for a better understanding of the phenomena and the factors that determine the ability of PM to induce pro-inflammatory effects in the nose, lungs and cardiovascular system (Li et al., 2003, . Sheesley et al., 2003; Donaldson et al., 2001). However, recent studies (Yang et al., 2014; Simonetti et al., 2017 submitted to Atmospheric Environment) put into evidence that each PO assays behave differently towards the hundreds of chemical species contained in PM. Further studies are then needed to better understand the mechanisms at the basis of OP assays results and the reliability of these tests in simulating oxidative processes in living organisms.

Only a few studies concern the dependence of the OP values on the dimensional distribution of PM and on its chemical composition (Boogaard et al., 2012; Hu et al., 2008; Shi et al., 2003a; Fang et al., 2017 Shafer et al., 2016). These studies generally considered only the two dimensional fraction PM_{10} and $PM_{2.5}$ and regarded only one or two OP assays. In this paper, we examined the dimensional distribution of three different OP assays (dithiothreitol (DTT), the ascorbic acid (AA) and the 2′,7′-dichlorofluorescin (DCFH)), chosen among the most used in the literature. The purpose of these methods is to quantify a measure of oxidation by ROS species present in the PM samples using three different molecules. In Fact, DTT is considered a chemical surrogate of the cellular reductants, such as NADH or NADPH, which reduces O_2 to superoxide anion (O_2^-) and induces oxidative stress (Kumagai et al., 2002), while the AA is a physiological antioxidant that prevents the oxidation of lipids and proteins Valko et al., (2005). Concerning the DCFH is a non-fluorescent molecule that is oxidized to the fluorescent dichlorofluorescein (DCF) by ROS in the presence of horseradish peroxidase (HRP). In DTT and AA cases, the ability of the aerosol redox-active species to transfer electrons from DTT or AA to oxygen has been demonstrated through the antioxidant loss rate (Cho et al., 2005; Fang et al., 2016), while in the DCFH assay the ROS production was calculated as the increase in fluorescence intensity over time.The three assays were applied to size-segregated samples

collected by a 10-stage impactor at two sites, characterized by different emission sources and meteo-climatic conditions. The chemical analysis (ions and elements) of the same samples was also performed, in order to verify the possible correlation of the OP results with single chemical components able to trace the principal PM sources.

Experimental

Sampling

The study was carried out during two Special Observation Periods (SOPs), performed in different geographical and environmental conditions.

The first SOP was carried out from March 16th to March 30th, 2017 at Sapienza University of Rome, sited in the center of the city, 26 km from the Thyrrenian Sea (Google Earth co-ordinates:Lat. 41.902433° Long. 12.517505°). The site is characterised by duty traffic, particularly during working days. The second SOP was carried out from February 17th to March 17st, 2017; samples were taken in Cassana, a hamlet at 6 km from Ferrara, a medium-size city located in the Po Valley (Northern Italy) at a distance of about 50 Km from the Adriatic Sea (Google Earth co-ordinates: Lat. 44.848774° Long. 11.561354°). The sampling site was in a residential area close to a major industrial area; road traffic emission was mainly due to the highway, running at about 500 m. Due to the geographical position of the Po Valley area, long periods of atmospheric stability are frequently experienced during the winter, resulting in very high concentration of PM, notably of secondary pollutants (Perrino et al., 2014; Caserini et al., 2017).During each SOP, size-segregated PM samples were collected by a Uniform Deposition Impactors (MOUDI; mod. 110.R, MSP) operating at the flow rate of 30 L min-1 and having stage cut-sizes of 0.18, 0.32, 0.56, 1.0, 1.8, 3.2, 5.6, 10 and 18 µm in aerodynamic diameter (AD): the impactor was equipped with Teflon membrane filters (TEFLO, 47 mm, 2.0 micron pore size, PALL Life Sciences).

Analysis

The PM mass concentration was obtained gravimetrically by using an automated microbalance (1 µg sensitivity, mod. ME5, Sartorius AG, Goettingen, Germany). To all the collected samples it was applied the analytical procedure described in Simonetti et al., 2017 submitted to Atmospheric Enviroment. Briefly, the samples were extracted in deionized water (H_2O ultrapure level, obtained by a deionizer Elga LabWater Purelab Plus) under mechanical agitation (Falc Instrument F205G-2/40RPM agitator; 1 h). The solution was filtered on nitrocellulose membranes (NC Millipore, pore

size 0.45 μm) and splitted in several aliquots to perform a quite detailed chemical analysis of the soluble fraction. The inorganic ions (Cl^-, NO_3^-, SO_4^2 , Na^+, NH_4^+, Mg^{2+}, Ca^{2+}) were determined by ion chromatography ((DX 120, ICS-1000, DIONEX Co., CA-USA) while the soluble fraction of elements (Li, Be, B, Na, Mg, Al, Si, P, K, Ca, Ti, V, Cr, Mn, Fe, Co, Ni, Cu, Zn, Ga, As, Se, Rb, Sr, Zr, Nb, Mo, Cd, Sn, Sb, Te, Cs, Ba, La, Ce, W, Tl, Pb, Bi and U) was analysed by inductively coupled plasma – mass spectrometry (Bruker 820, equipped with a reaction cell, CRI, and a 400 μl/min MicroMist nebulizer). Water-soluble organic carbon (WSOC) was analysed by Total Organic Carbon Analyser (TOC-VCSH, Shimadzu) and was determined by the Non-Purgeable Organic Carbon (NPOC) method, in order to measures non-volatile organic carbon remaining in an acidified sample after purging the sample with gas (Timonen, et al., 2008). One aliquot of the solution was used for OP assays. The oxidative potential of the collected PM samples was determined using dichlorofluorescein diacetate (DCFH-DA), the dithiothreitol (DTT) and the ascorbic acid (AA) assays. DTT and AA absorbance was recorded by UV-Vis spectroscopy (Spectra MAX 190: Molecular Devices, Sunnyvale, USA) at 412 nm and 216 nm, respectively. The respective oxidative potential (OP^{DTT} and OP^{AA}) were expressed as the AA or DTT consumption rate per sampled volume or per mg of PM (nmol min^{-1} m^{-3} or nmol $min^{-1}mg^{-1}$). The OP values obtained from the DCFH assay (OP^{DCFH}) were instead measured through the emitted radiation at 530 nm (excitation wavelength 427 nm) by a Fluorescence detector (Jasco FP-920; excitation wavelength: 427 nm). A calibration curve was obtained daily using standard H_2O_2 solutions (5×10^{-6}, 1×10^{-7}, 2×10^{-7}, 5×10^{-7} and 1×10^{-6} M) instead of the sample solution and the results, expressed in nmol H_2O_2 per sampled volume or per mg of PM, were obtained by converting the fluorescence intensity into H_2O_2 equivalents. The information relative to the chemicals preparation and the detailed procedure are reported in appendix (F1).

Finally, the insoluble fraction of samples was subjected to microwave-assisted digestion in HNO_3/H_2O_2 mixture (2:1) and analysed by ICP-MS for the same elements determined in the soluble fraction. Further experimental details about the elemental analyses are given in Canepari et al. 2006, 2010; Protano et al., 2016.

RESULTS AND DISCUSSION

Dimensional distribution of PM and tracers

In figure 1 the dimensional distribution relative to PM mass concentration in both the monitoring campaigns is reported. As it can be seen, in the Ferrara's area the particles within the *fine* mode were shifted to larger aerodynamic diameters (maximum in 1.0-1.8 μm cut size) compared to those in the

Roma area (maximum in the 0.56-1.0 µm size range). These results are in accordance with the different meteo-climatic characteristics of the two different geographic areas. In fact, Rome is generally characterized by frequent windy events and by quite good mixing properties of the air masses (Perrino et al., 2008; Di Giovane et al., 2000); these conditions does not favour the ageing processes of PM. The Ferrara area, instead, is characterized, especially during the winter season, by long periods of atmospheric stability, which favour the PM permanence time in the atmosphere and thus the size increase of particles in the fine mode (Perrino et al., 2008; Canepari et al., 2014 Perrino et al., 2014). The bimodal dimensional profile is more evident in Rome than in Ferrara, where the *coarse* fraction is much less pronounced and partially superimposed to the fine fraction. This difference can be again partially explained by considering the different permanence time of particles in the atmosphere, as ageing processes cause, in the coarse mode, a shift towards lower diameters. Furthermore, coarse particles are greatly influenced by the contribution of road-dust-resuspension due to the vehicular traffic, more intense at the urban monitoring site.

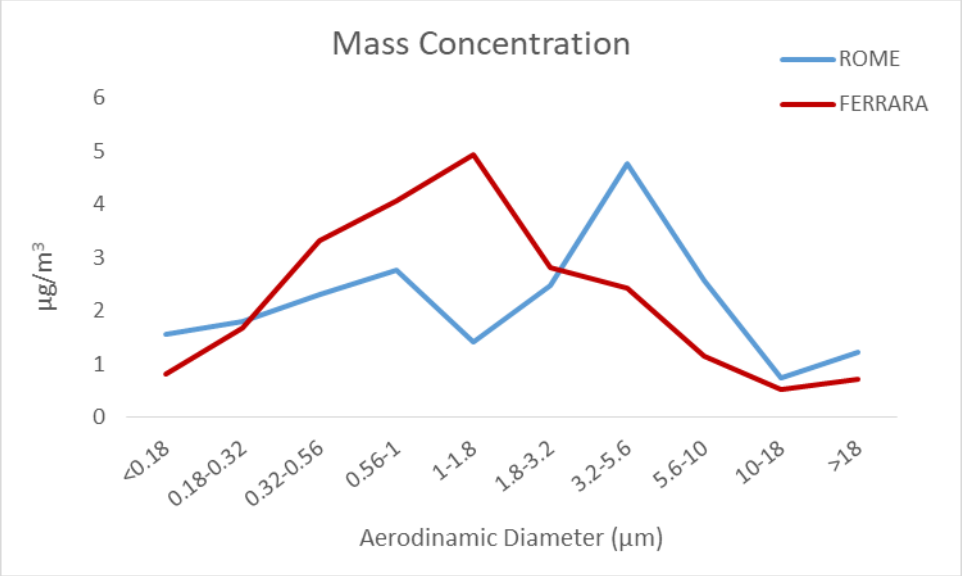

Figure 1: *Dimensional profiles of PM mass concentration in Rome and Ferrara during the monitoring period*

Figure 2 reports the dimensional distribution relative to NO_3^- and NH_4^+ ions, which are the main constituent of secondary inorganic particles, to Na^+, a tracer of the sea spray contribute, and Ca^{2+}, a tracer of soil sources (Perrino et al., 2008; Farao et al., 2014). As it can be seen, secondary ions are more abundant at the Ferrara site; even in this case, the difference was due to the persistence of poor re-mixing conditions of air masses typical of the Po Valley area, which facilitates the formation of

secondary species. The maximum of concentration is registered for 1-1.8 µm and indicates the presence of aged dusts. In Rome the concentration of secondary species was much lower, and the lower stagnation of the air masses did not favour the aging phenomena (maximum concentration at 0.32-0.56 um, *fine* particles range). The sea spray component (traced by Na^+) is present almost exclusively in the *coarse* fraction and the concentration is significantly higher at the Rome site, because of its closeness to the sea and to the frequent events of marine aerosol transport. The soil component (traced by Ca^{2+}) is present at higher concentrations in Rome than in Ferrara, probably due to its association to resuspension source due to the vehicular traffic (Canepari et al., 2008; Harrison *et al*., 2003; Viana *et al*., 2008a; Amato *et al*., 2011). Further information on the dimensional distribution of individual PM components can be obtained by elemental analysis. In this study, elemental analysis was performed by dividing the soluble and insoluble fractions. The study of the soluble fraction chemical composition allows us to understand the relationships between chemical composition and OP values, as the same solution was subjected to both chemical and OP analysis. Furthermore, the adoption of a chemically fractionated methods had been demonstrated to increase the selectivity of elements as source tracers, thus improving the dimensional characterization of specific source contributes.

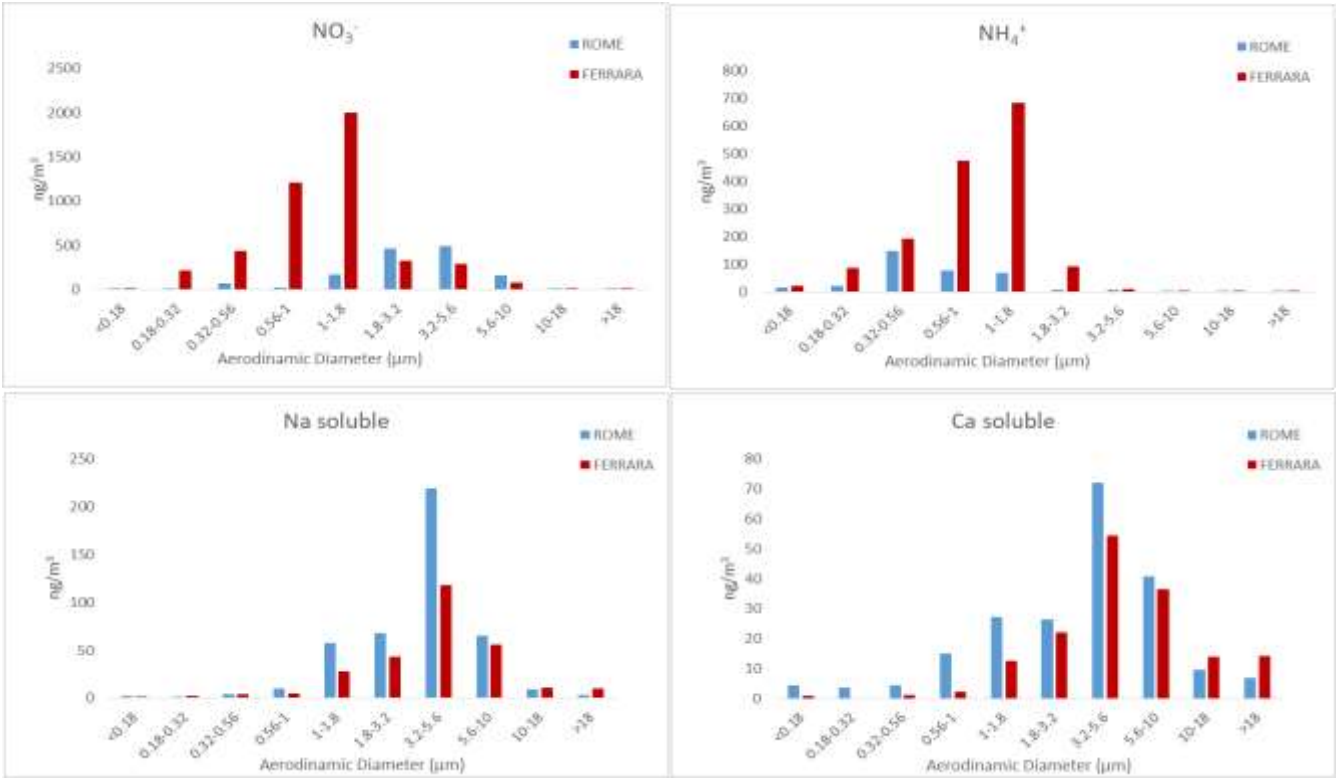

Figure 2: *Dimensional profiles of NO_3^- NH_4^+ $Na^+$and Ca^{2+}in Rome and Ferrara during the monitoring period*

As an example, figure 3 reports the dimensional distribution of extracted and residual fractions of Sb; it can be easily noted that the two chemical fractions showed a very different dimensional distribution. In the literature, many studies (Canepari et al., 2011) indicated the brake pads abrasion as one of the main sources of Sb; this element, in the form of Sb_2S_3, is in fact used as a lubricant to reduce vibrations and to improve friction stability, and is released into the environment during breaking. This contribute, generated by mechanical abrasion, is almost completely confined in the coarse fraction of PM. On the other hands, forest fires, volcanic eruptions and waste incineration are the main sources of Sb in the fine fraction of PM (Miravet et al., 2007; Takaoka et al., 2005; Nirel et al., 2008). Figure 3 shows that the soluble fraction is almost completely associated to the combustive processes (*fine* particles) while the residual fraction is mainly influenced by the *coarse* contribute due to brake abrasion. As already remarked, particles in the *fine* fraction were more subjected to ageing processes in Ferrara than in Rome and concentrations in the coarse mode are higher in Rome, due to the higher contribute from traffic. Many other elements show remarkable differences between the size distributions of the two chemical fractions, reflecting a different solubility of the chemical species of the same element, which derive from different sources (appendices F2,F3).

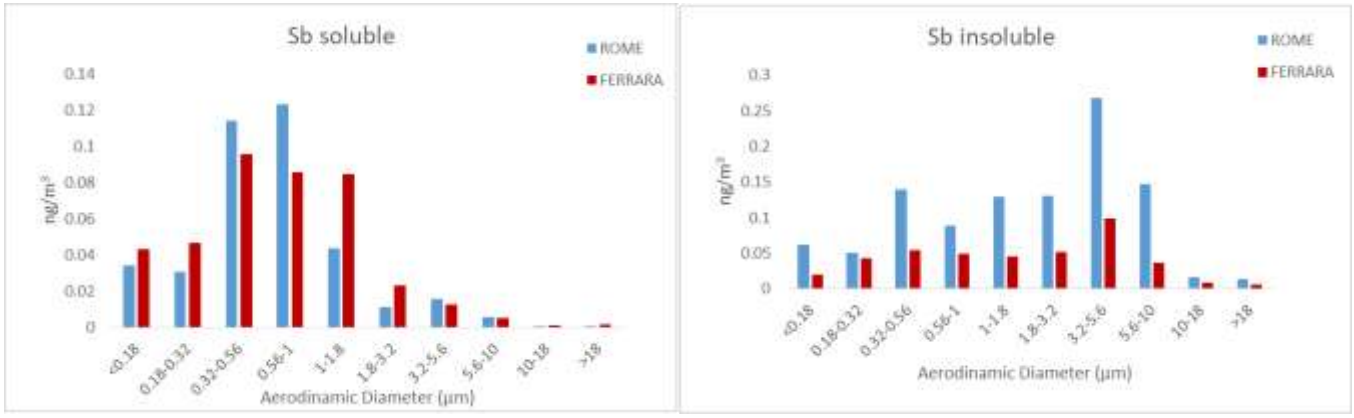

Figure 3: *Dimensional profiles of Sb obtained by the analysis of impactor (SOP1and SOP$_2$)*

In most cases (e.g., Be, Li, Rb, V, , Be, Sn), the elements are contained in both *fine* and *coarse* particles, but *fine* particles, contains more soluble, and thus more bio-accessible, species than the *coarse* fraction (Canepari et al. 2010).

Oxidative Potential Results

Figure 4 shows the results obtained by the analysis of the samples by the three oxidative potential assays. A comparison of the data obtained in the two SOPs shows that, despite the different dust composition at the two sites, the dimensional behavior of the three methods is poorly dependent on the sampling site. In addition, the results clearly indicate a different behaviour for each assays, confirming the non-interchangeability of the methods (Janssen et al., 2014; Yang et al., 2014; Simonetti et al., 2017 submitted in Atmospheric Environment). AA assays was particular sensitive to the coarse fraction of PM, with OP^{AA} maximum values in the 3.2-5.6 µm size fraction at both sites. The same dimensional profile was observed for all the tracers of road dust resuspension (insoluble fraction of Ba, Cu, Fe, Mn, reported in appendix F3; Canepari et al., 2008). OP^{AA} values are higher at the Roma site, accordingly to the higher contribute from traffic-related resuspension processes. Conversely, OP^{DTT} values were mostly affected by particles in the fine mode, with a dimensional profile similar to those of some tracers of the industrial-related contributes (soluble fraction of As, Cd, Se, Pb, Ni; Canepari et al., 2009; 2014). The fine mode of OP^{DTT} at Ferrara site, accordingly to the higher permanence time of particles, is slightly shifted towards higher size fractions respect to the Rome site. Particles in the coarse mode gave a small, but not negligible, contribute to OP^{DTT} in the size fractions range 1.8-10 µm. However, the OP dimensional profile was different from those of the re-suspension tracers and OP values at the two sites are comparable; the DTT assay seems then to be scarcely influenced by the road dust resuspension contribute.

The DCFH assay showed to be the less selective method; the OP^{DCFH} values were higher in the fine mode, but a bimodal size distribution was observed at both sites. As in the case of the OP^{DTT}, the dimensional distribution in the fine mode was shifted towards higher diameter at the Ferrara site; values in the coarse mode are higher at the Rome site, particularly in the size fraction 3.2-5.6 µm, where the maximum concentration of road dust resuspension tracers was observed.

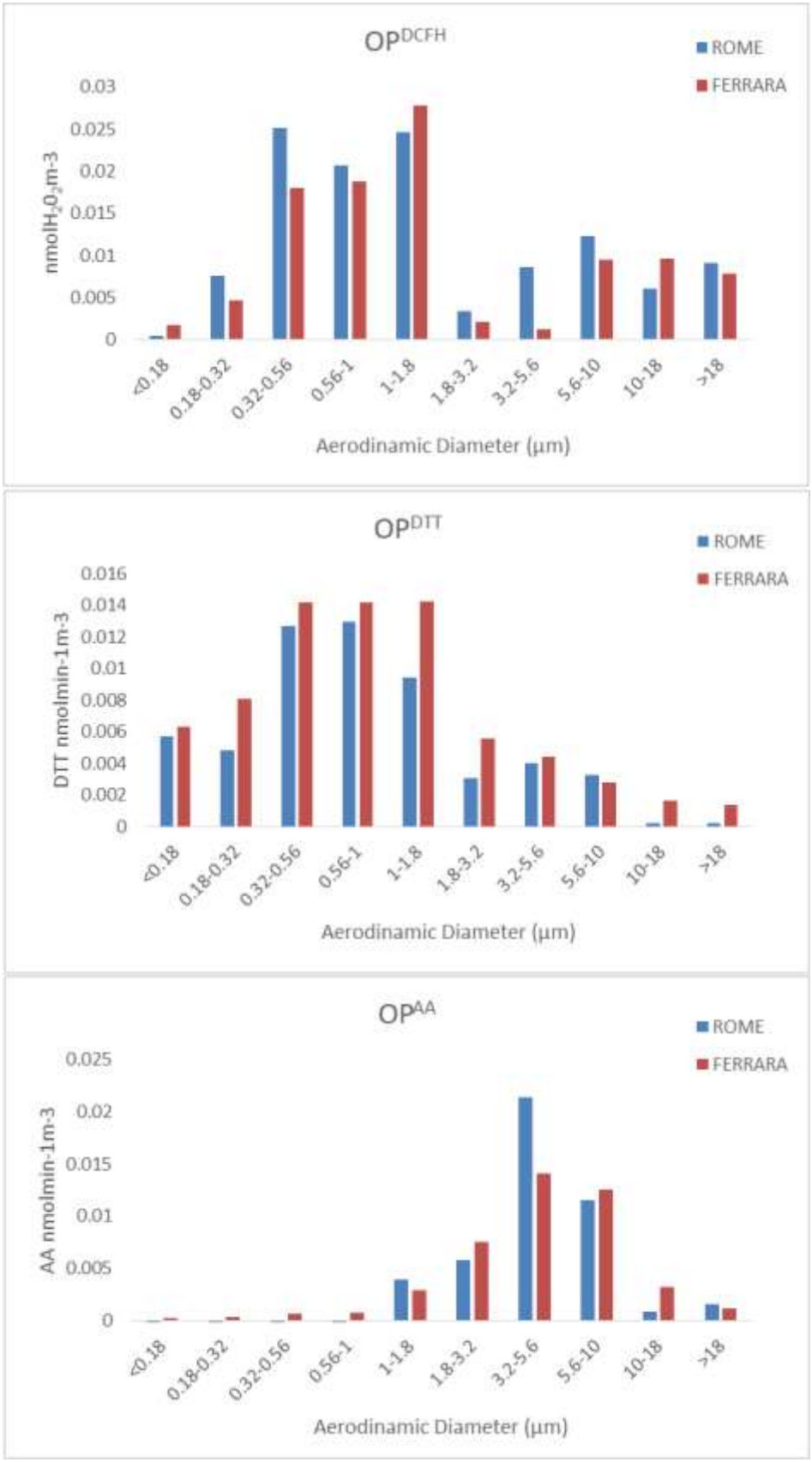

Figure 4: *Comparison of the oxidative potential results obtained with the three methods on multistage filters in Rome and Ferrara.*

Conclusion

This study concerned a detailed chemical analysis of size-segregated PM samples and the assessment of oxidative potential by different assays (AA, DTT and DCFH). This allowed us to focus our attention on the correspondence among the origins of the particles, their emitting sources and their ability to generate different types of oxidative processes.

The AA assay resulted to be particularly sensitive to particles in the *coarse* mode, especially to those generated by vehicular traffic, such as the abrasion of brake pads and the re-suspension of road dust. OP^{DCFH} and OP^{DTT} had a very different size profile, moved to the *fine* mode. These two methods were less selective towards specific emission sources and their correlation with PM chemical composition need to be further deepened.

This suggests that either OP^{DCFH} or OP^{AA} and OP^{DTT} should be use in a complement way in order to providing information regarding the oxidative properties of PM, which can subsequently be used to study its health effects.

In conclusion, it can be affirmed that the oxidative potential is influenced by different sources and that the origin of the particles has a role of primary importance in the generation of oxidative stress.

*3.6.4 The "Carbonaceous aerosol in Rome and Environs (CARE)" project: first results**

Introduction

The "Carbonaceous Aerosol in Rome and Environs (CARE)" experiment is focus on a specific question: what is the colour, size, composition, and toxicity of the carbonaceous aerosol in the Mediterranean urban background area of Rome? In recent years, scientific research has focused on the understanding of microphysical, chemical and optical properties of the carbonaceous aerosol in the ambient atmosphere due to its impact on both climate and human health (Ramana et al., 2010; Shindell et al., 2012). Carbonaceous aerosol is a complex mixture of components resulting from the processing in the atmosphere of combustion-generated aerosol particles. It consists of both light absorbing and light scattering material in particles with sizes varying from few nanometres to few micrometres, black carbon (BC), brown carbon (BrC) and organic aerosols (OAs) being its major components. BC and OAs are mainly in sub-micrometre particles, typically produced by pyrolysis in fossil fuel combustion (i.e. road traffic) and biomass burning processes. BC is a distinct type of carbonaceous material found in accumulation mode (particle diameter of 0.1-1 μ m) and ultrafine (diameter <100nm) particles that is formed primarily in flames and then directly emitted to the atmosphere, has a strong wavelength-independent visible light absorption, is refractory and insoluble in water (Bond et al., 2013). BC and BrC are carbonaceous aerosols in their chemical composition, but are named after their visual colour appearance: BC because it looks blackish, BrC because it looks brownish. Recent development of single-particle instruments capable of detecting BC (i.e., the single-particle soot photometer, SP2) has provided a method to obtain number size distributions and mixing state of refractory BC (rBC). These are however not fully resolved because of the narrow size detection limits (about 80-300 nm). No instrument allows measuring the ultrafine BC alone. This is why no reference method has been developed yet for measuring carbonaceous aerosol components.
Carbonaceous aerosols are likely to vary largely across the different regions in Europe (Kulmala et al., 2011; Alves et al., 2012; Querol et al., 2013). Although both road traffic and biomass burning from domestic heating contribute to increase primary carbonaceous components in European urban areas, both their emissions and processing may differ across Europe. In the Mediterranean basin, an area of particular sensitivity as far as air pollution and climate change are concerned (e.g., Lelieveld et al., 2002), carbonaceous aerosols levels are uncertain.

**Paper in preparation. Possible publication on October.*

Italian Mediterranean urban areas and Rome in particular, are therefore potential carbonaceous aerosol hot spots for Europe. Several studies have suggested a link between the carbonaceous aerosol and health effects (WHO, 2012; REVIHAAP report, WHO, 2013). There are evidences that ambient particulate matter (PM_{10} and $PM_{2,5}$) pollution poses severe risks to the human health (WHO 2013; Lim et al., 2012, US EPA, 2009). However, since PM_{10} is a heterogeneous mix of solid and liquid particles, the specific constituents that are responsible for these findings remain uncertain. As some of the organics are highly toxic and BC is present largely as solid insoluble ultrafine particles, carbonaceous aerosol could have a larger health impact than other PM_{10} constituents (Cassee et al., 2013; WHO 2013). In particular, BC effects on human health has been increasingly considered, either in its own right or as a carrier of other chemicals (WHO, 2013; Janssen et al. 2012; Shindell et al., 2012; UNEP-WMO, 2011; US National Academy of Sciences, 2004; CAFE, 2004; HEI, 2002). Despite the chemical composition, literature studies (WHO, 2013) indicate that physical properties (size, particle number and surface area) may play a role. Though yet limited, there is epidemiological evidence on the association between short-term exposures to ultrafine particles (no matter what the composition is) and cardiorespiratory health, as well as the health of the central nervous system (WHO, 2013). Finally, there is an increasing awareness that various PM components, and particularly ultrafine particles, induce pulmonary inflammation through the generation of oxidative stress [6]. In this paper, we present first results of carbonaceous aerosol measurements carried out in February 2017 in the downtown urban area of Rome. Spatially resolved measurements with high time resolution of Black and elemental carbon (EC), organic carbon (OC), water-soluble organic carbon (WSOC) and BrC, major components of nor-refractory PM_1 (NH_4^+, SO_4^{2-}, NO_3^-, Chl), and particle size distribution from 0.008 to 10 µm were carried out. The aim of this paper is to provide baseline levels of carbonaceous aerosols for the urban Mediterranean urban area of Rome reducing the assessment uncertainties of aerosol optical, chemical and microphysical properties, and to address future research directions. Thanks to this project, a robust dataset of optical–microphysical–chemical properties of the carbonaceous aerosol in the urban Mediterranean background area of Rome was collected, together with relevant data of human health exposure. Different techniques for measuring carbonaceous aerosol properties were coupled with the aim to improve data reliability. Number size distribution, composition, mass concentration, and wavelength-dependent optical properties of the bulk aerosol were measured at a fixed location in the downtown Rome with time resolution of minutes. Mobile measurements were carried out to assess the spatial gradients of BC particles near urban roadways and building surfaces, and the connections between these gradients and the atmospheric turbulence will be assessed through Computational fluid dynamics modelling (CFD).

Human cells were in-vitro exposed, relevant doses assessed, and the oxidative stress associated to particulate matter measured, to investigate the toxicity of the carbonaceous aerosol.

Materials and Methods

Measurement site

Measurements were carried out from 27 January to 28 February 2017 in downtown Rome. Measurement site is located in the center of Rome, into a garden, in between three last traffic roads 100-800 m far (41°52’52”N, 12°29’50”E). Figure 1 showed the maps of Rome and the monitoring areas located in an important traffic area.

Figure 1. : *Map of sampling sites in Rome.*

Major chemical component

Major chemical components were measured through different techniques: Aerodyne Aerosol Chemical Speciation Monitor (ACSM), EcoChem Photoelectric Aerosol Sensor (PAS) 2000, OCEC Carbon Aerosol Analyser, Sunset Laboratory, OR-USA and Particle into Liquid Sampler.

The Aerodyne Aerosol Chemical Speciation Monitor (ACSM) is a mass spectrometer capable of analysing in real-time, with a temporal resolution of 30 minutes, the non-refractory at 600 deg C component of the fine (<1 *m* m) particulate (NR-PM1) (Ng et al., 2011). The instrument analyses the mass spectrum of NR-PM1 by acquiring 100 different macromolecules (associated to pre-fixed mass-

to-charge, m/z), providing the measurement of the main organic and inorganic chemical components (Organic matter, OM; Ammonium, NH4; Sulfate, SO4; Nitrate, NO3; Chloride, Cl). The EcoChem Photoelectric Aerosol Sensor (PAS) 2000 is a real-time monitor that measures the surface-associated total polycyclic aromatic hydrocarbons (PAHs) concentration (Marr et al., 2004). The PAS 2000 works on the principle of the photoionization of the particle-bound PAHs: the fine particles on whose surface PAHs are adsorbed are ionized by UV radiation, the charged particles are collected on a filter element and the resulting piezoelectric current is measured and proportionally related to the particle-bound PAHs. The logged data in 5 min intervals (expressed as total PAH concentration in *m*g/m^3), were averaged over 30 min intervals for correlation with ACSM data.

OCEC Carbon Aerosol Analyser, Sunset Laboratory, OR-USA was used to determinate EC and OC on 24-h quartz fiber filters by thermo-optical analysis by applying the NIOSH-QUARTZ temperature protocol. Water-soluble organic carbon (WSOC) was also analysed on 24-h quartz fiber filters by TOC-VCSH (Shimadzu) by using the NPOC (non-purgeable organic carbon) procedure (Sanna Saarikosk at al., 2007). WSOC was determined by the Non-Purgeable Organic Carbon (NPOC) method, which measures non-volatile OC present in the sample Inorganic carbon (carbonates, hydrogen carbonates and dissolved carbon dioxide) In the NPOC method the samples was acidified with 1% acid (Timonen, et al., 2008). For the determination of levoglucosan, 24-h quartz fiber filters were extracted in de-ionized water and the solution analysed by high-performance anion-exchange chromatography with pulsed amperometric detection (HPAEC-PAD), using a DC ICS-3000 oven, a GP40 gradient pump, a CarboPac™ PA10 analytical and guard column and a Dionex ED50/ED50A electrochemical cell. The same analytical method was used for the analysis of the solutions collected by the particle-into-liquid sampler. A particle-into-liquid sampler (PILS) was used for on-line measurement of levoglucosan and oxidative potential. The air flow is denuded of gaseous species and aerosol particles are grown in a saturated water vapor chamber to form droplets that are collected by inertial impact on a collection plate that is washed by deionized water. The resulting solution was collected every 2 hours for subsequent analyses (Perrino et al. 2015). Oxidative potential (OP) was determined by the 2'7'-dichlorofluorescein (DCFH) essay (Hung and Wang, 2001).

First Results

Figure 2 showed the summary of the daily trends obtained from the organic component analysis (EC, OC, Levoglucosan and WSOC) during the monitoring campaign. It can be seen that the profiles have a similar trend profile, recording a maximum OC value on February 23 (about 12 μg/m^3). Finally, it

can be seen how the WSOC represents an important contribution to the organic components analyzed, about 20% of the OC. Further considerations will be made in future studies.

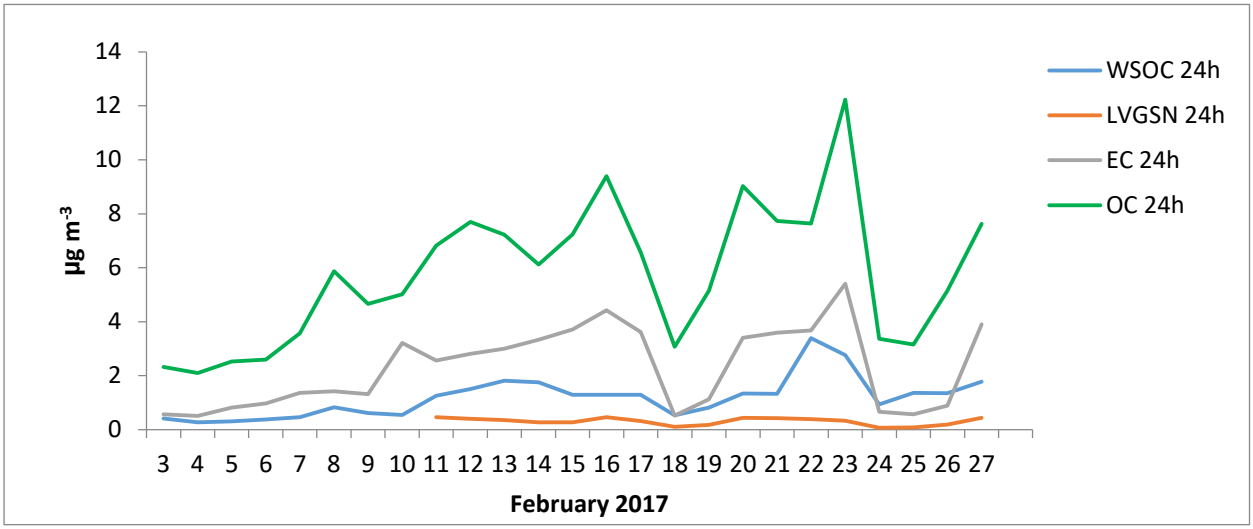

Figure 2: *Comparison of results obtained by the analysis of OC, EC, LVGSN and WSOC*

The further analysis in which I have been involved in this research project was the OP analysis in atmospheric particulate matter samples collected with high time resolution. In fact, samples collected with PILS, with a time resolution of 2h, were subsequent analysed by the 2'7'-dichlorofluorescein (DCFH) assay, one of the important assays, using in literature, as measures of the inherent capacity of PM to oxidize target molecules. In fact, in the last yeas several studies were focused on the analysis of this new alternative air quality exposure metric used in combination with PM mass concentrations analysis. OP analysis could be justify possible association of oxidative stress to the three different aerosol conditions found to have peculiar physicochemical properties of the carbonaceous aerosol. The premise for this exercise is the increasing awareness that carbonaceous aerosols may induce health effects through the generation of oxidative stress, e.g., (Li et al., 2003). Figure 9 presents the oxidative stress dependence on eBC mass concentration, OC mass concentration, BC-to-OC ratios, and particle size. In panel a data are coloured by the hours of day: red markers show case (i), blue markers show case (ii), and green markers show case (iii). In panel b, these cases are indicated by red, blue, and green colours, respectively.

It is evident that the aerosol occurring at the evening peak hour (case ii) does correspond to the lowest values of oxidative stress.

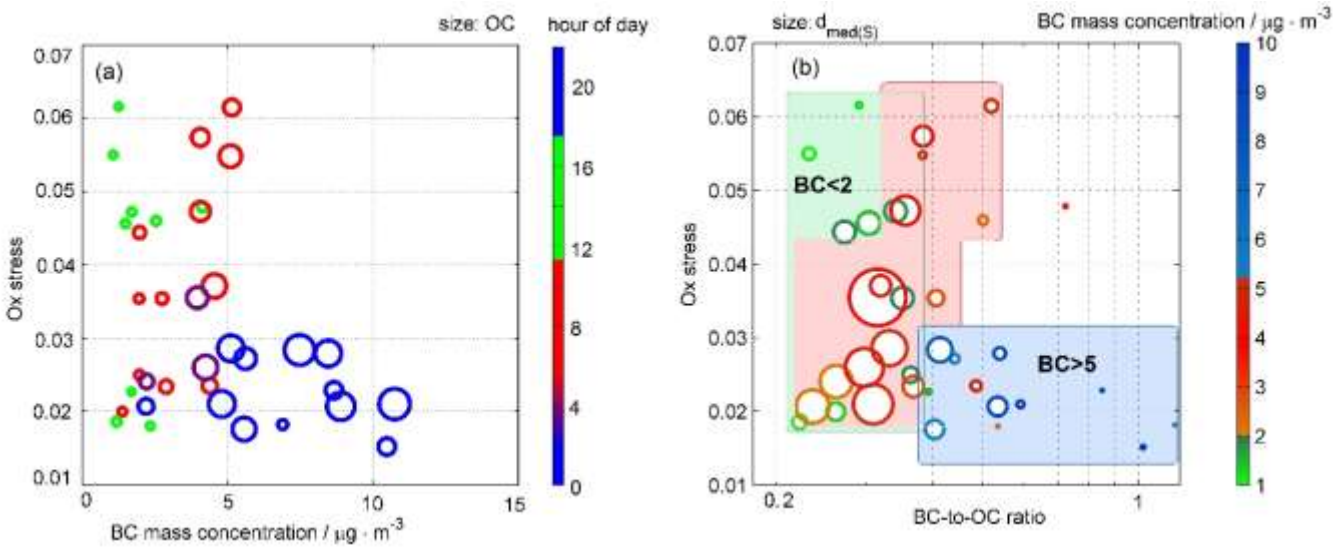

Figure 9. *Size-dependent oxidative stress.*

Data of case (i) and (ii) show a particle size-dependent oxidative stress - and a very weak dependence on the BC-to-OC ratios: the oxidative stress increases with decreasing aerosol diameter. Future research should better evaluate these relationships. Despite this is a very preliminary analysis, it is clear that possible aerosol health effects cannot be evaluated without a clear knowledge on particle size, composition and colour properly measured with high time resolution. The currently regulated aerosol metric cannot recognise some differences that may be however relevant for human health effects. It is clear that even with a proper time resolution (at least 2 hour instead of the currently regulated 24 hours) the PMx metric could in principle recognise only differences between low concentrations (case iii) and high concentrations (case i and ii), but cannot distinguish important properties in aerosol size, composition and colour separating traffic emissions (case i) from case ii, and influencing so differently human health.

Conclusion

It important to underline that the great amount of datas collected in this important project will need to an important interpretative work and will be the subject of further publications. However the first CARE experimental results, reported in this paper, indicate an urban background level of the eBC mass concentration in Rome in winter of 2.6-2.5 *m*g / m^3, which is comparable to that observed across other European cities, but larger - particularly at the rush hour when we observed a mean value of 5.2 (95%CI=5.0-5.5) *m*g /m^3. In fact, we found peculiar physicochemical properties of the carbonaceous aerosol at the rush hour, and speculated on relevant health effects. The premise for this exercise is the increasing awareness that carbonaceous aerosols may induce health effects through the generation of

oxidative stress. We observed a particle mass, size, and composition dependent relationship between eBC and the oxidative stress explaining significantly different values associated to road traffic and biomass burning aerosols. First findings of the CARE project therefore strongly indicate that the air quality legislation currently in effect in Europe (based on 24-h averaged PM10 and PM2.5) is not enough to assess aerosol health impact, and that future air quality legislation has to consider new metrics based on particle size, colour and composition measurements with a higher time resolution, in addition to particle mass.

References

Ayres, J. G., Borm, P., Cassee, F. R., Castranova, V., Donaldson, K., Ghio, A., Harrison, R.M., Hider, R., Kelly, F., Kooter, I.M., Maynard, R.L., Mudway, I., Nel, A., Sioutas, C., Smith, S., Baeza-Squiban, A., Cho, A, Duggan, S., Froines, J., & Marano, F. (2008). Evaluating the toxicity of airborne particulate matter and nanoparticles by measuring oxidative stress potential—a workshop report and consensus statement. *Inhalation toxicology*, 20(1), 75-99.

Alaghmand, M., & Blough, N. V. (2007). Source-dependent variation in hydroxyl radical production by airborne particulate matter. *Environmental science & technology*, 41(7), 2364-2370.

Alves, C., Vicente, A., Pio, C., Kiss, G., Hoffer, A., Decesari, S., Prevot A. S. H., Minguillon, M. C., Querol, X., Hillamo, R., Swietlicki E & Spindler, G. (2012). Organic compounds in aerosols from selected European sites–Biogenic versus anthropogenic sources. *Atmospheric Environment*, *59*, 243-255.

Amato, F., Pandolfi, M., Moreno, T., Furger, M., Pey, J., Alastuey, A., Bukowiecki, N., Prevot, A.S.H., Baltensperger, U., & Querol, X. (2011). Sources and variability of inhalable road dust particles in three European cities. *Atmospheric Environment*, *45*(37), 6777-6787.

Aust, A. E., Ball, J. C., Hu, A. A., Lighty, J. S., Smith, K. R., Straccia, A. M., Veranth, J.M., & Young, W. C. (2002). Particle characteristics responsible for effects on human lung epithelial cells. *Research Report (Health Effects Institute)*, 110, 1-65.

Barry, R. G., & Chorley, R. J. (1992). *Atmosphere, weather and climate*. 6th ed. Routledge, London.

Bond, T. C., Doherty, S. J., Fahey, D. W., Forster, P. M., Berntsen, T., DeAngelo, B. J., Flanner, M. G., Ghan,S., Kärcher, B., Koch, D., Kondo, Y., Quinn, P. K., Sarofim, M. C., Schultz, M. G., Schulz, M., Venkataraman, C., Zhang, H., Zhang, S., Bellouin, N., Guttikunda, S. K., Hopke, P. K., Jacobson, M. Z., Kaiser, J.W., Klimont, Z., Lohmann, U., Schwarz, J. P., Shindell, D., Storelvmo, T.,Warren, S. G., and Zender, C. S.,& Kinne, S. (2013). Bounding the role of black carbon in the climate system: A scientific assessment. *Journal of Geophysical Research: Atmospheres*, *118*(11), 5380-5552.

Boogaard, H., Janssen, N. A., Fischer, P. H., Kos, G. P., Weijers, E. P., Cassee, F. R., Van der Zee, S. C., De Hartog, J. J., Brunekreef, B., & Hoek, G. (2012). Contrasts in oxidative potential and other particulate matter characteristics collected near major streets and background locations. *Environmental health perspectives*, *120*(2), 185.

Borm, P. J., Kelly, F., Künzli, N., Schins, R. P., & Donaldson, K. (2007). Oxidant generation by particulate matter: from biologically effective dose to a promising, novel metric. *Occupational and environmental medicine*, 64(2), 73-74.

Brereton, R.G. (1990). Chemometrics: application of mathematics and statistics to laboratory systems. Chichester, UK, Ellis Horwood.

Brook, R.D.; Rajagopalan, S.; Pope, C.A.; Brook, J.R.; Bhatnagar, A.; Diez-Roux, A.V.; Holguin, F.; Hong, Y.; Luepker, R.V.; Mittleman, M.; Peters, A.; Siscovick, D.; Smith, S.C.; Whitsel, L.; Kaufman, J.D.; (2010). Particulate matter air pollution and cardiovascular disease. *Circulation,* 121(21), 2331-2378.

Brunekreef, B., & Holgate, S. T. (2002). Air pollution and health. *The lancet*, 360(9341), 1233-1242.

Brunekreef, B., & Forsberg, B. (2005). Epidemiological evidence of effects of coarse airborne particles on health. *European Respiratory Journal*, 26(2), 309-318.

Burnett, R. T., Cakmak, S., Brook, J. R., & Krewski, D. (1997). The role of particulate size and chemistry in the association between summertime ambient air pollution and hospitalization for cardiorespiratory diseases. *Environmental health perspectives*, 105(6), 614.

Burnett, R. T., Smith-Doiron, M., Stieb, D., Cakmak, S., & Brook, J. R. (1999). Effects of particulate and gaseous air pollution on cardiorespiratory hospitalizations. *Archives of Environmental Health: An International Journal*, 54(2), 130-139.

Canepari, S., Cardarelli, E., Pietrodangelo, A. & Strincone, M. (2006b). Determination of Metals, Metalloids and Non-Volatile Ions in Airborne Particulate Matter by a New Two-Step Sequential Leaching Procedure. Part B: Validation on Real Equivalent Samples. *Talanta* 69: 588–595.

Canepari, S., Perrino, C., Olivieri, F., & Astolfi, M. L. (2008). Characterisation of the traffic sources of PM through size-segregated sampling, sequential leaching and ICP analysis. *Atmospheric Environment*, 42(35), 8161-8175.

Canepari, S., Perrino, C., Astolfi, M. L., Catrambone, M., & Perret, D. (2009). Determination of soluble ions and elements in ambient air suspended particulate matter: inter-technique comparison of XRF, IC and ICP for sample-by-sample quality control. *Talanta*, 77(5), 1821-1829.

Canepari, S., Pietrodangelo, A., Perrino, C., Astolfi, M. L., & Marzo, M. L. (2009). Enhancement of source traceability of atmospheric PM by elemental chemical fractionation. *Atmospheric Environment*, 43(31), 4754-4765.

Canepari, S., Marconi, E., Astolfi, M. L., & Perrino, C. (2010). Relevance of Sb (III), Sb (V), and Sb-containing nano-particles in urban atmospheric particulate matter. *Analytical and bioanalytical chemistry*, 397(6), 2533-2542.

Canepari, S., Astolfi, M. L., Farao, C., Maretto, M., Frasca, D., Marcoccia, M., & Perrino, C. (2014). Seasonal variations in the chemical composition of particulate matter: a case study in the Po Valley. Part II: concentration and solubility of micro-and trace-elements. *Environmental Science and Pollution Research*, 21(6), 4010-4022.

Caserini, S., Giani, P., Cacciamani, C., Ozgen, S., & Lonati, G. (2017). Influence of climate change on the frequency of daytime temperature inversions and stagnation events in the Po Valley: historical trend and future projections. *Atmospheric Research*, *184*, 15-23.

Cassee, F. R., Héroux, M. E., Gerlofs-Nijland, M. E., & Kelly, F. J. (2013). Particulate matter beyond mass: recent health evidence on the role of fractions, chemical constituents and sources of emission. *Inhalation toxicology*, *25*(14), 802-812.

Cathcart, R., Schwiers, E., & Ames, B. N. (1983). Detection of picomole levels of hydroperoxides using a fluorescent dichlorofluorescein assay. *Analytical biochemistry*, 134(1), 111-116.

Charrier, J. G., & Anastasio, C. (2012). On dithiothreitol (DTT) as a measure of oxidative potential for ambient particles: evidence for the importance of soluble transition metals. *Atmospheric chemistry and physics*, 12(5), 11317.

Chen, Y., Yang, Q., Krewski, D., Shi, Y., Burnett, R. T., & McGrail, K. (2004). Influence of relatively low level of particulate air pollution on hospitalization for COPD in elderly people. *Inhalation toxicology*, 16(1), 21-25.

Chen, C. Y., Misztal, I., Aguilar, I., Legarra, A., & Muir, W. M. (2011). Effect of different genomic relationship matrices on accuracy and scale. *Journal of Animal Science*, *89*(9), 2673-2679

Chen, R., Li, Y., Ma, Y., Pan, G., Zeng, G., Xu, X., Chen, B., & Kan, H. (2011). Coarse particles and mortality in three Chinese cities: the China Air Pollution and Health Effects Study (CAPES). *Science of the Total Environment*, *409*(23), 4934-4938.

Cheung, K., Shafer, M. M., Schauer, J. J., & Sioutas, C. (2012). Diurnal trends in oxidative potential of coarse particulate matter in the Los Angeles Basin and their relation to sources and chemical composition. *Environmental science & technology*, 46(7), 3779-3787.

Chirizzi, D., Cesari, D., Guascito, M. R., Dinoi, A., Giotta, L., Donateo, A., & Contini, D. (2017). Influence of Saharan dust outbreaks and carbon content on oxidative potential of water-soluble fractions of PM 2.5 and PM 10. *Atmospheric Environment*, 163, 1-8.

Cho, A. K., Sioutas, C., Miguel, A. H., Kumagai, Y., Schmitz, D. A., Singh, M., Fernandez, F.A., & Froines, J. R. (2005). Redox activity of airborne particulate matter at different sites in the Los Angeles Basin. *Environmental Research*, 99(1), 40-47.

Cho, S. H., Tong, H., McGee, J. K., Baldauf, R. W., Krantz, Q. T., & Gilmour, M. I. (2009). Comparative toxicity of size-fractionated airborne particulate matter collected at different distances from an urban highway. *Environmental health perspectives*, *117*(11), 1682.

Conti, M.E., Iacobucci, M., & Cecchetti, G.(2005). A statistical approach applied to trace metal data from biomonitoring studies. *International Journal of Environment and Pollution,* 23(1), 29–41.

Conti, M.E., Iacobucci, M., Cucina, D., & Mecozzi, M. (2007). Multivariate statistical methods applied to biomonitoring studies. *International Journal of Environment and Pollution*, 29(1–3), 333–343.

Conti, M.E., Bocca, B., Iacobucci, M., Finoia, M.G., Mecozzi, M., Pino, A., & Alimonti, A. (2010). Baseline trace metals in seagrass, algae and molluscs in a southern Tyrrhenian cosystem (Linosa Island, Sicily). *Archives of Environmental Contamination an Toxicology. 58,79–95.*

De Oliveira Alves, N., Loureiro, A. L. M., dos Santos, F. C., Nascimento, K. H., Dallacort, R., de Castro Vasconcellos, P., ... & de Medeiros, S. R. B. (2011). Genotoxicity and composition of particulate matter from biomass burning in the eastern Brazilian Amazon region. *Ecotoxicology and environmental safety*, 74(5), 1427-1433.

Di Giovine, M., Canofani, A., Colombari, F., & Donato, E. (2000). Relazione sullo stato dell'ambiente; qualità dell'aria a Roma.

DiStefano, E., Eiguren-Fernandez, A., Delfino, R. J., Sioutas, C., Froines, J. R., & Cho, A. K. (2009). Determination of metal-based hydroxyl radical generating capacity of ambient and diesel exhaust particles. *Inhalation toxicology*, 21(9), 731-738.

Di Menno Di Bucchianico A, Catrambone M, Perrino C, Passariello B, Quaresima S (2002), La valutazione del materiale particellare alla luce del DM 2/4/2002, Marina di Carrara 11/10/2002, Eventi di trasporto di sabbie sahariane nell'Italia centrale.

Dockery, D. W., Pope, C. A., Xu, X., Spengler, J. D., Ware, J. H., Fay, M. E., Ferris B.G. Jr., & Speizer, F. E. (1993). An association between air pollution and mortality in six US cities. *New England journal of medicine*, 329(24), 1753-1759.

Donaldson, K., Stone, V., Seaton, A., & MacNee, W. (2001). Ambient particle inhalation and the cardiovascular system: potential mechanisms. *Environmental health perspectives*, 109(Suppl 4), 523.

Donaldson, K.; Stone, V.; Borm, P.J.; Jimenez, L.A.; Gilmour, P.S.; Schins, R.P.; , Knaapen; A.M.; Rahman, I.; Faux, S.P.; Brown, D.M.; MacNee, W.. (2003). Oxidative stress and calcium signaling in the adverse effects of environmental particles (PM 10). *Free Radical Biology and Medicine*, 34(11), 1369-1382.

Dray, S., Dufour, A.B., & Chessel, D. (2007). The ade4 package-II: Two-table and K-table methods. R News. 7(2), 47-52.

Fang, T., Verma, V., Bates, J. T., Abrams, J., Klein, M., Strickland, M. J., Sarnat, S. E., Chang, H. H., Mulholland, J. A., Tolbert, P. E. & Russell, A. G. (2015). Oxidative potential of ambient water-soluble PM 2.5 measured by Dithiothreitol (DTT) and Ascorbic Acid (AA) assays in the southeastern United States: contrasts in sources and health associations. *Atmospheric Chemistry & Physics Discussions*, *15*(21) 30609-30644.

Fang, T; Verma, V.; Bates, J. T.; Abrams, J.; Klein, M.; Strickland, M.J.; Sarnat, S.E.; Chang , H.H.; Mulholland, J.A; Tolbert, P.E.; Russell, A.G.;& Weber R.J (2016). Oxidative potential of ambient water-soluble PM 2.5 in the southeastern United States: contrasts in sources and health associations between ascorbic acid (AA) and dithiothreitol (DTT) assays. Atmospheric Chemistry and Physics, 16(6), 3865-3879.

Fang, T., Zeng, L., Gao, D., Verma, V., Stefaniak, A. B., & Weber, R. J. (2017). Ambient Size Distributions and Lung Deposition of Aerosol Dithiothreitol-Measured Oxidative Potential: A Contrast Between Soluble and Insoluble Particles. Environmental Science & Technology.

Falissard, B. (1999). Focused Principal Components Analysis: looking at a correlation matrix with a particular interest in a given variable. *Journal of Computational and Graphical Statistics*, 8(4), 906-912.

Falissard, B. (2012). psy: Various procedures used in psychometry. R package version 1.1. http://CRAN.R-project.org/package=psy.

Goodarzi, F., & Huggins, F. E. (2001). Monitoring the species of arsenic, chromium and nickel in milled coal, bottom ash and fly ash from a pulverized coal-fired power plant in western CanadaPresented at the Whistler 2000 Speciation Symposium, Whistler Resort, BC, Canada, June 25–July 1, 2000. Geological Survey of Canada (GSC) Contribution No. 2000113. *Journal of Environmental Monitoring*, 3(1), 1-6.

Goudie, A. S. (2014). Desert dust and human health disorders. *Environment international*, 63, 101-113.

Halliwell, B., & Whiteman, M. (2004). Measuring reactive species and oxidative damage in vivo and in cell culture: how should you do it and what do the results mean?. *British journal of pharmacology*, 142(2), 231-255.

Harrison, R. M., Jones, A. M., & Lawrence, R. G. (2003). A pragmatic mass closure model for airborne particulate matter at urban background and roadside sites. *Atmospheric Environment*, *37*(35), 4927-4933.

Hasson, A. S., & Paulson, S. E. (2003). An investigation of the relationship between gas-phase and aerosol-borne hydroperoxides in urban air. *Journal of Aerosol Science*, 34(4), 459-468.

Hlavay, J., Polyak, K., & Weisz, M. (2001). Monitoring of the natural environment by chemical speciation of elements in aerosol and sediment samplesPresented at the Whistler 2000 Speciation Symposium, Whistler Resort, BC, Canada, June 25–July 1, 2000. *Journal of Environmental Monitoring*, 3(1), 74-80.

Hoek, G., Krishnan, R. M., Beelen, R., Peters, A., Ostro, B., Brunekreef, B., & Kaufman, J. D. (2013). Long-term air pollution exposure and cardio-respiratory mortality: a review. *Environmental Health*, 12(1), 43.

Host, S., Larrieu, S., Pascal, L., Blanchard, M., Declercq, C., Fabre, P., Jusot, J.F., Chardon, B., Le Tertre, A., Wagner, V., Lefranc, A., & Prouvost, H. (2008). Short-term associations between fine and coarse particles and hospital admissions for cardiorespiratory diseases in six French cities. *Occupational and Environmental Medicine*, *65*(8), 544-551

Hu, S., Polidori, A., Arhami, M., Shafer, M. M., Schauer, J. J., Cho, A., & Sioutas, C. (2008). Redox activity and chemical speciation of size fractioned PM in the communities of the Los Angeles-Long Beach harbor. *Atmospheric Chemistry and Physics*, *8*(21), 6439-6451.

Huang, M. F., Lin, W. L., & Ma, Y. C. (2005). A study of reactive oxygen species in mainstream of cigarette. *Indoor air*, 15(2), 135-140.

Huang, W., Zhang, Y., Zhang, Y., Fang, D., & Schauer, J. J. (2016). Optimization of the Measurement of Particle-Bound Reactive Oxygen Species with 2′, 7′-dichlorofluorescin (DCFH). *Water, Air, & Soil Pollution*, 227(5), 164.

Hung, H. F., & Wang, C. S. (2001). Experimental determination of reactive oxygen species in Taipei aerosols. *Journal of Aerosol Science*, 32(10), 1201-1211.

Janssen, N. A., Hoek, G., Simic-Lawson, M., Fischer, P., Van Bree, L., Ten Brink, H., Keuken, M., Atkinson, R.W., Anderson, H.R., Brunekreef, B., & Cassee, F. R. (2011). Black carbon as an additional indicator of the adverse health effects of airborne particles compared with PM10 and PM2. 5. *Environmental health perspectives*, *119*(12), 1691.

Janssen, N. A., Yang, A., Strak, M., Steenhof, M., Hellack, B., Gerlofs-Nijland, M. E., Kuhlbusch T., Kelly, F., Harrison R., Brunekreef, B., Flemming Cassee & Hoek, G. (2014). Oxidative potential of particulate matter collected at sites with different source characteristics. *Science of the Total Environment*, 472, 572-581.

Kelly, F. J., & Fussell, J. C. (2012). Size, source and chemical composition as determinants of toxicity attributable to ambient particulate matter. *Atmospheric environment*, 60, 504-526.

Keston, A. S., & Brandt, R. (1965). The fluorometric analysis of ultramicro quantities of hydrogen peroxide. *Analytical biochemistry*, 11(1), 1-5.

Knaapen, A. M., Shi, T., Borm, P. J., & Schins, R. P. (2002). Soluble metals as well as the insoluble particle fraction are involved in cellular DNA damage induced by particulate matter. *Molecular and Cellular Biochemistry*, 234(1), 317-326.

Kumagai, Y., Koide, S., Taguchi, K., Endo, A., Nakai, Y., Yoshikawa, T., & Shimojo, N. (2002). Oxidation of proximal protein sulfhydryls by phenanthraquinone, a component of diesel exhaust particles. *Chemical research in toxicology*, 15(4), 483-489.

Kulmala, M., Asmi, A., Lappalainen, H. K., Baltensperger, U., Brenguier, J.-L., Facchini, M. C., Hansson, H.-C., Hov, Ø., O'Dowd, C. D., Pöschl, U., Wiedensohler, A., Boers, R., Boucher, O., de Leeuw, G., Denier van der Gon, H. A. C., Feichter, J., Krejci, R., Laj, P., Lihavainen, H., Lohmann, U., McFiggans, G., Mentel, T., Pilinis, C., Riipinen, I., Schulz, M., Stohl, A., Swietlicki, E., Vignati, E., Alves, C., Amann, M., Ammann, M., Arabas, S., Artaxo, P., Baars, H., Beddows, D. C. S., Bergström, R., Beukes, J. P., Bilde, M., Burkhart, J. F., Canonaco, F., Clegg, S. L., Coe, H., Crumeyrolle, S., D'Anna, B., Decesari, S., Gilardoni, S., Fischer, M., Fjaeraa, A. M., Fountoukis, C., George, C., Gomes, L., Halloran, P., Hamburger, T., Harrison, R. M., Herrmann, H., Hoffmann, T., Hoose, C., Hu, M., Hyvärinen, A., Hõrrak, U., Iinuma, Y., Iversen, T., Josipovic, M., Kanakidou, M., Kiendler-Scharr, A., Kirkevåg, A., Kiss, G., Klimont, Z., Kolmonen, P., Komppula, M., Kristjánsson, J.-E., Laakso, L., Laaksonen, A., Labonnote, L., Lanz, V. A., Lehtinen, K. E. J., Rizzo, L. V., Makkonen, R., Manninen, H. E., McMeeking, G., Merikanto, J., Minikin, A., Mirme, S., Morgan, W. T., Nemitz, E., O'Donnell, D., Panwar, T. S., Pawlowska, H., Petzold, A., Pienaar, J. J., Pio, C., Plass-Duelmer, C., Prévôt, A. S. H., Pryor, S., Reddington, C. L., Roberts, G., Rosenfeld, D., Schwarz, J., Seland, Ø., Sellegri, K., Shen, X. J., Shiraiwa, M., Siebert, H., Sierau, B., Simpson, D., Sun, J. Y., Topping, D., Tunved, P., Vaattovaara, P., Vakkari, V., Veefkind, J. P., Visschedijk, A., Vuollekoski, H., Vuolo, R., Wehner, B., Wildt, J., Woodward, S., Worsnop, D. R., van Zadelhoff, G.-J., Zardini, A. A., Zhang, K., van Zyl, P. G., Kerminen, V.-M., S Carslaw, K., and Pandis, S. N. (2011). General overview: European Integrated project on Aerosol Cloud Climate and Air Quality interactions (EUCAARI) – integrating aerosol research from nano to global scales, *Atmospheric Chemistry and Physics*, 11, 13061-13143, https://doi.org/10.5194/acp-11-13061-2011.

Landreman, A. P., Shafer, M. M., Hemming, J. C., Hannigan, M. P., & Schauer, J. J. (2008). A macrophage-based method for the assessment of the reactive oxygen species (ROS) activity of atmospheric particulate matter (PM) and application to routine (daily-24 h) aerosol monitoring studies. *Aerosol Science and Technology*, 42(11), 946-957.

LeBel, C. P., Ischiropoulos, H., & Bondy, S. C. (1992). Evaluation of the probe 2', 7'-dichlorofluorescin as an indicator of reactive oxygen species formation and oxidative stress. *Chemical research in toxicology*, 5(2), 227-231.

Lelieveld, J., Berresheim, H., Borrmann, S., Crutzen, P. J., Dentener, F. J., Fischer, H., ... & Korrmann, R. Feichter, J., Flatau, P. J., Heland, J., Holzinger, R., Korrmann, R., Lawrence, M. G., Levin, Z., Markowicz, K. M., Mihalopoulos, N., Minikin, A., Ramanathan, V., de Reus, M., Roelofs, G. J., Scheeren, H. A., Sciare, J., Schlager, H., Schultz, M., Siegmund, P., Steil, B., Stephanou, E.G., Stier, P., Traub,M.,Warneke, C.,Williams, J., and Ziereis, H. (2002). Global air pollution crossroads over the Mediterranean. *Science*, *298*(5594),

Li, N., Sioutas, C., Cho, A., Schmitz, D., Misra, C., Sempf, J., Wang M, Oberley T, Froines J, & Nel, A. (2003). Ultrafine particulate pollutants induce oxidative stress and mitochondrial damage. *Environmental health perspectives*, *111*(4), 455.

Lim, S. S., Vos, T., Flaxman, A. D., Danaei, G., Shibuya, K., Adair-Rohani, H., & Aryee, M. (2012). A comparative risk assessment of burden of disease and injury attributable to 67 risk factors and risk factor clusters in 21 regions, 1990–2010: a systematic analysis for the Global Burden of Disease Study 2010. *The lancet*, *380*(9859), 2224-2260.

Lin, M., Stieb, D. M., & Chen, Y. (2005). Coarse particulate matter and hospitalization for respiratory infections in children younger than 15 years in Toronto: a case-crossover analysis. *Pediatrics*, 116(2), e235-e240.

Mahowald, N., Albani, S., Kok, J. F., Engelstaeder, S., Scanza, R., Ward, D. S., & Flanner, M. G. (2014). The size distribution of desert dust aerosols and its impact on the Earth system. *Aeolian Research*, *15*, 53-71.

Malig, B. J., & Ostro, B. D. (2009). Coarse particles and mortality: evidence from a multi-city study in California. *Occupational and environmental medicine*, *66*(12), 832-839.

Manahan (2000), Chimica dell'ambiente, Editor: L Zoccolillo, Chapter 10, PICCIN.

Marcoccia, M., Ronci, L., De Matthaeis, E., Setini, A., Perrino, C., & Canepari, S. (2017). In-vivo assesment of the genotoxic and oxidative stress effects of particulate matter on Echinogammarus veneris. *Chemosphere*, 173, 124-134.

Mark, D., (1999), *Atmospheric Aerosol Sampling* in: Harrison R M and. Van Grieken R E, *Atmospheric Particles* Vol 5.

Marr, L. C., Grogan, L. A., Wöhrnschimmel, H., Molina, L. T., Molina, M. J., Smith, T. J., & Garshick, E. (2004). Vehicle traffic as a source of particulate polycyclic aromatic hydrocarbon exposure in the Mexico City metropolitan area. *Environmental science & technology*, *38*(9), 2584-2592.

Mates, J. M., Pérez-Gómez, C., & De Castro, I. N. (1999). Antioxidant enzymes and human diseases. *Clinical biochemistry*, 32(8), 595-603.

Miljevic, B., Fairfull-Smith, K. E., Bottle, S. E., & Ristovski, Z. D. (2010). The application of profluorescent nitroxides to detect reactive oxygen species derived from combustion-generated particulate matter: Cigarette smoke–A case study. *Atmospheric Environment*, 44(18), 2224-2230.

Miljevic, B., Hedayat, F., Stevanovic, S., Fairfull-Smith, K. E., Bottle, S. E., & Ristovski, Z. D. (2014). To sonicate or not to sonicate PM filters: reactive oxygen species generation upon ultrasonic irradiation. *Aerosol Science and Technology*, 48(12), 1276-1284.

Miravet, R., López-Sánchez, J. F., Rubio, R., Smichowski, P., & Polla, G. (2007). Speciation analysis of antimony in extracts of size-classified volcanic ash by HPLC–ICP-MS. *Analytical and bioanalytical chemistry*, *387*(5), 1949-1954.

Mirowsky, J., Hickey, C., Horton, L., Blaustein, M., Galdanes, K., Peltier, R. E., Lippmann, M., Chillrud, S., Chen, L.C., Ross, J., Nadas, A., & Gordon, T. (2013). The effect of particle size, location and season on the toxicity of urban and rural particulate matter. *Inhalation toxicology*, *25*(13), 747-757.

Miyazaki, Y.; Kondo, Y.; Shiraiwa, M.; Takegawa, N.; Miyakawa, T.; Han, S.; Kita, K.; Hu, M.; Deng, Z.Q.; Zhao, Y.; Sugimoto, N.; Blake, D.R.; Weber R. J.; . (2009). Chemical characterization of water-soluble organic carbon aerosols at a rural site in the Pearl River Delta, China, in the summer of 2006. *Journal of Geophysical Research: Atmospheres*, *114*(D14).

Morselli, L. (Ed.). (1991). Deposizioni acide: i precursori, l'interazione con l'ambiente ei materiali. Maggioli.

Mudway, I. S., Stenfors, N., Duggan, S. T., Roxborough, H., Zielinski, H., Marklund, S. L., Blomberg, A., Frew, A.J, Sandström, T.,& Kelly, F. J. (2004). An in vitro and in vivo investigation of the effects of diesel exhaust on human airway lining fluid antioxidants. *Archives of Biochemistry and Biophysics*, 423(1), 200-212.

Nel, A. (2005). Air pollution-related illness: effects of particles. *Science*, 308(5723), 804-806.

Ng, N. L., Herndon, S. C., Trimborn, A., Canagaratna, M. R., Croteau, P. L., Onasch, T. B., & Jayne, J. T. (2011). An Aerosol Chemical Speciation Monitor (ACSM) for routine monitoring of the composition and mass concentrations of ambient aerosol. *Aerosol Science and Technology*, *45*(7), 780-794.

Nirel, P. M., Pomian-Srzednicki, I., Meyer, M., & Filella, M. (2008). Dissolved antimony concentrations in contrasted watersheds: the importance of lithogenic origin. *Journal of Environmental Monitoring*, *10*(2), 256-260

Ning, L.; Sioutas, C.; Cho, A.; Schmitz, D.; Misra, C.; Meiying Wang, J.S.; Oberley, T.; Froines, J.; Nel A. (2003). Ultrafine particulate pollutants induce oxidative stress and mitochondrial damage. *Environmental health perspectives*, *111*(4), 455.

Ntziachristos, L., Froines, J. R., Cho, A. K., & Sioutas, C. (2007). Relationship between redox activity and chemical speciation of size-fractionated particulate matter. *Particle and fibre toxicology*, 4(1), 5.

Oberdörster, G. (2000). Pulmonary effects of inhaled ultrafine particles. *International archives of occupational and environmental health*, *74*(1), 1-8.

Ostro, B., Roth, L., Malig, B., & Marty, M. (2009). The effects of fine particle components on respiratory hospital admissions in children. *Environmental Health Perspectives*, *117*(3), 475.

Pant, P., & Harrison, R. M. (2013). Estimation of the contribution of road traffic emissions to particulate matter concentrations from field measurements: a review. *Atmospheric Environment*, 77, 78-97.

Peng, R. D., Chang, H. H., Bell, M. L., McDermott, A., Zeger, S. L., Samet, J. M., & Dominici, F. (2008). Coarse particulate matter air pollution and hospital admissions for cardiovascular and respiratory diseases among Medicare patients. *Jama*, *299*(18), 2172-2179.

Perrino, C., Catrambone, M., & Pietrodangelo, A. (2008). Influence of atmospheric stability on the mass concentration and chemical composition of atmospheric particles: a case study in Rome, Italy. *Environment international*, 34(5), 621-628.

Perrino, C., Canepari, S., Catrambone, M., Dalla Torre, S., Rantica, E., & Sargolini, T. (2009). Influence of natural events on the concentration and composition of atmospheric particulate matter. *Atmospheric Environment*, 43(31), 4766-4779.

Perrino, C., Catrambone, M., Dalla Torre, S., Rantica, E., Sargolini, T., & Canepari, S. (2014). Seasonal variations in the chemical composition of particulate matter: a case study in the Po Valley. Part I: macro-components and mass closure. *Environmental Science and Pollution Research*, *21*(6), 3999-4009

Perrone, M. G., Zhou, J., Malandrino, M., Sangiorgi, G., Rizzi, C., Ferrero, L., Dommen, J. & Bolzacchini, E. (2016). PM chemical composition and oxidative potential of the soluble fraction of particles at two sites in the urban area of Milan, Northern Italy. *Atmospheric Environment*, 128, 104-113.

Pietrodangelo, A., Salzano, R., Rantica, E., & Perrino, C. (2013). Characterisation of the local topsoil contribution to airborne particulate matter in the area of Rome (Italy). Source profiles. *Atmospheric environment*, 69, 1-14.

.Pi, J. B., Kumagai, Y., Yamauchi, H., Nikaido, M., Horikuchi, S., Sun, Y., & Shimojo, N. (2001, June). A possible mechanism for nitric oxide dysfunction induced by prolonged arsenic exposure. In *China Fluoride and Arsenic Society 2nd Conference on Flouride and Arsenic Research* (pp. 2-5).

Pope III, C. A., Burnett, R. T., Thun, M. J., Calle, E. E., Krewski, D., Ito, K., & Thurston, G. D. (2002). Lung cancer, cardiopulmonary mortality, and long-term exposure to fine particulate air pollution. *Jama*, *287*(9), 1132-1141.

Pope, C. A., Burnett, R. T., Thurston, G. D., Thun, M. J., Calle, E. E., Krewski, D., & Godleski, J. J. (2004). Cardiovascular mortality and long-term exposure to particulate air pollution. *Circulation*, *109*(1), 71-77.

Protano, C., Astolfi, M. L., Canepari, S., & Vitali, M. (2016). Urinary levels of trace elements among primary school-aged children from Italy: The contribution of smoking habits of family members. *Science of the Total Environment*, *557*, 378-385.

Puett, R,C., Hard, J,E,, Yanosky, J.D., Paciorek, C., Schwartz, J., Suh, H., Speizer, F.E., & Laden, F. (2009). Chronic fine and coarse particulate exposure, mortality, and coronary heart disease in the Nurses' Health Study. *Environmental Health Perspectives*, 117,1697–701.

Querol, X., Alastuey, A., Viana, M., Moreno, T., Reche, C., Minguillón, M. C., Ripoll, A., Pandolfi, M., Amato, F., Karanasiou, A., Pey, J., Cusack, M., Vázquez, R., Plana, F., Dall'Osto, M., de la Rosa, J., Sánchez de la Campa, A., Fernández-Camacho, R., Rodríguez, S., Pio, C., Alados-Arboledas, L., Titos, G. and Artíñano, B. and Salvador, P., García Dos Santos, S., Fernández Patier, R., & Pérez, N. (2013). Variability of carbonaceous aerosols in remote, rural, urban and industrial environments in Spain: implications for air quality policy. *Atmospheric Chemistry and Physics*, *13*(13), 6185-6206.

Ramana, M. V., Ramanathan, V., Feng, Y., Yoon, S. C., Kim, S. W., Carmichael, G. R., & Schauer, J. J. (2010). Warming influenced by the ratio of black carbon to sulphate and the black-carbon source. *Nature Geoscience*, *3*(8), 542.

Reche, C., Viana, M., Amato, F., Alastuey, A., Moreno, T., Hillamo, R., Teinilä, K.; Saarnio, K.; Seco R.; Peñuelas J.; Mohr C.; Prévôt A.S., Querol X. (2012). Biomass burning contributions to urban aerosols in a coastal Mediterranean City. *Science of the Total Environment*, 427, 175-190.

Ricci, P. F., & Cirillo, M. C. (1985). Uncertainty in health risk analysis. *Journal of hazardous materials*, 10(2-3), 433-447.

Saarikoski, S., Sillanpää, M., Sofiev, M., Timonen, H., Saarnio, K., Teinilä, K., Karppinen, A.; Kukkonen, J., Hillamo R. (2007). Chemical composition of aerosols during a major biomass burning episode over northern Europe in spring 2006: Experimental and modelling assessments. *Atmospheric Environment*, 41(17), 3577-3589.

Sarnat, S. E., Klein, M., Sarnat, J. A., Flanders, W. D., Waller, L. A., Mulholland, J. A., Russell, A.G., & Tolbert, P. E. (2010). An examination of exposure measurement error from air pollutant spatial variability in time-series studies. *Journal of exposure science & environmental epidemiology*, *20*(2), 135.

Sauvain, J. J., Rossi, M. J., & Riediker, M. (2013). Comparison of three acellular tests for assessing the oxidation potential of nanomaterials. *Aerosol Science and Technology*, 47(2), 218-227.

Schwarze, P. E., Øvrevik, J., Låg, M., Refsnes, M., Nafstad, P., Hetland, R. B., & Dybing, E. (2006). Particulate matter properties and health effects: consistency of epidemiological and toxicological studies. *Human & experimental toxicology*, 25(10), 559-579.

See, S. W., Wang, Y. H., & Balasubramanian, R. (2007). Contrasting reactive oxygen species and transition metal concentrations in combustion aerosols. *Environmental Research*, 103(3), 317-324.

Shafer, M. M., Hemming, J. D., Antkiewicz, D. S., & Schauer, J. J. (2016). Oxidative potential of size-fractionated atmospheric aerosol in urban and rural sites across Europe. *Faraday discussions*, *189*, 381-405.

Sheesley, R. J., Schauer, J. J., Chowdhury, Z., Cass, G. R., & Simoneit, B. R. (2003). Characterization of organic aerosols emitted from the combustion of biomass indigenous to South Asia. *Journal of Geophysical Research: Atmospheres*, 108(D9).

Sheppard, L., Levy, D., Norris, G., Larson, T. V., & Koenig, J. Q. (1999). Effects of ambient air pollution on nonelderly asthma hospital admissions in Seattle, Washington, 1987-1994. *Epidemiology*, 23-30.

Shi, T., Knaapen, A. M., Begerow, J., Birmili, W., Borm, P. J. A., & Schins, R. P. F. (2003). Temporal variation of hydroxyl radical generation and 8-hydroxy-2′-deoxyguanosine formation by coarse and fine particulate matter. *Occupational and environmental medicine*, *60*(5), 315-321.

Shi, T., Schins, R. P., Knaapen, A. M., Kuhlbusch, T., Pitz, M., Heinrich, J., & Borm, P. J. (2003). Hydroxyl radical generation by electron paramagnetic resonance as a new method to monitor ambient particulate matter composition. *Journal of Environmental Monitoring*, *5*(4), 550-556.

Shindell, D., Kuylenstierna, J. C., Vignati, E., van Dingenen, R., Amann, M., Klimont, Z., Anenberg, S. C., Muller, N., Maenhout, G.J., Raes, F., Schwartz, J., Faluvegi, G., Pozzoli, L., Kupiainen, K., Höglund-Isaksson, L., Emberson, L., Streets, D., Ramanathan, V., Hicks, K., Oanh, N.T.K., Milly, G., Williams M., Demkine, V., Fowler, D., & Schwartz, J. (2012). Simultaneously mitigating near-term climate change and improving human health and food security. *Science*, *335*(6065), 183-189.

Shinyashiki, M., Rodriguez, C. E., Di Stefano, E. W., Sioutas, C., Delfino, R. J., Kumagai, Y., Froines, J.R.,& Cho, A. K. (2008). On the interaction between glyceraldehyde-3-phosphate dehydrogenase and airborne particles: evidence for electrophilic species. *Atmospheric Environment*, 42(3), 517-529.

Shridhar, V., Khillare, P. S., Agarwal, T., & Ray, S. (2010). Metallic species in ambient particulate matter at rural and urban location of Delhi. *Journal of Hazardous Materials*, *175*(1), 600-607.

Simoneit, B. R., Schauer, J. J., Nolte, C. G., Oros, D. R., Elias, V. O., Fraser, M. P., Rogge W.F.; & Cass, G. R. (1999). Levoglucosan, a tracer for cellulose in biomass burning and atmospheric particles. *Atmospheric Environment*, 33(2), 173-182

Simonetti; G., Conte; E., Massimi; L., Perrino, C., & Canepari S. (2017) Oxidative potential of selected particulate matter components. Submitted in *Atmopheric Enviroment*.

Simoni, M., Baldacci, S., Maio, S., Cerrai, S., Sarno, G., & Viegi, G. (2015). Adverse effects of outdoor pollution in the elderly. *Journal of thoracic disease*, 7(1), 34.

Sigaud, S., Evelson, P., & González-Flecha, B. (2005). H2O2-induced proliferation of primary alveolar epithelial cells is mediated by MAP kinases. *Antioxidants & redox signaling*, 7(1-2), 6-13.

Squadrito, G. L., Cueto, R., Dellinger, B., & Pryor, W. A. (2001). Quinoid redox cycling as a mechanism for sustained free radical generation by inhaled airborne particulate matter. *Free Radical Biology and Medicine*, *31*(9), 1132-1138.

Steenhof, M., Gosens, I., Strak, M., Godri, K. J., Hoek, G., Cassee, F. R., Mudway, I.S., Kelly, F.J., Harrison, R.M., Lebret, E., Janssen, N.A.H., Pieters, R.H.H., & Brunekreef, B. (2011). In vitro toxicity of particulate matter (PM) collected at different sites in the Netherlands is associated with PM composition, size fraction and oxidative potential-the RAPTES project. *Particle and fibre toxicology*, 8(1), 26.

Stéphanie, V., Laurent, M., Hélène, C., Abderrazak, Y., & Hélène, M. (2011). Role of size and composition of traffic and agricultural aerosols in the molecular responses triggered in airway epithelial cells. *Inhalation toxicology*, *23*(11), 627-640.

Stoeger, T., Takenaka, S., Frankenberger, B., Ritter, B., Karg, E., Maier, K., Schulz, H., & Schmid, O. (2009). Deducing in vivo toxicity of combustion-derived nanoparticles from a cell-free oxidative potency assay and metabolic activation of organic compounds. *Environmental Health Perspectives*, 117(1), 54.

Taioli, E., Sram, R. J., Garte, S., Kalina, I., Popov, T. A., & Farmer, P. B. (2007). Effects of polycyclic aromatic hydrocarbons (PAHs) in environmental pollution on exogenous and oxidative DNA damage (EXPAH project): description of the population under study. *Mutation Research/Fundamental and Molecular Mechanisms of Mutagenesis*, 620(1), 1-6.

Takaoka, M., Yamamoto, T., Tanaka, T., Takeda, N., Oshita, K., & Uruga, T. (2005). Direct speciation of lead, zinc and antimony in fly ash from waste treatment facilities by XAFS spectroscopy. *Physica Scripta*, *2005*(T115), 943.

Timonen, H. J., Saarikoski, S. K., Aurela, M. A., Saarino, K. M., & Hillamo, R. E. (2008). Water-soluble organic carbon in urban aerosol: concentrations, size distributions and contribution to particulate matter. *Boreal environment research*, 13(4), 335-346.

Thorpe, A., & Harrison, R. M. (2008). Sources and properties of non-exhaust particulate matter from road traffic: a review. *Science of the total environment*, 400(1), 270-282.

Turner, M. C., Krewski, D., Pope III, C. A., Chen, Y., Gapstur, S. M., & Thun, M. J. (2011). Long-term ambient fine particulate matter air pollution and lung cancer in a large cohort of never-smokers. *American journal of respiratory and critical care medicine*, *184*(12), 1374-1381.

UNEP, W. (2011). Integrated assessment of black carbon and tropospheric ozone: Summary for Decision Makers. *Nairobi: United Nations Environment Programme*.

U.S. EPA. 2009. "Integrated Science Assessment for Particulate Matter." EPA/600/R-. http://ofmpub.epa.gov/eims/eimscomm.getfile?p_download_id=494959 [accessed 17 July 2017]

Valko, M. M. H. C. M., Morris, H., & Cronin, M. T. D. (2005). Metals, toxicity and oxidative stress. *Current medicinal chemistry*, 12(10), 1161-1208.

Verma, V., Pakbin, P., Cheung, K. L., Cho, A. K., Schauer, J. J., Shafer, M. M., Kleinman, M. T.,& Sioutas, C. (2011). Physicochemical and oxidative characteristics of semi-volatile components of quasi-ultrafine particles in an urban atmosphere. *Atmospheric environment*, 45(4), 1025-1033.

Venkatachari, P., Hopke, P. K., Grover, B. D., & Eatough, D. J. (2005). Measurement of particle-bound reactive oxygen species in Rubidoux aerosols. *Journal of Atmospheric Chemistry*, 50(1), 49.

Venkatachari, P., Hopke, P. K., Brune, W. H., Ren, X., Lesher, R., Mao, J., & Mitchell, M. (2007). Characterization of wintertime reactive oxygen species concentrations in Flushing, New York. *Aerosol Science and Technology*, 41(2), 97-111.

Venkatachari, P., & Hopke, P. K. (2008). Development and laboratory testing of an automated monitor for the measurement of atmospheric particle-bound reactive oxygen species (ROS). *Aerosol Science and Technology*, 42(8), 629-635.

Vernile, P., Tutino, M., Bari, G., Amodio, M., Spagnuolo, M., de Gennaro, G., & de Lillo, E. (2013). Particulate matter toxicity evaluation using bioindicators and comet assay. *Aerosol and Air Quality Research*, 13, 172-178.

Viana, M., Kuhlbusch, T. A. J., Querol, X., Alastuey, A., Harrison, R. M., Hopke, P. K., Winiwarter, W., Vallius, M., Szidat, S., Prevot, A.S.H., Bloemen, H., Wahlin, P., Vecchi, R., Miranda, A.I., Kasper-Giebl, A., Maenhaut, W., Hitzenberger, R., & Hueglin, C. (2008). Source apportionment of particulate matter in Europe: a review of methods and results. *Journal of aerosol science*, *39*(10), 827-849.

Vidrio, E., Jung, H., & Anastasio, C. (2008). Generation of hydroxyl radicals from dissolved transition metals in surrogate lung fluid solutions. *Atmospheric Environment*, 42(18), 4369-4379.

Zielinski, H., Mudway, I. S., Bérubé, K. A., Murphy, S., Richards, R., & Kelly, F. J. (1999). Modeling the interactions of particulates with epithelial lining fluid antioxidants. American *Journal of Physiology-Lung Cellular and Molecular Physiology*, 277(4), L719-L726.

Wang, H., & Joseph, J. A. (1999). Quantifying cellular oxidative stress by dichlorofluorescein assay using microplate reader. *Free Radical Biology and Medicine*, 27(5), 612-616.

Wang, M., Beelen, R., Eeftens, M., Meliefste, K., Hoek, G., & Brunekreef, B. (2012). Systematic evaluation of land use regression models for NO_2. *Environmental science & technology*, 46(8), 4481-4489.

WHO 2012: Health effects of black carbon. Janssen, N. A. H., Gerlofs-Nijland, M. E., Lanki, T., Salonen, R. O., Cassee, F.,Hoek, G., Fischer, P., Brunekreef, B., and Krzyzanowski, M.: WHO's Regional Office for Europe, Copenhaguen, 86 pp., ISBN 9789289002653, http://www.euro.who.int/ data/assets/pdf file/ 0004/162535/e96541.pdf, 2012.

WHO 2013: Review of evidence on health aspects of air pollution – REVIHAAP. First Results. WHO's Regional Office for Europe, Copenhaguen, 28 pp., http://www.euro.who.int/ data/ assets/pdf file/0020/182432/e96762-final.pdf, 2013.

Xing, Y. F., Xu, Y. H., Shi, M. H., & Lian, Y. X. (2016). The impact of PM2. 5 on the human respiratory system. *Journal of thoracic disease*, *8*(1), E69.

Yang, A., Jedynska, A., Hellack, B., Kooter, I., Hoek, G., Brunekreef, B., Kuhlbusch , T.A.J., Cassee , F.R., & Janssen, N. A. (2014). Measurement of the oxidative potential of PM 2.5 and its constituents: the effect of extraction solvent and filter type. *Atmospheric environment*, 83, 35-42.

Yang, A. X. (2015). *Oxidative potential of particulate matter as a health-relevant exposure metric* (Doctoral dissertation, Utrecht University).

Yang, A., Hellack, B., Leseman, D., Brunekreef, B., Kuhlbusch, T. A., Cassee, F. R., Hoek, G., & Janssen, N. A. (2015). Temporal and spatial variation of the metal-related oxidative potential of PM $_{2.5}$ and its relation to $PM_{2.5}$ mass and elemental composition. *Atmospheric Environment*, 102, 62-69.

Yi, S., Zhang, F., Qu, F., & Ding, W. (2014). Water-insoluble fraction of airborne particulate matter (PM10) induces oxidative stress in human lung epithelial A549 cells. *Environmental toxicology*, 29(2), 226-233.

Zanobetti, A., & Schwartz, J. (2011). Ozone and survival in four cohorts with potentially predisposing diseases. *American journal of respiratory and critical care medicine*, *184*(7), 836-841.

Zou, Y., Jin, C., Su, Y., Li, J., & Zhu, B. (2016). Water soluble and insoluble components of urban PM 2.5 and their cytotoxic effects on epithelial cells (A549) in vitro. *Environmental Pollution*, 212, 627-635.

Zomer, B., Collé, L., Jedyńska, A., Pasterkamp, G., Kooter, I., & Bloemen, H. (2011). Chemiluminescent reductive acridinium triggering (CRAT)—mechanism and applications. *Analytical and bioanalytical chemistry*, *401*(9), 2945.

CHAPTER IV: PhD CONCLUSION AND PERSPECTIVES

The first part of this work concerned the development and the application to field campaigns of new analytical methods that allowed us improving our knowledge about the PM chemical composition and its relations with emissive sources and climatic conditions. This knowledge is of primary relevance for a reliable estimation of contributes to PM given from individual sources, whose environmental and health concerns may be very different.

In particular, we focused our attention on high-time resolved sampling and analysis methods; having information about the time variability of single chemical compounds allows for a comparison with meteo-climatic parameters and emission sources strength, both variable at short time intervals. These optimized methods permitted a reliable tracing of important PM sources, such as vehicular traffic and wood burning, and the definition of elemental profile of several contributes to PM in indoor and outdoor environments, such as cigarette smoke, incense burning, brushwood burning, pellet burning and road dust resuspension. Particular attention was also given to the determination of inorganic secondary ions (mainly ammonium nitrate and sulphate) that constitute a very relevant PM fraction. These ions are formed by reaction in the atmosphere of gaseous precursors like NOx and SO_2 and may behave as oxidant species, being thus relevant for PM health and environment risk assessment. The formation of secondary species is a complex and still partly unknown mechanism, in which atmospheric and particle bound water play a primary role. A part of this doctoral work was then focused measuring particle bound water and of its relations with secondarily formed species. Our results showed a strong synergic correlation between water and ammonium nitrate, particularly when high relative humidity and poor mixing of atmosphere are present: in these conditions, ammonium nitrate and particle bound water accounted for about half of the total PM mass amount.

The second part of this work concerned the study of the relations between PM individual sources (traced by chemical analyses) and the generation of ossidative processes. In this thesis, three different oxidative potential assays (ascorbic acid, AA; dithiothreitol ,DTT and dichlorofluorescein diacetate, DCFH) were used as an exposure metric in assessing long-term health effects. The results obtained in this PhD thesis showed that each OP method could not be used individually. In fact, their basic mechanisms respond differently depending on the chemical composition of PM samples. The study of oxidative potential in unsupported dust, in daily PM10 samples, and in dimensionally segregated field samples, showed that the three methods are not interchangeable, since they measure different values in the same samples. These results suggest that further research efforts are needed to assess the predictive capabilities of these acellular procedures, nowadays largely used to estimate the PM's

ability to generate ROS. In our view, the application of different methods may be a more reliable tool to simulate the different ROS generation mechanisms, although targeted studies would be needed to better correlate OP values and in-vivo generation of oxidative stress. In particular, the application of the three methods to all the field dusts showed that the DCFH and DTT methods are more sensitive to organic substances, exhibiting higher levels of oxidative potential for dust in which organic carbon is the predominant species, while the AA method is more sensitive towards dusts rich in metals and metalloids. However, multivariate statistical analysis (focused on principal constituents' analysis) of chemical and OP data evidenced that AA and DTT variability is correlated to the same chemical components of PM, although the sensitivity of the two assays towards the single components is very different.

The interpretation of the results obtained by the DCFH assay has been particularly difficult. In fact, DCFH results appear to be driven by a competition between several factors, some of which increase the response while others suppress it. As this method is the one that better simulate the cellular ROS generation mechanism, and is largely used in cellular experiment to evaluate intracellular oxidative stress, this result, that to our knowledge had not been previously evidenced in the literature, certainly need to be studied further.

Another very interesting issue of this work, particularly innovative compared to the studies already reported in the literature, was the application of the three assays to both the soluble and insoluble fractions of some environmentally relevant dusts. This study showed that the insoluble fraction, which is generally neglected in the OP measurements, has a determining role in the generation of oxidative potential. In addition, thanks to the work focus on the analysis OPs in different monitoring campaigns it was possible to conclude that the results obtained by the OP analysis of the PM samples do not depend on the PM's total concentration, but are strongly linked to its chemical composition, sources emission and particles' size. As an example, our study allowed identifying a strong correlation between the DTT assay results and secondary ions: the presence of unfavorable climatic conditions (high relative humidity and low air masses mixing properties) could increase the health concern of PM, also when anthropic sources are not particularly active.

In the last months, we have applied OP assay to time-resolved samples, collected by the previously optimized system during an intensive monitoring campaign that involved almost all the Italian researchers working on PM. This study generated a very important database that is still being elaborated; the first results, however, show a significant correlation between OP measured by the DCFH assay and black carbon, one of the most reliable tracer of emission from diesel vehicular traffic.

It is worth noting that the findings described in this PhD thesis opened up new perspectives and challenge related to PM research.

One important focus is the comprehension of the role of adsorbed and bound water in chemical transoformation of species present as solid, liquid or vapour phases. In particular, we evidenced a strong influence of water on the formation of inorganic secondary species; a similar influence could be exerted also on the formation of secondary organic species and on the interconversion between organic compounds. As most of the reaction in the atmosphere include redox equilibria, a better comprehension of these precesses could be very helpful to understand the role of PM in inducing oxidative stress.

A second new finding concerned the behaviour of DCFH assay, which is one the most used method to assess PM's oxidative potential; in particular, we evidenced for the first time that the assay is sensitive to components able to suppress the OP^{DCFH}. It is reasonable to hypothesize that this effect depends on the presence in PM of enzyme inibitors or of reducing species. As a similar mechanism could be active also in cellular systems, this result needs to be properly confirmed and deepened. In our laboratory are currently being undertaken studies about the measurement of reductans species in PM samples and about the identification in PM of possible HRP inibitors.

A last very interesting issue regards the study of the relations between black carbon and generation of ROS. The results that we obtained in CARE project showed that OP^{DCFH} is anti-correlated to black carbon (BC) mass concentration; however, the finest BC particles (diamenters in the nanometer range) resulted to be much more active than larger one in producing oxidative processes. BC constitutes one of the main anthropic contributions to nanoparticles in the atmosphere: its role in the inducing adverse effects on human health, and in particular in the generation of ROS is one of key point that need to be understood.

APPENDICES

A1: Meteorological data recorded during the first SOP.

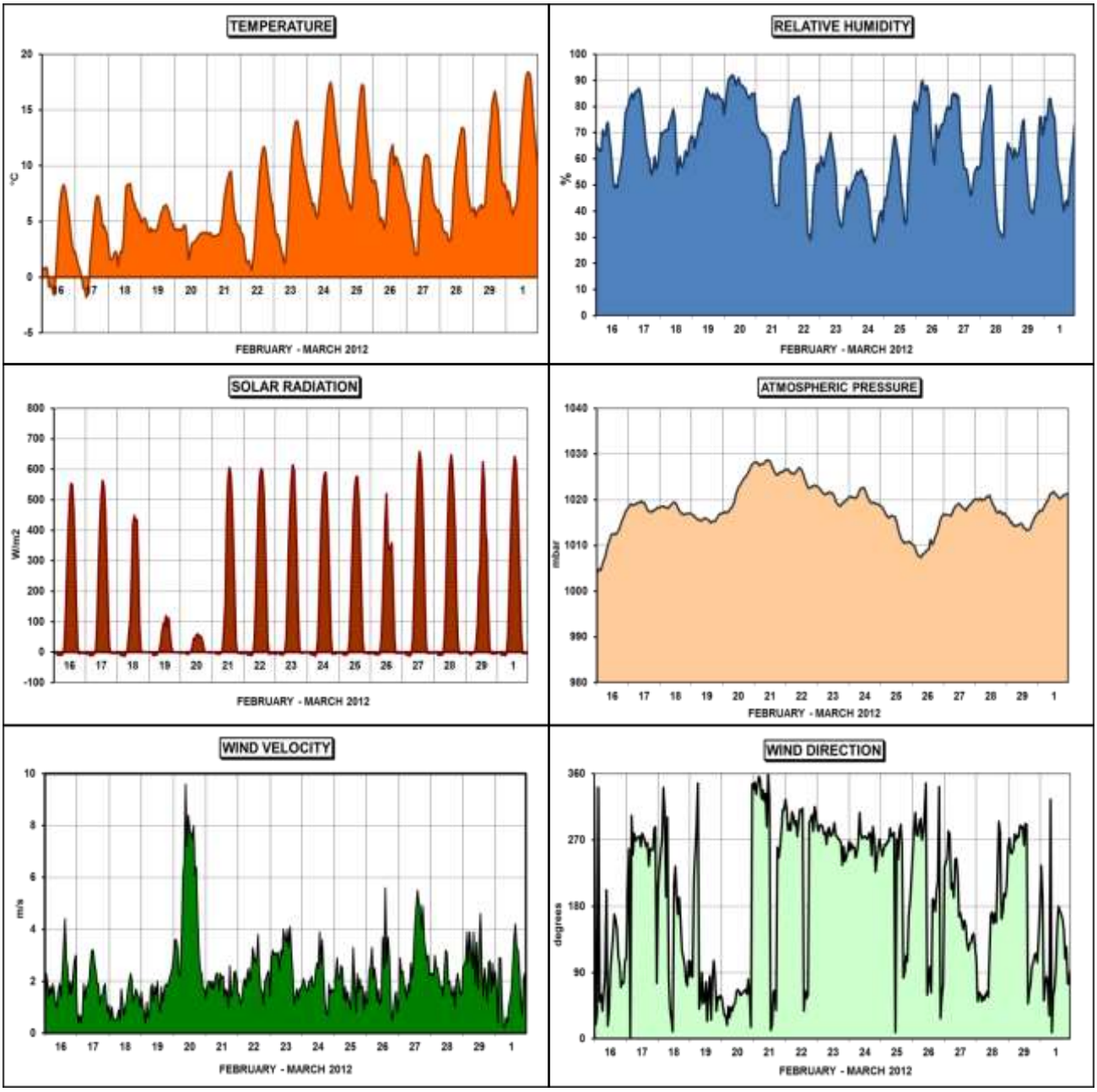

A2: a. Thermal ramp - Karl Fisher analysis of the 24-h samples collected during SOP1.

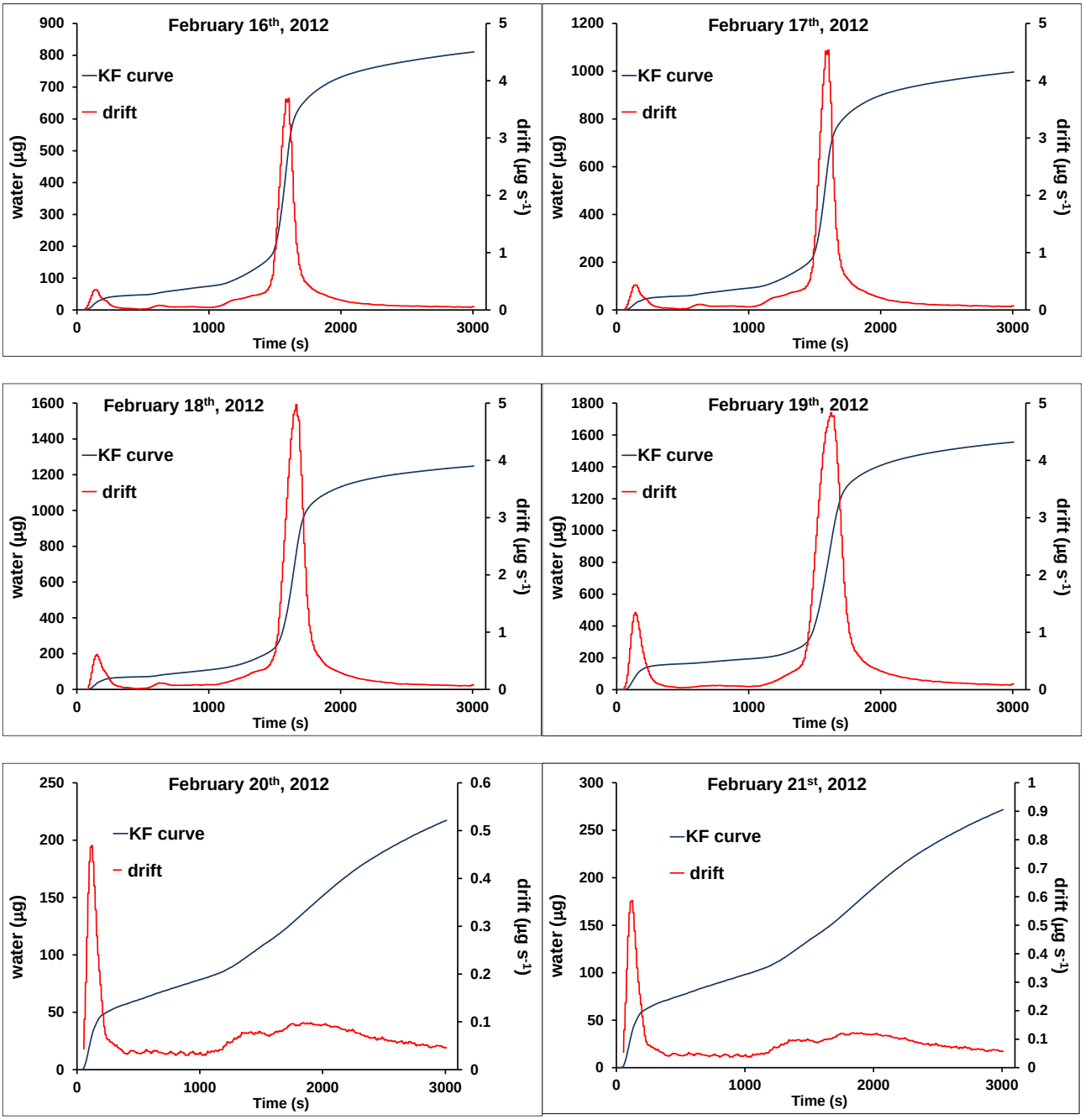

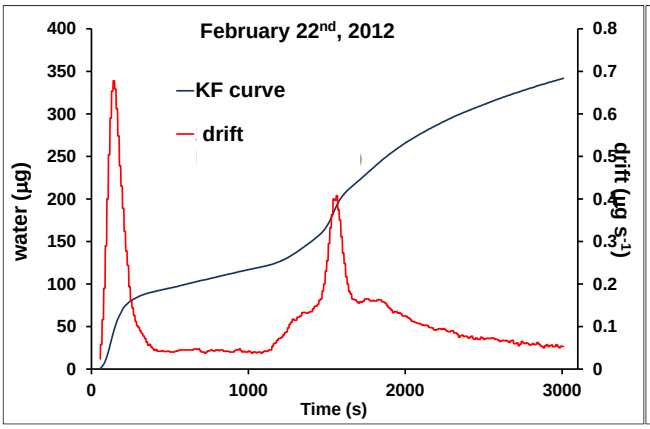
February 22nd, 2012
KF curve
drift
water (µg)
drift (µg s-1)
Time (s)

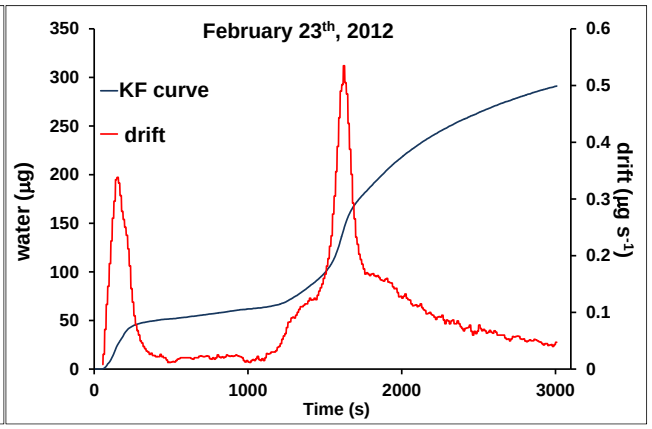
February 23th, 2012
KF curve
drift
water (µg)
drift (µg s-1)
Time (s)

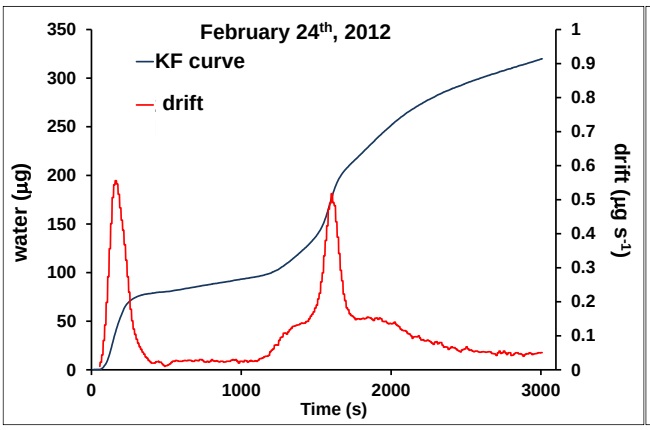
February 24th, 2012
KF curve
drift
water (µg)
drift (µg s-1)
Time (s)

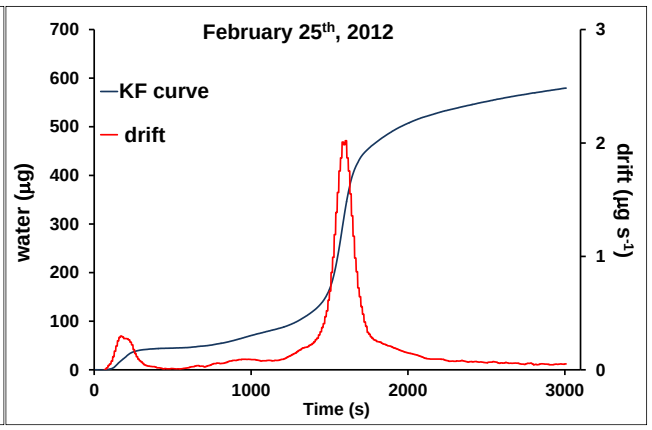
February 25th, 2012
KF curve
drift
water (µg)
drift (µg s-1)
Time (s)

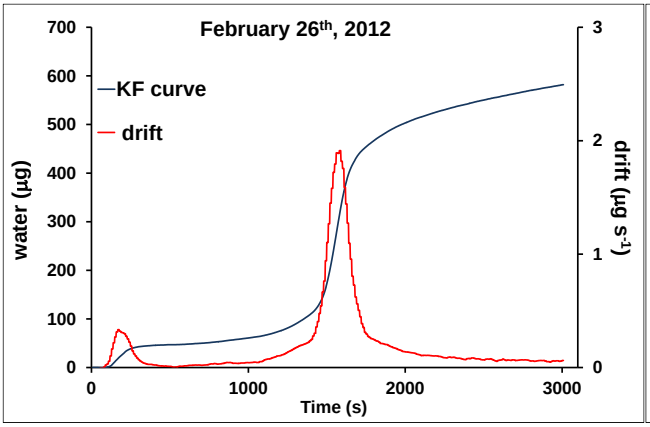
February 26th, 2012
KF curve
drift
water (µg)
drift (µg s-1)
Time (s)

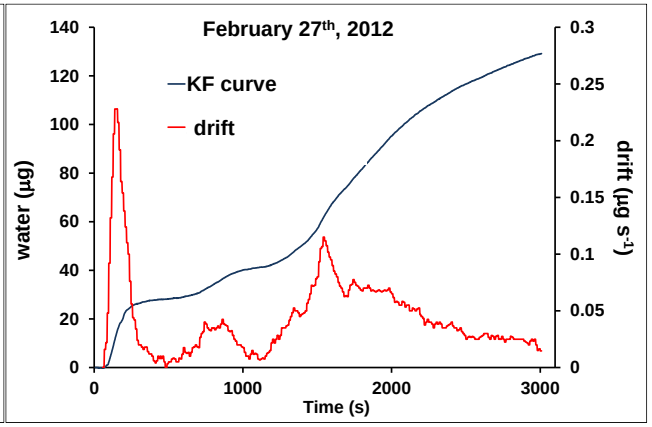
February 27th, 2012
KF curve
drift
water (µg)
drift (µg s-1)
Time (s)

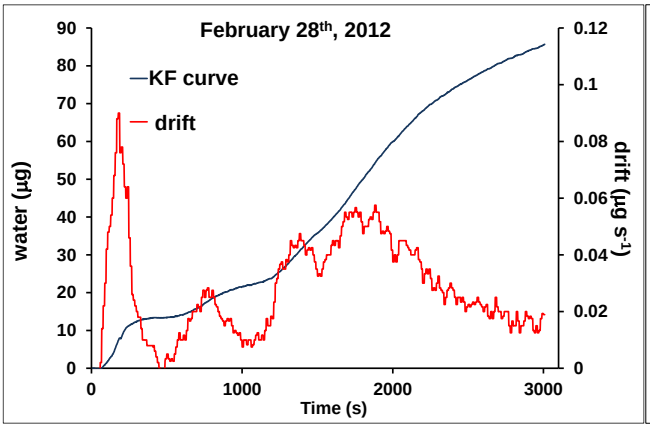
February 28th, 2012
KF curve
drift
water (µg)
drift (µg s-1)
Time (s)

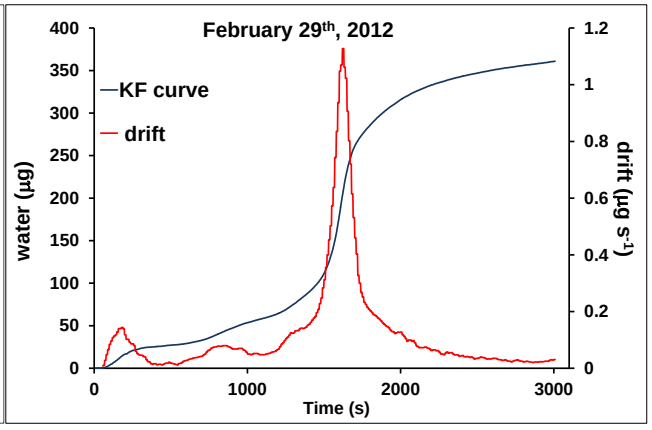
February 29th, 2012
KF curve
drift
water (µg)
drift (µg s-1)
Time (s)

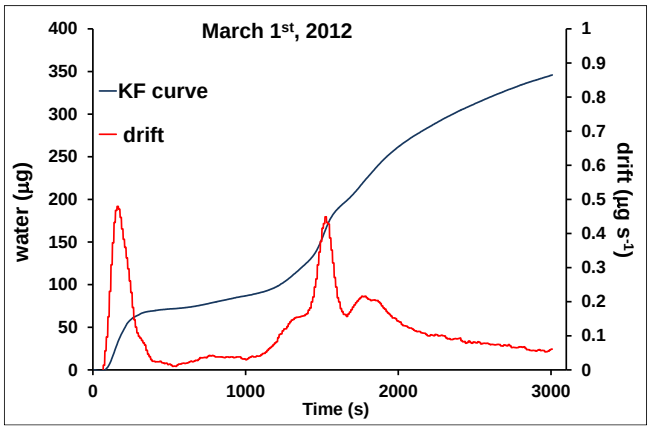
March 1st, 2012
KF curve
drift
water (µg)
drift (µg s-1)
Time (s)
400
350
300
250
200
150
100
50
0
1
0.9
0.8
0.7
0.6
0.5
0.4
0.3
0.2
0.1
0
0
1000
2000
3000

A2: b. Thermal ramp - Karl Fisher analysis of the size-segregated samples collected during SOP1.

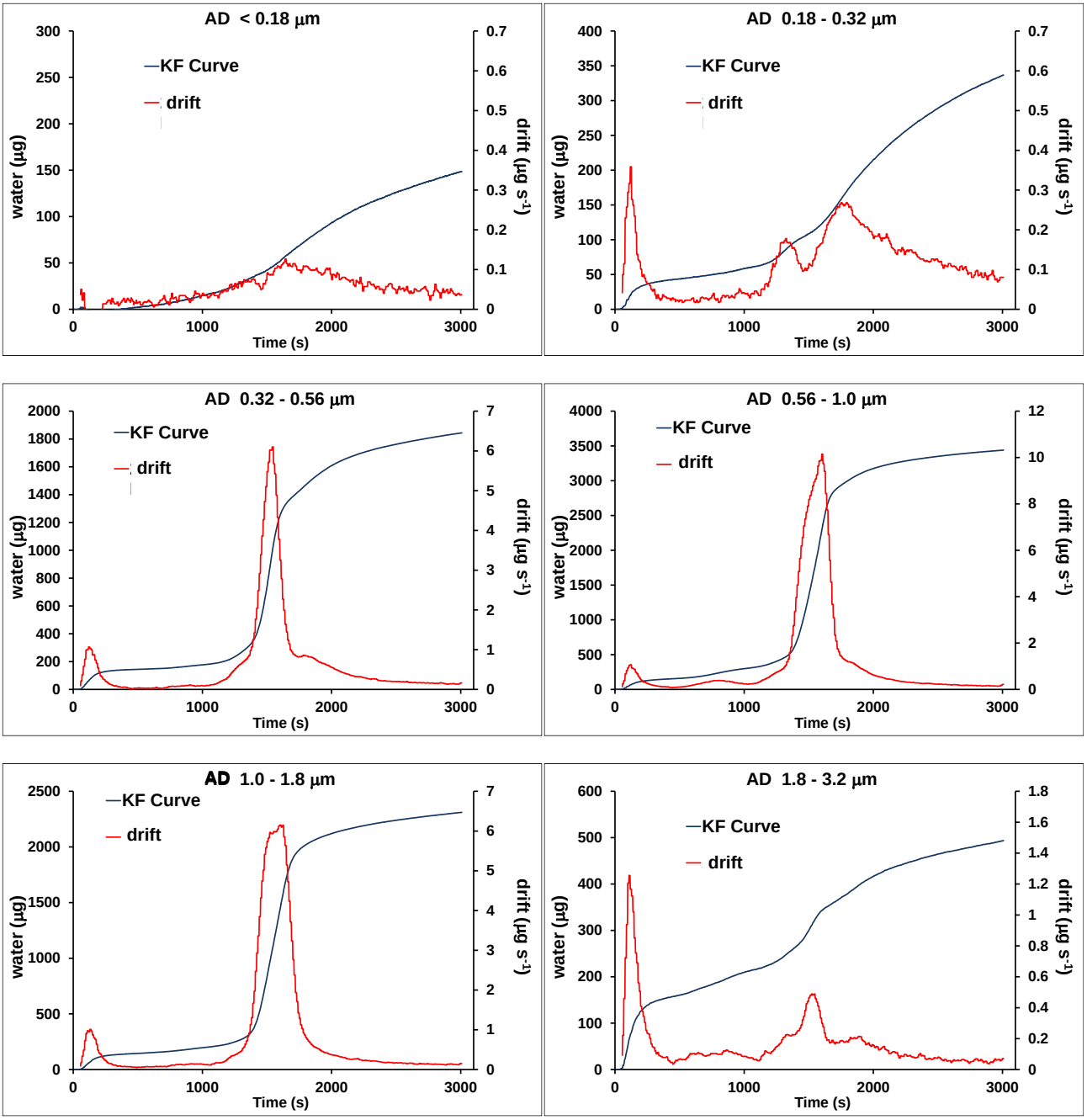

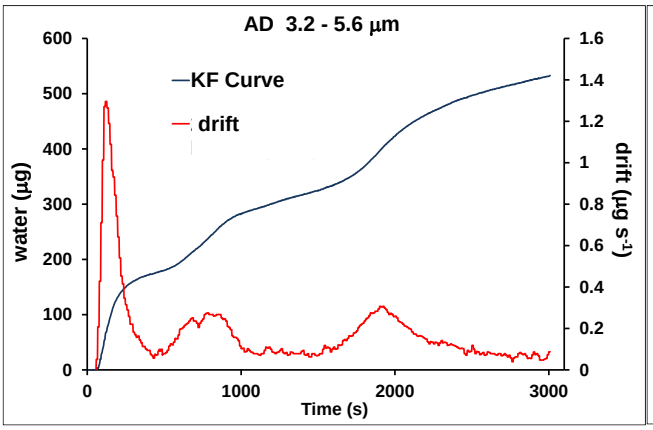
AD 3.2 - 5.6 µm
KF Curve
drift
water (µg)
drift (µg s-1)
Time (s)
0
100
200
300
400
500
600
0
0.2
0.4
0.6
0.8
1
1.2
1.4
1.6
0
1000
2000
3000

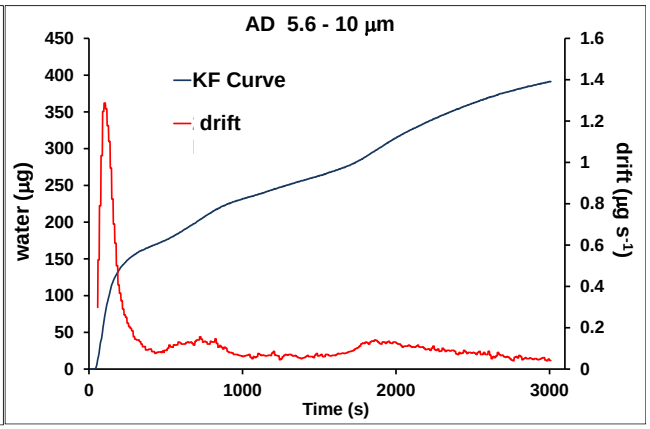
AD 5.6 - 10 µm
KF Curve
drift
water (µg)
drift (µg s-1)
Time (s)
0
50
100
150
200
250
300
350
400
450
0
0.2
0.4
0.6
0.8
1
1.2
1.4
1.6
0
1000
2000
3000

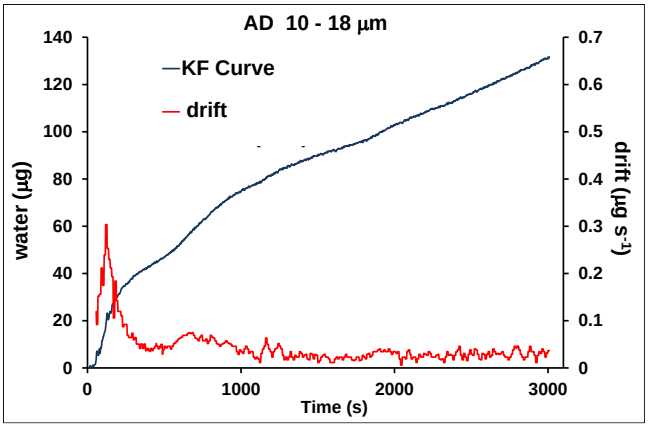
AD 10 - 18 µm
KF Curve
drift
water (µg)
drift (µg s-1)
Time (s)
0
20
40
60
80
100
120
140
0
0.1
0.2
0.3
0.4
0.5
0.6
0.7
0
1000
2000
3000

A3: Percentage of water (w/w) with respect to the PM mass amount during the four SOPs. Red figures indicate values between LOD and LOQ.

	SOP1	SOP2	SOP3	SOP4
	water (w/w %)	water (w/w %)	water (w/w %)	water (w/w %)
<0.18	5.6	6.8	1.2	10
0.18-0.32	8.8	3.0	3.2	6.6
0.32-0.56	30	4.8	3.8	9.1
0.56-1	35	6.0	3.4	11
1-1.8	31	5.8	1.3	1.8
1.8-3.2	20	3.4	2.0	8.0
3.2-5.6	15	3.1	2.2	10
5.6-10	20	1.5	2.4	6.5
10-18	18	2.8	4.4	1.9
>18	16	1.9	3.7	3.4

A4: Thermal ramp - Karl Fisher analysis of the size-segregated samples collected during SOP2. The analysis of stages AD 0.56 – 1.0 µm and AD 10 – 18 µm were below the LOQ (25 µ g).

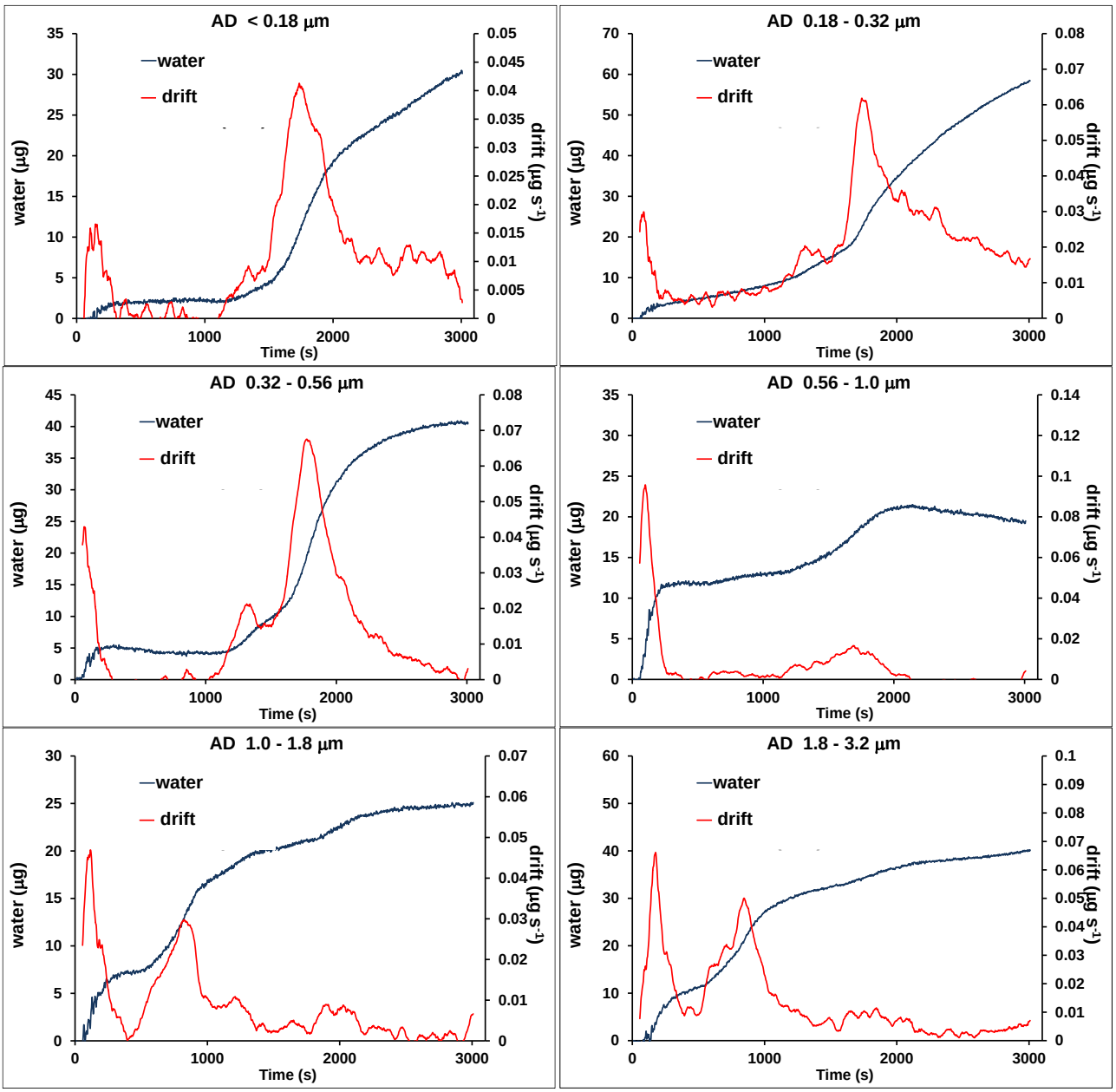

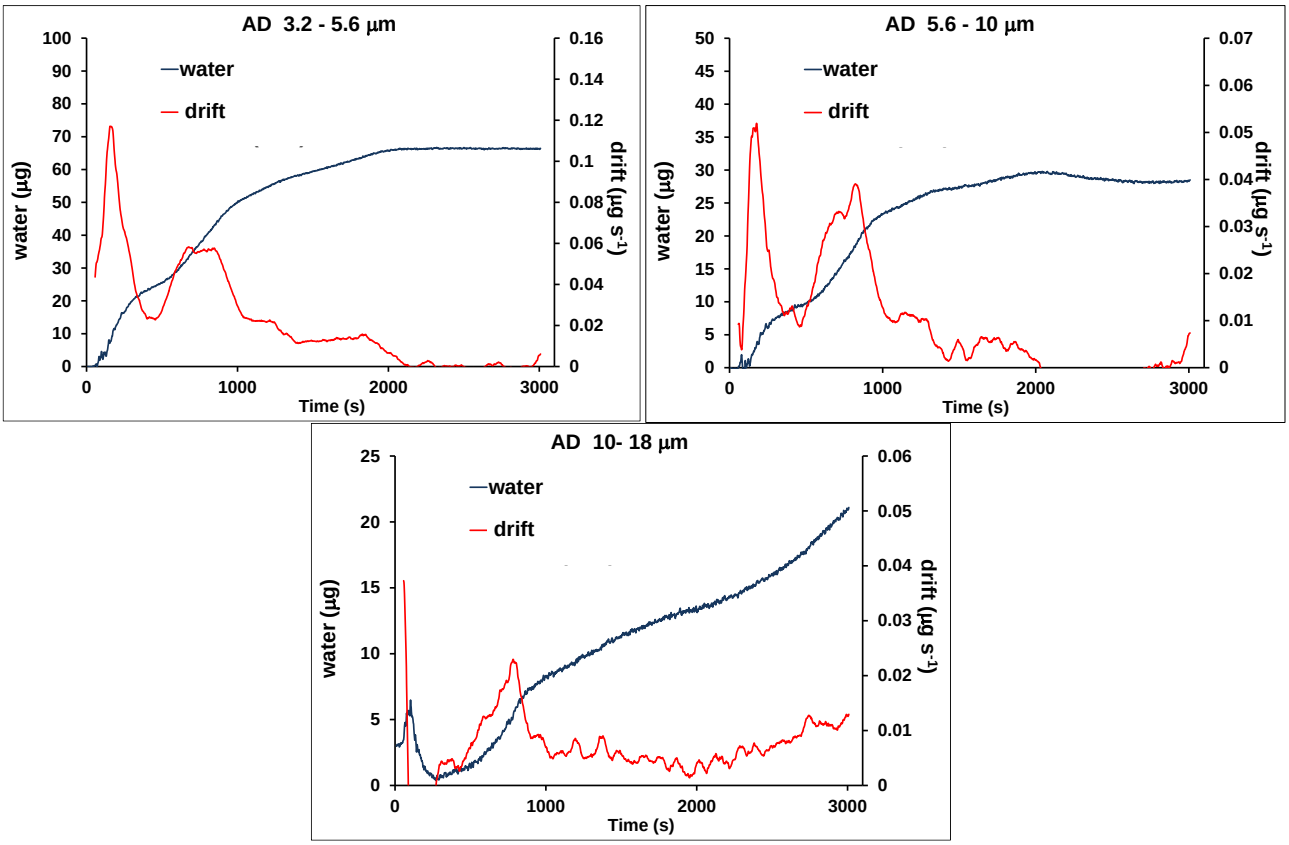
AD 3.2 - 5.6 µm
water
drift
water (µg)
drift (µg s-1)
Time (s)
AD 5.6 - 10 µm
water
drift
water (µg)
drift (µg s-1)
Time (s)
AD 10- 18 µm
water
drift
water (µg)
drift (µg s-1)
Time (s)

A5: Size-distribution of nitrate, sulfate and ammonium during SOP3.

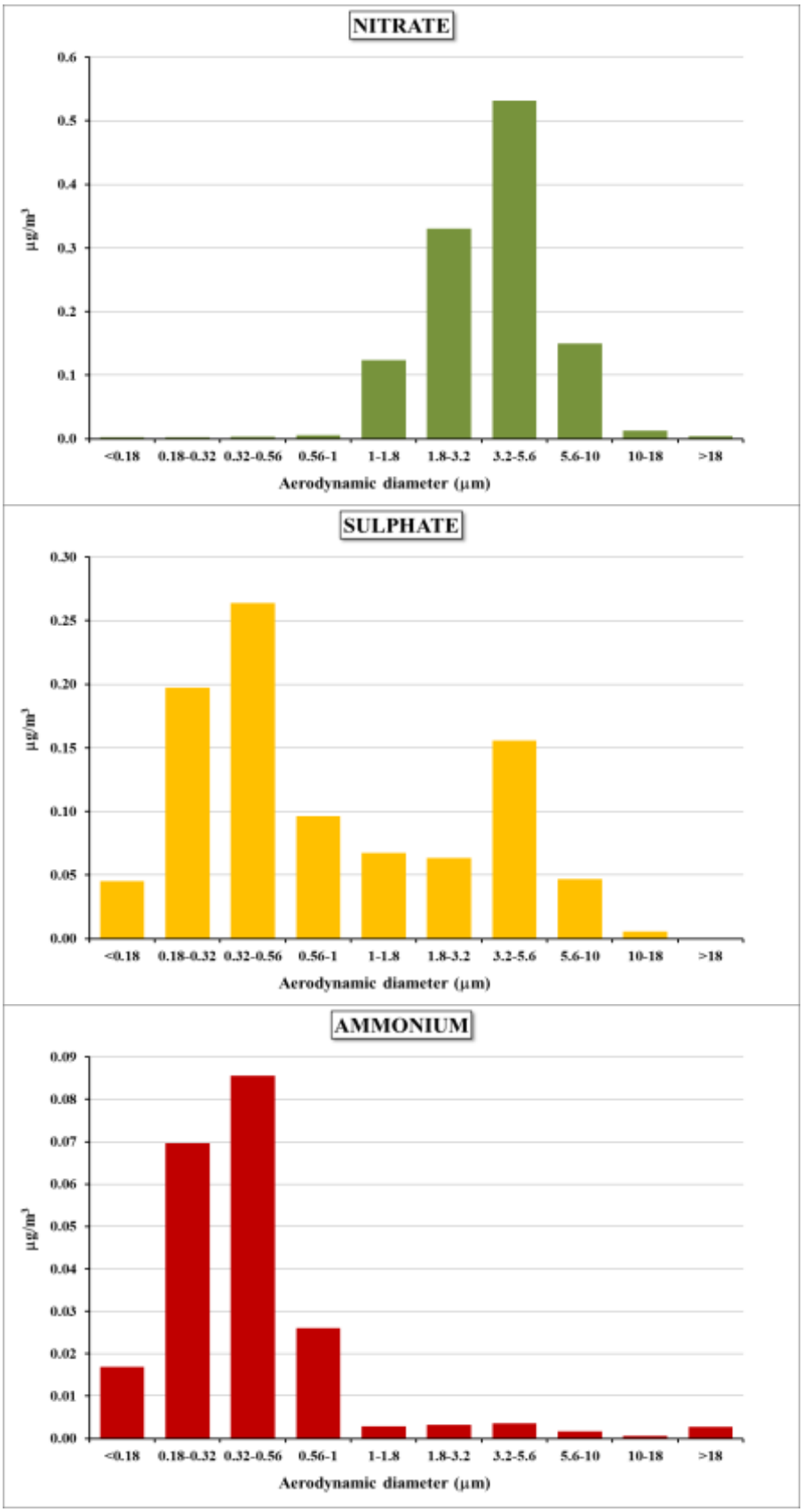

A6: Thermal ramp - Karl Fisher analysis of the size-segregated samples collected during SOP4. The analysis of stages AD 1.0 – 1.8 µm and AD 10 – 18 µm were below the LOQ (25 µg).

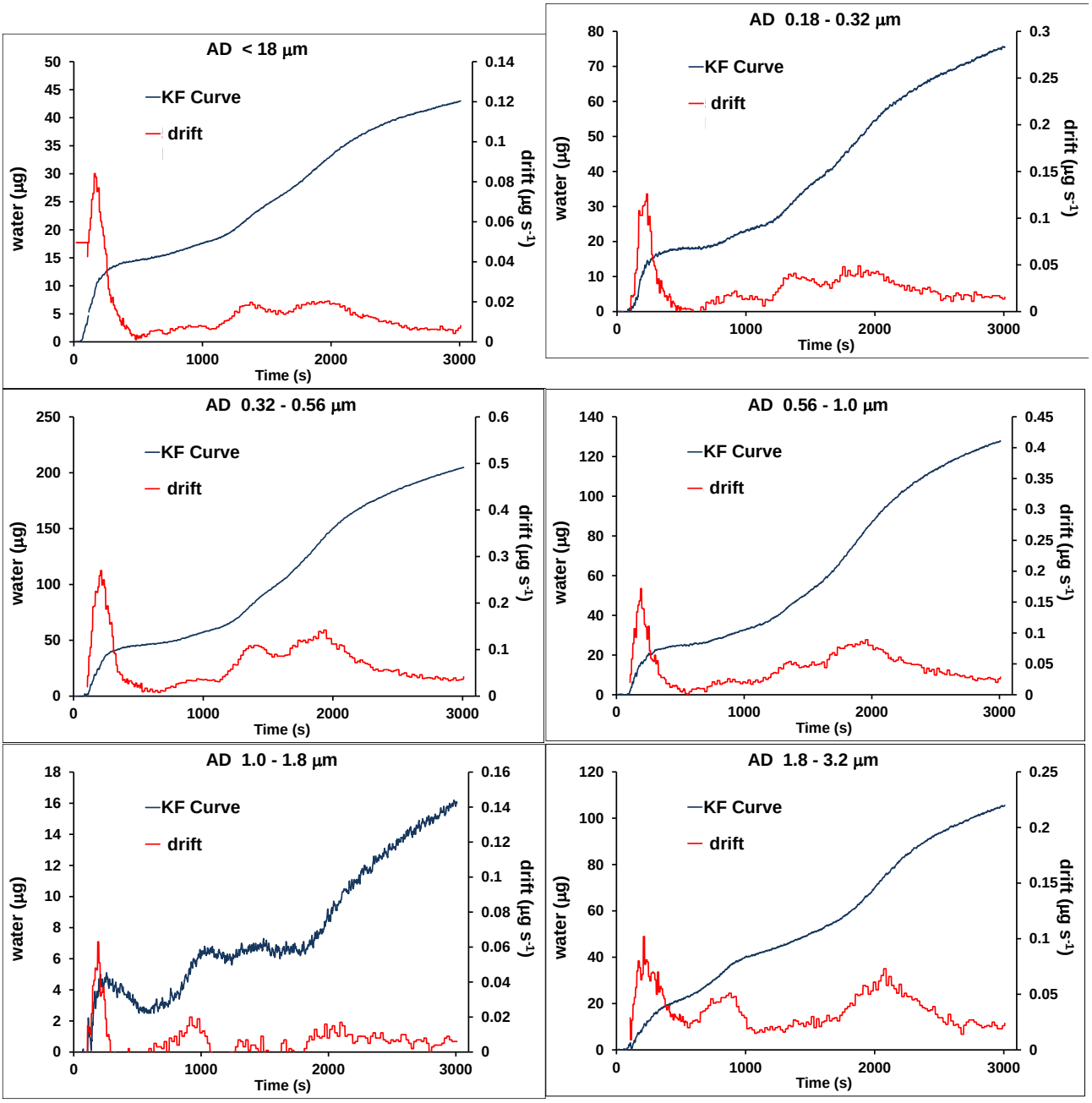

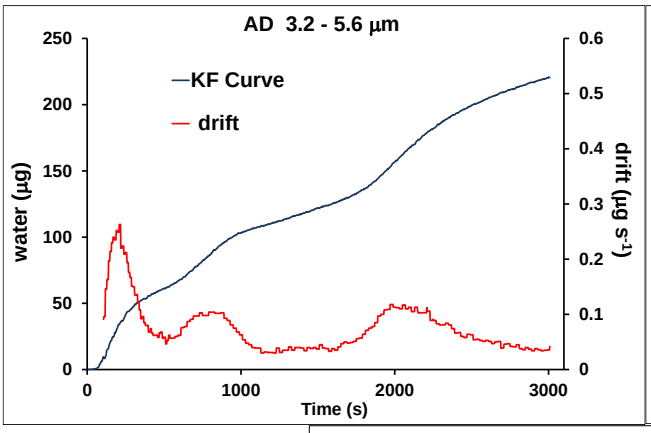
AD 3.2 - 5.6 µm
KF Curve
drift
water (µg)
drift (µg s-1)
Time (s)
0
50
100
150
200
250
0
0.1
0.2
0.3
0.4
0.5
0.6
0
1000
2000
3000

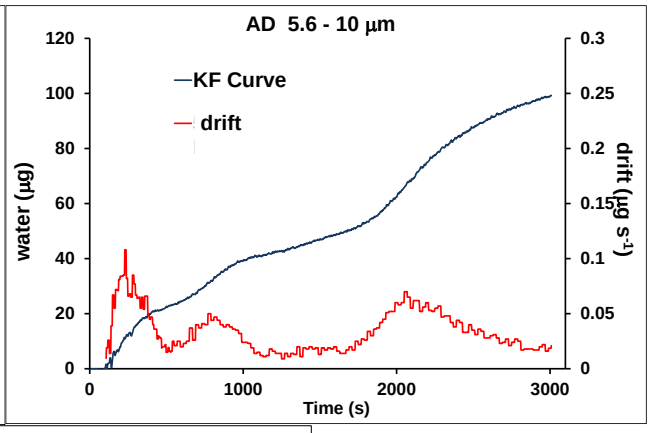
AD 5.6 - 10 µm
KF Curve
drift
water (µg)
drift (µg s-1)
Time (s)
0
20
40
60
80
100
120
0
0.05
0.1
0.15
0.2
0.25
0.3
0
1000
2000
3000

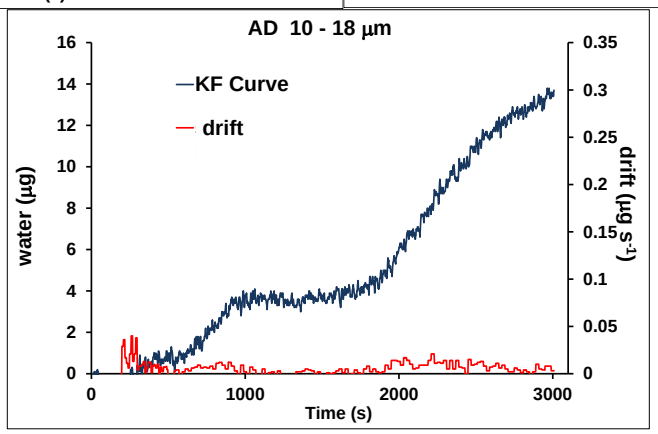
AD 10 - 18 µm
KF Curve
drift
water (µg)
drift (µg s-1)
Time (s)
0
2
4
6
8
10
12
14
16
0
0.05
0.1
0.15
0.2
0.25
0.3
0.35
0
1000
2000
3000

C1. Schematic assembly of the PILS-IC

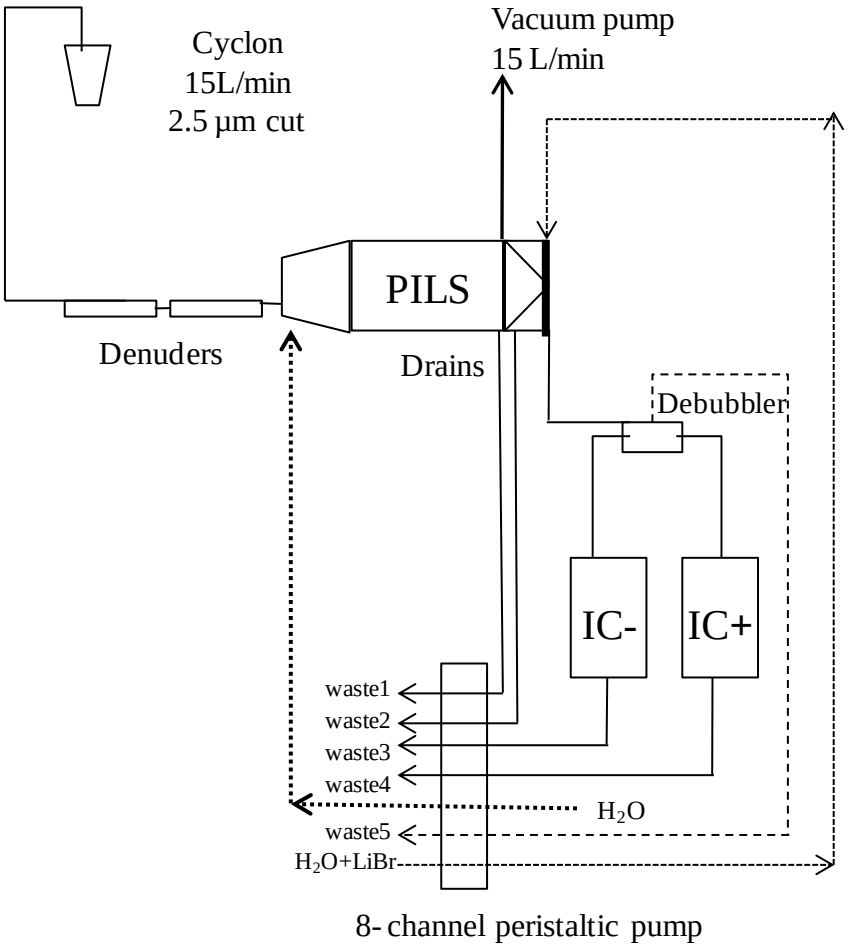

C2. Operative flow rates of the PILS-IC.

PILS line	**Flow rate (mL min^{-1})**
Water vapor generator (H_2O)	1.5
Grown chamber drain (waste 1)	0.9
Impactor plate drain (waste 2)	0.8
Washing solution (H_2O+LiBr)	0.8
Anion chromatograph drain (waste 3)	0.3
Cation chromatograph drain (waste 4)	0.2
Debubbler drain (waste 5)	0.3

C3. Scatter plot of the ion concentrations measured by the modified PILS-IC and by the diffusion lines. Data are reported for all ions but nitrite, as these values were frequently below the LOQ of the diffusion lines.

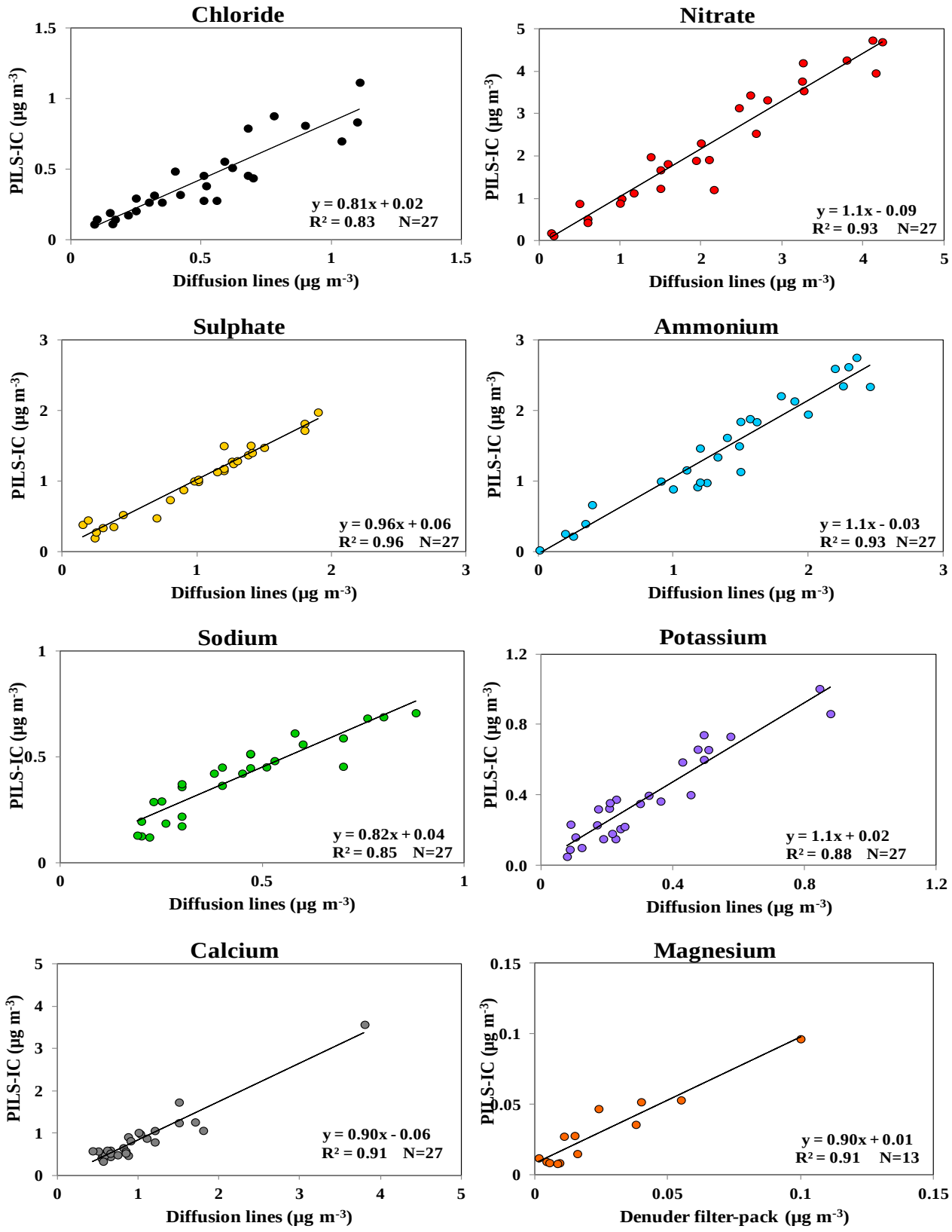

C4.48-h back-trajectories of the air masses calculated every hour from 12:00 a.m. to 12:00 p.m. of February 2nd.

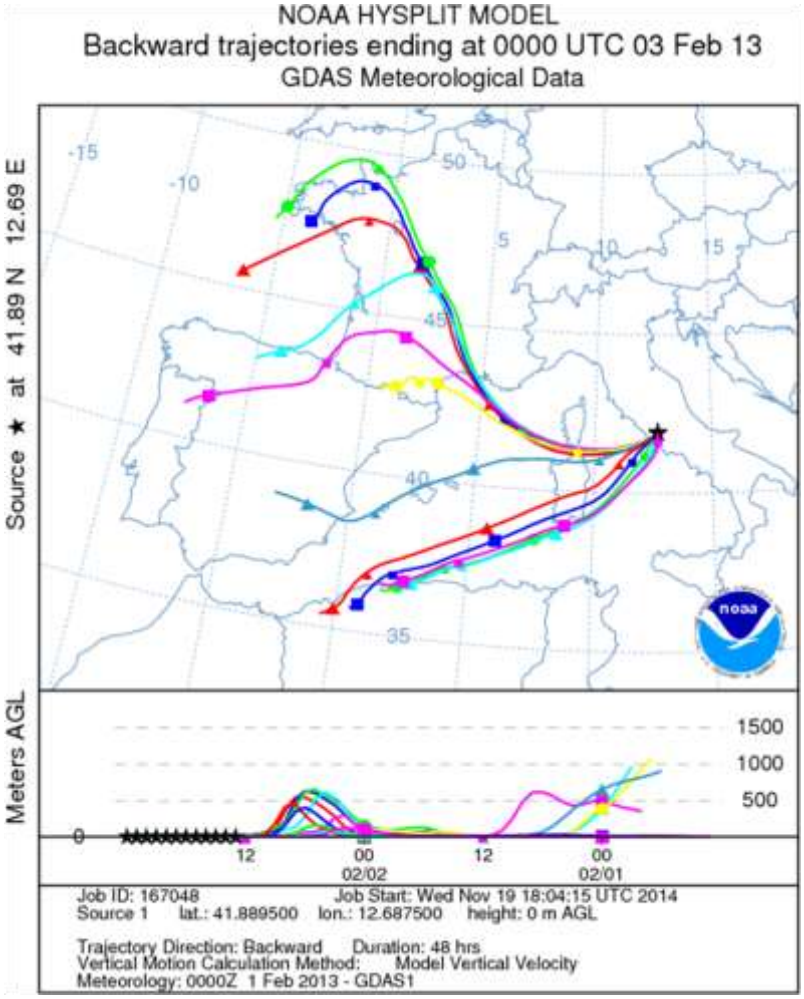

D1: Principal component analysis of OP assays' results and chemical characteristics of dusts' insoluble fraction

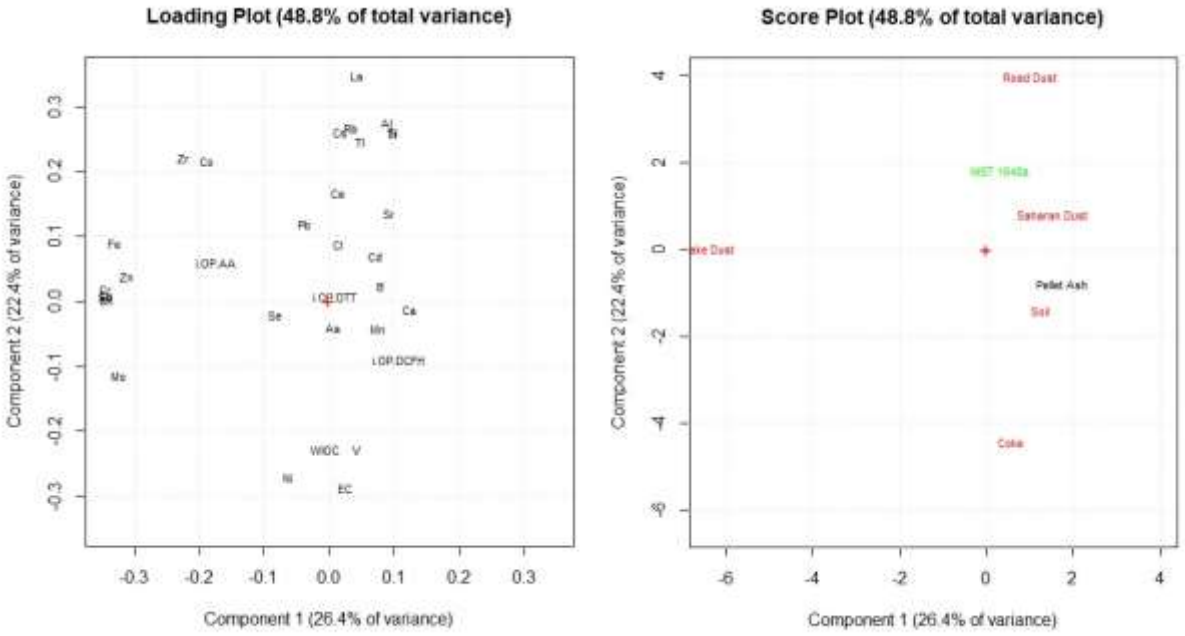

E1: The mean concentration, 10 and 90 ° percentile of PM mass concentration and of the measured PM macro components obtained by the XRF, IC, WSOC and EC/OC analysis of $PM_{2.5}$ and PM_{10} samples collected at the Ferrara site and of PM_{10} samples collected at the Rome site

		FERRARA								ROME			
		PM_{10} (ng/m^3)				$PM_{2.5}$ (ng/m^3)				PM_{10} (ng/m^3)			
	tecnique	average	median	10%	90%	average	median	10%	90%	average	median	10%	90%
MASS		31901	27500	14123	56167	25843	24030	9122	45713	29419	32573	15527	36498
Al	XRF	97	79	57	197	48	40	36	59	194	184	133	263
Ca	XRF	577	413	256	965	99	79	63	141	1479	1439	891	2247
Cl	XRF	386	350	143	752	182	177	63	377	771	322	175	1906
Cr	XRF	5.7	5.5	4.6	7.1	4.4	4.2	3.7	5.1	9.1	8.5	6.6	13
Fe	XRF	97	79	57	197	47	33	3.0	84	625	599	328	936
K	XRF	308	275	183	454	276	260	135	424	460	495	244	569
Mg	XRF	118	113	58	190	34	30	11	64	196	173	109	316
Na	XRF	347	286	133	592	138	107	72	233	756	531	342	1563
S	XRF	525	483	179	667	488	420	133	800	675	664	376	959
Si	XRF	315	256	186	640	101	84	76	126	802	764	511	1156
Ti	XRF	10	7.0	3.4	24	1.3	0.43	0.43	1.9	27	28	16	40
V	XRF	2.5	1.8	0.6	4.7	2.1	1.2	0.43	4.6	5.4	5.5	3.7	7.0
Zn	XRF	32	29	12	60	24	22	8.4	40	27	28	17	37
Cl^-	IC	352	321	118	556	157	124	37	300	808	321	154	2050
NO_3^-	IC	9700	7090	1370	21700	8480	6360	1440	18900	3168	3109	1035	5234
$SO_4^=$	IC	1740	1370	392	3430	1550	1360	449	3140	2038	2056	984	3024
Na^+	IC	218	146	59	423	78	71	37	142	1014	563	364	2402
NH_4^+	IC	3820	1420	330	9970	3700	1770	519	9020	951	1075	374	1456
Mg^{++}	IC	69	52	33	117	17	14	7.0	32	174	117	70	372
Ca^{++}	IC	311	228	127	554	74	58	12	128	1197	1173	798	1786
OC	TOA	4830	4760	2400	6280	4410	4010	1990	5980	5884	5995	3382	7794
EC	TOA	819	787	289	1280	768	770	250	1180	1513	1629	883	1964
WSOC	TOC	376	176	452	330	324	376	176	437	342	343	179	522

E2: Data obtained by the soluble, insoluble fraction analysis of $PM_{2.5}$ and PM_{10} samples collected at the Ferrara site and of PM_{10} samples collected at the Rome site

PM_{10} - ROME												
	Soluble Fraction (ng/m³)				Insoluble Fraction (ng/m³)				Total (ng/m³)			
	average	median	10%	90%	average	median	10%	90%	average	median	10%	90%
Li	0.083	0.085	0.045	0.12	0.14	0.14	0.08	0.18	0.23	0.23	0.17	0.28
Be	0.0042	0.0047	0.0012	0.0061	0.015	0.016	0.007	0.024	0.019	0.021	0.0088	0.029
B	3.5	3.5	2.1	4.8	0.58	0.30	0.15	1.2	4.1	3.7	2.3	5.9
Na	600	272	7.8	1856	106	102	89	128	707	371	102	1978
Mg	104	71	44	217	51	49	33	66	156	130	86	261
Al	11	12	3	16	140	145	83	183	151	159	89	198
Si	0.0	0.0	0.0	0.0	347	338	249	466	347	338	249	466
P	0.0	0.0	0.0	0.0	70	61	45	109	70	61	45	109
Ca	648	604	518	862	154	146	111	191	802	771	640	1011
Ti	0.14	0.15	0.074	0.19	7.8	7.5	4.6	11	8.0	7.6	4.8	11
V	1.429	1.4	0.44	2.8	1.1	1.0	0.56	1.6	2.5	2.5	1.2	4.2
Cr	0.063	0.010	0.010	0.19	7.4	6.3	4.5	10	7.4	6.3	4.6	10
Mn	3.856	4.0	2.3	5.3	6.1	5.6	3.3	9.5	10	9.2	5.3	15
Fe	26	28	8.8	38	624	579	343	895	650	610	361	927
Co	0.059	0.07	0.03	0.075	0.11	0.11	0.069	0.15	0.17	0.18	0.11	0.22
Ni	0.91	0.91	0.33	1.4	1.6	1.7	0.97	2.2	2.5	2.8	1.4	3.3
Cu	14	15	5.9	18	17	15	10	28	31	32	18	45
Zn	20	21	12	26	19	19	15	22	39	42	29	46
Ga	0.0078	0.0075	0.0040	0.012	0.068	0.066	0.043	0.091	0.076	0.074	0.05	0.097
As	0.24	0.23	0.15	0.34	0.16	0.18	0.079	0.22	0.40	0.44	0.23	0.56
Se	0.38	0.39	0.14	0.59	0.12	0.11	0.053	0.21	0.51	0.53	0.21	0.79
Rb	0.98	0.99	0.29	1.7	0.62	0.62	0.38	0.88	1.60	1.61	0.74	2.5
Sr	2.7	2.7	1.8	3.3	1.9	2.0	1.4	2.5	4.6	4.7	3.5	5.6
Zr	0.081	0.078	0.021	0.11	1.4	1.3	0.72	1.9	1.5	1.4	0.76	2.0
Nb	0.0024	0.0029	0.0010	0.0037	0.073	0.067	0.034	0.11	0.075	0.070	0.035	0.11
Mo	0.39	0.24	0.12	0.91	1.1	0.98	0.59	1.5	1.5	1.19	0.71	2.4
Cd	0.15	0.16	0.05	0.24	0.039	0.041	0.016	0.063	0.19	0.21	0.09	0.27
Sn	0.18	0.16	0.09	0.29	4.0	3.8	2.1	6.1	4.2	4.1	2.2	6.3
Sb	0.87	0.88	0.36	1.3	1.8	1.9	0.81	2.8	2.6	3.0	1.2	3.8
Te	0.0029	0.0026	0.0006	0.0048	0.0033	0.0025	0.00087	0.0049	0.0062	0.0065	0.00244	0.0096
Cs	0.030	0.028	0.015	0.046	0.066	0.072	0.033	0.10	0.097	0.10	0.049	0.14
Ba	4.1	4.2	1.9	5.9	14	14	7.1	21	18	18	9.7	26
La	0.017	0.017	0.0085	0.022	0.36	0.36	0.24	0.49	0.38	0.38	0.25	0.50
Ce	0.035	0.038	0.019	0.045	0.71	0.73	0.48	0.96	0.74	0.78	0.51	1.0
W	0.019	0.016	0.010	0.033	0.053	0.049	0.027	0.089	0.071	0.063	0.038	0.12
Hg	0.0	0.0	0.0	0.0	0.0	0.0	0.0	0.0	0.0	0.0	0.0	0.0
Tl	0.060	0.049	0.024	0.10	0.032	0.026	0.011	0.070	0.092	0.073	0.034	0.16
Pb	0.70	0.69	0.25	1.1	4.4	4.7	2.4	6.3	5.1	5.3	2.9	7.0
Bi	0.017	0.019	0.0074	0.024	0.24	0.21	0.13	0.40	0.26	0.24	0.14	0.42
U	0.0029	0.0029	0.0011	0.0038	0.020	0.020	0.010	0.029	0.023	0.023	0.012	0.032
S	1643	1532	804	2338	0.0	0.0	0.0	0.0	1643	1532	804	2338

PM_{10} - FERRARA												
	Soluble Fraction (ng Nm^{-3})				Insoluble Fraction (ng Nm^{-3})				Total (ng Nm^{-3})			
	average	median	10%	90%	average	median	10%	90%	average	median	10%	90%
Li	0.097	0.094	0.057	0.13	0.084	0.068	0.031	0.16	0.18	0.18	0.11	0.25
Be	0.00084	0.00066	0.00019	0.0018	0.0028	0.0022	0.0011	0.0054	0.0037	0.0030	0.0015	0.0066
B	5.1	4.1	1.4	10	0.58	0.51	0.21	0.92	5.6	4.7	1.7	11
Na	331	248	98	580	83	81	73	93	414	320	178	661
Mg	62	62	33	89	42	38	17	74	104	99	54	160
Al	6.3	4.8	1.8	12	57	48	23	96	63	53	27	108
Si	19	17	8.0	26	3534	3555	2895	3944	3553	3574	2909	3963
P	7.8	7.5	3.6	13	0.0	0.0	0.0	0.0	7.8	7.5	3.6	13
K	241	237	139	358	13	8.4	0.74	29	254	249	145	369
Ca	399	346	218	645	131	110	84	191	529	445	312	792
Ti	0.11	0.10	0.031	0.24	2.5	2.1	0.94	4.4	2.6	2.2	1.0	4.6
V	1.1	0.60	0.21	2.6	0.48	0.38	0.19	0.89	1.6	0.8	0.5	3.4
Cr	0.28	0.24	0.083	0.49	4.0	4.0	2.9	5.0	4.3	4.2	3.0	5.5
Mn	3.9	3.3	1.8	5.8	3.6	3.5	1.5	5.9	7.5	6.5	3.4	12
Fe	28	20	5.5	61	252	234	117	401	280	277	128	438
Co	0.032	0.029	0.013	0.051	0.057	0.054	0.027	0.10	0.089	0.075	0.042	0.14
Ni	0.58	0.48	0.18	1.1	1.1	1.1	0.51	1.5	1.7	1.6	0.70	2.6
Cu	5.0	4.8	2.0	7.8	6.8	6.6	2.9	11	12	11	5.7	18
Zn	29	25	10	48	15	13	10	21	44	39	22	66
Ga	0.0092	0.0073	0.0018	0.020	0.034	0.028	0.012	0.063	0.043	0.036	0.017	0.080
As	0.44	0.41	0.15	0.75	0.14	0.098	0.0096	0.27	0.58	0.55	0.16	1.0
Se	0.50	0.47	0.24	0.71	0.15	0.14	0.0035	0.30	0.64	0.63	0.27	0.97
Rb	0.53	0.50	0.27	0.83	0.147	0.120	0.065	0.27	0.68	0.70	0.37	0.96
Sr	1.2	1.0	0.58	2.0	0.40	0.37	0.24	0.58	1.6	1.3	0.78	2.5
Zr	0.059	0.033	0.0064	0.15	0.43	0.37	0.19	0.78	0.49	0.41	0.25	0.81
Nb	0.0025	0.0011	0.000032	0.0046	0.024	0.020	0.010	0.037	0.026	0.022	0.011	0.041
Mo	0.48	0.41	0.13	0.81	0.39	0.39	0.19	0.61	0.87	0.79	0.31	1.4
Cd	0.16	0.13	0.048	0.30	0.029	0.019	0.0087	0.055	0.19	0.15	0.06	0.36
Sn	0.30	0.23	0.060	0.57	2.2	2.1	0.84	3.7	2.5	2.4	0.91	4.1
Sb	0.74	0.65	0.31	1.2	0.77	0.61	0.29	1.3	1.5	1.4	0.62	2.5
Te	0.0032	0.0028	0.00080	0.0066	0.0042	0.0029	0.00091	0.0094	0.0074	0.0060	0.00036	0.015
Cs	0.016	0.014	0.0065	0.030	0.012	0.0083	0.0047	0.022	0.027	0.023	0.011	0.047
Ba	1.7	1.4	0.77	2.7	3.2	2.7	1.4	5.3	4.9	4.8	2.5	7.9
La	0.0079	0.0069	0.0029	0.013	0.087	0.068	0.038	0.16	0.10	0.074	0.046	0.17
Ce	0.015	0.012	0.0055	0.027	0.15	0.13	0.067	0.26	0.17	0.15	0.074	0.28
W	0.037	0.031	0.010	0.069	0.048	0.038	0.012	0.092	0.085	0.073	0.023	0.16
Hg	0.0	0.0	0.0	0.0	0.0	0.0	0.0	0.0	0.0	0.0	0.0	0.0
Tl	0.018	0.017	0.0053	0.031	0.0018	0.0013	0.000064	0.0045	0.018	0.017	0.0053	0.031
Pb	1.4	1.1	0.34	2.6	3.5	3.6	1.8	5.1	1.4	1.1	0.34	2.6
Bi	0.033	0.025	0.0068	0.064	0.17	0.16	0.070	0.30	3.5	3.7	1.8	5.1
U	0.0027	0.0021	0.00076	0.0053	0.0060	0.0053	0.0028	0.010	0.17	0.16	0.072	0.30
S	0.0	0.0	0.0	0.0	0.0	0.0	0.0	0.0	0.0060	0.0053	0.0028	0.010

$PM_{2.5}$ - FERRARA												
	Soluble Fraction (ng Nm^{-3})				Insoluble Fraction (ng Nm^{-3})				Total (ng Nm^{-3})			
	average	median	10%	90%	average	median	10%	90%	average	median	10%	90%
Li	0.074	0.065	0.037	0.12	0.025	0.019	0.013	0.054	0.10	0.087	0.059	0.14
Be	0.00030	0.00032	0.000048	0.00063	0.00073	0.00064	0.00016	0.0016	0.0010	0.00085	0.00022	0.0021
B	4.7	4.1	1.6	9.9	0.93	0.71	0.30	1.6	5.6	4.6	2.1	11
Na	89	68	35	161	80	80	67	91	169	155	121	239
Mg	16	16	7.4	25	12	11	7.9	17	27	28	16	38
Al	3.1	2.4	1.3	5.2	20	16	7.7	42	23	18	10	45
Si	13	12	10	16	3538	3467	3229	3811	3551	3478	3240	3825
P	3.7	3.5	0.91	6.6	0.0	0.0	0.0	0.0	3.7	3.5	0.91	6.6
K	214	210	118	349	5.4	4.5	1.5	10	220	212	126	358
Ca	86	80	53	130	114	105	87	142	200	180	153	258
Ti	0.062	0.054	0.019	0.13	0.8	0.7	0.3	1.3	0.83	0.77	0.35	1.4
V	1.0	0.59	0.19	2.5	0.24	0.17	0.08	0.47	1.3	0.73	0.33	2.9
Cr	0.22	0.21	0.051	0.40	2.7	2.6	2.3	3.2	3.0	2.8	2.4	3.5
Mn	1.9	1.6	0.65	3.4	1.8	1.4	0.67	3.1	3.7	3.1	1.5	6.4
Fe	16	12	2.5	32	74	69	40	105	90	85	46	129
Co	0.015	0.013	0.0059	0.025	0.022	0.021	0.010	0.032	0.037	0.036	0.018	0.055
Ni	0.46	0.31	0.13	0.92	0.78	0.74	0.45	1.0	1.2	1.1	0.58	2.0
Cu	1.8	1.9	0.73	2.7	2.3	2.1	1.2	3.7	4.1	4.2	2.1	5.8
Zn	22	19	8.2	39	11	10	8.7	14	33	29	17	51
Ga	0.011	0.0083	0.0022	0.024	0.013	0.012	0.0061	0.022	0.024	0.022	0.0093	0.04
As	0.41	0.35	0.11	0.72	0.16	0.16	0.05	0.24	0.56	0.52	0.17	1.0
Se	0.43	0.43	0.19	0.60	0.12	0.12	0.0045	0.26	0.55	0.57	0.18	0.77
Rb	0.49	0.47	0.24	0.82	0.053	0.046	0.034	0.075	0.54	0.52	0.27	0.86
Sr	0.28	0.27	0.17	0.37	0.26	0.24	0.19	0.35	0.54	0.52	0.40	0.74
Zr	0.042	0.022	0.0049	0.076	0.11	0.088	0.043	0.17	0.15	0.12	0.054	0.23
Nb	0.0015	0.0006	0.00012	0.0039	0.0069	0.0061	0.0031	0.011	0.0084	0.0071	0.0031	0.016
Mo	0.41	0.32	0.10	0.73	0.22	0.19	0.10	0.40	0.63	0.52	0.21	1.1
Cd	0.15	0.12	0.049	0.30	0.026	0.020	0.014	0.046	0.18	0.15	0.065	0.34
Sn	0.20	0.13	0.038	0.43	1.2	1.1	0.40	2.1	1.4	1.3	0.45	2.7
Sb	0.62	0.63	0.26	0.96	0.43	0.34	0.15	0.80	1.0	0.97	0.44	1.9
Te	0.0037	0.0035	0.00083	0.0075	0.0028	0.0016	0.0012	0.0058	0.0066	0.0042	0.00014	0.012
Cs	0.014	0.013	0.0060	0.022	0.0033	0.0026	0.0017	0.0059	0.017	0.016	0.0077	0.028
Ba	0.71	0.66	0.38	1.0	0.49	0.22	0.37	1.5	1.2	0.97	0.059	2.2
La	0.0049	0.0046	0.0031	0.0068	0.029	0.025	0.014	0.048	0.034	0.031	0.019	0.053
Ce	0.010	0.0092	0.0059	0.014	0.056	0.049	0.030	0.089	0.066	0.059	0.036	0.10
W	0.028	0.022	0.0071	0.052	0.025	0.022	0.0054	0.051	0.053	0.047	0.014	0.11
Hg	0.0	0.0	0.0	0.0	0.0	0.0	0.0	0.0				
Tl	0.016	0.016	0.0050	0.026	0.00046	0.00037	0.00046	0.0014	0.02	0.016	0.0050	0.026
Pb	1.6	1.4	0.56	2.8	2.6	2.4	1.3	3.5	1.6	1.4	0.56	2.8
Bi	0.030	0.024	0.0058	0.063	0.097	0.076	0.039	0.17	2.6	2.4	1.4	3.6
U	0.0017	0.0013	0.0006	0.0032	0.0023	0.0019	0.0013	0.0036	0.10	0.079	0.040	0.17
S	0.0	0.0	0.0	0.0	0.0	0.0	0.0	0.0	0.0023	0.0019	0.0013	0.0036

F1: assays chemicals preparations

DTT assay:

0.7 mL of PM extract, was incubated in a thermostat bath at 37 ° C, 0.2 mL of phosphate buffer and 0.1 mL of DTT 1 mM are added. At regular intervals corresponding to times 0, 5 ', 10', 15 ', 20', 1 mL of TCA 10% is added. At the end of the addition, 1 mL of each vial of reaction is taken and 2 mL of Tris-buffer and 50 µL of DTNB are added. The compound is stable for about 2 hours. They wait for 5 minutes and continue reading the 412 nm wavelength spectrophotometer.

Preparation of reagents:

-*DTT 1mM*: DTT 1M vial is extracted 100 µL and taken to 100 mL with deionized H_2O (to be stored in the dark).

- *Phosphate Buffer1M a pH7.4:* Prepare 1M monobasic solution by weighing 13.609 g of KH_2PO_4 in 100 mL of H2O and 1M dibasic solution by weighing 17.4 g of K_2HPO_4 in 100 mL of H_2O. 11 mL of 1M KH_2PO_4 solution and 16 mL of 1M K_2HPO_4 are mixed and brought to 100 mL with deionized H_2O.

- *Trichloroacetic Acid 10% w/v:* Weigh 10 g of TCA and bring to 100 ml with deionized water.

-*DTNB 10mM*: Weigh 0.198 g in 50 ml of methanol (keep in the dark).

-*Tris-buffer 0. 4M, pH 8.9, in EDTA 20 mM:* Weigh 4,846 g of Tris and 0.8324 g of EDTA in 100 ml of deionized water. The final pH of buffer solutions is controlled by potentiometry.

DCFH assay

The DCFH solution was prepared by dissolving 4.873 mg of reagent in 5 mL of CH_3CH_2OH in the dark. Then, 20 mL of NaOH 0.01 M is added and the solution is dark at room temperature for 30 minutes. The HRP solution was prepared by dissolving 3.15 mg HRP in 1 L of 25 mM phosphate buffer, and incubated at 37 ° C.

At a rate of 1.5 mL of filter extract, in a thermostated bath at 37 ° C, are added 125 µL of DCFH solution and 5 mL of HRP in buffer solution. After 15 ' minutes at 37 ° C it is possible read the sample with a spectrophotometer at 427 nm (absorption) wavelengths and 530 nm (emission).

The instrument calibration is prepared with standard H_2O_2 solutions at concentrations of 5x 10-6, 1 × 10-7, 2 × 10-7, 5x10-7, 1x10-6, analysed according to the above procedure.

Preparation of reagents:

- *Phosphate Buffer1M :* The KH_2PO_4 1M solution is prepared by weighing 13.609 g of KH_2PO_4 in 100 ml of H_2O and the K_2HPO_4 1 M solution by weighing 17.4 g of K_2HPO_4 in 100 ml of H_2O. 11 mL of 1M KH_2PO_4 solution and 16 mL of 1M K_2HPO_4 are mixed and brought to 100 mL with H_2O. From the 1M mix solution, 25 mL was taken and taken to 1 L with deionized water.

- *NaOH 0.01 M*: Weigh 2 grams of NaOH in pastes and dissolve in 500 mL of deionized water. From this solution, 500 µl of this solution areis brought to 50 ml volume with deionized water.

Acid Ascorbic Assay:

In a 37 ° C thermostat bath, 2.4 ml of PM extract solution is added 0.3 ml of phosphate buffer 0.5 mmol and 100 µL of ascorbic acid. The sample is read by a UV spectrophotometer at a wavelength of 265 nm at the time the reagent is added (time 0 '), and in the following time: 5', 10 ', 15', 20 ', measuring the depletion in the ascorbic acid time.

Preparation of reagents:

- *Ascorbic Acid 2 mM*: Weigh 0.0352 g of reagent and bring to 100 ml with deionized H_2O.

-*Phosphate Buffer 0. 5mM:* From 1 M phosphate buffer (prepared according to the procedure described in the DTT method), 50 µL are taken and brought to 100 mL with H_2O.

F2: Chemical analysis of soluble fraction

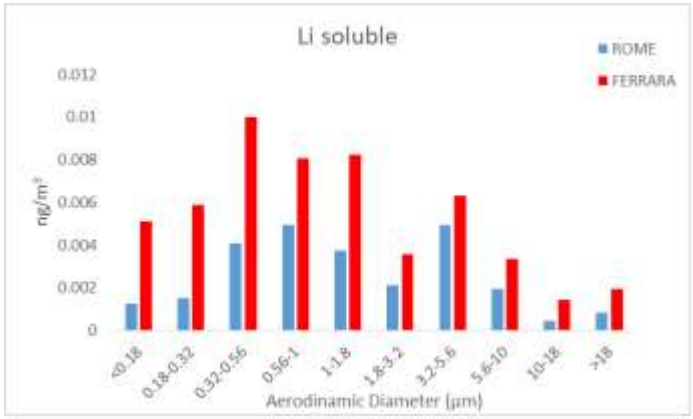

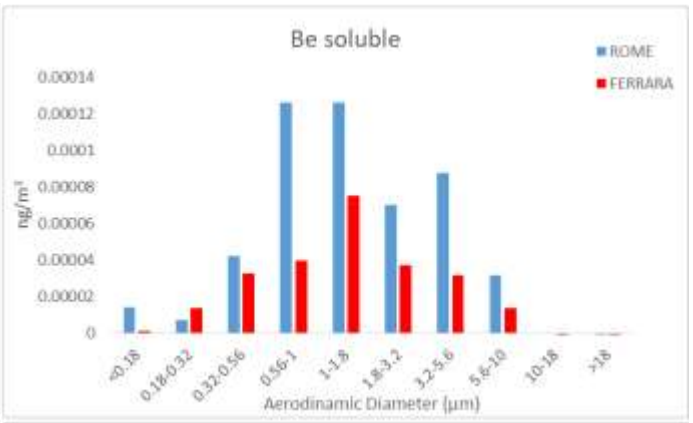

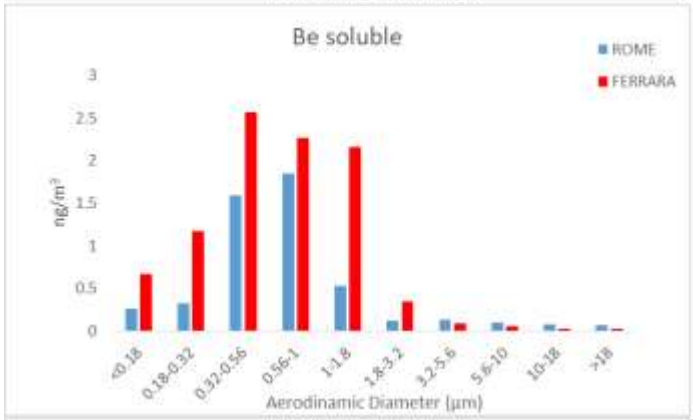

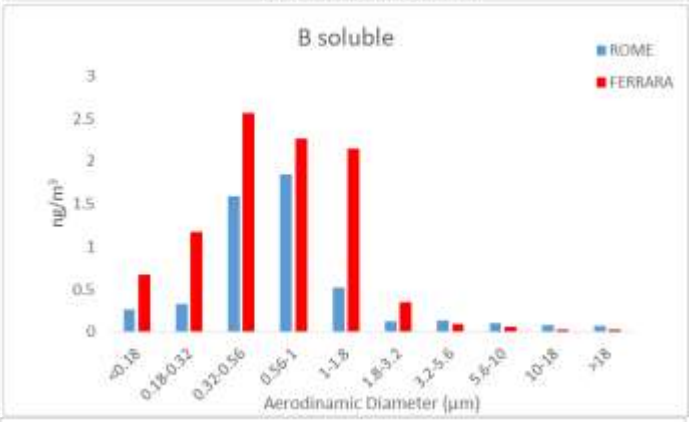

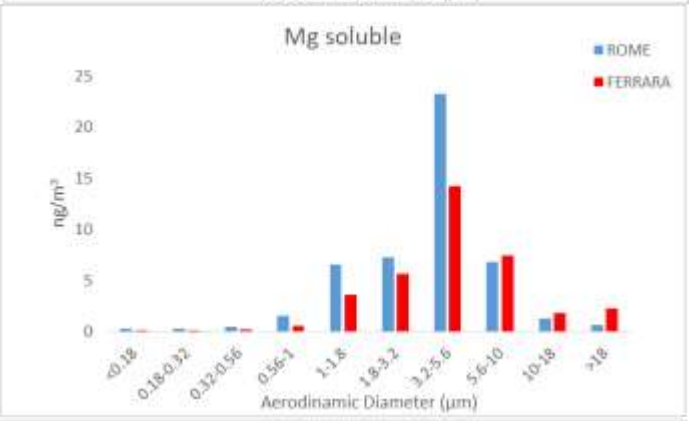

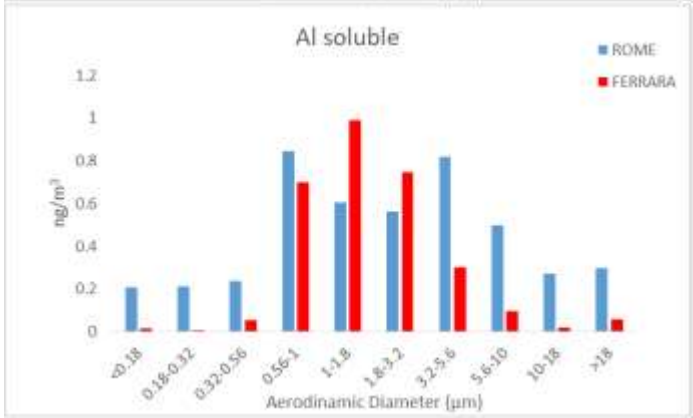

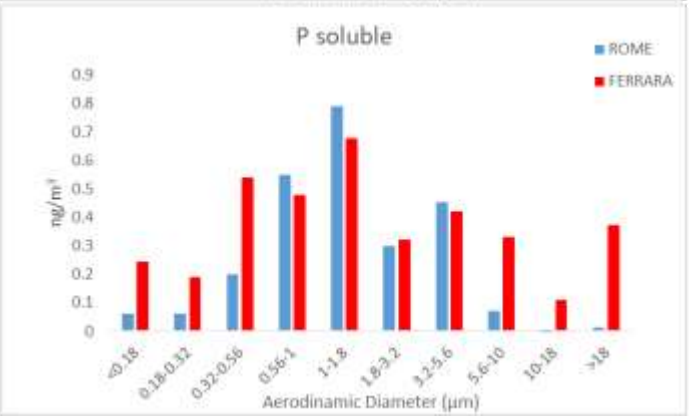

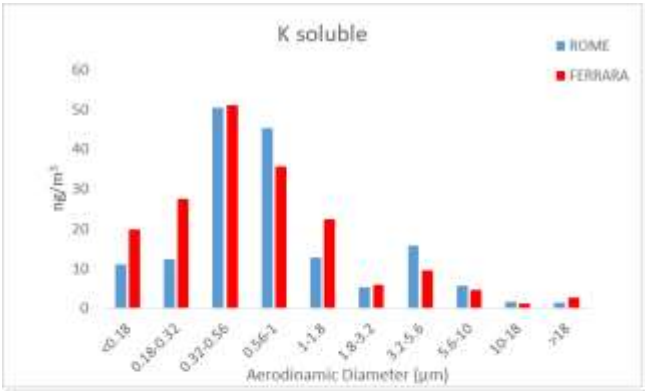
K soluble
ROME
FERRARA
ng/m³
Aerodinamic Diameter (µm)

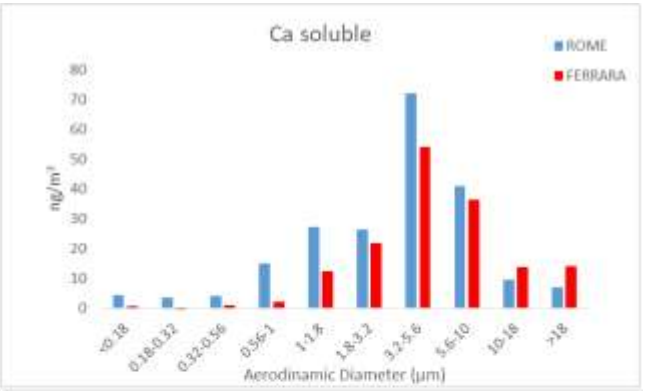
Ca soluble
ROME
FERRARA
ng/m³
Aerodinamic Diameter (µm)

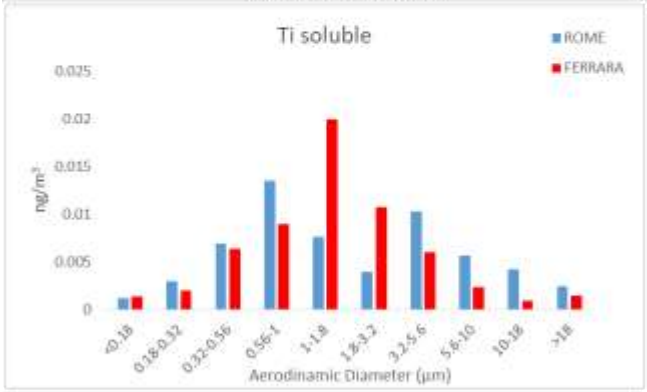
Ti soluble
ROME
FERRARA
ng/m³
Aerodinamic Diameter (µm)

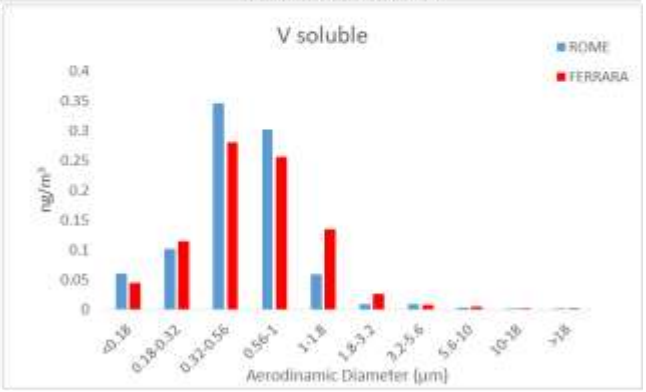
V soluble
ROME
FERRARA
ng/m³
Aerodinamic Diameter (µm)

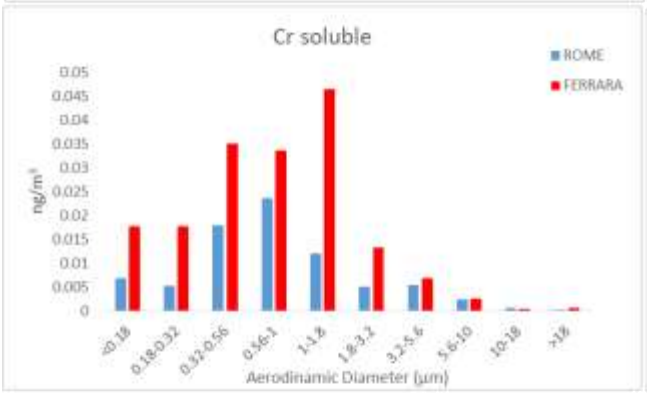
Cr soluble
ROME
FERRARA
ng/m³
Aerodinamic Diameter (µm)

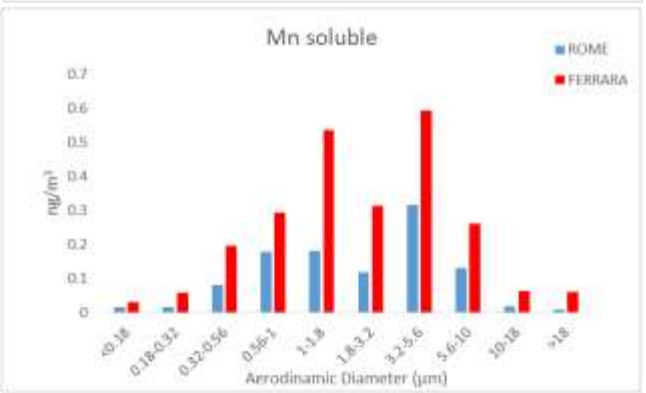
Mn soluble
ROME
FERRARA
ng/m³
Aerodinamic Diameter (µm)

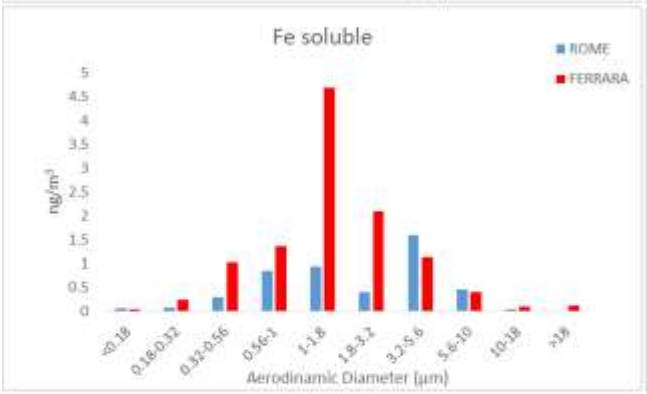
Fe soluble
ROME
FERRARA
ng/m³
Aerodinamic Diameter (µm)

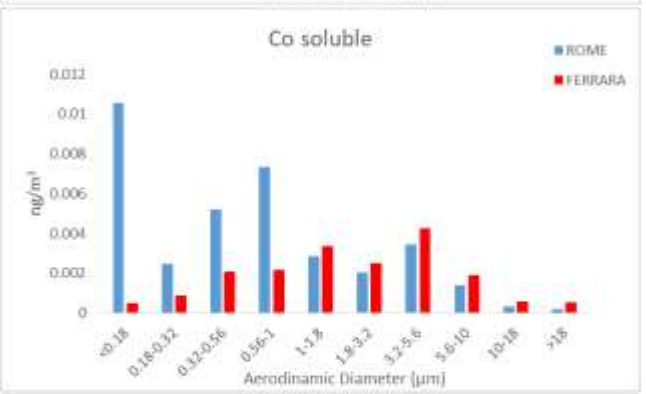
Co soluble
ROME
FERRARA
ng/m³
Aerodinamic Diameter (µm)

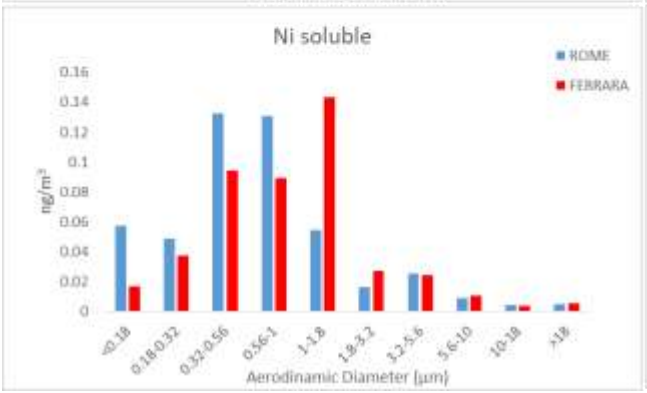
Ni soluble
ROME
FERRARA
ng/m³
Aerodinamic Diameter (µm)

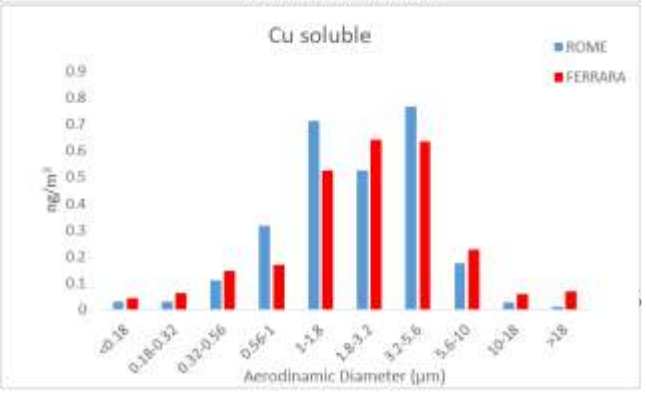
Cu soluble
ROME
FERRARA
ng/m³
Aerodinamic Diameter (µm)

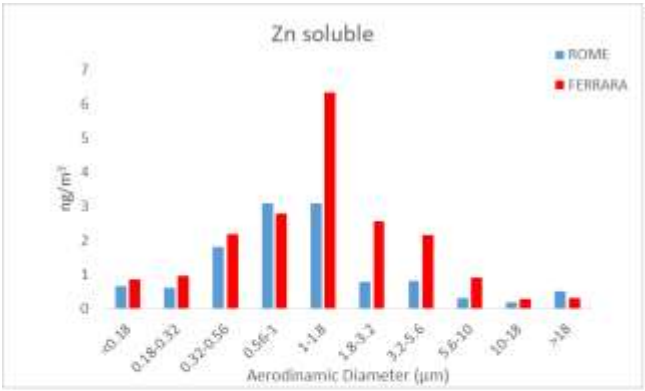
Zn soluble
ROME
FERRARA
ng/m³
Aerodinamic Diameter (µm)

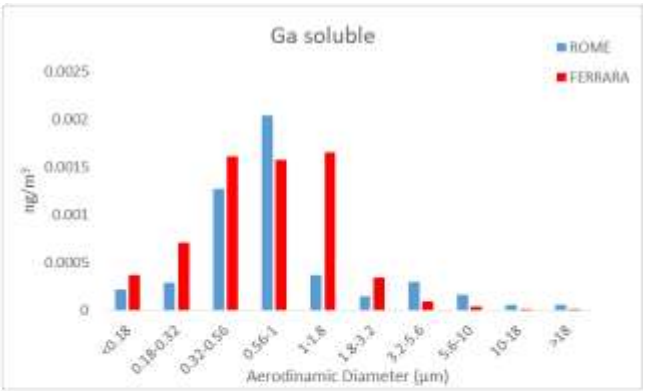
Ga soluble
ROME
FERRARA
ng/m³
Aerodinamic Diameter (µm)

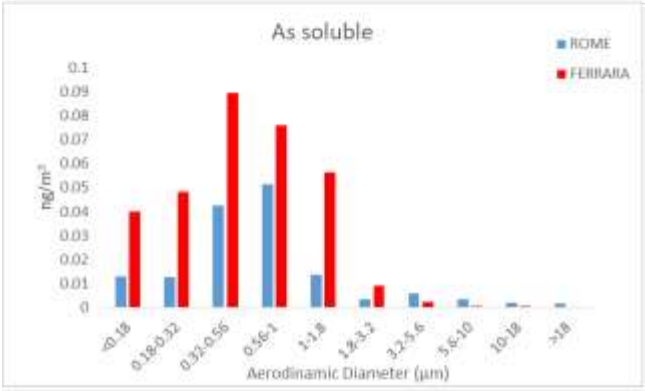
As soluble
ROME
FERRARA
ng/m³
Aerodinamic Diameter (µm)

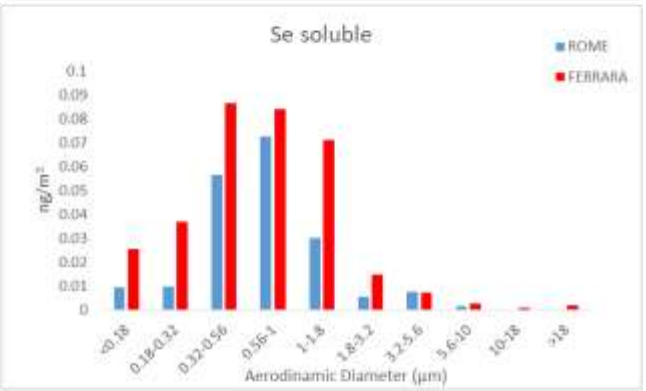
Se soluble
ROME
FERRARA
ng/m³
Aerodinamic Diameter (µm)

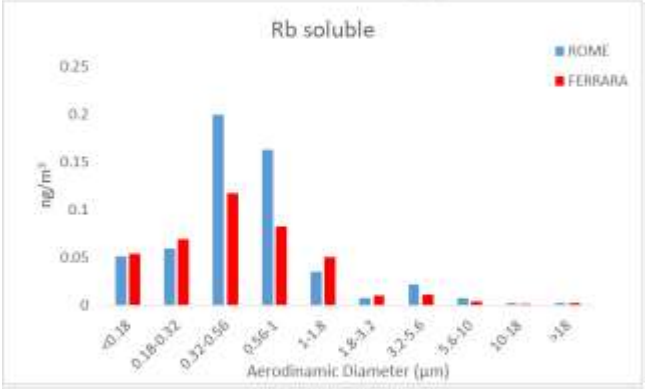
Rb soluble
ROME
FERRARA
ng/m³
Aerodinamic Diameter (µm)

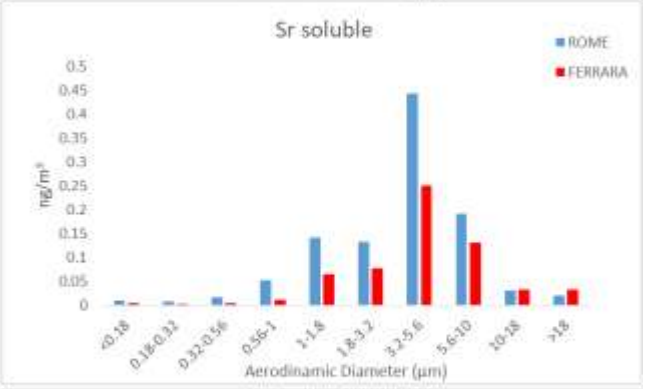
Sr soluble
ROME
FERRARA
ng/m³
Aerodinamic Diameter (µm)

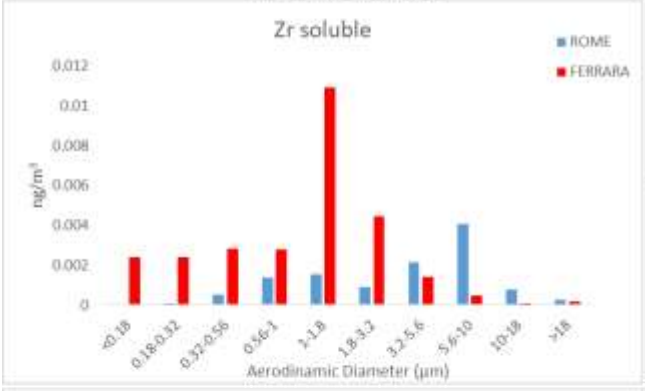
Zr soluble
ROME
FERRARA
ng/m³
Aerodinamic Diameter (µm)

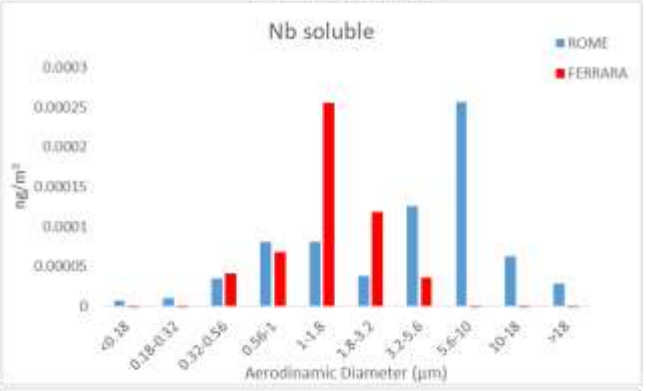
Nb soluble
ROME
FERRARA
ng/m³
Aerodinamic Diameter (µm)

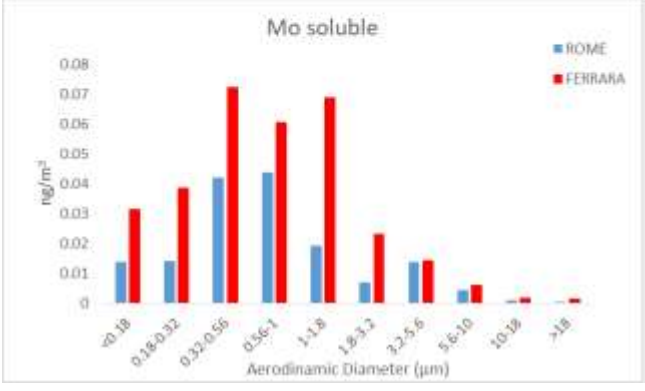
Mo soluble
ROME
FERRARA
ng/m³
Aerodinamic Diameter (µm)

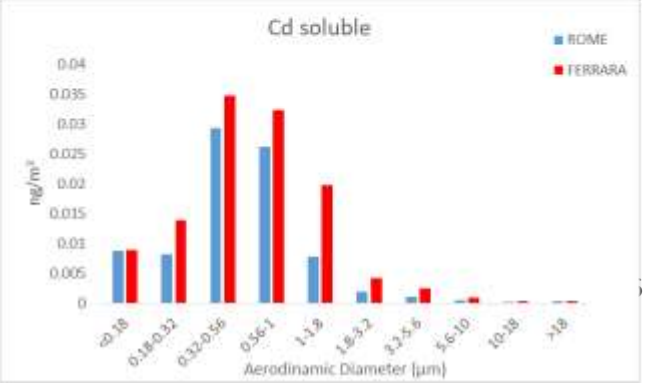
Cd soluble
ROME
FERRARA
ng/m³
Aerodinamic Diameter (µm)

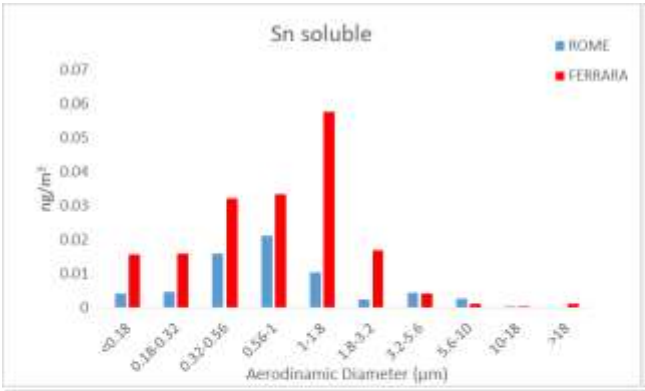
Sn soluble
ROME
FERRARA
ng/m³
0.07
0.06
0.05
0.04
0.03
0.02
0.01
0
<0.18
0.18-0.32
0.32-0.56
0.56-1
1-1.8
1.8-3.2
3.2-5.6
5.6-10
10-18
>18
Aerodinamic Diameter (µm)

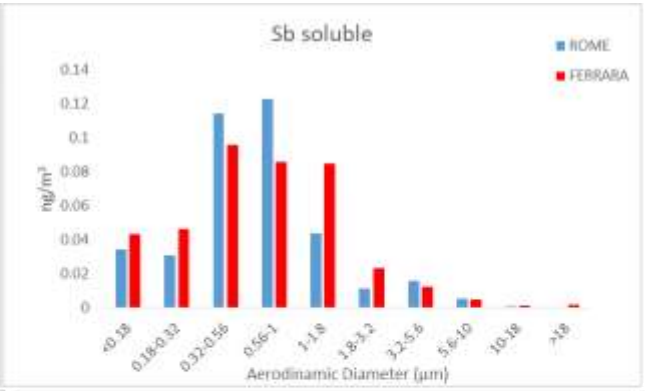
Sb soluble
ROME
FERRARA
ng/m³
0.14
0.12
0.1
0.08
0.06
0.04
0.02
0
<0.18
0.18-0.32
0.32-0.56
0.56-1
1-1.8
1.8-3.2
3.2-5.6
5.6-10
10-18
>18
Aerodinamic Diameter (µm)

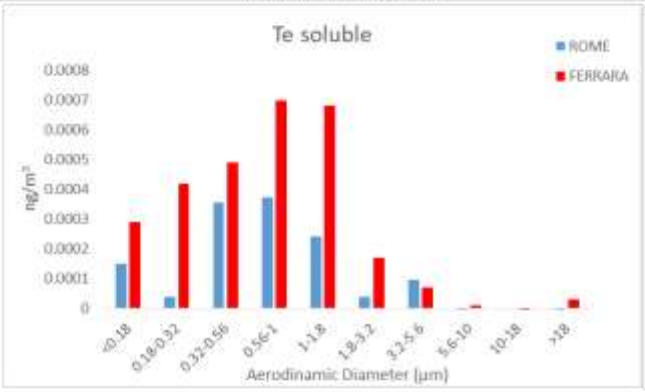
Te soluble
ROME
FERRARA
ng/m³
0.0008
0.0007
0.0006
0.0005
0.0004
0.0003
0.0002
0.0001
0
<0.18
0.18-0.32
0.32-0.56
0.56-1
1-1.8
1.8-3.2
3.2-5.6
5.6-10
10-18
>18
Aerodinamic Diameter (µm)

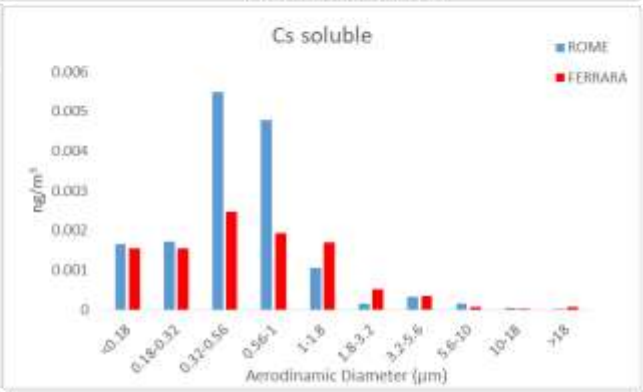
Cs soluble
ROME
FERRARA
ng/m³
0.006
0.005
0.004
0.003
0.002
0.001
0
<0.18
0.18-0.32
0.32-0.56
0.56-1
1-1.8
1.8-3.2
3.2-5.6
5.6-10
10-18
>18
Aerodinamic Diameter (µm)

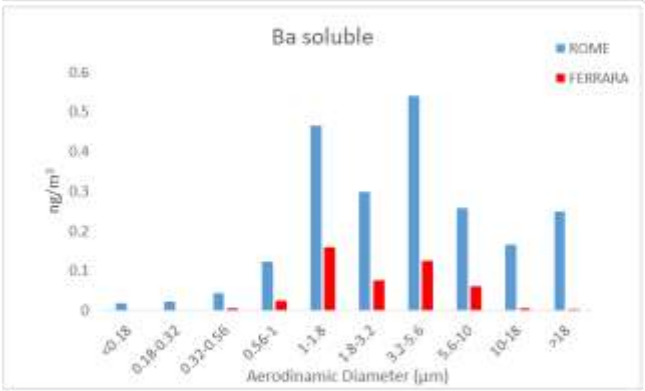
Ba soluble
ROME
FERRARA
ng/m³
0.6
0.5
0.4
0.3
0.2
0.1
0
<0.18
0.18-0.32
0.32-0.56
0.56-1
1-1.8
1.8-3.2
3.2-5.6
5.6-10
10-18
>18
Aerodinamic Diameter (µm)

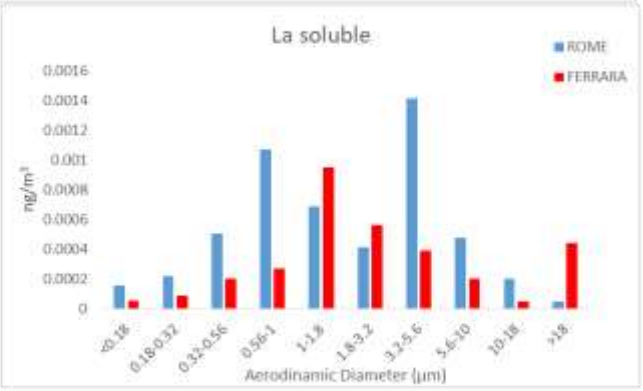
La soluble
ROME
FERRARA
ng/m³
0.0016
0.0014
0.0012
0.001
0.0008
0.0006
0.0004
0.0002
0
<0.18
0.18-0.32
0.32-0.56
0.56-1
1-1.8
1.8-3.2
3.2-5.6
5.6-10
10-18
>18
Aerodinamic Diameter (µm)

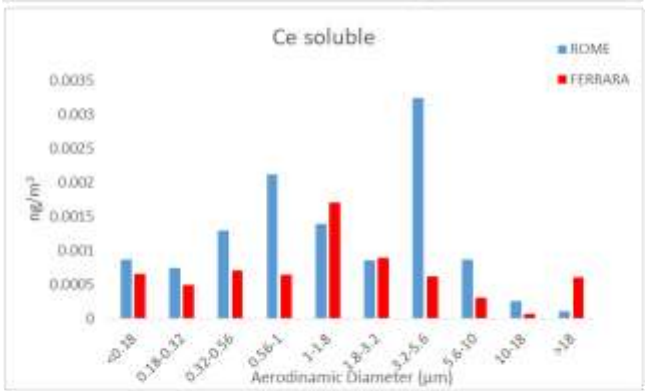
Ce soluble
ROME
FERRARA
ng/m³
0.0035
0.003
0.0025
0.002
0.0015
0.001
0.0005
0
<0.18
0.18-0.32
0.32-0.56
0.56-1
1-1.8
1.8-3.2
3.2-5.6
5.6-10
10-18
>18
Aerodinamic Diameter (µm)

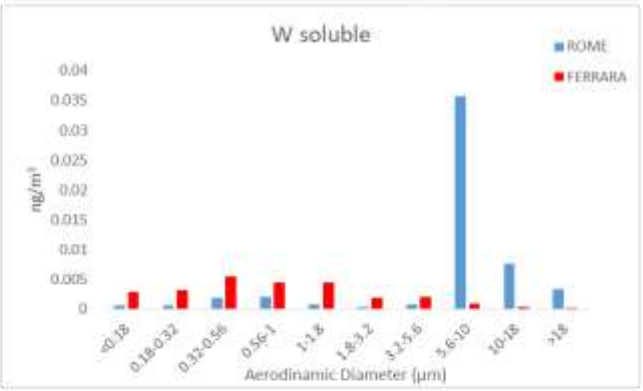
W soluble
ROME
FERRARA
ng/m³
0.04
0.035
0.03
0.025
0.02
0.015
0.01
0.005
0
<0.18
0.18-0.32
0.32-0.56
0.56-1
1-1.8
1.8-3.2
3.2-5.6
5.6-10
10-18
>18
Aerodinamic Diameter (µm)

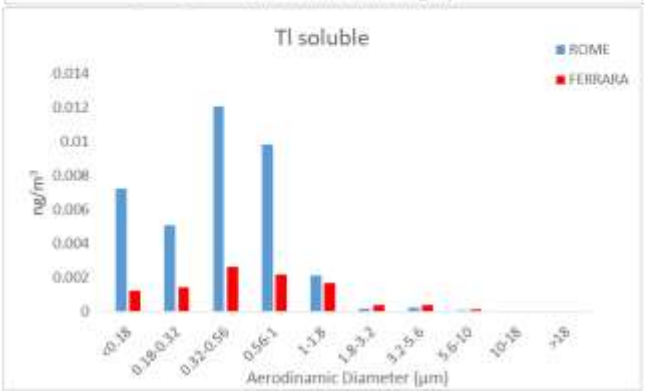
Tl soluble
ROME
FERRARA
ng/m³
0.014
0.012
0.01
0.008
0.006
0.004
0.002
0
<0.18
0.18-0.32
0.32-0.56
0.56-1
1-1.8
1.8-3.2
3.2-5.6
5.6-10
10-18
>18
Aerodinamic Diameter (µm)

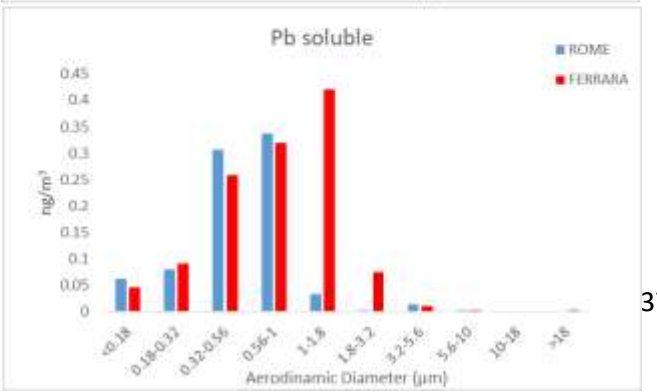
Pb soluble
ROME
FERRARA
ng/m³
0.45
0.4
0.35
0.3
0.25
0.2
0.15
0.1
0.05
0
<0.18
0.18-0.32
0.32-0.56
0.56-1
1-1.8
1.8-3.2
3.2-5.6
5.6-10
10-18
>18
Aerodinamic Diameter (µm)

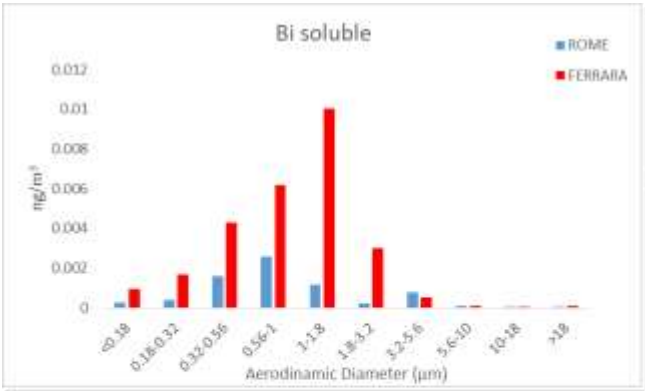
Bi soluble
ROME
FERRARA
ng/m³
0.012
0.01
0.008
0.006
0.004
0.002
0
<0.18
0.18-0.32
0.32-0.56
0.56-1
1-1.8
1.8-3.2
3.2-5.6
5.6-10
10-18
>18
Aerodinamic Diameter (µm)

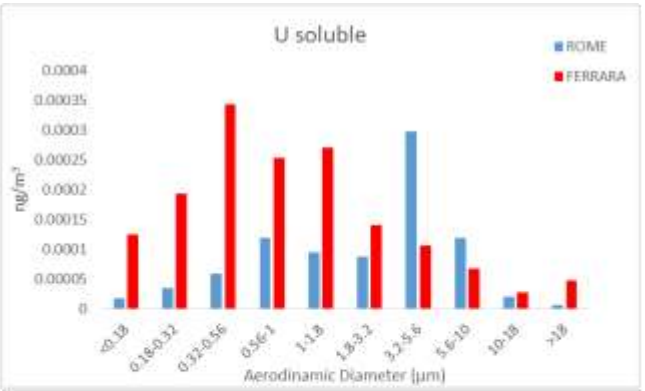
U soluble
ROME
FERRARA
ng/m³
0.0004
0.00035
0.0003
0.00025
0.0002
0.00015
0.0001
0.00005
0
<0.18
0.18-0.32
0.32-0.56
0.56-1
1-1.8
1.8-3.2
3.2-5.6
5.6-10
10-18
>18
Aerodinamic Diameter (µm)

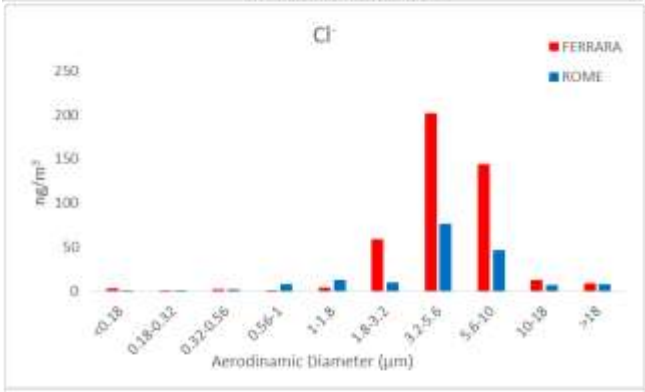
Cl⁻
FERRARA
ROME
ng/m³
250
200
150
100
50
0
<0.18
0.18-0.32
0.32-0.56
0.56-1
1-1.8
1.8-3.2
3.2-5.6
5.6-10
10-18
>18
Aerodinamic Diameter (µm)

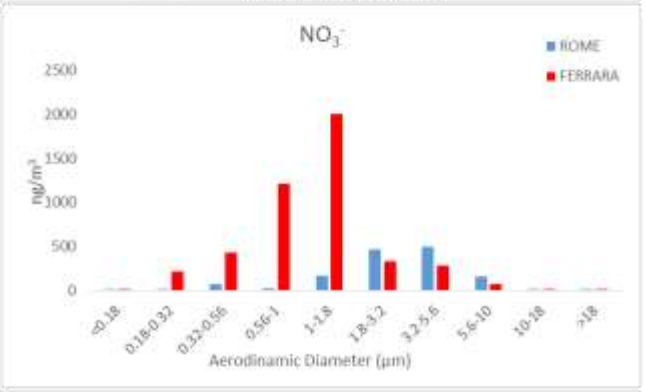
NO3⁻
ROME
FERRARA
ng/m³
2500
2000
1500
1000
500
0
<0.18
0.18-0.32
0.32-0.56
0.56-1
1-1.8
1.8-3.2
3.2-5.6
5.6-10
10-18
>18
Aerodinamic Diameter (µm)

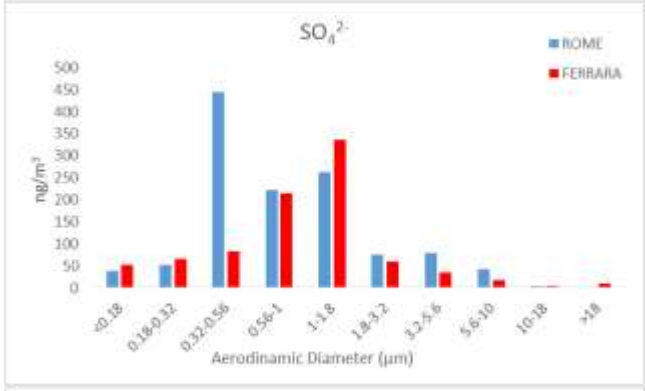
SO4 2-
ROME
FERRARA
ng/m³
500
450
400
350
300
250
200
150
100
50
0
<0.18
0.18-0.32
0.32-0.56
0.56-1
1-1.8
1.8-3.2
3.2-5.6
5.6-10
10-18
>18
Aerodinamic Diameter (µm)

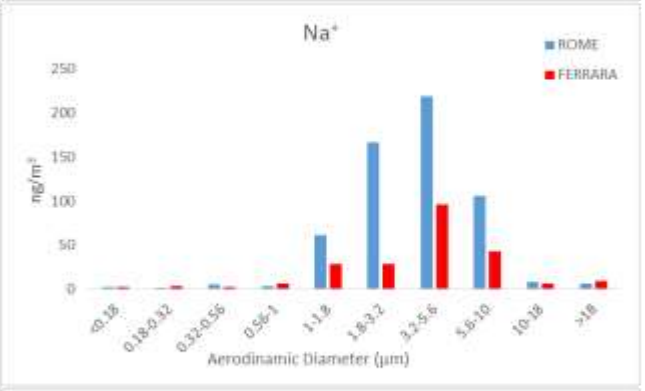
Na+
ROME
FERRARA
ng/m³
250
200
150
100
50
0
<0.18
0.18-0.32
0.32-0.56
0.56-1
1-1.8
1.8-3.2
3.2-5.6
5.6-10
10-18
>18
Aerodinamic Diameter (µm)

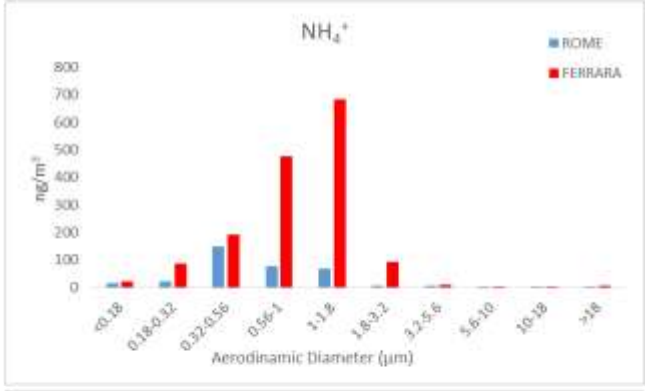
NH4+
ROME
FERRARA
ng/m³
800
700
600
500
400
300
200
100
0
<0.18
0.18-0.32
0.32-0.56
0.56-1
1-1.8
1.8-3.2
3.2-5.6
5.6-10
10-18
>18
Aerodinamic Diameter (µm)

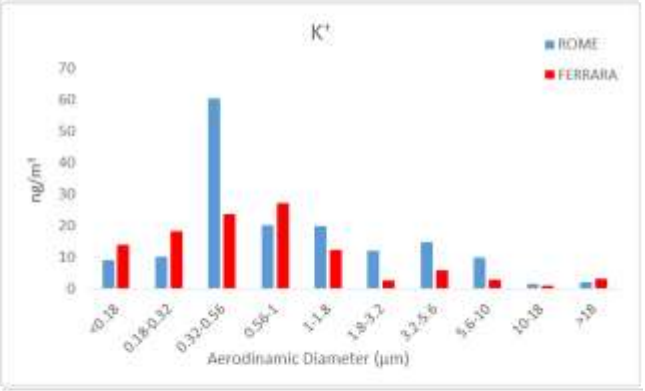
K+
ROME
FERRARA
ng/m³
70
60
50
40
30
20
10
0
<0.18
0.18-0.32
0.32-0.56
0.56-1
1-1.8
1.8-3.2
3.2-5.6
5.6-10
10-18
>18
Aerodinamic Diameter (µm)

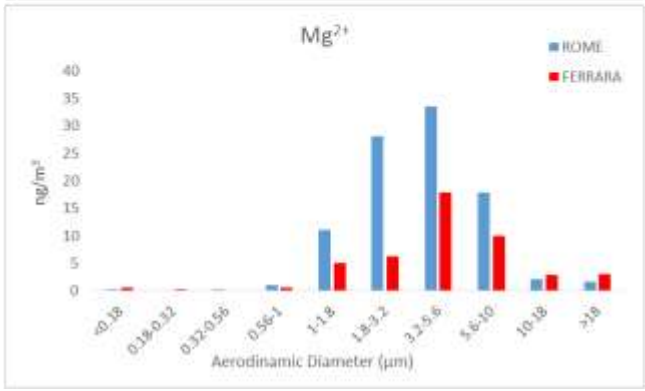
Mg2+
ROME
FERRARA
ng/m³
40
35
30
25
20
15
10
5
0
<0.18
0.18-0.32
0.32-0.56
0.56-1
1-1.8
1.8-3.2
3.2-5.6
5.6-10
10-18
>18
Aerodinamic Diameter (µm)

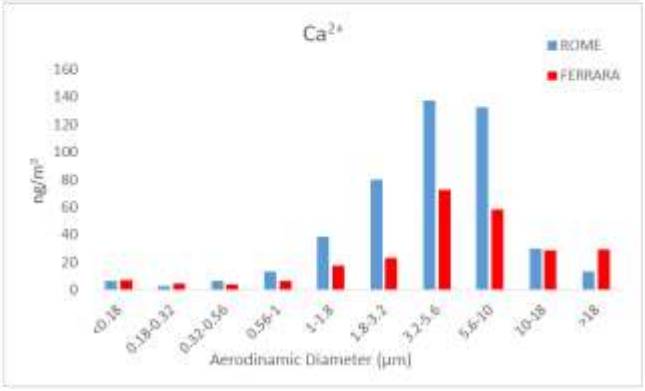
Ca2+
ROME
FERRARA
ng/m³
160
140
120
100
80
60
40
20
0
<0.18
0.18-0.32
0.32-0.56
0.56-1
1-1.8
1.8-3.2
3.2-5.6
5.6-10
10-18
>18
Aerodinamic Diameter (µm)

F3: CHEMICAL ANALYSIS OF INSOLUBLE FRACTION

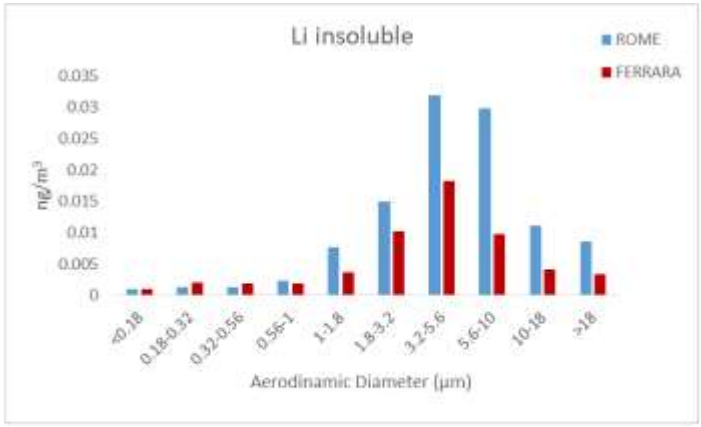

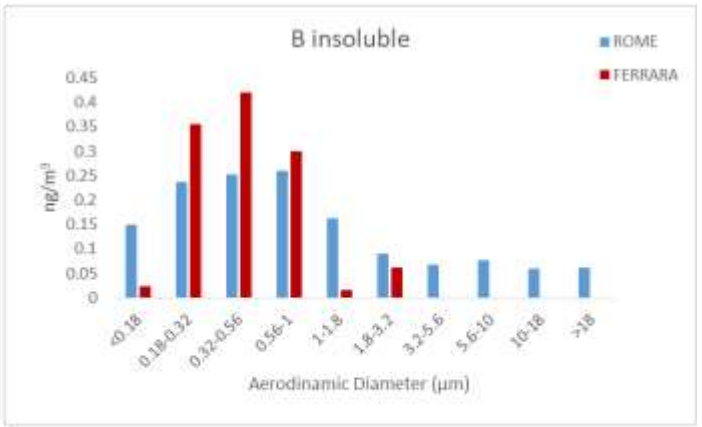

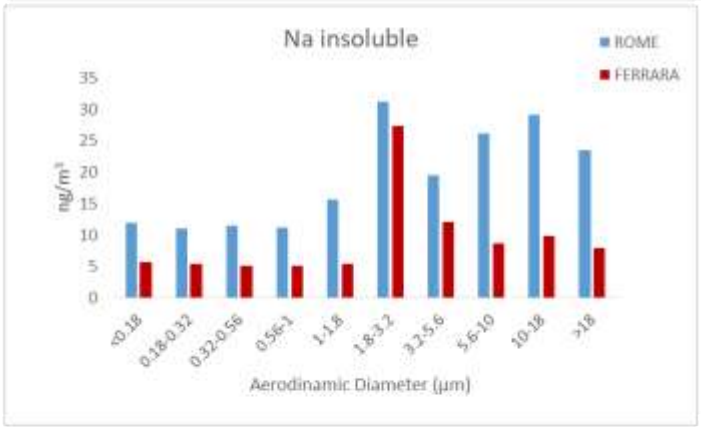

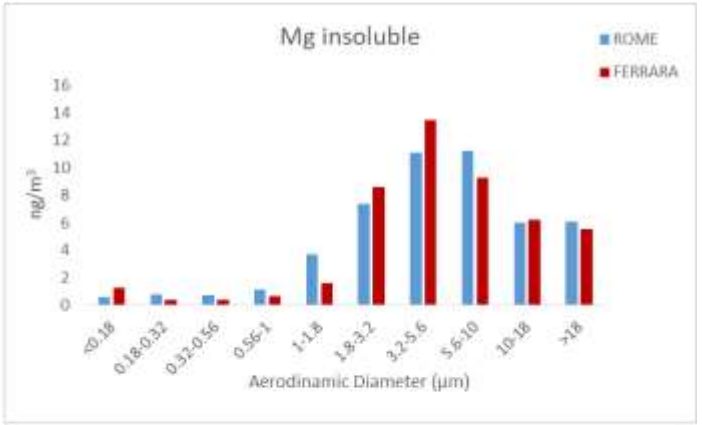

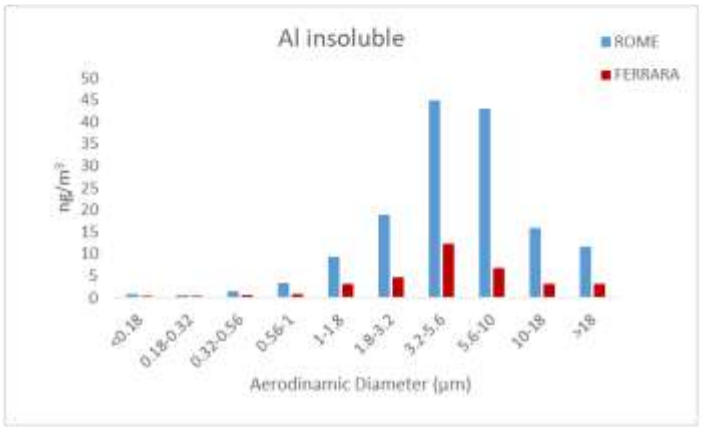

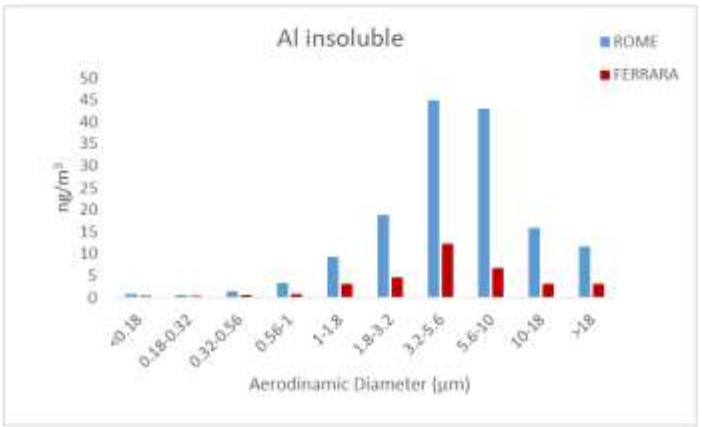

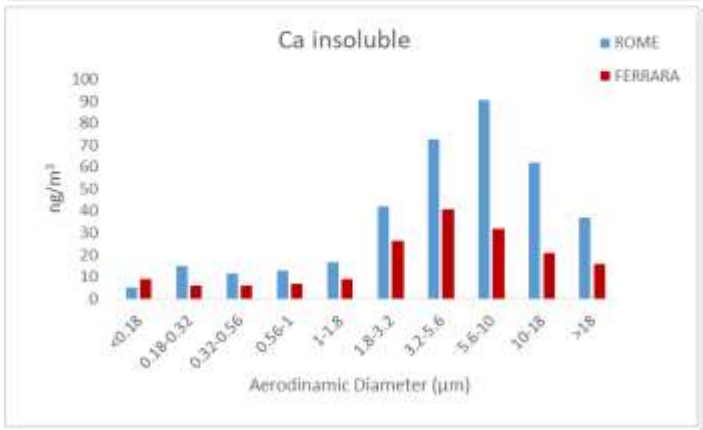

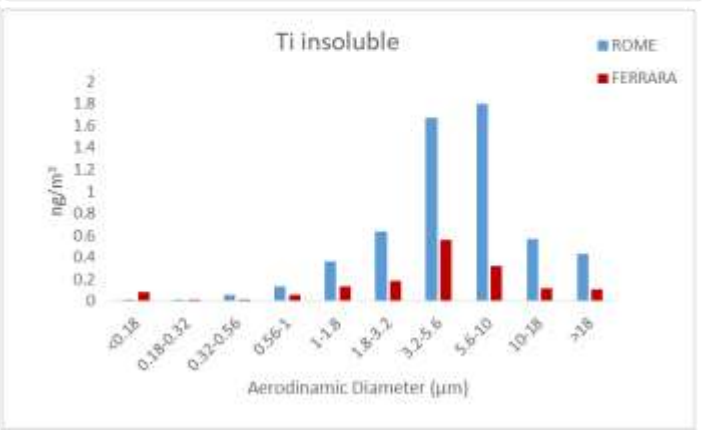

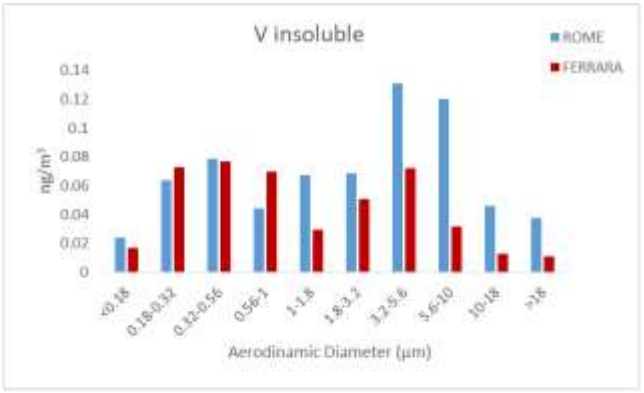
V insoluble
ROME
FERRARA
ng/m³
0.14
0.12
0.1
0.08
0.06
0.04
0.02
0
<0.18
0.18-0.32
0.32-0.56
0.56-1
1-1.8
1.8-3.2
3.2-5.6
5.6-10
10-18
>18
Aerodinamic Diameter (µm)

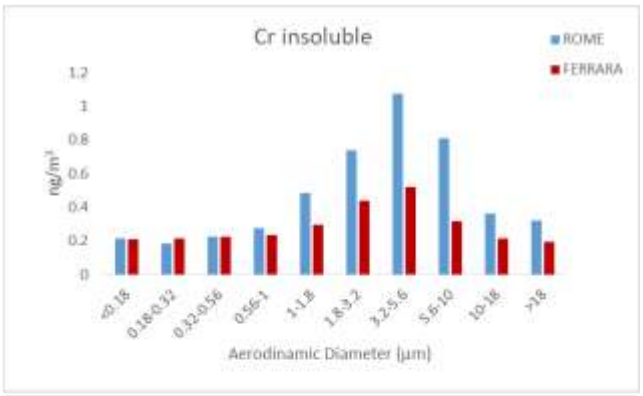
Cr insoluble
ROME
FERRARA
ng/m³
1.2
1
0.8
0.6
0.4
0.2
0
<0.18
0.18-0.32
0.32-0.56
0.56-1
1-1.8
1.8-3.2
3.2-5.6
5.6-10
10-18
>18
Aerodinamic Diameter (µm)

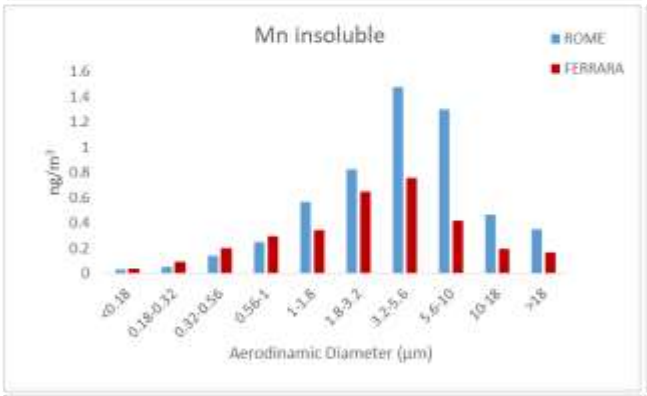
Mn insoluble
ROME
FERRARA
ng/m³
1.6
1.4
1.2
1
0.8
0.6
0.4
0.2
0
<0.18
0.18-0.32
0.32-0.56
0.56-1
1-1.8
1.8-3.2
3.2-5.6
5.6-10
10-18
>18
Aerodinamic Diameter (µm)

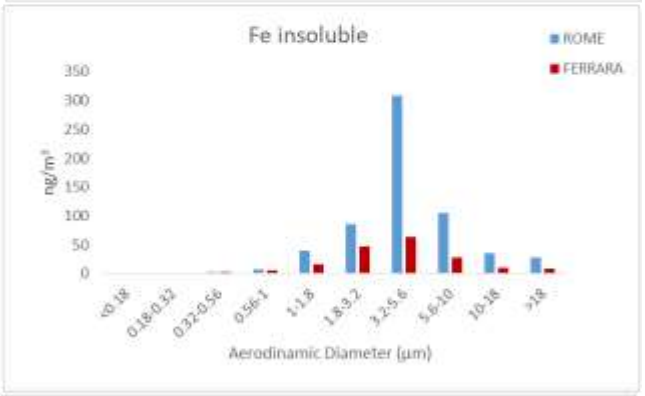
Fe insoluble
ROME
FERRARA
ng/m³
350
300
250
200
150
100
50
0
<0.18
0.18-0.32
0.32-0.56
0.56-1
1-1.8
1.8-3.2
3.2-5.6
5.6-10
10-18
>18
Aerodinamic Diameter (µm)

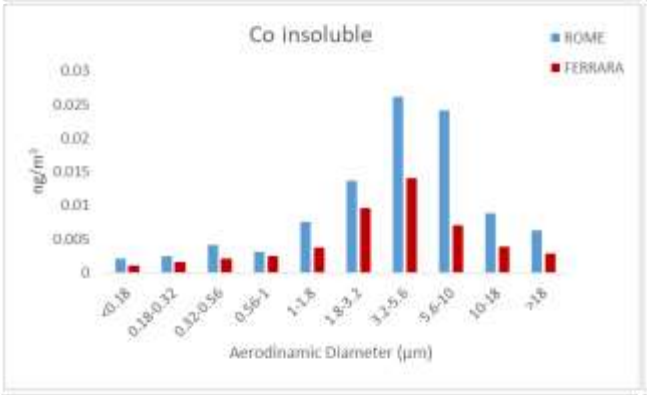
Co insoluble
ROME
FERRARA
ng/m³
0.03
0.025
0.02
0.015
0.01
0.005
0
<0.18
0.18-0.32
0.32-0.56
0.56-1
1-1.8
1.8-3.2
3.2-5.6
5.6-10
10-18
>18
Aerodinamic Diameter (µm)

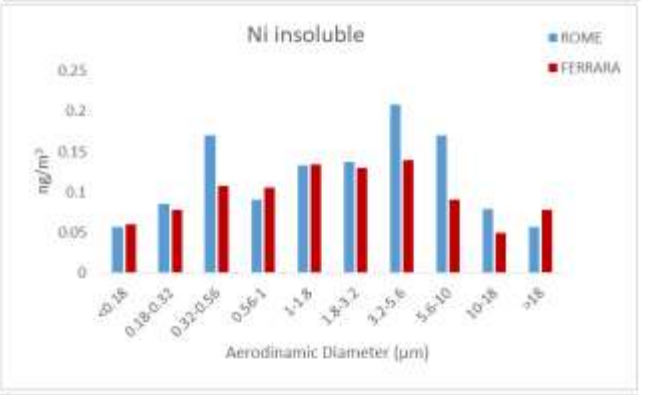
Ni insoluble
ROME
FERRARA
ng/m³
0.25
0.2
0.15
0.1
0.05
0
<0.18
0.18-0.32
0.32-0.56
0.56-1
1-1.8
1.8-3.2
3.2-5.6
5.6-10
10-18
>18
Aerodinamic Diameter (µm)

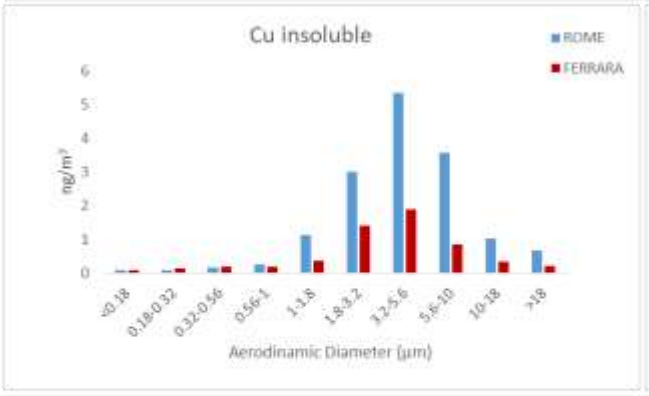
Cu insoluble
ROME
FERRARA
ng/m³
6
5
4
3
2
1
0
<0.18
0.18-0.32
0.32-0.56
0.56-1
1-1.8
1.8-3.2
3.2-5.6
5.6-10
10-18
>18
Aerodinamic Diameter (µm)

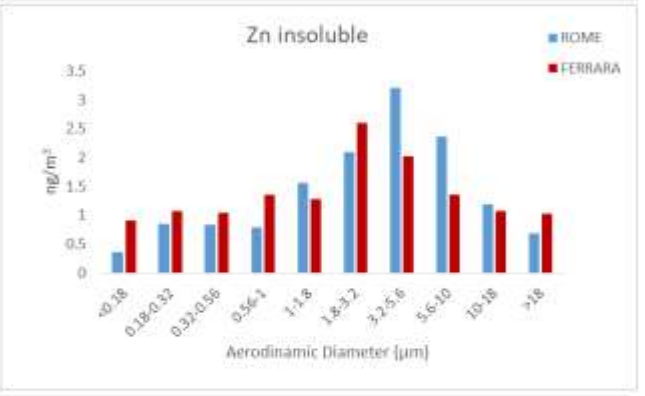
Zn insoluble
ROME
FERRARA
ng/m³
3.5
3
2.5
2
1.5
1
0.5
0
<0.18
0.18-0.32
0.32-0.56
0.56-1
1-1.8
1.8-3.2
3.2-5.6
5.6-10
10-18
>18
Aerodinamic Diameter (µm)

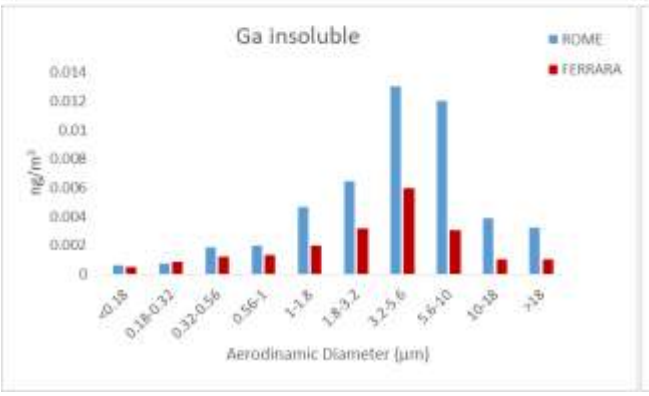
Ga insoluble
ROME
FERRARA
ng/m³
0.014
0.012
0.01
0.008
0.006
0.004
0.002
0
<0.18
0.18-0.32
0.32-0.56
0.56-1
1-1.8
1.8-3.2
3.2-5.6
5.6-10
10-18
>18
Aerodinamic Diameter (µm)

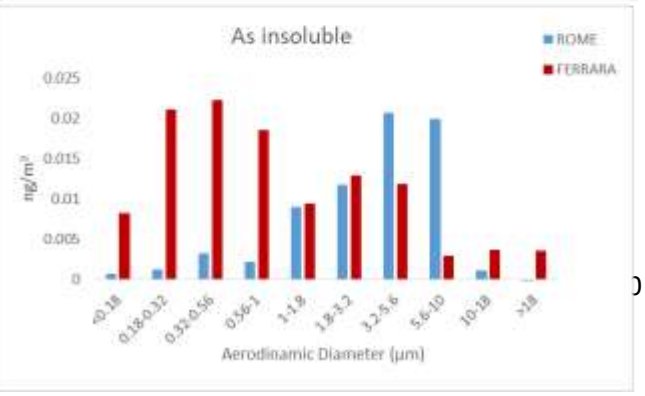
As insoluble
ROME
FERRARA
ng/m³
0.025
0.02
0.015
0.01
0.005
0
<0.18
0.18-0.32
0.32-0.56
0.56-1
1-1.8
1.8-3.2
3.2-5.6
5.6-10
10-18
>18
Aerodinamic Diameter (µm)

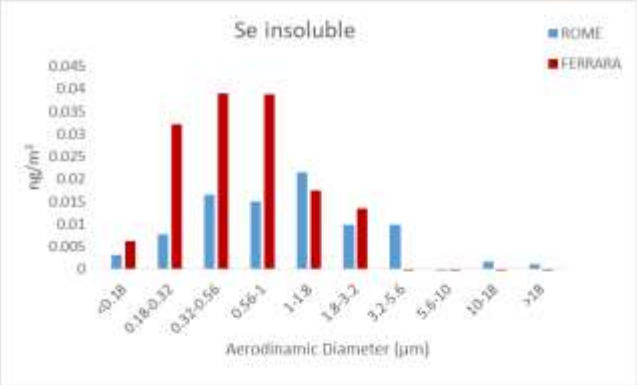
Se insoluble
ROME
FERRARA
ng/m³
0.045
0.04
0.035
0.03
0.025
0.02
0.015
0.01
0.005
0
<0.18
0.18-0.32
0.32-0.56
0.56-1
1-1.8
1.8-3.2
3.2-5.6
5.6-10
10-18
>18
Aerodinamic Diameter (µm)

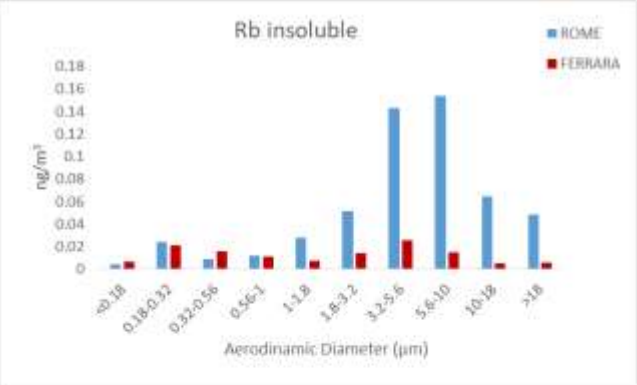
Rb insoluble
ROME
FERRARA
ng/m³
0.18
0.16
0.14
0.12
0.1
0.08
0.06
0.04
0.02
0
<0.18
0.18-0.32
0.32-0.56
0.56-1
1-1.8
1.8-3.2
3.2-5.6
5.6-10
10-18
>18
Aerodinamic Diameter (µm)

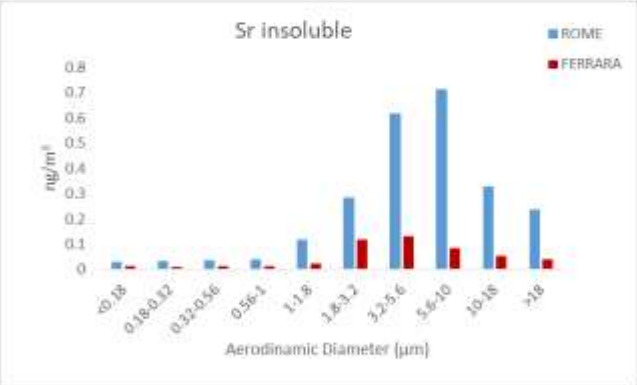
Sr insoluble
ROME
FERRARA
ng/m³
0.8
0.7
0.6
0.5
0.4
0.3
0.2
0.1
0
<0.18
0.18-0.32
0.32-0.56
0.56-1
1-1.8
1.8-3.2
3.2-5.6
5.6-10
10-18
>18
Aerodinamic Diameter (µm)

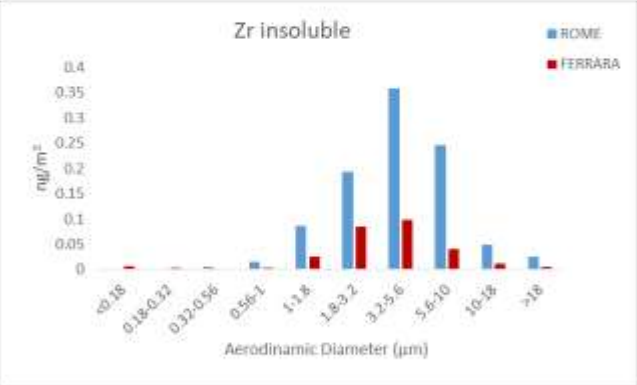
Zr insoluble
ROME
FERRARA
ng/m³
0.4
0.35
0.3
0.25
0.2
0.15
0.1
0.05
0
<0.18
0.18-0.32
0.32-0.56
0.56-1
1-1.8
1.8-3.2
3.2-5.6
5.6-10
10-18
>18
Aerodinamic Diameter (µm)

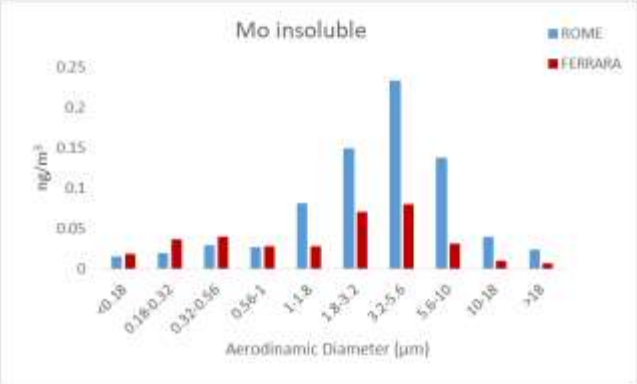
Mo insoluble
ROME
FERRARA
ng/m³
0.25
0.2
0.15
0.1
0.05
0
<0.18
0.18-0.32
0.32-0.56
0.56-1
1-1.8
1.8-3.2
3.2-5.6
5.6-10
10-18
>18
Aerodinamic Diameter (µm)

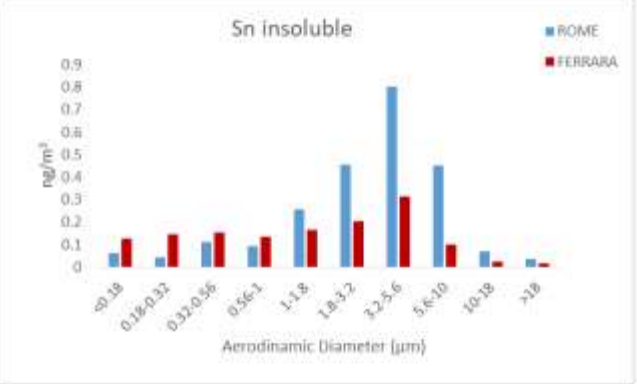
Sn insoluble
ROME
FERRARA
ng/m³
0.9
0.8
0.7
0.6
0.5
0.4
0.3
0.2
0.1
0
<0.18
0.18-0.32
0.32-0.56
0.56-1
1-1.8
1.8-3.2
3.2-5.6
5.6-10
10-18
>18
Aerodinamic Diameter (µm)

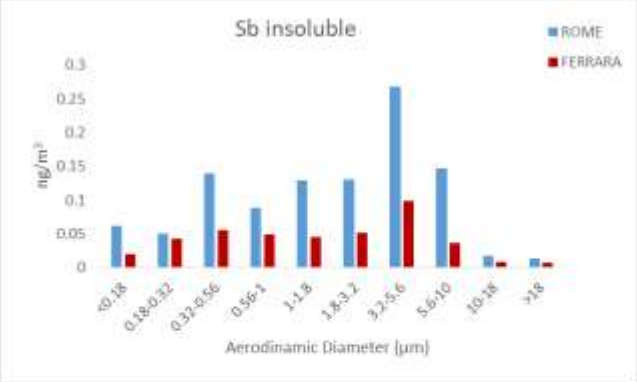
Sb insoluble
ROME
FERRARA
ng/m³
0.3
0.25
0.2
0.15
0.1
0.05
0
<0.18
0.18-0.32
0.32-0.56
0.56-1
1-1.8
1.8-3.2
3.2-5.6
5.6-10
10-18
>18
Aerodinamic Diameter (µm)

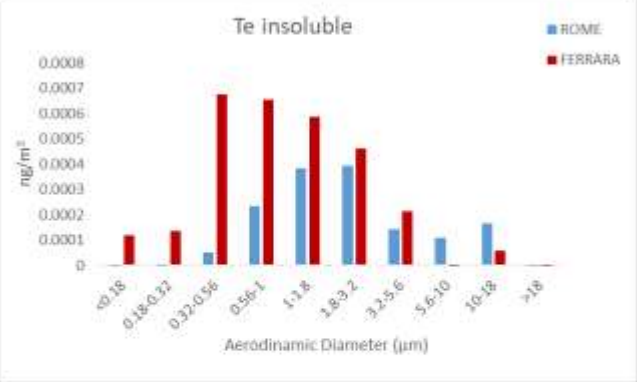
Te insoluble
ROME
FERRARA
ng/m³
0.0008
0.0007
0.0006
0.0005
0.0004
0.0003
0.0002
0.0001
0
<0.18
0.18-0.32
0.32-0.56
0.56-1
1-1.8
1.8-3.2
3.2-5.6
5.6-10
10-18
>18
Aerodinamic Diameter (µm)

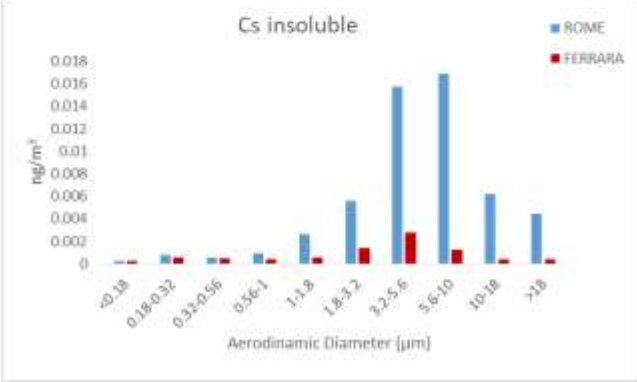
Cs insoluble
ROME
FERRARA
ng/m³
0.018
0.016
0.014
0.012
0.01
0.008
0.006
0.004
0.002
0
<0.18
0.18-0.32
0.32-0.56
0.56-1
1-1.8
1.8-3.2
3.2-5.6
5.6-10
10-18
>18
Aerodinamic Diameter (µm)

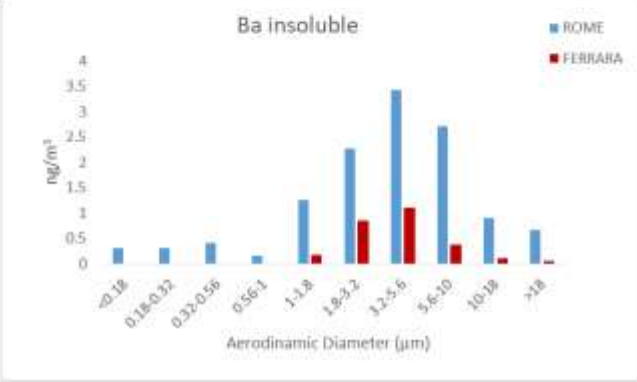
Ba insoluble
ROME
FERRARA
ng/m³
4
3.5
3
2.5
2
1.5
1
0.5
0
<0.18
0.18-0.32
0.32-0.56
0.56-1
1-1.8
1.8-3.2
3.2-5.6
5.6-10
10-18
>18
Aerodinamic Diameter (µm)

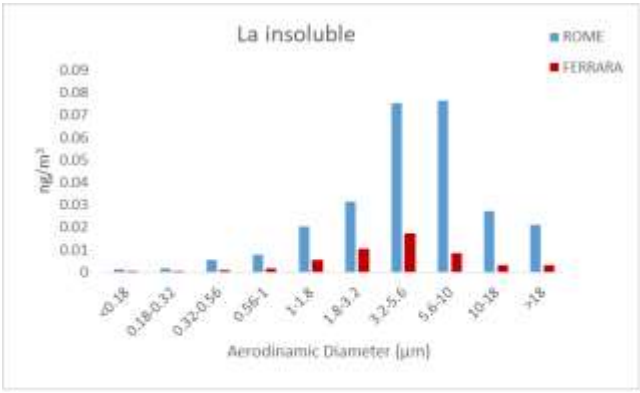
La insoluble
ROME
FERRARA
ng/m³
0.09
0.08
0.07
0.06
0.05
0.04
0.03
0.02
0.01
0
<0.18
0.18-0.32
0.32-0.56
0.56-1
1-1.8
1.8-3.2
3.2-5.6
5.6-10
10-18
>18
Aerodinamic Diameter (µm)

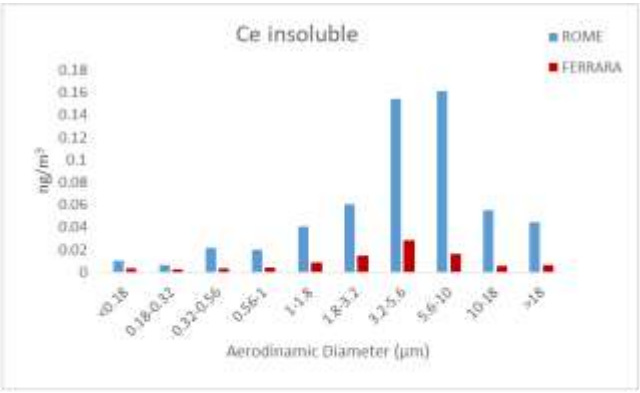
Ce insoluble
ROME
FERRARA
ng/m³
0.18
0.16
0.14
0.12
0.1
0.08
0.06
0.04
0.02
0
<0.18
0.18-0.32
0.32-0.56
0.56-1
1-1.8
1.8-3.2
3.2-5.6
5.6-10
10-18
>18
Aerodinamic Diameter (µm)

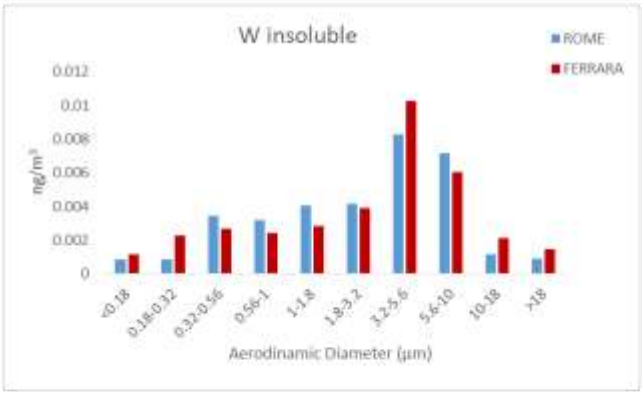
W insoluble
ROME
FERRARA
ng/m³
0.012
0.01
0.008
0.006
0.004
0.002
0
<0.18
0.18-0.32
0.32-0.56
0.56-1
1-1.8
1.8-3.2
3.2-5.6
5.6-10
10-18
>18
Aerodinamic Diameter (µm)

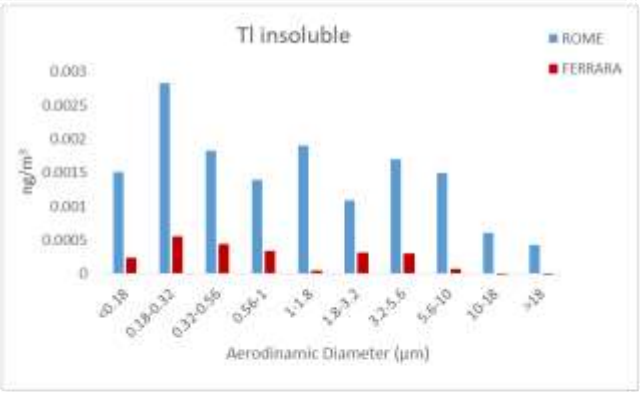
Tl insoluble
ROME
FERRARA
ng/m³
0.003
0.0025
0.002
0.0015
0.001
0.0005
0
<0.18
0.18-0.32
0.32-0.56
0.56-1
1-1.8
1.8-3.2
3.2-5.6
5.6-10
10-18
>18
Aerodinamic Diameter (µm)

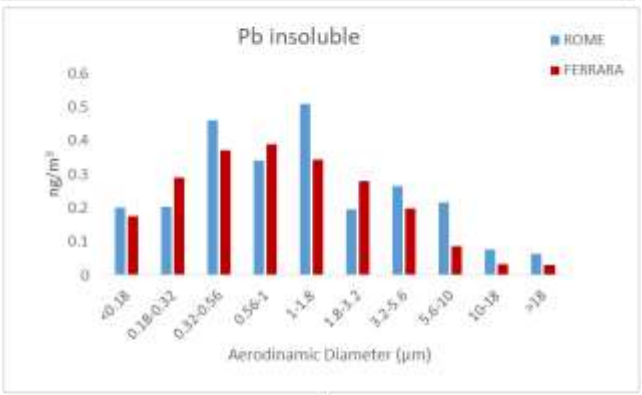
Pb insoluble
ROME
FERRARA
ng/m³
0.6
0.5
0.4
0.3
0.2
0.1
0
<0.18
0.18-0.32
0.32-0.56
0.56-1
1-1.8
1.8-3.2
3.2-5.6
5.6-10
10-18
>18
Aerodinamic Diameter (µm)

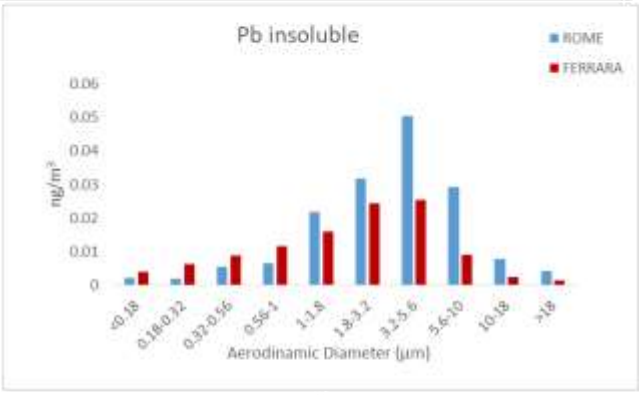
Pb insoluble
ROME
FERRARA
ng/m³
0.06
0.05
0.04
0.03
0.02
0.01
0
<0.18
0.18-0.32
0.32-0.56
0.56-1
1-1.8
1.8-3.2
3.2-5.6
5.6-10
10-18
>18
Aerodinamic Diameter (µm)

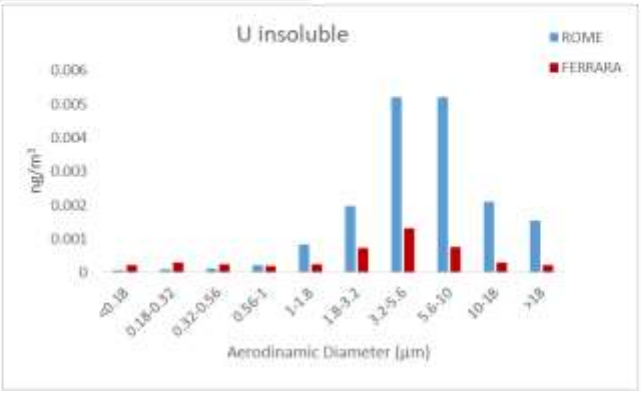
U insoluble
ROME
FERRARA
ng/m³
0.006
0.005
0.004
0.003
0.002
0.001
0
<0.18
0.18-0.32
0.32-0.56
0.56-1
1-1.8
1.8-3.2
3.2-5.6
5.6-10
10-18
>18
Aerodinamic Diameter (µm)